THE INTERFACE CRACK PROBLEM IN NONHOMOGENEOUS BONDED MATERIALS OF FINITE THICKNESS

by

Yaofeng Chen and F. Erdogan

Lehigh University, Bethlehem, PA

August 1992

FINAL PROJECT REPORT

OFFICE OF NAVAL RESEARCH CONTRACT NO. N0O014-89-3188

THE INTERFACE CRACK PROBLEM IN NONHOMOGENEOUS BONDED MATERIALS OF FINITE THICKNESS

by

Yaofeng Chen and F. Erdogan

Lehigh University, Bethlehem, PA

August 1992

FINAL PROJECT REPORT

OFFICE OF NAVAL RESEARCH CONTRACT NO. N0014-89-3188

St-A per telecom, Mr. Rajatakse,
ONR/Code 1132sm, Arl., VA.
JK 10-16-92

Abstract

In a recently developed material forming method called Functionally Gradient Materials as well as applications of material deposition processes such as ion plating, composite materials are being created where the interface possesses a gradually varying material composition and properties. This study was directed at the mechanics of such materials when there is a crack on the interface, and sought to find parameters that govern the crack growth such as the crack tip stress intensity factors, strain energy release rate and probable direction of crack extension. The mixed boundary value problem involved two bonded materials having finite thicknesses with an interface crack under plane strain or generalized plane stress conditions. One material is homogeneous and the other nonhomogeneous with an exponential property variation in the y-direction.

Fourier transforms was applied to Navier's equations to derive a system of singular integral equations with a simple Cauchy kernel and Fredholm kernels. The x-derivatives of the two crack opening displacements are assumed to be the unknowns. Extensive asymptotic expansions of the kernels, which were the algebraic sum of rational functions of 7 by 7 and 8 by 8 determinants as the numerator and denominator were carried out in order to separate the Cauchy kernel and to facilitate the integral equations numerical computation. The problem was solved numerically by converting to a system of linear algebraic equations and by using a collocation technique. The stress field near the crack tip is mixed mode and is shown to have a standard square root singularity.

Cases for a wide range of degrees of nonhomogeneity and combinations of

material thickness to crack length ratios were computed with loadings of uniform normal stress and uniform shear. The results of a special case where both materials have very large thicknesses compare very well with the previous results for two bonded half planes.

The technique developed in this study is useful for fracture mechanics studies of composite materials that have a nonhomogeneous interfacial zone. The results compiled are especially well suited for studying the delamination problem in nonhomogeneous thin films bonded to elastic substrates.

Chapter 1
Introduction

1.1 Introduction

Materials of composite nature have found their applications perhaps as early as the recorded history. One of the earliest applications may have been in protection against corrosion by using a variety of coatings. The majority of the more recent applications of composite materials seek to utilize the strengths or mechanical properties of component materials in order to optimize the properties of the combined system. For example, blades in gas turbine engines are subject to high stresses and highly corrosive environment of oxygen, sulfur and chlorine gases. A monolithic material such as a high temperature alloy is incapable of providing both functions. The solution is to design the bulk for the mechanical properties and use a coating of another alloy to provide the corrosion resistance. Another example of composite materials is dry film lubricant coatings, as in the case of, for example, using thin gold films bearing and sliding parts. Such dry film lubricants are important for critical parts where conventional organic fluid lubricants are susceptible to degradation.

In the quest of finding an optimal composite for a particular need, the problem of thermal mismatch at the bimaterial interface has always been one of the major reasons that cause the material to fail to perform its intended function. Thermal mismatch and residual stresses occur because the temperature under which the composites are processed does not fall in the temperature range where it is supposed to perform, and usually far from it.

With the help of novel material forming processes and innovative apparatuses,

material scientists have found ways to produce new materials with maximum efficiency as never before. In laboratories and manufacturing facilities, physical vapor deposition (PVD), chemical vapor deposition (CVD)[1] and their derivatives have been used to create materials from the very elemental building blocks, i.e. atoms and molecules for applications ranging from semiconductors to machine tools. A notable derivative of the physical vapor deposition process is one called ion plating[2]. In the ion plating process, the coating material, in atomic or molecular form, is to be charged and accelerated in an electric field so that the charged particles impinge on the substrate with a very high kinetic energy. The impact of the charges particles causes sputtering of the substrate and a great deal of physical mixing of the coating and substrate materials. Usually what results is a coating of gradual change in material composition from the substrate to the coating material. These processes have demonstrated that composite materials with distinctive material properties but a gradually varying interfacial zone composition and, as a result, varying interface properties can be achieved; see for example [3]. The immediate benefit of this achievement is perhaps the relief of residual stresses in the composite. Because the material characteristics at the interface is no longer an abrupt change of properties but rather a smooth transition from one material to another, thermal mismatch and residual stresses are reduced substantially.

In another area of the development of composite materials, a concept that seeks to design engineering composites to optimize material properties for particular applications is producing more new material forming processes. Prompted by the "Space Plane Project" that requires high temperature materials to protect the space vehicle from thermal damage during reentry, one such "Functionally Gradient

Materials" describes a successful laboratory testing of a TiB_2-Cu system to be used on the exterior of the spacecraft. The TiB_2:Cu ratio decreases from exterior of the surface to the interior[4].

In high temperature engine combustion chambers and gas turbine air foils, where good heat resistant property near the surface, heat dissipation in the bulk, minimal residual stresses and overall mechanical toughness are required, this new way of materials design can succeed where traditional design methods fail. There are several methods to produce such "gradient" effect in composite materials, such as Chemical Vapor Deposition[5], Centrifugal Casting[6], and Combustion Sintering [7]. Composite materials so produced possess mechanical and thermal properties, instead of changing abruptly from one to the other as traditional composites do, that vary continuously through the thickness of the composite[8]. The resulting continuously varying material composition leads to reduced residual stresses.

This study is directed toward the fracture mechanics of an interface at a two material junction where both materials are of finite thickness. The material is isotropic, but near the interface it is nonhomogeneous. This nonhomogeneity results either from intentional material mixing or through the particular process used. To study the fracture mechanics of the interface we assume the existence of initial defects in the form of a crack, and then try to find certain fracture parameters that govern the tendency of the crack to grow. In brittle fracture and fatigue crack growth, the most important parameter we seek is the stress intensity factor, which combines the effects of applied loads, crack geometry and material properties. To be more specific, we shall phrase the problem as follows: To study the fracture mechanics problem of a crack at the interface of a two bonded finite thickness materials. Both materials

will be isotropic one being homogeneous and the other nonhomogeneous in the thickness direction. The problem will be formulated as a plane strain or generalized plane stress problem.

The analysis of this interface crack problem will be performed within the confines of the linear theory of elasticity, which we solve as a plane strain or generalized plane stress problem in a straightforward manner, under self equilibrating surface tractions. The crack problem is of the mixed boundary value type and is reduced to a system of singular integral equations. Except under very special circumstances where a closed form solution can be found, most often the system of SIE's are solved by a numerical method to obtain the crack tip stress intensity factors, the strain energy release rate and the direction of probable crack extension. Once the integral equations are solved, the stress field can be readily computed if one so desires.

1.2 Literature survey

In studying the fracture mechanics of bonded materials, in recent past considerable attention has been directed toward studying the mechanical behavior of the interfacial regions where defects usually in the form of voids or cracks often exist. Numerous publications have addressed the mechanics of interfacial regions in bonded materials (see for example [9] through [13]). It has been shown that for interface cracks the material properties, in particular the ratio of Young's moduli, plays an important role in their fracture mechanics behavior. In the simplest case of two bonded materials where both are homogeneous and isotropic, the Young's moduli are constant, and therefore a jump discontinuity exists at the interface. With such a

discontinuity it is well known that the stress state around the crack tip exhibits an oscillation[9][10][11]. This is physically inadmissible, as it implies wrinkling and overlapping of the crack surfaces near the crack tips[12]. It could be argued that this affects a very small region near the crack tip and consequently is not important.

The crack-contact model tries to resolve this inconsistency by assuming that the crack surfaces close near the crack tips and form a cusp and the shear stress in the contact region is zero[13]. However, the general belief is that the resolution to this physical anomaly has to come from a more realistic modeling of the interfacial region of the bonded materials. Research has shown that this stress oscillation disappears as long as the material property is continuous around the crack tip [9][14][15][16]. For the interface cracks there is a model that treats the interfacial region as a third nonhomogeneous material with steep property gradients thus eliminating the jump discontinuity in the material properties[16]. This model eliminates the stress oscillations since the material properties are continuous throughout the domain.

In light of the discussions in the previous section on composites that possess varying material properties near the interface, material nonhomogeneity is something that has to be taken into account in the study of interface crack problems in a wide variety of applications. Reference [16] exemplifies such a case by assuming one material to be nonhomogeneous with the material parameters varying through the thickness in a certain exponential manner and provides the interface crack solution for two bonded half planes. In many practical applications where the crack size is small as compared to the thickness dimension, often the bonding of two materials can

be modeled by two half planes. In some other applications, however, this may be realistic. Thus, in cases such as the dry-film lubricant coatings discussed earlier, thin layer of refractory coatings on cutting tools and variety of components involving thin films in microelectronics where the film thickness is sometimes less than 1.0μm (10^{-6} meter) [3], it may be necessary to investigate the interfacial crack problem for finite domains.

1.3 Overview

The main objectives of this study are to study the interface crack problem in a two-layered solid with finite thickness. The medium is nonhomogeneous, and particular attention is focused on thin film cases where numerical computation is difficult. The study admits any general loading configurations, covers a very wide range of material nonhomogeneity, and does not place limits on the material thickness to crack length ratio. However, if the material is strongly nonhomogeneous and at the same time the thickness to crack length ratio very small, the effort in numerical computation would increase in a dis-proportionate manner.

In Chapter 2 the problem is formulated under considerations of plane elasticity by using the two displacement components as the primary unknowns. Through integral transform the problem is transformed to solving a pair of coupled second order ODE's. With the introduction of yet another new set of unknowns, i.e. the derivative of the crack opening displacements, and applying the mixed boundary conditions, for the plane problem the original formulation is reduced to a system of singular integral equations with the derivative of the crack opening displacements as the unknown functions. The pair of singular integral equations are of the first kind

and both have a simple Cauchy kernel. As a result the stress field around the crack tips exhibits the well-known square-root singularity.

Chapter 3 describes the method to solve the pair of SIE's, namely the step by step procedure of transforming the SIE's to a system of linear algebraic equations, the solutions of which are the finite part of the density functions. Of particular interest is the numerical computation scheme to compute the infinite oscillating integrals for the evaluation of the related Fredholm kernels. Special attention is paid to the case where the material is strongly nonhomogeneous, and the material thickness to crack length ratio is small, and as a consequence the convergence of the solution is slow. An important point that is addressed in Chapter 3 involves the integration of a sign (step) function and a logarithm function. Failure to pay special attention to these integrals deters convergence of the numerical scheme.

In Chapter 4, a particular case of very large thickness to crack length ratio is computed so as to compare with known results. This serves as a benchmark of verification, even though the two problems are not exactly the same. General cases considered to be of practical use is computed under the opening mode and shear mode. Also, the results are discussed and interpretation of the trends of the crack tip characteristics as a function of the nonhomogeneity parameter and geometry changes is examined. Chapter 5 gives the conclusions and points to direction of future research.

Hidden in the straightforwardness of the derivation in Chapter 2 is the analytical formulation of the interface crack problem. The complexity of the expressions of the Fredholm kernels in terms of the basic variables such as thicknesses, Poisson's ratio and the nonhomogeneity parameter can be seen in

Appendix A. In it, all the elements of the determinants that form the numerators and denominators of the expressions in Fredholm kernels are listed. These expressions were first derived using the symbolic manipulation program MACSYMA[17] on a VAX-8300 and later verified by similar program MAPLE[18] on a VAX-8530.

Appendix B describes the asymptotic expansion of the rational polynomials where the numerators and denominators are determinants the elements of which are depicted in Appendix A. In theory, only the leading terms need to be extracted in order to derive the pair of SIE's with the proper Cauchy kernel, which is to be expected for the problem defined. For the sake of numerically solving the SIE's in a more efficient manner, the asymptotic expansion is carried out to as many terms using the symbolic manipulator MAPLE, as the limit of computer resources would allow. To tackle potential practical cases applicable to this work, which usually involves thin films deposited on substrates with film thicknesses in the micron range, the successful asymptotic analysis to as many terms as possible proved to be absolutely essential.

Appendix C gives some useful formulas to evaluate those infinite integrals, whose integrands have been known in closed form through asymptotic expansions carried out in Appendix B. Appendix D illustrates, by way of simple examples, several schemes to numerically integrate a step function and logarithm function both of which have a discontinuity within the interval of integration. It explains the technique used in Chapter 3 to separate the integrals involving step function and the logarithm function from other infinite integrals. Failing to do so would very nearly guarantee the breakdown of convergence in the numerical scheme.

Appendix E addresses two aspects that are very important in the numerical computation in this work. One is the limit of floating point calculations that can be

carried out for the Fredholm kernels, which depends on the range of a real number defined in FORTRAN language resided in the computer and used to perform the computation. The other is how such cases involving thin films on thick substrates are to be successfully tackled within the numerical scheme.

Appendix F shows the derivation of the Cauchy integral which is necessary to study the singular behavior of the solution around the crack-tips and to compute the stress intensity factors.

Chapter 2

Formulation Of The Problem

2.1 Introduction

The crack problem under consideration is shown in Figure 1. Two plates are bonded together and it is assumed that there is a crack at the interface. It is a plane strain, isotropic, but nonhomogeneous, elasticity problem. However, the derivation in what follows is also good for a generalized plane stress problem should any physical interpretation warrant. Material 1 (occupying $y < 0$) is homogeneous, whereas material 2 (occupying $y > 0$) is nonhomogeneous in the y-direction. The elastic properties of material 2 may vary very steeply near the interface but continuity of the material parameters is maintained across the interface. The nonhomogeneity of material 2 is assumed to be such that its shear modulus varies across the thickness as an exponential function. This assumption is broad enough to accommodate most practical applications. The real advantage made possible by this assumption, however, is that it leads to a system of differential equations with constant coefficients. Given the complexity of the nonhomogeneous problem, this feat is vital in the formulation of our problem. As for the Poisson's ratio ν , we shall consider it constant.

To solve the linear elasticity problem under general loading conditions defined above, we use the method of superposition as shown in Figure 2. First the elasticity problem of the configuration as defined in the absence of any cracks under a prescribed loading is formulated, Figure 2(b). The crack problem as shown in Figure 2(c), the solution of which is of the main interest in this study, is solved by

applying loadings at the two crack surfaces that is equal in magnitude, but opposite in sign, to the tractions at the same locations of the elasticity problem in Figure 2(b). Since only the crack problem (Figure 2(c)) carries the characteristic stress singularities that we seek, the solution of it alone will tell us the fracture mechanics characteristics of the problem. Only when we seek to know the stress field need we superpose the solutions of the two elasticity problems.

2.2 Formulation of the crack problem

Referring to Figure 1, let the shear modulus of material 1 be μ_1, which is a constant, and that of material 2 be $\mu_2 = \mu_1 e^{\gamma y}$. The thicknesses of the two materials are h_1 and h_2, respectively. We use the two components of displacement u and v as the primary unknowns. Let $\kappa = 3 - 4\nu$ for plane strain and $\kappa = \frac{3-\nu}{1+\nu}$ for generalized plane stress, where ν is the Poisson's ratio. Hooke's Law may then be expressed as

$$\sigma_{xx} = \frac{\mu_i}{\kappa-1}[(\kappa+1)\frac{\partial u}{\partial x} + (3-\kappa)\frac{\partial v}{\partial y}],$$

$$\sigma_{yy} = \frac{\mu_i}{\kappa-1}[(3-\kappa)\frac{\partial u}{\partial x} + (\kappa+1)\frac{\partial v}{\partial y}], \qquad (1)$$

$$\sigma_{xy} = \mu_i\,(\frac{\partial u}{\partial x} + \frac{\partial v}{\partial y}),$$

$$i = 1,\ 2.$$

In the absence of body forces, the equations of equilibrium are expressed as

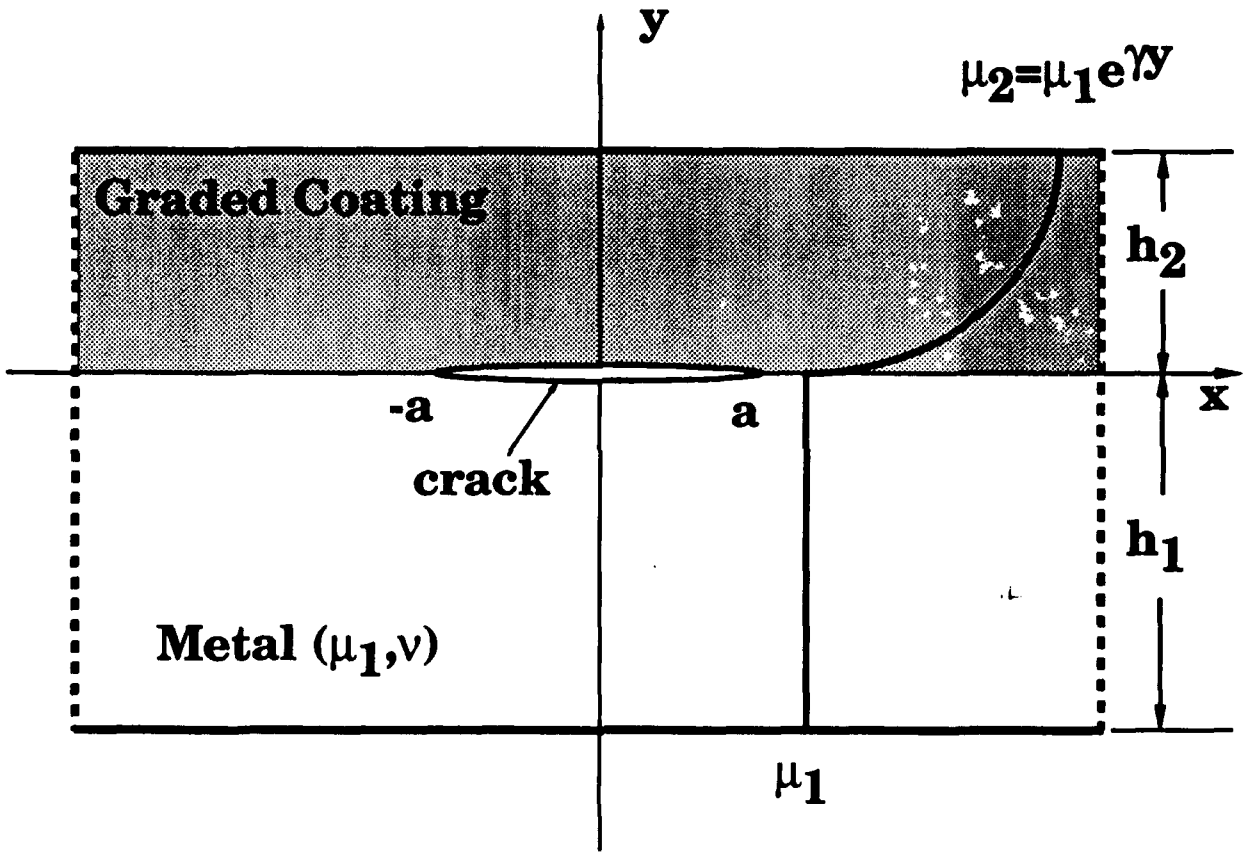

Figure 1. A crack in the interface of two materials with finite thicknesses. One material is homogeneous and another non-homogeneous.

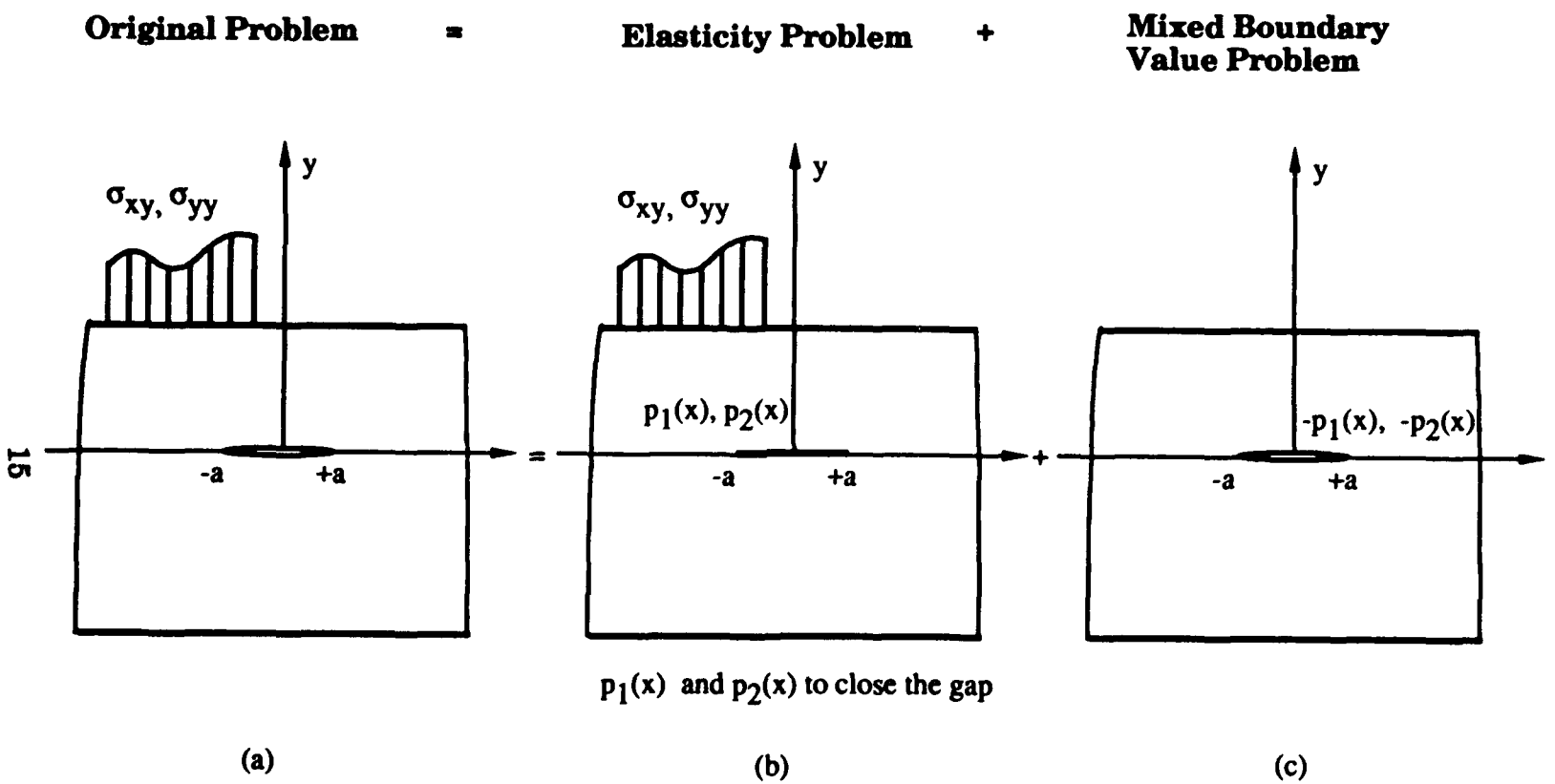

Figure 2. Superpose an elasticity problem and a MBVP to solve the original problem.

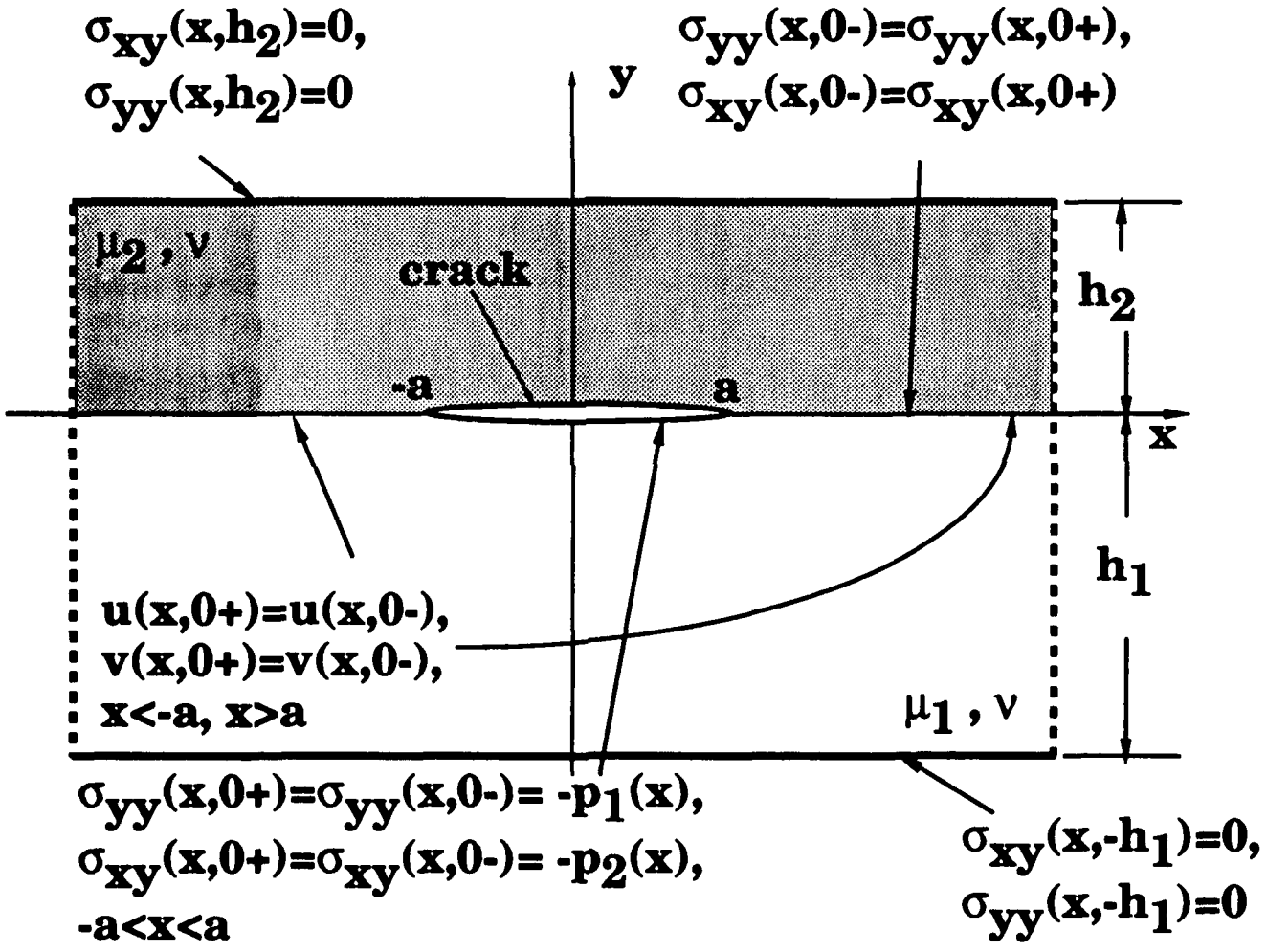

Figure 3. Boundary conditions.

$$\frac{\partial \sigma_{xx}}{\partial x} + \frac{\partial \sigma_{xy}}{\partial y} = 0,$$

$$\frac{\partial \sigma_{xy}}{\partial x} + \frac{\partial \sigma_{yy}}{\partial y} = 0. \tag{2}$$

Substituting Eqn. (1) into Eqn. (2) for $0 < y < h_2$ we find the Navier's equations as

$$(\kappa+1)\frac{\partial^2 u}{\partial x^2} + (\kappa-1)\frac{\partial^2 u}{\partial y^2} + 2\frac{\partial^2 v}{\partial x \partial y} + \gamma(\kappa-1)\frac{\partial u}{\partial y} + \gamma(\kappa-1)\frac{\partial v}{\partial x} = 0,$$

$$(\kappa-1)\frac{\partial^2 v}{\partial x^2} + (\kappa+1)\frac{\partial^2 v}{\partial y^2} + 2\frac{\partial^2 u}{\partial x \partial y} + \gamma(3-\kappa)\frac{\partial u}{\partial x} + \gamma(\kappa+1)\frac{\partial v}{\partial y} = 0. \tag{3}$$

Equation (3) and similar equations obtained for material 2 must be solved under the following boundary and continuity conditions (Figure 3):

$$\sigma_{yy}(x,h_2) = 0,\ \sigma_{xy}(x,h_2) = 0,\ -\infty<x<\infty, \tag{4}$$

$$\sigma_{yy}(x,-h_1) = 0,\ \sigma_{xy}(x,-h_1) = 0,\ -\infty<x<\infty, \tag{5}$$

$$\sigma_{yy}(x,0+) = \sigma_{yy}(x,0-),\ \sigma_{xy}(x,0+) = \sigma_{xy}(x,0-),\ -\infty<x<\infty, \tag{6}$$

$$\sigma_{yy}(x,0+) = \sigma_{yy}(x,0-) = -p_1(x),\ \sigma_{xy}(x,0+) = \sigma_{xy}(x,0-) = -p_2(x),\ -a<x<a,$$
$$u(x,0+) = u(x,0-),\ v(x,0+) = v(x,0-),\ x\le -a,\ x\ge a, \tag{7}$$

where $p_1(x)$ and $p_2(x)$ are the normal and shear stresses, respectively, at the location of the crack in the elasticity solution of the corresponding uncracked problem (Figure 2(a)). The notations 0+ and 0- are necessary since there is a discontinuity of displacement field at the crack surface.

To solve Eqn. (3), define the Fourier transforms of the two displacement components, u and v, respectively, as follows:

$$U(\alpha,y) = \int_{-\infty}^{\infty} u(x,y)\, e^{-i\alpha x}\, dx,$$

$$V(\alpha,y) = \int_{-\infty}^{\infty} v(x,y)\, e^{-i\alpha x}\, dx. \tag{8}$$

By definition, u and v become

$$u(x,y) = \frac{1}{2\pi}\int_{-\infty}^{\infty} U(\alpha,y) e^{i\alpha x}\, d\alpha,$$

$$v(x,y) = \frac{1}{2\pi}\int_{-\infty}^{\infty} V(\alpha,y) e^{i\alpha x}\, d\alpha. \tag{9}$$

From Eqns. (3) and (8) it can be shown that

$$(\kappa-1)\frac{d^2U}{dy^2} + \gamma(\kappa-1)\frac{dU}{dy} - (\kappa+1)\alpha^2 U + 2i\alpha\frac{dV}{dy} + \gamma(\kappa-1)i\alpha V = 0,$$

$$(\kappa+1)\frac{d^2V}{dy^2} + \gamma(\kappa+1)\frac{dV}{dy} + (\kappa-1)\alpha^2 V + 2i\alpha\frac{dU}{dy} + \gamma(3-\kappa)i\alpha U = 0. \tag{10}$$

Solving Eqn. (10) we find

$$U(\alpha,y) = C_1(\alpha)e^{n_1 y} + C_2(\alpha)e^{n_2 y} + C_3(\alpha)e^{n_3 y} + C_4(\alpha)e^{n_4 y},$$

$$V(\alpha,y) = D_1(\alpha)e^{n_1 y} + D_2(\alpha)e^{n_2 y} + D_3(\alpha)e^{n_3 y} + D_4(\alpha)e^{n_4 y}, \tag{11}$$

$$0 < y < h_2,$$

where, n_1, n_2, n_3 and n_4 are solutions of the following characteristic equation:

$$n^4 + 2\gamma n^3 - (2\alpha^2 - \gamma^2)n^2 - 2\alpha^2\gamma n + \frac{3-\kappa}{1+\kappa}\alpha^2\gamma^2 + \alpha^4 = 0. \tag{12}$$

Eqn. (12), a polynomial equation of the fourth degree, has the following roots:

$$n_1 = \frac{1}{2}(R\cos\theta - \gamma + iR\sin\theta),$$

$$n_2 = \overline{n_1} = \frac{1}{2}(R\cos\theta - \gamma - iR\sin\theta),$$

$$n_3 = -\frac{1}{2}(R\cos\theta + \gamma - iR\sin\theta), \tag{13}$$

$$n_4 = \overline{n_3} = -\frac{1}{2}(R\cos\theta + \gamma + iR\sin\theta).$$

Note that n_2 and n_4 are the respective complex conjugates of n_1 and n_3. In addition, R and θ may be expressed as

$$R = \sqrt[4]{(\gamma^2 + 4\alpha^2)^2 + 16\alpha^2\gamma^2\frac{3-\kappa}{1+\kappa}},$$

$$\theta = \frac{1}{2}\tan^{-1}\left(\frac{4\alpha\gamma}{\gamma^2 + 4\alpha^2}\sqrt{\frac{3-\kappa}{\kappa+1}}\right). \tag{14}$$

In Eqn. (11), the functions $C_j(\alpha)$ and $D_j(\alpha)$, ($j = 1 \cdots 4$) are not independent. Their relationship can be established by substituting Eqn. (11) into either one of Eqn. (10) and noting that the identity is true for all y, therefore the coefficients of the y dependent terms must be identically zero, giving

$$D_j(\alpha) = \frac{-i\alpha[2n_j + \gamma(3-\kappa)]\ C_j(\alpha)}{(\kappa+1)n_j^2 + \gamma(\kappa+1)n_j - (\kappa-1)\alpha^2}, \quad j = 1 \cdots 4. \tag{15}$$

The above derivation is for the nonhomogeneous material. For material 1, which is homogeneous ($\gamma = 0$) or for $-h_2 < y < 0$, Eqn. (10) becomes

$$(\kappa-1)\frac{d^2U}{dy^2}-(\kappa+1)\alpha^2U+2\alpha\frac{dV}{dy}=0,$$

$$(\kappa+1)\frac{d^2V}{dy^2}-(\kappa-1)\alpha^2V+2i\alpha\frac{dU}{dy}=0. \tag{16}$$

The corresponding characteristic equation, which can be obtained by letting $\gamma = 0$ in Eqn. (12), becomes

$$(n^2-\alpha^2)^2=0. \tag{17}$$

From Eqns. (17) the solution of Eqn. (16) may be obtained as

$$U(\alpha,y)=[A_1(\alpha)+A_2(\alpha)y]e^{|\alpha|y}+[A_3(\alpha)+A_4(\alpha)y]e^{-|\alpha|y},$$

$$V(\alpha,y)=[B_1(\alpha)+B_2(\alpha)y]e^{|\alpha|y}+[B_3(\alpha)+B_4(\alpha)y]e^{-|\alpha|y}, \tag{18}$$

$$-h_1 < y < 0.$$

Similar to the nonhomogeneous case, the functions $A_j(\alpha)$ and $B_j(\alpha)$, ($j = 1 \cdots 4$) are inter-dependent. Their relationships, obtained by substituting Eqn. (18) into either one of Eqn. (16), are found as follows:

$$B_1(\alpha)=-i[\frac{\alpha}{|\alpha|}A_1(\alpha)-\frac{\kappa}{\alpha}A_2(\alpha)],$$

$$B_2(\alpha)=-i\frac{\alpha}{|\alpha|}A_2(\alpha),$$

$$B_3(\alpha)=i[\frac{\alpha}{|\alpha|}A_3(\alpha)+\frac{\kappa}{\alpha}A_4(\alpha)], \tag{19}$$

$$B_4(\alpha)=i\frac{\alpha}{|\alpha|}A_4(\alpha).$$

The original problem has only two unknowns, i.e. the two displacement components. After Fourier transform, we have instead eight unknown coefficients in the solution to the two ODE's. Now we need to utilize the homogeneous boundary conditions, Eqns. (4) through (7), to determine the unknown functions A_j's and C_j's. Before we apply Fourier transforms to the boundary conditions, define density functions as follows:

$$f_1(x) = \frac{\partial}{\partial x}[v_2(x,0+) - v_1(x,0-)],$$
$$f_2(x) = \frac{\partial}{\partial x}[u_2(x,0+) - u_1(x,0-)]. \tag{20}$$

It follows that $f_1(x) = f_2(x) = 0$, $-\infty < x < -a$, $a < x < \infty$, which is a direct result of the fact that $v_2(x,0+) = v_1(x,0-)$ and $u_2(x,0+) = u_1(x,0-)$ outside of the crack. Let the Fourier transforms of f_1 and f_2 be F_1 and F_2, respectively, that is, let

$$F_1(\alpha) = \int_{-a}^{a} f_1(x)\, e^{-i\alpha x}\, dx,$$
$$F_2(\alpha) = \int_{-a}^{a} f_2(x)\, e^{-i\alpha x}\, dx. \tag{21}$$

The Fourier transforms of Eqns. (4) - (7) may then be expressed as follows:

$$\sigma_{xy}(x,h_2) = 0,\ -\infty<x<\infty,\ \rightarrow \frac{dU}{dy}(\alpha,h_2) + i\alpha V(\alpha,h_2) = 0, \tag{22}$$

$$\sigma_{yy}(x,h_2) = 0,\ -\infty<x<\infty,\ \rightarrow (3-\kappa) i\alpha U(\alpha,h_2) + (\kappa+1)\frac{dV}{dy}(\alpha,h_2) = 0, \tag{23}$$

$$\sigma_{xy}(x,-h_1) = 0,\ -\infty<x<\infty,\ \rightarrow \frac{dU}{dy}(\alpha,-h_1) + i\alpha V(\alpha,-h_1) = 0, \tag{24}$$

$$\sigma_{yy}(x,-h_1) = 0,\ -\infty<x<\infty,\ \rightarrow (3-\kappa)i\alpha U(\alpha,-h_1)+(\kappa+1)\frac{dV}{dy}(\alpha,-h_1) = 0, \tag{25}$$

$$\sigma_{yy}(x,0+) = \sigma_{yy}(x,0-),\ -\infty<x<\infty,\ \rightarrow$$

$$(3-\kappa)i\alpha U(\alpha,0+)+(\kappa+1)\frac{dV}{dy}(\alpha,0+) = (3-\kappa)i\alpha U(\alpha,0-)+(\kappa+1)\frac{dV}{dy}(\alpha,0-), \tag{26}$$

$$\sigma_{xy}(x,0+) = \sigma_{xy}(x,0-),\ -\infty<x<\infty,\ \rightarrow$$

$$\frac{dU}{dy}(\alpha,0+)+i\alpha V(\alpha,0+) = \frac{dU}{dy}(\alpha,0-)+i\alpha V(\alpha,0-). \tag{27}$$

Note that the Fourier transforms of the density functions are identically zero outside of the crack and are the new unknowns inside of the crack. We can now express the transforms of the mixed and final boundary condition as

$$i\alpha[V(\alpha,0+)-V(\alpha,0-)] = F_1(\alpha),$$

$$i\alpha[U(\alpha,0+)-U(\alpha,0-)] = F_2(\alpha). \tag{28}$$

We now substitute the appropriate expressions for U's and V's from Eqns. (11) and (18) into Eqns. (22) to (27). By taking advantage of the inter-dependence between A_j's and B_j's, $j = 1 \cdots 4$, and C_j's and D_j's, $j = 1 \cdots 4$, we obtain a system of eight linear equations for the unknown functions A_j's and C_j's, ($j = 1 \cdots 4$) in terms of the Fourier transforms of the density functions as follows

$$\begin{bmatrix} 0 & 0 & 0 & 0 & a_{15} & a_{16} & a_{17} & a_{18} \\ 0 & 0 & 0 & 0 & a_{25} & a_{26} & a_{27} & a_{28} \\ a_{31} & a_{32} & a_{33} & a_{34} & 0 & 0 & 0 & 0 \\ a_{41} & a_{42} & a_{43} & a_{44} & 0 & 0 & 0 & 0 \\ a_{51} & a_{52} & a_{53} & a_{54} & a_{55} & a_{56} & a_{57} & a_{58} \\ a_{61} & a_{62} & a_{63} & a_{64} & a_{65} & a_{66} & a_{67} & a_{68} \\ a_{71} & a_{72} & a_{73} & a_{74} & a_{75} & a_{76} & a_{77} & a_{78} \\ a_{81} & 0 & a_{83} & 0 & a_{85} & a_{86} & a_{87} & a_{88} \end{bmatrix} \begin{bmatrix} A_1(\alpha) \\ A_2(\alpha) \\ A_3(\alpha) \\ A_4(\alpha) \\ C_1(\alpha) \\ C_2(\alpha) \\ C_3(\alpha) \\ C_4(\alpha) \end{bmatrix} = \begin{bmatrix} 0 \\ 0 \\ 0 \\ 0 \\ 0 \\ 0 \\ F_1(\alpha) \\ F_2(\alpha) \end{bmatrix} \tag{29}$$

where a_{ij}, $i, j = 1 \cdots 8$, the exact expressions of which are given in Appendix A, are functions of α, γ, κ, h_1, and h_2. We can solve Eqn. (29) for A_i, C_i, ($i = 1 \cdots 4$) in terms of the unknowns F_1, F_2 as

$$A_i = \sum_{j=1}^{2} \frac{D_{ij}}{D} F_j, \; i = 1 \cdots 4, \tag{30}$$

$$C_{i-4} = \sum_{j=1}^{2} \frac{D_{ij}}{D} F_j, \; i = 5 \cdots 8, \tag{31}$$

where D is the determinant of the 8 by 8 coefficient matrix, and D_{ij} are the appropriate cofactors of D. D_{ij} is defined as the 7 by 7 determinant computed from deleting the i-th column and the $j+6$-th row of the 8 by 8 matrix, then multiplied by the factor $(-1)^{(i+j+6)}$.

Up to this point, we have used all of the boundary conditions except the traction boundary conditions on the crack surfaces (Eqn. (7)), namely,

$$\sigma_{yy}(x,0-) = -p_1(x),\ \sigma_{xy}(x,0-) = -p_2(x),\ -a<x<a, \tag{32}$$

or

$$\sigma_{yy}(x,0+) = -p_1(x),\ \sigma_{xy}(x,0+) = -p_2(x),\ -a<x<a. \tag{33}$$

Either of (32) or (33) can be used; we chose, however, (32) for its simpler expressions because material 1 is homogeneous.

We now have two equations (32) in which we substitute stresses expressed in terms of Fourier transforms of the displacement components by using the Hooke's Law. These transformed displacement components are given by (11) and (18) in terms of eight undetermined coefficients or, indirectly in terms of Fourier transforms of the two density functions introduced by (21). Therefore, the two equations (32) are sufficient to determine the unknowns F_1 and F_2.

2.3 Derivation of the system of singular integral equations

Expressing Eqn. (32) in terms of Fourier transforms of the displacement components, we obtain

$$\begin{aligned} -p_1(x) &= \frac{\mu_1}{2\pi(\kappa-1)}\left[(3-\kappa)\int_{-\infty}^{\infty} U(\alpha,0-)i\alpha e^{i\alpha x}\,d\alpha + (\kappa+1)\int_{-\infty}^{\infty}\frac{dV}{dy}(\alpha,0-)e^{i\alpha x}\,d\alpha\right], \\ -p_2(x) &= \frac{\mu_1}{2\pi}\left[(3-\kappa)\int_{-\infty}^{\infty}\frac{dU}{dy}(\alpha,0-)e^{i\alpha x}\,d\alpha + (\kappa+1)\int_{-\infty}^{\infty} V(\alpha,0-)e^{i\alpha x}\,d\alpha\right]. \end{aligned} \tag{34}$$

By substituting from Eqn. (18) into Eqn. (34) it may be shown that

$$-\frac{2\pi}{\mu_1}p_1(x) = \lim_{y\to 0-}\int_{-\infty}^{\infty} -i\alpha(\{2A_1+[2y-i(\kappa+1)\frac{1}{|\alpha|}]A_2\}\ e^{i\alpha x+|\alpha|y}+$$

$$\{2A_3+[2y+i(\kappa+1)\frac{1}{|\alpha|}]A_4\}\ e^{i\alpha x-|\alpha|y})\ d\alpha, \tag{35}$$

$$-\frac{2\pi}{\mu_1}p_2(x) = \lim_{y\to 0-}\int_{-\infty}^{\infty}\{[2|\alpha|A_1+(2|\alpha|y-\kappa+1)A_2]\ e^{i\alpha x+|\alpha|y}+$$

$$[-2|\alpha|A_3-(2|\alpha|y+\kappa-1)A_4]\ e^{i\alpha x-|\alpha|y}\}d\alpha.$$

Now substituting (30) into (35), expressing F_1, and F_2 in their integral form (Eqn. (21)) and then changing the order of integration, we may write the integral equations with the density functions as unknowns as follows:

$$-\frac{\pi(\kappa+1)}{2\mu_1}p_i(x) = \int_{-a}^{a}\sum_{j=1}^{2}K_{ij}(x,t)f_j(t)dt,\ i = 1,\ 2,\ -a<x<a, \tag{36}$$

where

$$K_{1j}(x,t) = \lim_{y\to 0-}\frac{\kappa+1}{4}\int_{-\infty}^{\infty} -i\alpha(\{2\frac{D_{1j}}{D}+[2y-(\kappa+1)\frac{1}{|\alpha|}]\frac{D_{2j}}{D}\}\ e^{i\alpha(x-t)+|\alpha|y}+$$

$$\{2\frac{D_{3j}}{D}+[2y+(\kappa+1)\frac{1}{|\alpha|}]\frac{D_{4j}}{D}\}\ e^{i\alpha(x-t)-|\alpha|y})\ d\alpha,\ j = 1,\ 2, \tag{37}$$

$$K_{2j}(x,t) = \lim_{y\to 0-}\frac{\kappa+1}{4}\int_{-\infty}^{\infty}\{[2|\alpha|\frac{D_{1j}}{D}+(2|\alpha|y-\kappa+1)]\frac{D_{2j}}{D}]\ e^{i\alpha(x-t)+|\alpha|y}-$$

$$[2|\alpha|\frac{D_{3j}}{D}+(2|\alpha|y+\kappa-1)]\frac{D_{4j}}{D}]\ e^{i\alpha(x-t)-|\alpha|y})\ d\alpha,\ j = 1,2. \tag{38}$$

It should be pointed out that the integrands in Eqns. (37) and (38) are complex expressions involving determinants of several 7 by 7 and 8 by 8 matrices the elements of which are also long expressions of complex variables, as detailed in Appendix A.

But the boundedness of these integrands at $\alpha = 0$, can be seen by noting that the integrands vanish at $\alpha = 0$. We also note that the integrands in Eqns. (37) and (38) are continuous functions of α. It then becomes clear that any singularities the kernels K_{ij} must come from the asymptotic behavior of the integrands as $|\alpha|$ approaches infinity.

The details of asymptotic expansions of the kernels are given in Appendix B. In Eqns. (37) and (38), the behavior of $\frac{D_{ij}}{D}$ as α goes to ∞ and $-\infty$ respectively are as follows,

$$\frac{D_{11}}{D}(\alpha) = \frac{\kappa-1}{2\alpha(\kappa+1)} + O(\frac{1}{\alpha^2}),$$

$$\frac{D_{12}}{D}(\alpha) = \frac{i}{2\alpha} + O(\frac{1}{\alpha^2}),$$

$$\frac{D_{21}}{D}(\alpha) = \frac{1}{\kappa+1} + O(\frac{1}{\alpha}), \qquad \textbf{(39)}$$

$$\frac{D_{22}}{D}(\alpha) = \frac{i}{\kappa+1} + O(\frac{1}{\alpha}),$$

$$\frac{D_{11}}{D}(\beta) = \frac{\kappa-1}{2\beta(\kappa+1)} + O(\frac{1}{\beta^2}),$$

$$\frac{D_{12}}{D}(\beta) = -\frac{i}{2\beta} + O(\frac{1}{\beta^2}),$$

$$\frac{D_{21}}{D}(\beta) = \frac{1}{\kappa+1} + O(\frac{1}{\beta}), \qquad \textbf{(40)}$$

$$\frac{D_{22}}{D}(\beta) = -\frac{i}{\kappa+1} + O(\frac{1}{\beta}),$$

where $\beta = -\alpha$ in Eqn (40). We note that, as shown in Appendix B, terms like $\frac{D_{31}}{D}$,

$\frac{D_{32}}{D}$, $\frac{D_{41}}{D}$, and $\frac{D_{42}}{D}$ are analytic at $|\alpha| = \infty$ and they are of much lower order as compared to $\frac{D_{11}}{D}$, $\frac{D_{12}}{D}$, $\frac{D_{21}}{D}$, and $\frac{D_{22}}{D}$ and therefore no asymptotic expansion needs to be done.

Let us now try to separate the leading terms from Eqns. (37) and (38). Substituting the first terms in Eqns. (39) and (40) for $\frac{D_{ij}}{D}$, $i, j = 1, 2$, separating the infinite integral from $-\infty$ to ∞ into two parts at 0 and making a change of variable for the part from $-\infty$ to 0 by letting $\beta = -\alpha$, after some simplifications we obtain the leading term of $K_{11}(x,t)$ as follows:

$$\lim_{y \to 0-} \int_0^\infty (1+\alpha y)\, e^{\alpha y} \sin\alpha(t-x)\, d\alpha. \tag{41}$$

It is easily shown that

$$\lim_{y \to 0-} \int_0^\infty e^{\alpha y} \sin\alpha(t-x)\, d\alpha = \frac{t-x}{y^2+(t-x)^2} = \frac{1}{t-x}. \tag{42}$$

From Ref. [19], we obtain

$$\lim_{y \to 0-} \int_0^\infty \alpha y\, e^{\alpha y} \sin\alpha(t-x)\, d\alpha = 0. \tag{43}$$

Thus, in (37) the Cauchy kernel has been separated. The remainder of the integrand after the leading term of $\frac{D_{11}}{D}$ and $\frac{D_{12}}{D}$ has been separated is headed by a term no higher than $\frac{1}{\alpha}$. It is analytic everywhere and we can eliminate the limiting process by substituting $y = 0$ directly under the integral. This gives the Fredholm kernel $k_{11}(x,t)$ as follows

$$k_{11}(x,t) = \frac{\kappa+1}{4}\int_{-\infty}^{\infty} -i\alpha(\{2(\frac{D_{1j}}{D} - \frac{\kappa-1}{2\alpha(\kappa+1)}) - (\kappa+1)\frac{1}{|\alpha|}(\frac{D_{2j}}{D} - \frac{1}{\kappa+1})\}\ e^{i\alpha(x-t)} +$$

$$\{2\frac{D_{3j}}{D} + (\kappa+1)\frac{1}{|\alpha|}]\frac{D_{4j}}{D}\}\ e^{i\alpha(x-t)})\ d\alpha. \tag{44}$$

Likewise, the leading term of $K_{22}(x,t)$ is found to exhibit the same singular characteristics as Eqn. (42). The other Fredholm kernel $k_{22}(x,t)$ is obtained from Eqn. (38) in the same manner.

By a similar process, the leading term for $K_{12}(x,t)$ and $K_{21}(x,t)$ has the following form: (see [19])

$$\lim_{y\to 0-} \int_0^{\infty} \alpha y\ e^{\alpha y}\cos\alpha(x-t)d\alpha = 0. \tag{45}$$

Therefore, we do not need to separate the leading term from $K_{12}(x,t)$ and $K_{21}(x,t)$ and the Fredholm kernels $k_{12}(x,t)$ and $k_{21}(x,t)$ are formulated in an analogous manner as $k_{11}(x,t)$ done previously.

From the discussions above, we find that the singular behavior of the kernels come solely from K_{11} and K_{22} and we can write Eqn. (36) as a system of singular integral equation as follows

$$-\frac{\pi(\kappa+1)}{2\mu_1}p_1(x) = \int_{-a}^{a}\frac{f_1(t)}{t-x}dt + \int_{-a}^{a}k_{11}(x,t)f_1(t)dt + \int_{-a}^{a}k_{12}(x,t)f_2(t)\ dt,$$

$$-\frac{\pi(\kappa+1)}{2\mu_1}p_2(x) = \int_{-a}^{a}\frac{f_2(t)}{t-x}dt + \int_{-a}^{a}k_{21}(x,t)f_1(t)dt + \int_{-a}^{a}k_{22}(x,t)f_2(t)\ dt, \tag{46}$$

$$-a<x<a.$$

k_{11}, k_{12}, k_{21}, k_{22} are derived from the kernels in Eqns. (37) and (38), as described

previously. They may be expressed in the following form

$$k_{11}(x,t) = \int_0^\infty D_{11}^*(\alpha) \sin\alpha(t-x)\ d\alpha, \tag{47}$$

$$k_{12}(x,t) = \int_0^\infty D_{12}^*(\alpha) \cos\alpha(t-x)\ d\alpha, \tag{48}$$

$$k_{21}(x,t) = \int_0^\infty D_{21}^*(\alpha) \cos\alpha(t-x)\ d\alpha, \tag{49}$$

$$k_{22}(x,t) = \int_0^\infty D_{22}^*(\alpha) \sin\alpha(t-x)\ d\alpha, \tag{50}$$

where,

$$D_{11}^*(\alpha) = -\frac{\kappa+1}{2}[2\alpha(\frac{D_{11}}{D}+\frac{D_{31}}{D}-\frac{\kappa-1}{2\alpha(\kappa+1)})+(\kappa+1)(\frac{D_{21}}{D}-\frac{D_{41}}{D}-\frac{1}{\kappa+1})], \tag{51}$$

$$D_{12}^*(\alpha) = -\frac{\kappa+1}{2} i[2\alpha(\frac{D_{12}}{D}+\frac{D_{32}}{D})-(\kappa+1)(\frac{D_{22}}{D}-\frac{D_{42}}{D})], \tag{52}$$

$$D_{21}^*(\alpha) = \frac{\kappa+1}{2}[2\alpha(\frac{D_{11}}{D}-\frac{D_{31}}{D})-(\kappa-1)(\frac{D_{21}}{D}+\frac{D_{41}}{D})], \tag{53}$$

$$D_{22}^*(\alpha) = -\frac{\kappa+1}{2} i[2\alpha(\frac{D_{12}}{D}-\frac{D_{32}}{D}-\frac{i}{2\alpha})-(\kappa-1)(\frac{D_{22}}{D}+\frac{D_{42}}{D}-\frac{i}{\kappa+1})]. \tag{54}$$

We now have derived the system of singular integral equations (Eqn. (46)) with a Cauchy kernel. The SIE's will be solved for the density functions f_1 and f_2 which are the unknowns. There are two additional conditions, namely,

$$\int_{-a}^{a} f_i(t)\ dt = 0,\ i = 1,\ 2, \tag{55}$$

which are the so called single-valuedness conditions. Physically, they mean that the

crack opens at one end and closes at the other. We will show that with Eqns. (46) and (55), we can solve the SIE's numerically by transforming them to a system of linear algebraic equations.

Chapter 3

Solution Of Singular Integral Equations And Numerical Computations

3.1 Introduction

In Chapter 2, we have derived the system of singular integral equations for the interface crack perturbation problem for finite thickness materials. These SIE's each has a Cauchy kernel and two Fredholm kernels. The two unknowns to be solved are the density functions which are the derivatives of the difference of the two displacement components. The solutions of SIE's are generally obtained either through function theoretical technique as given by Muskhelishvili in [20], or through numerical methods [21], [22]. For the problem at hand the SIE's which have a simple Cauchy kernel and lengthy Fredholm kernels, it is most convenient to use a numerical method to obtain the solution. In this work the method of collocation with the unknown functions represented by Chebyshev polynomials described in [21] is used.

3.2 Solution of the integral equations

To facilitate solving the integral equations, let us make a change of variables as follows:

$$t = sa, \quad x = ra, \quad \Rightarrow \quad dt = ads, \quad dx = adr \tag{56}$$

The singular integral equations (Eqn. (46)) then become

$$-\frac{\pi(\kappa+1)}{2\mu_1}p_1(r) = \int_{-1}^{1}\frac{f_1(s)}{s-r}ds + \int_{-1}^{1}k_{11}(r,s)f_1(s)a\ ds + \int_{-1}^{1}k_{12}(r,s)f_2(s)a\ ds,$$

$$-\frac{\pi(\kappa+1)}{2\mu_1}p_2(r) = \int_{-1}^{1}\frac{f_2(s)}{s-r}ds + \int_{-1}^{1}k_{21}(r,s)f_1(s)a\ ds + \int_{-1}^{1}k_{22}(r,s)f_2(s)a\ ds, \tag{57}$$

$$-1 < r < 1.$$

$p_1(r)$ and $p_2(r)$ are the normal and shear stresses that need to be applied across the crack surface to close the gap in the elasticity problem and $f_1(s)$, $f_2(s)$ are the unknown density functions for which we wish to solve. After the change of variable Eqns. (47) through (50) now become

$$k_{11}(r,s) = \int_0^{\infty} D_{11}^{*}(\alpha)\sin\alpha a(s-r)\ d\alpha, \tag{58}$$

$$k_{12}(r,s) = \int_0^{\infty} D_{12}^{*}(\alpha)\cos\alpha a(s-r)\ d\alpha, \tag{59}$$

$$k_{21}(r,s) = \int_0^{\infty} D_{21}^{*}(\alpha)\cos\alpha a(s-r)\ d\alpha, \tag{60}$$

$$k_{22}(r,s) = \int_0^{\infty} D_{22}^{*}(\alpha)\sin\alpha a(s-r)\ d\alpha, \tag{61}$$

D_{11}^{*}, D_{12}^{*}, D_{22}^{*}, and D_{21}^{*} have been defined in Chapter 2.

3.2.1 The infinite integrals

To evaluate the Fredholm kernels which contain integrals with infinite upper limit (Eqns. (58) through (61)), we shall treat the integrands with sine and cosine terms separately. The integrals that contain sine functions as in Eqn. (58) may be expressed as

$$k_{11}(r,s) = \int_0^A (D_{11}^*(\alpha) - \frac{\gamma}{4\alpha})\sin\alpha a(s-r)\, d\alpha + \int_A^\infty (D_{11}^*(\alpha) - \frac{\gamma}{4\alpha})\sin\alpha a(s-r)\, d\alpha + \frac{\gamma}{4}\int_0^\infty \frac{\sin\alpha a(s-r)}{\alpha} d\alpha, \tag{62}$$

where the integrand of the first integral is bounded everywhere and is integrated numerically. The third integral has a closed form expression given by

$$\int_0^\infty \frac{1}{\alpha} \sin\alpha a(s-r)\, d\alpha = sign[a(s-r)]\frac{\pi}{2}, \tag{63}$$

where the *sign* function is defined as a function that gives only the sign of its argument with the numerical value 1.0. The second integral can be written as

$$\int_A^\infty (D_{11}^*(\alpha) - \frac{\gamma}{4\alpha})\sin\alpha a(s-r)\, d\alpha = \int_A^\infty (d_{11}^*(\alpha) - \frac{\gamma}{4\alpha})\sin\alpha a(s-r)\, d\alpha + \int_A^\infty [D_{11}^*(\alpha) - d_{11}^*(\alpha)]\sin\alpha a(s-r)\, d\alpha. \tag{64}$$

Let $O(\alpha^n)$ denote polynomials of degree n in α. Note that $d_{11}^*(\alpha)$ is a polynomial of finite degree in α shown in Appendix B. It represents the leading asymptotic terms of $D_{11}^*(\alpha)$ and the last term in the polynomial is a term like $(\frac{\gamma}{\alpha})^{11} O(0)$ (see Eqn. (B.59)). Therefore the leading term in the integrand in $[D_{11}^*(\alpha) - d_{11}^*(\alpha)]$ is a term like $(\frac{\gamma}{\alpha})^{12} O(0)$. Since γ is the parameter that determines the degree of nonhomogeneity in material 2 and is a constant, we can choose the value "A", which separates the infinite integral into two integrals, such that $(\frac{\gamma}{A})^{12}$ is small to any order we desire so that

$$\int_A^\infty [D_{11}^*(\alpha) - d_{11}^*(\alpha)]\sin\alpha a(s-r)\, d\alpha \tag{65}$$

is negligible.

A few words must be said here regarding the selection of the value "*A*" such that Eqn. (65) can be neglected. While it is true that we can choose "*A*" so that $(\frac{\gamma}{A})^{12}$ is small to any degree we want, for a particular nonhomogeneity constant, there is a point where any further increase in "*A*" will only serve to tax the numerical effort, whereas the final solution has become stabilized. The increased numerical effort that comes as a result of the increase in "*A*" can be seen from the first integral in Eqn. (62). Since that integral is to be evaluated by Gauss' formula, a larger upper limit of integration means more computing effort.

When a proper "*A*" has been chosen in Eqn. (62), Eqn. (64) can be evaluated in closed form since $(d_{11}^{*}(\alpha) - \frac{\gamma}{4\alpha})$ is a polynomial of finite degree in α. The closed form expressions for the integral are derived in Appendix C. Note that

$$d_{11}^{*}(\alpha) - \frac{\gamma}{4\alpha} = \sum_{j=2}^{11} c_{11,j}^{*} \frac{1}{\alpha^{j}}, \tag{66}$$

where $c_{11,j}^{*}$, $j = 2 \cdots 11$ are shown in Eqn. (B.59) in Appendix B. Eqn. (62) may now be written as follows

$$k_{11}(r,s) = \int_0^A (D_{11}^{*}(\alpha) - \frac{\gamma}{4\alpha})\sin\alpha a(s-r)\, d\alpha + \sum_{j=2}^{11} c_{11,j}^{*} \int_A^{\infty} \frac{\sin\alpha a(s-r)}{\alpha^{j}}\, d\alpha + \frac{\gamma}{4}\, sign\, a(s-r)\frac{\pi}{2}. \tag{67}$$

Similarly, $k_{22}(r,s)$ may be expressed in the following manner:

$$k_{22}(r,s) = \int_0^A \left(D_{22}^*(\alpha) - \frac{\gamma}{4\alpha}\right)\sin\alpha a(s-r)\, d\alpha + \sum_{j=2}^{11} c_{22_j}^* \int_A^\infty \frac{\sin\alpha a(s-r)}{\alpha^j}\, d\alpha + \frac{\gamma}{4}\, sign\, a(s-r)\frac{\pi}{2}. \tag{68}$$

We see that $k_{11}(r,s)$ and $k_{22}(r,s)$ are both bounded functions, even if $(s - r)$ goes to zero. In Eqns. (67) and (68), only the first term is to be integrated numerically; the second term, which is expressed in summation of integrals, can be expressed in closed form. The closed form expressions for these integrals are shown in Appendix C. The last term, however, is a step function. As $(s - r)$ goes from positive to negative, the value of the step function changes from $\frac{\gamma\pi}{8}$ to $-\frac{\gamma\pi}{8}$ While the reason for separation of this term from the Fredholm kernels $k_{11}(r,s)$ and $k_{22}(r,s)$ may not be immediately apparent, the fact remains that there is this term hidden in the kernel. We shall illustrate by way of examples in Appendix D that failure to take special precautions when dealing with functions that contain a step function in numerical evaluation of integrals will lead to erroneous results, thereby inhibiting convergence of the final solution. Furthermore, the definite integral (see Eqn. (57))

$$\int_{-1}^{1} \frac{\gamma\pi}{8}\, sign\, a(s-r)\, f_i(s)\, ds,\ i = 1, 2. \tag{69}$$

of the step function has a trivial closed form expression as will be shown later in the chapter. Had the step function not been separated, we will find that numerical convergence would be greatly hindered simply because of the inability of numerical quadrature to properly approximate the step function.

Having described the way to evaluate $k_{11}(r,s)$ and $k_{22}(r,s)$, we now do the same for $k_{12}(r,s)$ and $k_{21}(r,s)$. The kernel $k_{12}(r,s)$ may be expressed as

$$k_{12}(r,s) = \int_0^A D_{12}^*(\alpha)\cos\alpha a(s-r)\,d\alpha + \int_A^\infty (D_{12}^*(\alpha) - \frac{\gamma}{4\alpha})\cos\alpha a(s-r)\,d\alpha + \frac{\gamma}{4}\int_A^\infty \frac{\cos\alpha a(s-r)}{\alpha} d\alpha. \tag{70}$$

Again, the integrand of the first integral in Eqn. (70) is bounded everywhere within the limits of integration. The third integral has a closed form expression as follows (see also Appendix C)

$$\int_A^\infty \frac{\cos\alpha a(s-r)}{\alpha}\,d\alpha = -Ci(Aa(s-r)) = -\gamma_o - \log|Aa(s-r)| - \int_0^{|A\,a(s-r)|} \frac{\cos\alpha - 1}{\alpha}\,d\alpha, \tag{71}$$

where $\gamma_o = 0.57721566490$, is the Euler's constant. By following the same argument as used in evaluating the second integral in Eqn. (62), we can choose a sufficiently large "A" so that $(D_{12}^*(\alpha) - d_{12}^*(\alpha))$ is small to any order we desire, which reduces the second integral in Eqn. (70) to

$$\int_A^\infty (D_{12}^*(\alpha) - \frac{\gamma}{4\alpha})\cos\alpha a(s-r)\,d\alpha \cong \int_A^\infty (d_{12}^*(\alpha) - \frac{\gamma}{4\alpha})\cos\alpha a(s-r)\,d\alpha = \sum_{j=2}^{11} c_{12_j}^* \int_A^\infty \frac{1}{\alpha^j}\cos\alpha a(s-r)\,d\alpha. \tag{72}$$

Each term of the summation in Eqn. (72) is evaluated in closed form, similar to Eqn. (64). Therefore, the Fredholm kernel $k_{12}(r,s)$ may be written as

$$k_{12}(r,s) = \int_0^A D_{12}^*(\alpha)\cos\alpha a(s-r)\,d\alpha + \sum_{j=2}^{11} c_{12,j}^* \int_A^\infty \frac{\cos\alpha a(s-r)}{\alpha^j}\,d\alpha - \frac{\gamma}{4}Ci(A\,a(s-r)), \tag{73}$$

where Ci is defined in Appendix C. The reason that Eqn. (71) is separated from $k_{12}(r,s)$ is similar to why the step function is separated from the kernel $k_{11}(r,s)$. It is because $Ci(A\ a\ (s-r))$, which contains a logarithmic term, could not be properly approximated by numerical quadrature when integrated. This fact will be illustrated in Appendix D by way of examples to show the significant error encountered when using Gauss' formula to numerically integrate a logarithmic function. Therefore the logarithm term is separated to be integrated in closed form as will be seen in section 3.2.3.

Similarly, $k_{21}(r,s)$ may be written as

$$k_{21}(r,s) = \int_0^A D_{21}^*(\alpha)\cos\alpha a(s-r)\,d\alpha - \sum_{j=2}^{11} c_{12,j}^* \int_A^\infty \frac{\cos\alpha a(s-r)}{\alpha^j}\,d\alpha + \frac{\gamma}{4}Ci(Aa(s-r)). \tag{74}$$

It is worth noting that $k_{12}(r,s)$ and $k_{21}(r,s)$ differ only by a sign, as is the case for problems that possesses symmetry with respect to the y-axis.

3.2.2 Nature of the stress singularity

It is well known in fracture mechanics that the stress field near the crack tip possesses a characteristics that is proportional to r^{-p}, where r is a small distance measured from the crack tip where we evaluate the stresses. p is called the power of singularity, a measure of the unboundedness of the stress field, whose value should

lie between 0 and 1. If p is larger than 1, the displacement field and the energy are both unbounded at the crack tip, which is unacceptable. On the other hand, if p is smaller than 0, r^{-p} maintains a positive power and the stresses vanish as r approaches 0 and there is no stress singularity. In crack problems, we accept bounded displacements. The stresses, which are of the order of one less than the displacements, may be unbounded, but must be integrable.

From the derivation of the singular integral equation in Chapter 2 and the discussion earlier in this chapter, we know that the terms in Eqn. (57) that involve Fredholm kernels are bounded and analytic everywhere. It is only the terms with Cauchy kernel that have singular behavior. Furthermore, from the discussions in Appendix F concerning the characteristics of the density functions $f_1(s)$, $f_2(s)$, we note that they are of the form:

$$f_i(s) = \frac{F_i(s)}{(s+1)^{1/2}(1-s)^{1/2}} = F_i(s)w(s) \ , \ i = 1, 2. \tag{75}$$

where $F_i(s)$, $i = 1, 2$ satisfy the Hölder condition on the closed interval of $[-1, 1]$ and $F_i(-1) \neq 0$, $F_i(1) \neq 0$, $i = 1, 2$.

3.2.3 Converting to linear system

Having described the way these Fredholm kernels are evaluated, and the nature of the unknown functions, we are now ready to solve the singular integral equations by converting them into a linear system of algebraic equations to obtain the unknown functions at discrete collocation points.

Let us express our unknown functions in the singular integral equation in terms of Chebyshev polynomial. $T_j(s)$ and $U_j(s)$ are the Chebyshev polynomial of the first kind and second kind respectively, and they are defined as follows

$$T_j(s) = \cos j\theta,$$

$$U_j(s) = \frac{\sin(j+1)\theta}{\sin\theta}, \tag{76}$$

$$s = \cos\theta.$$

$$F_i(s) = \sum_{j=0}^{p} B_{ij}\, T_j(s),\ i = 1,\ 2. \tag{77}$$

B_{ij} are now the new unknowns to be solved in the linear system. Substitute Eqn. (77) into Eqn. (57), keeping in mind the following identity,

$$\frac{1}{\pi}\int_{-1}^{1} \frac{T_j(t)\ dt}{(t-x)\sqrt{1-t^2}} = 0, \qquad j = 0, \tag{78}$$

$$= U_{j-1}(x), \quad j > 0,$$

Eqn. (57) becomes

$$-\frac{\kappa+1}{2\mu_1}p_1(r) = \sum_{j=1}^{p} B_{1j}\, U_{j-1}(r) + \frac{1}{\pi}\left[\int_{-1}^{1} k_{11}(r,s)\, f_1(s)\, a\ ds + \int_{-1}^{1} k_{12}(r,s)\, f_2(s)\, a\ ds\right], \quad -1<r<1. \tag{79}$$

$$-\frac{\kappa+1}{2\mu_1}p_2(r) = \sum_{j=1}^{p} B_{2j}\, U_{j-1}(r) + \frac{1}{\pi}\left[\int_{-1}^{1} k_{21}(r,s)\, f_1(s)\, a\ ds + \int_{-1}^{1} k_{22}(r,s)\, f_2(s)\, a\ ds\right], \quad -1<r<1. \tag{80}$$

Let us evaluate the integrals in Eqns. (79) and (80) separately. Substituting Eqn. (67)

into the first integral in Eqn. (79), we obtain

$$\int_{-1}^{1} k_{11}(r,s)\, f_1(s)\, a\, ds = \sum_{j=0}^{p} B_{1j}\, a \int_{-1}^{1} k_{11}^{*}(r,s)\, \frac{T_j(s)}{\sqrt{1-s^2}}\, ds + \frac{\pi\gamma a}{8} \int_{-1}^{1} sign\, a(s-r)\, f_1(s)\, ds. \tag{81}$$

$$k_{11}^{*}(r,s) = \int_0^A (D_{11}^{*}(\alpha) - \frac{\gamma}{4\alpha}) \sin\alpha a(s-r)\, d\alpha + \sum_{i=2}^{11} c_{11,i}^{*} \int_A^{\infty} \frac{\sin\alpha a(s-r)}{\alpha^i}\, d\alpha. \tag{82}$$

Recall in Chapter 2 the definition of the density functions (See Eqn. (20)) and the change of variable we have made at the beginning of the chapter

$$f_1(s) = \frac{\partial}{\partial x} [v_2(x,0+) - v_1(x,0-)]\, a. \tag{83}$$

The integral of the second term in Eqn. (81) thus becomes

$$\begin{aligned} \int_{-1}^{1} sign\, a(s-r) f_1(s)\, ds &= \int_{-a}^{a} sign(t-x)\, f_1(t)\, dt \\ &= -\int_{-a}^{x} f_1(t)\, dt + \int_{x}^{a} f_1(t)\, dt \\ &= -[v_2(t,0+) - v_1(t,0-)]\Big|_{-a}^{x} + [v_2(t,0+) - v_1(t,0-)]\Big|_{x}^{a} \\ &= -2\, [v_2(x,0+) - v_1(x,0-)]. \end{aligned} \tag{84}$$

Because the crack opening displacement is zero at the crack tips, Eqn. (84) turns out to be exactly twice the negative vertical crack opening displacement at point "x". This crack opening displacement may be expressed as follows, after appropriate change of variables $x = r\, a$

$$v_2(x,0+) - v_1(x,0-) = \int_{-1}^{r} f_1(s)\, ds$$
$$= \sum_{j=0}^{P} B_{1j} \int_{-1}^{r} \frac{T_j(s)}{\sqrt{1-s^2}}\, ds \tag{85}$$

Again, make a simple change of variable in the integral in Eqn. (85) by letting $s = \cos\theta$, then $ds = -\sin\theta\, d\theta$, and we can easily show that it becomes

$$\int_{-1}^{r} \frac{T_j(s)}{\sqrt{1-s^2}}\, ds = -\int_{\pi}^{\cos^{-1}r} \cos j\theta\, d\theta$$
$$= -\frac{\sin j(\cos^{-1}r)}{j} \tag{86}$$
$$= -\frac{1}{j}\, U_{j-1}(r)\, \sqrt{1-r^2}\,.$$

Consider the Gauss-Chebyshev integration formula [23]

$$\frac{1}{\pi} \int_{-1}^{1} \frac{g(s)\, ds}{\sqrt{1-s^2}} \cong \frac{1}{n} \sum_{k=1}^{n} g(t_k), \quad T_n(t_k) = 0,$$
$$t_k = \cos\frac{\pi\,(2k-1)}{2n}, \quad k = 1 \cdots n. \tag{87}$$

Note that to use this formula, we need to know the function values of $g(s)$ at points t_k, $k = 1 \cdots n$, all zeroes of Chebyshev polynomial of the first kind of degree n. Applying this formula to the first integral in Eqn. (81), we obtain

$$\int_{-1}^{1} k_{11}^{*}(r,s)\, \frac{T_j(s)}{\sqrt{1-s^2}}\, ds = \frac{\pi}{n} \sum_{k=1}^{n} k_{11}^{*}(r,t_k)\, T_j(t_k). \tag{88}$$

At any point "r", and a particular choice of zero of the Chebyshev polynomial of the first kind, the first integral of $k_{11}^{*}(r,t_k)$ (see Eqn. (82)) is evaluated by straight-forward Gauss' formula of arbitrary interval as follows

$$\int_0^A [D_{11}^*(\alpha) - \frac{\gamma}{4}] \sin\alpha a(t_k - r)\, d\alpha \cong$$

$$\sum_{l=1}^{N} \{\frac{a_l - a_{l-1}}{2} \sum_{i=1}^{q} w_i\, [D_{11}^*(y_i) - \frac{\gamma}{4}] \sin y_i a(t_k - r)\}, \tag{89}$$

$$y_i = (\frac{a_l - a_{l-1}}{2}) x_i + (\frac{a_l + a_{l-1}}{2}),$$

$$a_0 = 0,\ a_{n_s} = A,\ a_l = a_0 + l\, d,\ l = 1 \cdots N,$$

where x_i is the i-th zero of Legendre polynomial $P_q(x)$, and w_i are the Gauss weights

$$w_i = \frac{2}{1 - x_i^2} [P_q'(x_i)]^2. \tag{90}$$

In Eqn. (89), N is the number of sub-intervals and it is equal to the integer part of A/d, q is the number of Gauss points and d is the sub-interval size for Gauss' formula evaluation. As discussed earlier in Section 3.2.1, the choice of "A" is dependent on the parameter γ, the degree of nonhomogeneity in material 2, and how small we wish the term $(\frac{\gamma}{A})^{12}$ to be. This limit of integration is therefore not a constant. The purpose of separating the integral in Eqn. (89) into several sub-intervals is to accommodate the changing "A" value so that a more uniform evaluation using the Gauss' formula is achieved. Choosing the number of Gauss points is somewhat arbitrary. When the Gauss points are too few, we might not have a good representation of the integrand hence an inaccurate evaluation of the integral results. On the other hand, it takes only a few trials to find that, above a certain number, increasing the Gauss points will only increase the computation effort with no discernible increase in the result of the integral. For the numerical computation in this work, a sub-interval size $d = 20$ and the number

of Gauss points $q = 20$ are used.

To complete the evaluation of Eqn. (81), we need to calculate the term that involves integrals with an infinite upper limit, which we have said in 3.2.1 to have closed form expressions. As mentioned earlier, the expressions for the integrals are derived in Appendix C, and the coefficients $c_{11,j}^{*}$ are obtained and listed in Appendix B. We write the integrals with infinite upper limit in two parts

$$\sum_{n=2}^{11} c_{11,n}^{*} \int_{A}^{\infty} \frac{\sin\alpha a(t_k - r)}{\alpha^n} d\alpha = \tag{91}$$

$$\sum_{n=1}^{5} c_{11,2n}^{*} \int_{A}^{\infty} \frac{\sin\alpha a(t_k - r)}{\alpha^{2n}} d\alpha + \sum_{n=2}^{6} c_{11,2n-1}^{*} \int_{A}^{\infty} \frac{\sin\alpha a(t_k - r)}{\alpha^{2n-1}} d\alpha.$$

Each part may in turn be written as

$$\sum_{n=1}^{5} c_{11,2n}^{*} \int_{A}^{\infty} \frac{\sin\alpha(t_k - r)}{\alpha^{2n}} d\alpha =$$

$$\sum_{n=1}^{5} c_{11.2n}^{*} \left[\cos A(t_k - r) \sum_{j=1}^{n-1} \frac{(-1)^{j+1}(t_k - r)^{2j-1}(2n-2j-1)!}{(2n-1)!A^{2n-2j}} + \right. \tag{92}$$

$$\sin A(t_k - r) \sum_{j=1}^{n} \frac{(-1)^{j+1}(t_k - r)^{2(j-1)}(2n-2j)!}{(2n-1)!A^{2n-2j+1}} +$$

$$\left. (-1)^n \frac{(t_k - r)^{2n-1}}{(2n-1)!} Ci(A(t_k - r))\right],$$

$$\sum_{n=2}^{6} c^{*}_{11,2n-1} \int_{A}^{\infty} \frac{\sin\alpha(t_k - r)}{\alpha^{2n-1}} d\alpha =$$

$$\sum_{n=2}^{6} c^{*}_{11,2n-1} \left[\cos A(t_k - r) \sum_{j=1}^{n-1} \frac{(-1)^{j+1}(t_k - r)^{2(j-1)}(2n-2j-2)!}{(2n-2)! A^{2n-2j-1}} + \right. \tag{93}$$

$$\sin A(t_k - r) \sum_{j=1}^{n-1} \frac{(-1)^{j+1}(t_k - r)^{2(j-1)}(2n-2j-1)!}{(2n-2)! A^{2n-2j}} +$$

$$\left. (-1)^{n+1} \frac{(t_k - r)^{2n-2}}{(2n-2)!} si(A(t_k - r)) \right].$$

In summary, the numerical evaluation of Eqn. (81) requires terms from Eqn. (86), Eqn. (89) and Eqns. (91) through (93), we may write it as follows

$$\int_{-1}^{1} k_{11}(r,s)\, f_1(s) a\, ds = \pi a \sum_{j=0}^{p} B_{1j} \left\{ \frac{1}{n} \sum_{k=1}^{n} \left[\sum_{l=1}^{N} \right. \right.$$

$$\left(\frac{a_l - a_{l-1}}{2} \sum_{i=1}^{q} w_i \left(D^{*}_{11}(y_i) - \frac{\gamma}{4} \right) \sin y_i a(t_k - r) \right) + \tag{94}$$

$$\left. \left. \sum_{i=2}^{11} c^{*}_{1,i} \int_{A}^{\infty} \frac{\sin\alpha a(t_k - r)}{\alpha^{i}} d\alpha \right] T_j(t_k) + \frac{\gamma}{4} \frac{U_{j-1}(r)}{j} \sqrt{1 - r^2} \right\},$$

where the only integral in the Eqn. (94) is expressed in terms of summations in Eqns. (91) through (93) and all appropriate variables are defined earlier in this section.

Following the same procedure, the integral involving $k_{22}(r,s)$ in Eqn. (80) may be expressed in terms of summations similar to that involving $k_{11}(r,s)$ as follows:

$$\int_{-1}^{1} k_{22}(r,s)\, f_2(s) a\, ds = \pi a \sum_{j=0}^{p} B_{2j} \{\frac{1}{n} \sum_{k=1}^{n} [\sum_{l=1}^{N}$$

$$(\frac{a_l - a_{l-1}}{2} \sum_{i=1}^{q} w_i\, (D_{22}^{*}(y_i) - \frac{\gamma}{4}) \sin y_i a(t_k - r)) + \qquad (95)$$

$$\sum_{i=2}^{11} c_{22,i}^{*} \int_{A}^{\infty} \frac{\sin\alpha a(t_k - r)}{\alpha^i}\, d\alpha\ ]\ T_j(t_k) + \frac{\gamma}{4} \frac{U_{j-1}(r)}{j} \sqrt{1 - r^2}\ \}.$$

The treatment of the integrals in Eqns. (79) and (80) with kernels $k_{12}(r,s)$ and $k_{21}(r,s)$ in converting them to summations is very similar to those with kernels $k_{11}(r,s)$ and $k_{22}(r,s)$ obtained earlier. The difference is that instead of having to deal with a step function in the integrand as shown in Eqn. (67), there is now a logarithmic term (see Eqn. (71)). Utilizing the following identity [24].

$$\int_{-1}^{1} \frac{T_j(s) \log |s - r|}{\sqrt{1 - s^2}}\, ds = -\frac{\pi}{j} T_j(r), \quad r < 1, \qquad (96)$$

The second integral in Eqn. (79) may be expressed as follows

$$\int_{-1}^{1} k_{12}(r,s)\, f_2(s) a\, ds = \pi a \sum_{j=0}^{p} B_{2j} \{\frac{1}{n} \sum_{k=1}^{n} [\sum_{l=1}^{N} (\frac{a_l - a_{l-1}}{2} \sum_{i=1}^{q}$$

$$w_i\, D_{12}^{*}(y_i) \cos y_i a(t_k - r)) + \sum_{i=2}^{11} c_{12,i}^{*} \int_{A}^{\infty} \frac{\cos\alpha a(t_k - r)}{\alpha^i}\, d\alpha - \qquad (97)$$

$$\frac{\gamma}{4}(\gamma_o + \log|A a| + \int_{0}^{|A\, a(t_k - r)|} \frac{\cos\alpha - 1}{\alpha}\, d\alpha)\ ]\ T_j(t_k) + \frac{\gamma}{4} \frac{T_j(r)}{j}\ \},$$

Again, all relevant variables are defined earlier in this section except for γ_o = 0.57721566490, the Euler's constant, which is mentioned in section 3.2.1. The integral

$$\int_0^{|A\,a(t_k-r)|} \frac{\cos\alpha - 1}{\alpha}\, d\alpha, \tag{98}$$

is evaluated using subroutine available in the IMSL software library. The subroutine is based on auxiliary functions described in [23]. As for the other integral in Eqn. (97), expressions derived in Appendix C gives

$$\sum_{n=2}^{11} c^{\bullet}_{12,n} \int_A^{\infty} \frac{\cos\alpha a(t_k-r)}{\alpha^n}\, d\alpha =$$

$$\sum_{n=1}^{5} c^{\bullet}_{12,2n} \int_A^{\infty} \frac{\cos\alpha a(t_k-r)}{\alpha^{2n}}\, d\alpha + \sum_{n=2}^{6} c^{\bullet}_{12,2n-1} \int_A^{\infty} \frac{\cos\alpha a(t_k-r)}{\alpha^{2n-1}}\, d\alpha, \tag{99}$$

where

$$\sum_{n=1}^{5} c^{\bullet}_{12,2n} \int_A^{\infty} \frac{\cos\alpha(t_k-r)}{\alpha^{2n}} d\alpha =$$

$$\sum_{n=1}^{5} c^{\bullet}_{12,2n} \left[\cos A(t_k-r) \sum_{j=1}^{n} \frac{(-1)^{j+1}(t_k-r)^{2(j-1)}(2n-2j)!}{(2n-1)!\, A^{2n-2j-1}} + \right.$$

$$\sin A(t_k-r) \sum_{j=1}^{n-1} \frac{(-1)^{j}(t_k-r)^{2j-1}(2n-2j-1)!}{(2n-1)!\, A^{2n-2j}} + \tag{100}$$

$$\left. (-1)^{n+1} \frac{(t_k-r)^{2n-1}}{(2n-1)!}\, si(A(t_k-r))\right],$$

$$\sum_{n=2}^{6} c^{*}_{12,2n-1} \int_{A}^{\infty} \frac{\cos\alpha(t_k - r)}{\alpha^{2n-1}}\, d\alpha =$$

$$\sum_{n=2}^{6} c^{*}_{12,2n-1} \left[\cos A(t_k - r) \sum_{j=1}^{n-1} \frac{(-1)^{j+1}(t_k - r)^{2(j-1)}(2n-2j-1)!}{(2n-2)!\, A^{2n-2j}} + \right.$$

$$\sin A(t_k - r) \sum_{j=1}^{n-1} \frac{(-1)^{j}(t_k - r)^{2j-1}(2n-2j-2)!}{(2n-2)!\, A^{2n-2j-1}} + \qquad (101)$$

$$\left. (-1)^{n} \frac{(t_k - r)^{2n-2}}{(2n-2)!}\, Ci(A(t_k - r))\right].$$

Using the same procedure, the integral with kernel $k_{21}(r,s)$ in Eqn. (80) may be expressed as

$$\int_{-1}^{1} k_{21}(r,s)\, f_1(s) a\, ds = \pi a \sum_{j=0}^{p} B_{1j} \left\{\frac{1}{n} \sum_{k=1}^{n} \left[\sum_{l=1}^{N} \left(\frac{a_l - a_{l-1}}{2}\right.\right.\right.$$

$$\left.\left.\sum_{i=1}^{q} w_i\, D^{*}_{21}(y_i) \cos y_i a(t_k - r)\right) + \sum_{i=2}^{11} c^{*}_{21,i} \int_{A}^{\infty} \frac{\cos\alpha a(t_k - r)}{\alpha^{i}}\, d\alpha - \right. \qquad (102)$$

$$\left.\frac{\gamma}{4}\left(\gamma_o + \log|Aa| + \int_{0}^{|A\,a(t_k - r)|} \frac{\cos\alpha - 1}{\alpha}\, d\alpha\right)\right] T_j(t_k) + \frac{\gamma}{4} \frac{T_j(r)}{j} \Big\}.$$

But as mentioned earlier, $k_{12}(r,s) = -k_{21}(r,s)$, Eqn. (102) therefore need not be computed, but can be obtained by simply changing the sign of $k_{12}(r,t_k)$ which has already been calculated.

We have shown that the sine integral $si(A(t_k - r))$, which contains a step function, is to be separated from the kernel and integrated in closed form. A similar procedure is applied to the cosine integral $Ci(A(t_k - r))$, which has a logarithm term (see Eqns. (84) and (96)). These steps are taken because the numerical procedure's inability to integrate properly either the step function or the log function. Recognizing the presence of additional sine integrals in Eqns. (93) and (100), as well as cosine integrals in Eqns. (92) and (101), one might suspect whether it is also necessary to

separate these terms which contain the discontinuous functions mentioned above. A closer look at Eqns. (92), (93) and (100), (101), however, reveals that the sine and cosine integrals have accompanying power functions. The presence of these power functions cause the discontinuity in the step function and the weak singularity in the logarithm function to be both continuous. Thus we can proceed with the Gaussian integration and get a good approximation without having to separate these sine and cosine integrals. In Appendix D, we shall illustrate this fact by way of examples to show the dampening effect of the power function on the step function as well as the logarithm function and the usage of Gauss' formula to evaluate integrals involving these functions.

We normalize the single-valuedness condition of Eqn. (55) so that the limits of integration become from -1 to 1

$$\int_{-1}^{1} f_i(s)\, ds = 0,\ i = 1,\ 2, \tag{103}$$

Substitute the representation of the density functions in terms of summation of Chebyshev polynomials and the unknown coefficients

$$f_i(s) = \sum_{j=0}^{p} B_{ij} \frac{T_j(s)}{\sqrt{1-s^2}},\quad i = 1,\ 2, \tag{104}$$

into Eqn. (103), and noting that $T_0(s) = 1$, we obtain

$$\sum_{j=0}^{p} B_{ij} \int_{-1}^{1} \frac{T_j(s)\ T_0(s)}{\sqrt{1-s^2}}\, ds = 0,\ i = 1,\ 2. \tag{105}$$

Since the Chebyshev polynomial of the first kind are orthogonal with respect to the weight function $\dfrac{1}{\sqrt{1-s^2}}$, we conclude that

$$B_{i0} = 0,\ i = 1,\ 2. \tag{106}$$

The unknowns in the linear system thus become, B_{1j} and B_{2j}, $j = 1 \cdots p$, a total of "$2p$" unknowns. To solve this linear system, we need to know "$2p$" distinct values in the forcing functions as the right hand side of the linear system. Let

$$r_m = \cos\frac{(2m-1)\pi}{2p},\quad m = 1 \cdots p. \tag{107}$$

r_m, $m = 1 \cdots p$ are the points where the forcing functions $p_1(r)$ and $p_2(r)$ are to be evaluated, thus forming the right hand side vector. Based on the foregoing discussion, we can write the system of singular integral equations as a system of linear equations as follows

$$\begin{aligned} -\frac{\kappa+1}{2\mu_1}p_1(r_m) = \sum_{j=1}^{p} B_{1j}\{U_{j-1}(r_m) + \frac{a}{n}\sum_{k=1}^{n} k'_{11}(t_k, r_m)\ T_j(t_k) + \\ \frac{\gamma a}{4}\frac{U_{j-1}(r_m)}{j}\sqrt{1-r_m^2}\} + B_{2j}\{\frac{a}{n}\sum_{k=1}^{n} k'_{12}(t_k, r_m)\ T_j(t_k) + \\ \frac{\gamma a}{4}\frac{T_j(r_m)}{j}\},\quad m = 1 \cdots p, \end{aligned} \tag{108}$$

$$\begin{aligned} -\frac{\kappa+1}{2\mu_1}p_2(r_m) = \sum_{j=1}^{p} B_{2j}\{U_{j-1}(r_m) + \frac{a}{n}\sum_{k=1}^{n} k'_{22}(t_k, r_m)\ T_j(t_k) + \\ \frac{\gamma a}{4}\frac{U_{j-1}(r_m)}{j}\sqrt{1-r_m^2}\} + B_{1j}\{\frac{a}{n}\sum_{k=1}^{n} k'_{21}(t_k, r_m)\ T_j(t_k) - \\ \frac{\gamma a}{4}\frac{T_j(r_m)}{j}\},\quad m = 1 \cdots p, \end{aligned} \tag{109}$$

where

$$k'_{11}(t_k,r_m) = \sum_{l=1}^{N} \left[\frac{a_l-a_{l-1}}{2} \sum_{i-1}^{q} w_i \left(D^*_{11}(y_i)-\frac{\gamma}{4}\right) \sin y_i a(t_k-r_m)\right] + \sum_{i=2}^{11} c^*_{11,i} \int_A^{\infty} \frac{\sin\alpha a(t_k-r_m)}{\alpha^i}\, d\alpha, \tag{110}$$

$$k'_{12}(t_k,r_m) = \sum_{l=1}^{N} \left[\frac{a_l-a_{l-1}}{2} \sum_{i-1}^{q} w_i D^*_{12}(y_i) \cos y_i a(t_k-r_m)\right] + \sum_{i=2}^{11} c^*_{12,i} \int_A^{\infty} \frac{\cos\alpha a(t_k-r_m)}{\alpha^i}\, d\alpha, \tag{111}$$

$$k'_{21}(t_k,r_m) = \sum_{l=1}^{N} \left[\frac{a_l-a_{l-1}}{2} \sum_{i-1}^{q} w_i D^*_{21}(y_i) \cos y_i a(t_k-r_m)\right] + \sum_{i=2}^{11} c^*_{21,i} \int_A^{\infty} \frac{\cos\alpha a(t_k-r_m)}{\alpha^i}\, d\alpha, \tag{112}$$

$$k'_{22}(t_k,r_m) = \sum_{l=1}^{N} \left[\frac{a_l-a_{l-1}}{2} \sum_{i-1}^{q} w_i \left(D^*_{22}(y_i)-\frac{\gamma}{4}\right) \sin y_i a(t_k-r_m)\right] + \sum_{i=2}^{11} c^*_{22,i} \int_A^{\infty} \frac{\sin\alpha a(t_k-r_m)}{\alpha^i}\, d\alpha. \tag{113}$$

Eqns. (108) and (109) form a "$2p$" by "$2p$" linear system.

It should be pointed out that the choice of collocation points r_m, $m = 1 \cdots p$ in Eqns. (108) and (109) is arbitrary. The only restriction is that $r_m \neq t_k$, which is imposed out of numerical convenience. Because $r_m = t_k$ would make any closed form evaluation of integrals that involves oscillatory sine and cosine functions invalid. On the other hand, the choice of collocation points affects convergence of the final solution. According to [25], it is best to choose them so that they are zeroes of

Chebyshev polynomials. Since t_k, $k = 1 \cdots n$ are also zeroes of Chebyshev polynomials by definition, we find that $r_m = t_k$ can simply be avoided by letting n be even and p odd, or vice versa.

3.3 Stress intensity factors

The stress intensity factors for our problem are defined as follows

$$k_1(-a) = \lim_{x \to -a} \sqrt{2(-a-x)}\ \sigma_{yy}(x,0), \tag{114}$$

$$k_1(a) = \lim_{x \to a} \sqrt{2(x-a)}\ \sigma_{yy}(x,0), \tag{115}$$

$$k_2(-a) = \lim_{x \to -a} \sqrt{2(-a-x)}\ \sigma_{xy}(x,0), \tag{116}$$

$$k_2(a) = \lim_{x \to a} \sqrt{2(x-a)}\ \sigma_{xy}(x,0), \tag{117}$$

In order to investigate the stress singularity near the crack tip, we need to obtain stress expressions for our problem. We recognize that while the stresses inside the crack give us the system of singular integral equations, these equations also provide us the stress expressions outside of the crack at $y = 0$, provided the density functions are known. Thus from Eqns. (46) we can write

$$\begin{aligned}
\frac{\pi(\kappa+1)}{2\mu_1}\sigma_{yy}(x,0) &= \int_{-a}^{a} \frac{f_1(t)}{t-x}dt + \int_{-a}^{a} k_{11}(x,t)f_1(t)\ dt + \int_{-a}^{a} k_{12}(x,t)f_2(t)\ dt, \\
\frac{\pi(\kappa+1)}{2\mu_1}\sigma_{xy}(x,0) &= \int_{-a}^{a} \frac{f_2(t)}{t-x}dt + \int_{-a}^{a} k_{21}(x,t)f_1(t)\ dt + \int_{-a}^{a} k_{22}(x,t)f_2(t)\ dt,
\end{aligned} \tag{118}$$

$$x < -a,\ x > a.$$

We expect the stresses to be singular at the crack tips. Furthermore from Eqns. (114) through (117), we know that any singular terms in the stresses weaker than the square root singularity, as well as regular terms, will vanish because of the expressions in the radical and the limiting process. Also recall that the terms

involving Fredholm kernels are bounded everywhere; hence the limiting process will serve to eliminate them and we need only concern ourselves with the singular terms. We may express the leading terms of normal stress at the beginning of the crack tip as

$$\lim_{x \to -a} \sigma_{yy}(x,0) = \lim_{x \to -a} \frac{2\mu_1}{\pi(\kappa+1)} \int_{-a}^{a} \frac{f_1(t)}{t-x} dt. \tag{119}$$

Recall that

$$f_i(t) = \frac{F_i(t)}{(t+a)^{1/2}(a-t)^{1/2}}, \quad i = 1, \ 2. \tag{120}$$

As will be discussed in Appendix F regarding the behavior of Cauchy integral, we can express it as follows (see Eqn. (F.18))

$$\int_{-a}^{a} \frac{f_1(t)}{t-x}\, dt = \pi \frac{\phi_1^*(-a)e^{\frac{\pi i}{2}}}{\sin\frac{\pi}{2}}(x+a)^{-\frac{1}{2}} - \pi \frac{\phi_2^*(a)e^{-\frac{\pi i}{2}}}{\sin\frac{\pi}{2}}(x-a)^{-\frac{1}{2}} + P(x), \tag{121}$$

$$= \pi\, i\, [\phi_1^*(-a)\,(x+a)^{-\frac{1}{2}} - \phi_2^*(a)\,(x-a)^{-\frac{1}{2}}] + P(x).$$

Also from Appendix F, we can show that

$$F_1(t) = \phi_1^*(t)\,(a-t)^{\frac{1}{2}} + i\,\phi_2^*(t)\,(t+a)^{\frac{1}{2}} + \phi_3^*(t)\,(t+a)^{\frac{1}{2}}\,(a-t)^{\frac{1}{2}}, \tag{122}$$

In Eqns. (121) and (122), $P(x)$ is bounded everywhere except possibly at the end points $-a$, a, where it has singularities no higher than the square-root singularity and ϕ_1^*, ϕ_2^* and ϕ_3^* are all bounded functions. Thus, we obtain

$$F_1(-a) = \phi_1^*(-a)\,\sqrt{2a}. \tag{123}$$

We can easily see that σ_{yy} is singular at $x = -a$ from Eqns. (119) and (121). At the

crack tips, the stresses will be dominated by the singular term. We may write Eqn. (119), with the help of Eqn. (123), as follows:

$$\lim_{x\to -a} \sigma_{yy}(x,0) = \lim_{x\to -a} \frac{2\mu_1}{\kappa+1} \frac{\phi_1^*(-a)}{\sqrt{-a-x}} = \lim_{x\to -a} \frac{2\mu_1}{\kappa+1} \frac{F_1(-a)}{\sqrt{2a(-a-x)}}. \tag{124}$$

Substituting Eqn. (124) into Eqn. (114), we obtain the Mode I stress intensity factor at the crack tip $x = -a$ as

$$k_1(-a) = \frac{2\mu_1}{(\kappa+1)\sqrt{a}} F_1(-a). \tag{125}$$

Similar to Eqn. (123), from Eqn. (122) we obtain $F_1(a) = i\,\phi_2^*(a)\sqrt{2a}$. The dominant term of σ_{yy} at the other end of the crack tip may then be written as

$$\lim_{x\to a} \sigma_{yy}(x,0) = \lim_{x\to a} -\frac{2\mu_1}{\kappa+1} \frac{i\,\phi_2^*(a)}{\sqrt{x-a}} = \lim_{x\to a} -\frac{2\mu_1}{\kappa+1} \frac{F_1(a)}{\sqrt{2a(x-a)}}. \tag{126}$$

Substituting Eqn. (126) into Eqn. (115), we obtain

$$k_1(a) = -\frac{2\mu_1}{(\kappa+1)\sqrt{a}} F_1(a). \tag{127}$$

The mode II stress intensity factors at either end of the crack tip are obtained by the same process. They are

$$k_2(-a) = \frac{2\mu_1}{(\kappa+1)\sqrt{a}} \; (-a). \tag{128}$$

$$k_2(a) = -\frac{2\mu_1}{(\kappa+1)\sqrt{a}} F_2(a). \tag{129}$$

These stress intensity factors may be conveniently evaluated from

$$F_i(s) = \sum_{j=1}^{p} B_{ij} \, T_j(s), \; i = 1, 2, \tag{130}$$

where B_{ij}, $i = 1, 2, j = 1 \cdots p$, come directly out of the solution of the linear system from Eqns. (108) and (109).

3.4 Crack opening displacements

As a result of discussions carried out in section 3.2.3, the crack opening displacements may readily be computed. Combining Eqns. (85) and (86), we obtain the y component of the COD as

$$v_2(x,0+) - v_1(x,0-) = \sum_{j=1}^{p} -B_{1j} \frac{U_{j-1}(\frac{x}{a})}{j} \sqrt{1-(\frac{x}{a})^2}. \tag{131}$$

It is not difficult to show that the x component of the crack opening displacement would be

$$u_2(x,0+) - u_1(x,0-) = \sum_{j=1}^{p} -B_{2j} \frac{U_{j-1}(\frac{x}{a})}{j} \sqrt{1-(\frac{x}{a})^2}. \tag{132}$$

Since the stresses have a square-root singularity, the crack opening displacements are

bounded at the crack tips and they vanish as the square-root of the distance measured from the crack tip, as shown in Eqns. (131) and (132).

3.5 Strain energy release rates

The strain energy release rate, is defined as one half the rate of change of strain energy per distance of crack propagation

$$G = \frac{1}{2}\frac{\partial W}{\partial a}. \tag{133}$$

The strain energy release rate may be seen as the force tending to open the crack surface. Its evaluation requires only a knowledge of the stresses and displacements near the crack tip. From reference [26], we may express the strain energy release rate solely in terms of the stress intensity factor and some material constants. The opening mode and sliding mode strain energy release rate are found to be

$$G_1 = \frac{\pi(\kappa+1)}{8\mu_1} k_1^2,$$
$$G_2 = \frac{\pi(\kappa+1)}{8\mu_1} k_2^2, \tag{134}$$

respectively. The total strain energy release rate becomes

$$G = \frac{\pi(\kappa+1)}{8\mu_1} (k_1^2 + k_2^2). \tag{135}$$

Let G_0 be the strain energy release rate of a crack of length $2a$ in an infinite elastic homogeneous medium with the same material properties as those of material 1 under uniform normal stress $\sigma_{yy} = \sigma_0$ at infinity. We then obtain

$$G_0 = \frac{\pi(\kappa+1)}{8\mu_1} k_{1,\infty}^2, \tag{136}$$

$k_{1,\infty}$ is the Mode I stress intensity factor under the configuration mentioned, and from [27] we know that $k_{1,\infty} = \sigma_0\sqrt{a}$. Therefore

$$\frac{G}{G_0} = \frac{k_1^2+k_2^2}{k_{1,\infty}^2}. \tag{137}$$

3.6 Convergence

Near the end of section 3.2.3, we have successfully converted the system of singular integral equations to a linear system of the size "$2p$" by "$2p$" (Eqns. (108) and (109)), where "p", is the number of terms in the summation that make up the density functions which are the unknowns in the SIE's. "p" is also the number of collocation points which we evaluate the forcing function to form the right-hand-side vector of the linear system. A look into the previously mentioned equations reveals that the number of terms in the Gauss-Chebyshev integration formula "n" is something we should also determine when solving the linear system. Furthermore, we shall decide the "A" value which is the integration cut-off point for the semi-infinite integral in Eqn. (65). Therefore, there are still these three parameters that need to be fixed for the linear system. We say the solution to the system of the singular integral equations has converged when changing any of the three parameters does not affect the numerical value of the solution of the linear system.

Of the three parameters that we mentioned earlier, the Gauss terms "n" and the collocation points "p" are both integers, the integration cut-off point "A", however, is a real number. While the relative magnitude of the two integer parameter are easier to measure in attempting to achieve convergence of the solution, since one could

start with an arbitrary small integer, we need to establish the magnitude of the third parameter. Recall in Eqns. (64) and (70) that "A" is the value which makes the integral

$$\int_A^{\infty} [D_{ij}^*(\alpha) - d_{ij}^*(\alpha)] \begin{matrix} \sin\alpha(t-x) \\ or \\ \cos\alpha(t-x) \end{matrix} d\alpha, \quad i, j = 1, 2, \tag{138}$$

negligible. A look at Eqns. (B.59) through (B.62) shows that the last term of $d_{ij}^*(\alpha)$, $i, j = 1, 2$ is in the form of $\frac{\gamma^{11}}{4096\alpha^{11}} O(0)$. Therefore, even though we do not know the exact expressions of $D_{ij}^*(\alpha)$, since $d_{ij}^*(\alpha)$ is the first 11 terms of $D_{ij}^*(\alpha)$ when it is expanded asymptotically, the leading term of $D_{ij}^*(\alpha) - d_{ij}^*(\alpha)$ must be a term like $\frac{\gamma^{12}}{8192\alpha^{12}} O(0)$. This gives us a basis of determining the value "A". Assume that when

$$\frac{\gamma^{12}}{8192\, A^{12}} = \varepsilon, \tag{139}$$

where ε is a very small number, we can ignore Eqn. (138). We can easily deduce that

$$A = \frac{|\gamma|}{\sqrt[12]{8192\ \varepsilon}}. \tag{140}$$

Granted that the initial assumption of ε might not render an "A" such that Eqn. (138) is close to zero, just as the initial guess of the other two parameters "p" and "n" might not render the solution anywhere near convergence, however, it provides something that we can improve on.

From the stand point of solving the singular integral equation, we say that the solution has converged when changing the "A" value produces the same numerical value, provided the other two parameters have been determined. With the perspective of numerically computing the integral in Eqn. (65), however, the stabilization of solution takes on a different meaning. As will be described in detail in Appendix E,

when "*A*" reaches to a point where it makes the value of some component terms in $D_{11}^{*}(\alpha)$ to reach the limit of floating point overflow for a real number, the ter n $D_{11}^{*}(\alpha)$ - $d_{11}^{*}(\alpha)$ is identically zero from the numerical computation stand point. Any further increase in "*A*" will only serve the same purpose. As a matter of fact, it is even possible to have "*A*" so large, that in evaluating the kernel $k_{11}(r,s)$ the second integral in Eqn. (62) can be completely ignored. But to do so is to defeat the whole purpose of going through the exercise of asymptotic expansions detailed in Appendix B. But as we will show in Appendix E, for the majority of the cases considered in this study, it does not take a large "*A*" to make the terms in $D_{11}^{*}(\alpha)$ to reach the machine constant. From the above discussion we conclude that as ε gets smaller, Eqn. (138) will diminish and the solution of the SIE's must converge.

We start a pilot case by taking for the value of the material constants, Poisson's ratio, $\nu = 0.3$, the non-homogeneity parameter of material 2, $\gamma = -3.0$, geometry constants such as the thickness of material 1, $h_1 = 10\,a$, that of material 2, $h_2 = a$ (a is half the crack length). A uniform unit normal stress over the entire crack length acts as the forcing function. To save computer time a liberal value of $\varepsilon = 1.0 \times 10^{-11}$ is used. To our pleasant surprise, we find that the solution, even though far from being converged for the "*p*" and "*n*" parameters we have selected, does not depend on "*n*", the number of terms in Gauss-Chebyshev integration formula. Figure 4 shows one of the parameters obtained as part of the solution, the Mode I stress intensity factor, changes as the number of collocation points "*p*" increases, but remains virtually constant with respect to the changes in the number of Gauss terms "*n*".

Having fixed one parameter, namely the gauss terms, in the quest of a converged solution of our linear system, the next logical step would be to see how the solution changes with respect to variations in the number of collocation points.

Figure 5 shows that as the number of collocation points increases, the solution converges quickly. A number of no more than 24 collocation points is sufficient to make the solution to reach the asymptote as shown in Figure 5. The final convergence of the problem is reached when the solution remains accurate to a certain digit with respect to the variance of the last parameter ε.

To ensure convergence of the solution for all the cases computed in this study, every number is computed at least six times; each time varying one parameter. The parameters used for each computation is listed in Table I. An accuracy of four significant figures is maintained for each of the six computations in every case calculated in this work.

As we have mentioned earlier and as will be explained in Appendix E in detail, for most cases it does not take a very large "A" for Eqn. (138) to become negligible. From the vantage point of numerical computation we want to keep "A" as small as possible, provided we can still obtain a converged solution. The reason for this is that a smaller "A" means less effort in integrating Eqn. (89). From Eqn. (140) we can easily see that "A" is indeed rather small. For $\gamma = 1.0$ and $\varepsilon = 1.0 \times 10^{-11}$ we need only to integrate Eqn. (89) from 0 to $A = 3.90$. When $\gamma = 0.1$, A becomes 0.39 according to Eqn. (140). But there is a limit below which the "A" value will make Eqn. (138) no longer negligible. Figure 6 illustrates this by showing a plot of the normalized strain energy release rate vs. the nonhomogeneity constant (γ) for the case $h_1/a = 100$, $h_2/a = 0.5$, $\nu = 0.3$. We see a pronounced dip in the computed parameter when $|\gamma| < 1.0$, where it should have been a very smooth transition as γ varies.

Let us keep in mind that this deviation occurs because we want to keep "A" small to reduce numerical computing effort. If we have kept the same "A" (the largest) for the worst case, namely $|\gamma| = 3.0$, and use it for computing any other case which has a smaller γ, the deviation would not have happened. We would at most

wind up with a less efficient use of computing time. But to put the anomaly just described in a different perspective, let us explain it as follows.

As $|\gamma|$ gets smaller, the magnitude of every term in the Fredholm kernel is getting smaller at the same time. But the basis we use to determine "*A*", is built on dropping certain terms when the leading term is less than an absolute number ε, as shown in Eqn. (139). Therefore the relative importance of these terms that are being dropped increases as $|\gamma|$ gets smaller and smaller, hence the deviations as shown in Figure 6. These deviations are something on which changing the parameters as shown in Table I has no affect; meaning we will still have convergence on the surface. Only when we examine any of the parameters that we seek, such as SIF or strain energy release rate, with respect to the changes in the nonhomogeneity constant, do we notice the aberrations.

The remedy for this situation is of course trivial; we could simply use a larger "*A*". For those cases of nonhomogeneity constant that fall into this range, we merely substitute a γ value in Eqn. (140) that is outside of the range, $|\gamma| = 1.5$, to be conservative in this particular example, instead of using the actual γ value.

Table I. Different parameters used for each computation in order to obtain a converged solution.

No.	ε	p	n
1	1.0×10^{-11}	22	51
2	1.0×10^{-11}	22	61
3	1.0×10^{-11}	24	51
4	1.0×10^{-11}	24	61
5	1.0×10^{-13} (1)	24	51
6	1.0×10^{-13} (1)	24	61

Note: (1) Except for the two cases (a). $h_1 = 100a$, $h_2 = 0.5a$ (b) $h_1 = 100a$, $h_2 = 0.25a$, where $\varepsilon = 1.0 \times 10^{-15}$.

(2) These parameters are used for all the cases compiled in Chapter 4 except as noted in (1).

(3) A uniform accuracy of four significant figures convergence is obtained for each computation with the parameters used as listed.

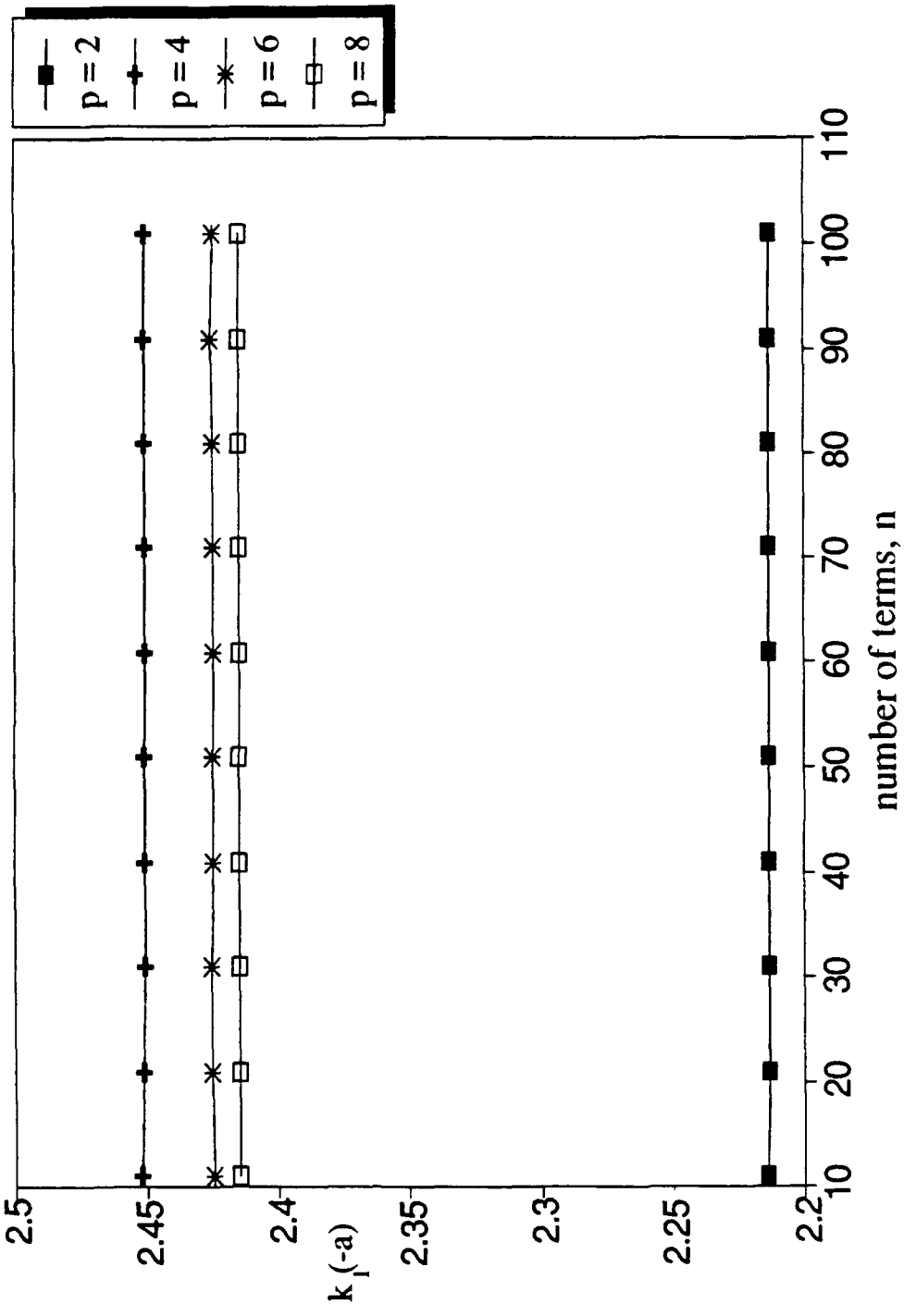

Figure 4. Mode I SIF vs. number of Gauss terms with collocation points 2, 4, 6, 8 for $\varepsilon = 1.0 \times 10^{-11}$. Material constants: $\nu = 0.3$, $\gamma = -3.0$. Geometry constants: $h_1 = 10\,a$, $h_2 = a$.

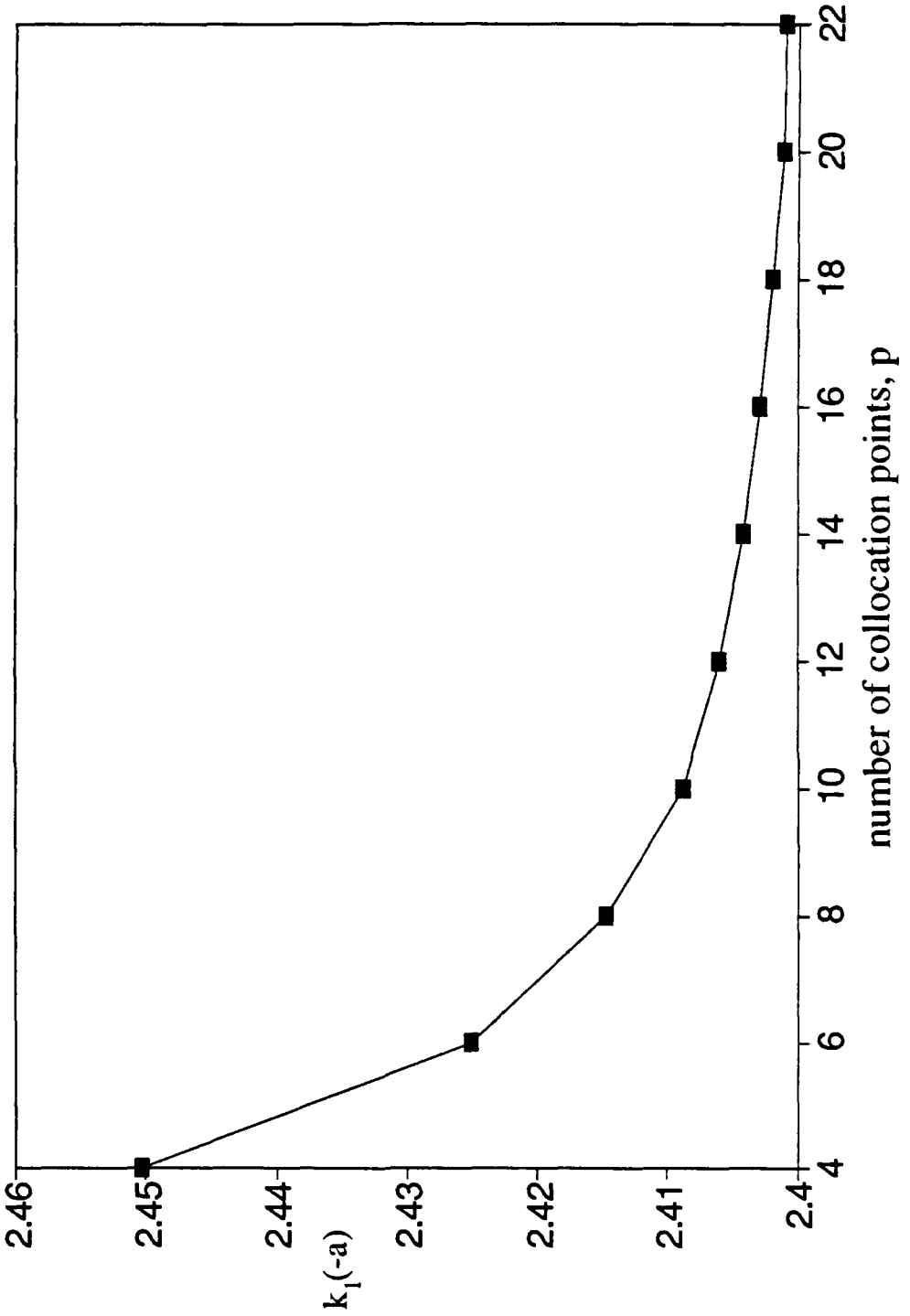

Figure 5. Mode I SIF vs. collocation points for $\varepsilon = 1.0 \times 10^{-11}$, n = 31. Material constants: $\nu = 0.3$, $\gamma = -3.0$. Geometry constants: $h_1 = 10a$, $h_2 = a$.

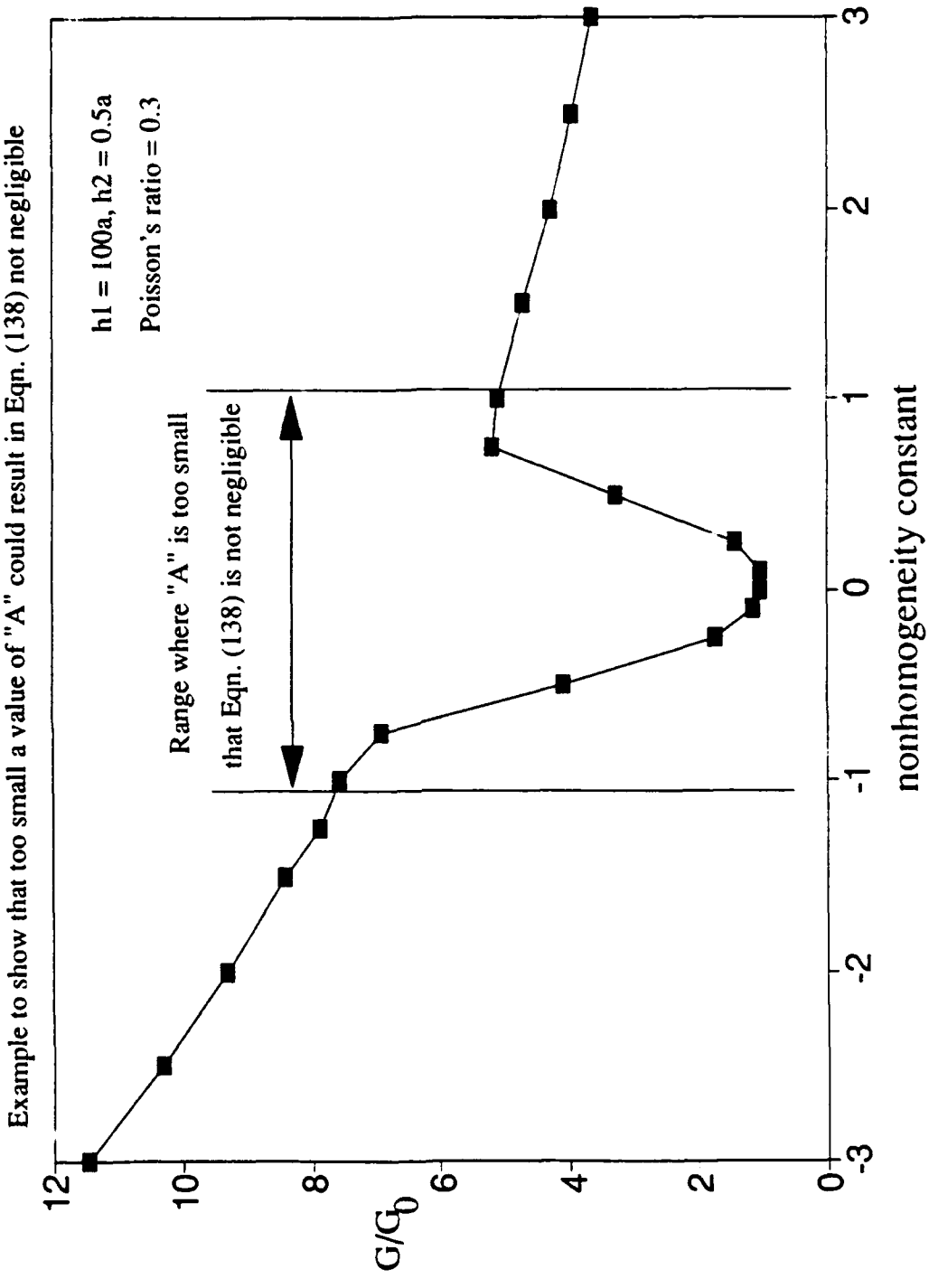

Figure 6. Example to show that too small a value of "A" could result in Eqn. (138) not negligible.

3.7 Direction of crack growth

We observe that, due to lack of symmetry in our problem since material 2 is non-homogeneous in the y-direction, and mixed-mode condition exists regardless of whether the loading is of one mode or mixed. That is why we'll see in Chapter 4 that both k_1 and k_2 are non-zero for all the loading conditions computed. With this mixed-mode conditions, it is apparent that the crack will not advance along the interface. In order to predict the direction in which the crack grows, one needs to examine the stress state in the near field of crack tip. The stress state, in polar coordinates (see Figure 7), in the neighborhood of the crack tip can be written as follows [28]:

$$\sigma_{rr} = \frac{1}{\sqrt{2r}}\cos\frac{\theta}{2}[k.(1+\sin^2\frac{\theta}{2})+\frac{3}{2}k_2\sin\theta-2k_2\tan\frac{\theta}{2}]+O(r^{\frac{1}{2}}),$$

$$\sigma_{\theta\theta} = \frac{1}{\sqrt{2r}}\cos\frac{\theta}{2}[k_1\cos^2\frac{\theta}{2}-\frac{3}{2}k_2\sin\theta]+O(r^{\frac{1}{2}}), \qquad \textbf{(141)}$$

$$\sigma_{r\theta} = \frac{1}{2\sqrt{2r}}\cos\frac{\theta}{2}[k_1\sin\theta-k_2(3\cos\theta-1)]+O(r^{\frac{1}{2}}).$$

Following [29], [30], the direction of the probable crack propagation may be determined by the plane of the maximum cleavage stress $\sigma_{\theta\theta}(r,\theta)$ around the crack tip. We obtain this direction either by solving the following equation

$$\frac{\partial}{\partial\theta}[\sqrt{2r}\,\sigma_{\theta\theta}(r,\theta)] = 0. \qquad \textbf{(142)}$$

which is to find the direction where $\sigma_{\theta\theta}(r,\theta)$ remains stationary, or, if we recognize that it is equivalent to finding the directions of the principal stress, simply solving $\sigma_{r\theta}(r,\theta) = 0$. Whichever case is used, we obtain

$$\cos\frac{\theta}{2}[k_1\sin\theta + k_2(3\sin\theta - 1)] = 0. \tag{143}$$

$\cos\frac{\theta}{2} = 0$ gives $\theta = \pm\pi$, which corresponds to the surface of the crack. The second term in Eqn. (143) provides the non-trivial solution and it may be expressed in the following quadratic form so that it is more easily solved

$$\tan^2\frac{\theta}{2} - \frac{k_1}{2k_2}\tan\frac{\theta}{2} - \frac{1}{2} = 0, \tag{144}$$

Note that the direction of probable crack growth is dependent only on the stress state around the crack tip. Therefore $r^{\frac{1}{2}}$ and subsequent terms need not be included in the foregoing analysis because they vanish around the crack tip.

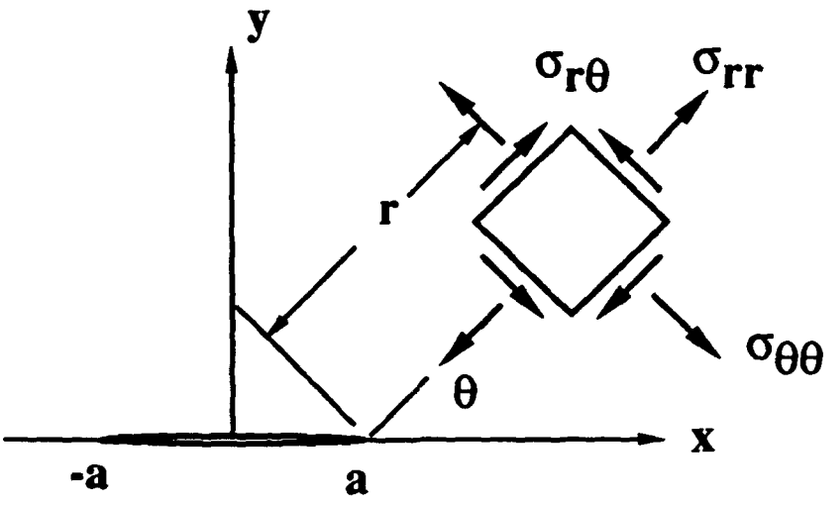

Figure 7. Stress components near the crack tip in polar coordinates.

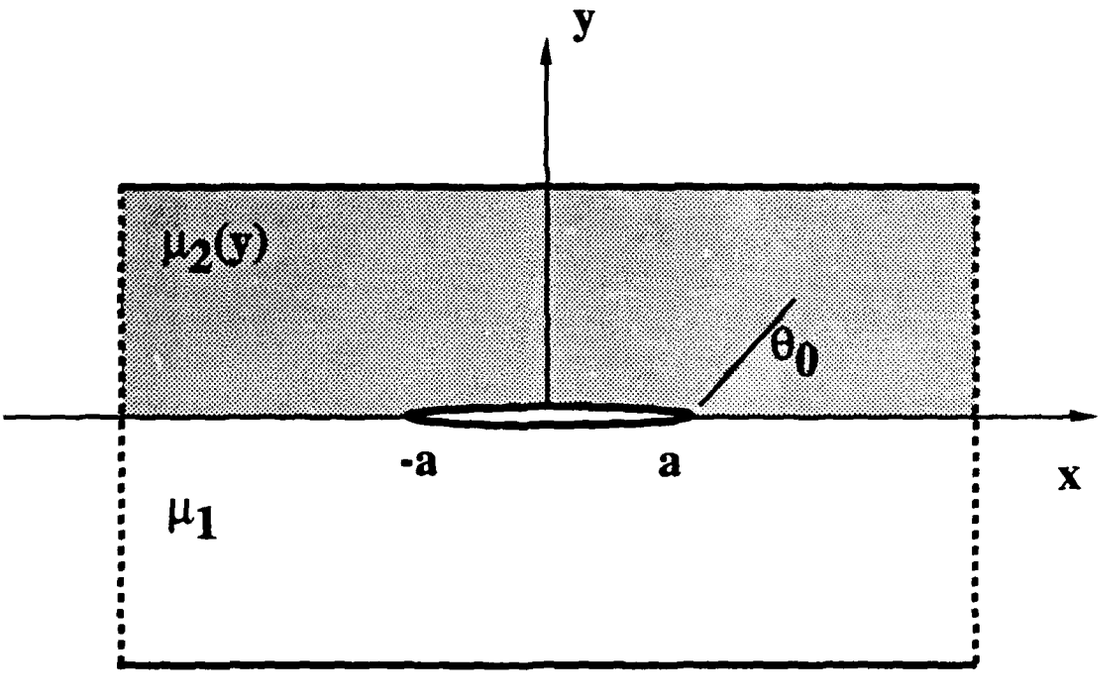

Figure 8. Probable direction of crack propagation.

Chapter 4

Results And Discussions

4.1 Introduction

In applying the solution of our problem to actual cases, we consider two material combinations. One that has a non-homogeneous material which is "softer" than the homogeneous material, as can be represented by $\gamma < 0$. For example, a thin film of gold, silver or lead to be deposited on Nickel or steel bearing and sliding parts as dry film lubricant[1][2] has this kind of characteristics. Gold has a modulus of elasticity of 10.8×10^6 psi., Nickel and steel have moduli of elasticity of 32×10^6 psi. and 29×10^6 psi. respectively. On the other hand, refractory heat-shield materials on metal substrates may or may not have a surface Young's moduli higher than those of the substrate. Refractory materials have Young's moduli anywhere from 10 to 70×10^6 psi. The range of Young's modulus for the metal substrate could be even more diverse. Thus we may have a homogeneous material either stiffer or softer than the nonhomogeneous layer, depending on the particular application.

The material and geometry constants used in the computation of the cases in this chapter are designed to cover a broad range of possible material and geometry combinations. The non-homogeneity constant used in the computation, ranges from -3 to 3. As for Poisson's ratio, a value of 0.3 was used in the computation. A separate investigation, however, on the effect of the changes in Poisson's ratio is done on one of the geometry combinations. The different cases of geometry and material constant combinations computed is shown in Table II. Only two loadings cases were investigated, namely the uniform normal stress and uniform shear applying at the

Table II. Material and geometry constants combinations computed in the present work.

Case No.	h_1/a	h_2/a	Poisson's ratio ν
1	100	100	0.3
2		10	
3		2	
4		1	
5		0.5	
6		0.25	
7	10	1	
8	4		
9	2		
10	1		
11	100	1	0.01, 0.1, 0.2, 0.3, 0.4, 0.499

top and bottom surfaces of the crack (Figure 9). Due to the myriad of loading combinations conceivable, these two loadings computed illustrate perhaps the most general cases. In addition, the result of these two loading cases for when the two materials are very thick provided verification and comparison of results of a similar problem with two half planes.

4.2 Results and discussions

The first thing to do after obtaining the solution of the system of integral equations is to compute a case with parameters very close to one whose solution has been known and to compare the results. Reference [16] solved an interface crack problem of a similar nature to what is done in the present work. The only differences are that in [16] the two materials are both half-spaces rather than of finite thicknesses and the Poisson's ratio exhibits the same nonhomogeneous properties as that of the Young's modulus for material 2, whereas in this study the Poisson's ratio is treated as a constant. To make a proper comparison, we can make the thickness of both materials to be very large, e.g., $h_1 = h_2 = 100a$. As for Poisson's ratio, a value of 0.3 is used. We will show later in this chapter that the effect of the changes in Poisson's ratio is not significant.

Figure 10 and Figure 11 show the Mode I and II stress intensity factors under the loading of normalized uniform normal stresses of the above mentioned two cases. Figure 12 and Figure 13 show the same stresses intensity factors under normalized shear stresses. Comparison of the these results shows that they can be very closely

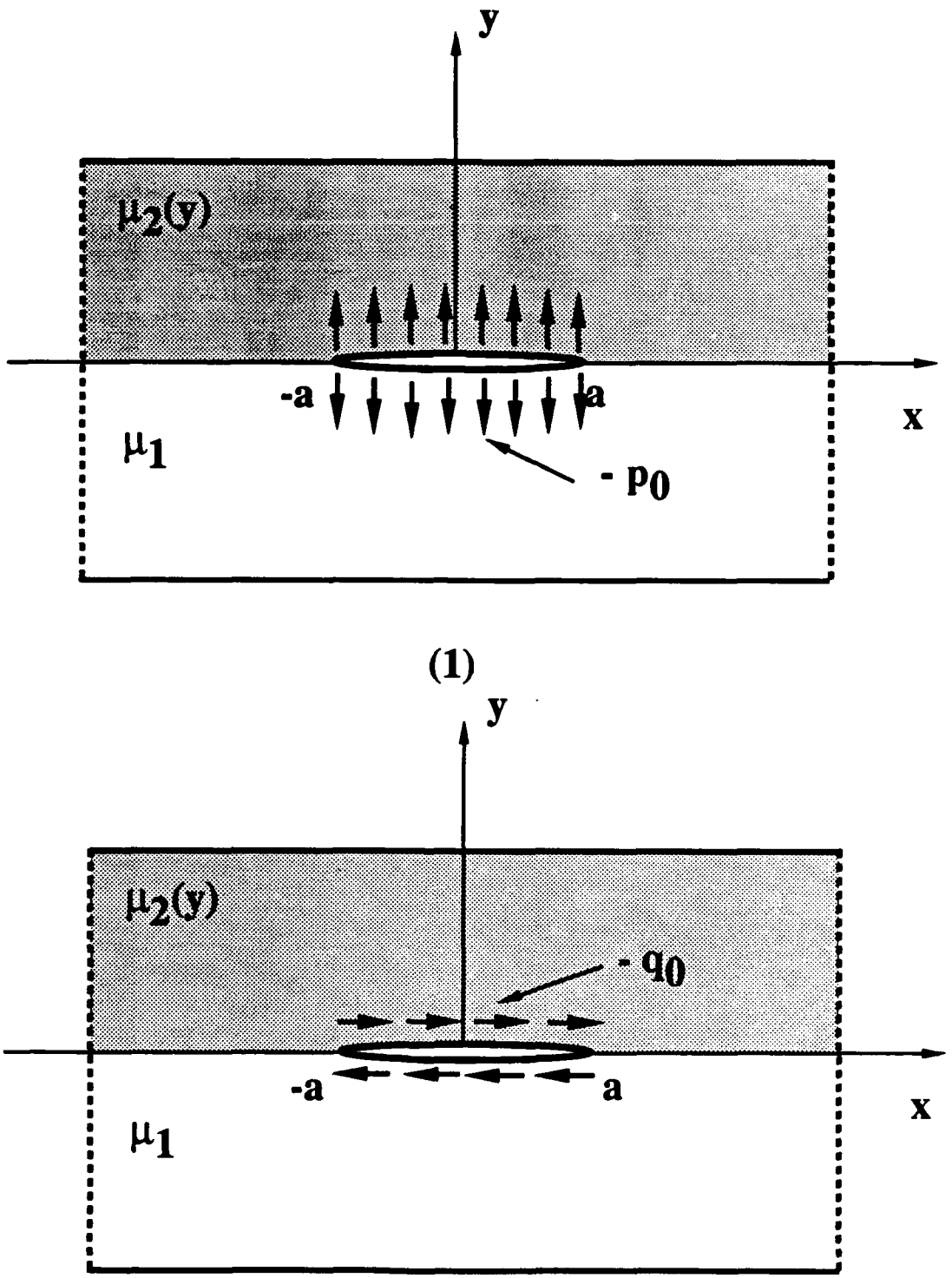

Figure 9. Loadings used in the present work, (1). uniform normal stress, (2). uniform shear.

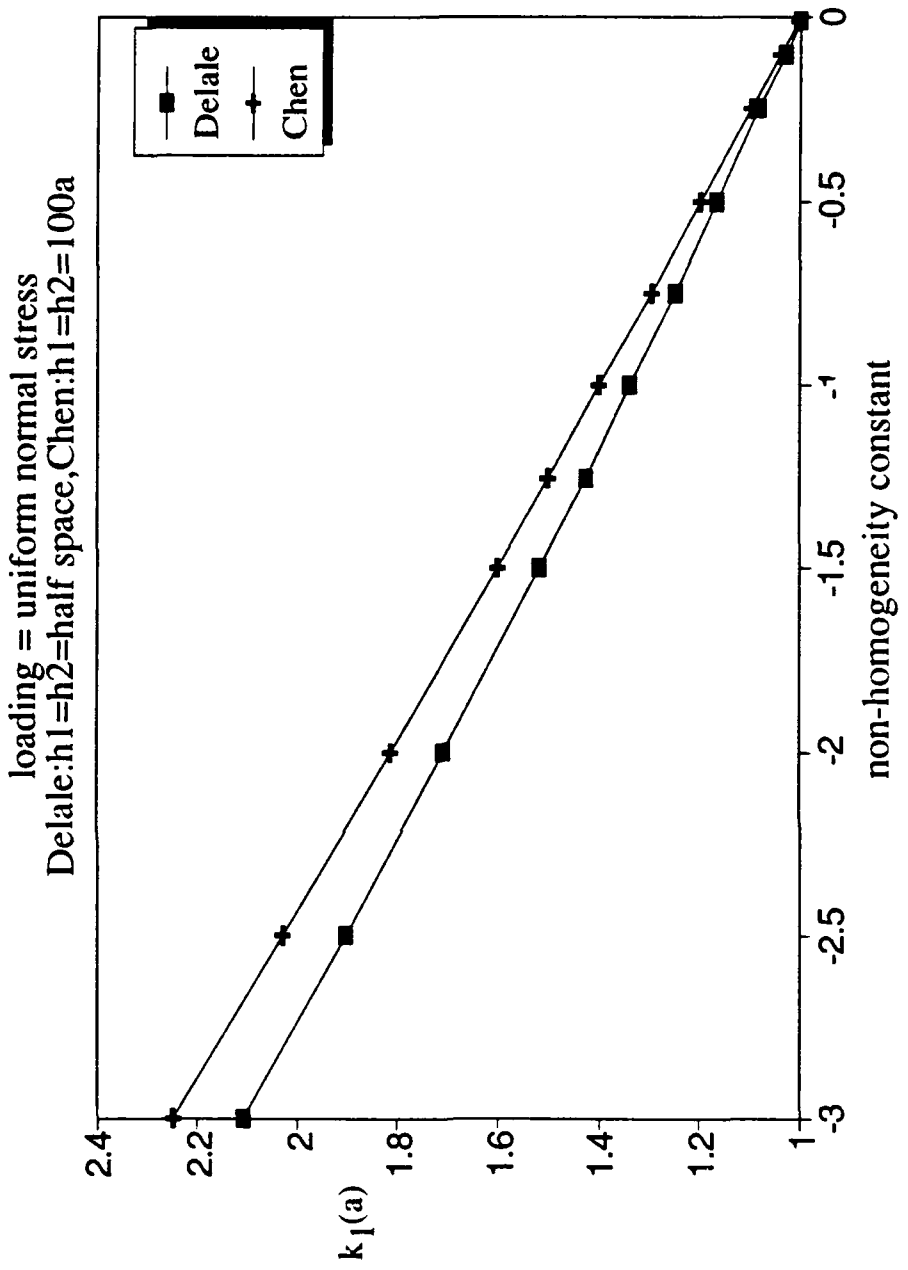

Figure 10. Comparison of Mode I SIF for interface crack between (1). two infinite half planes, and (2). $h_1=h_2=100a$ under loading of uniform normal stress.

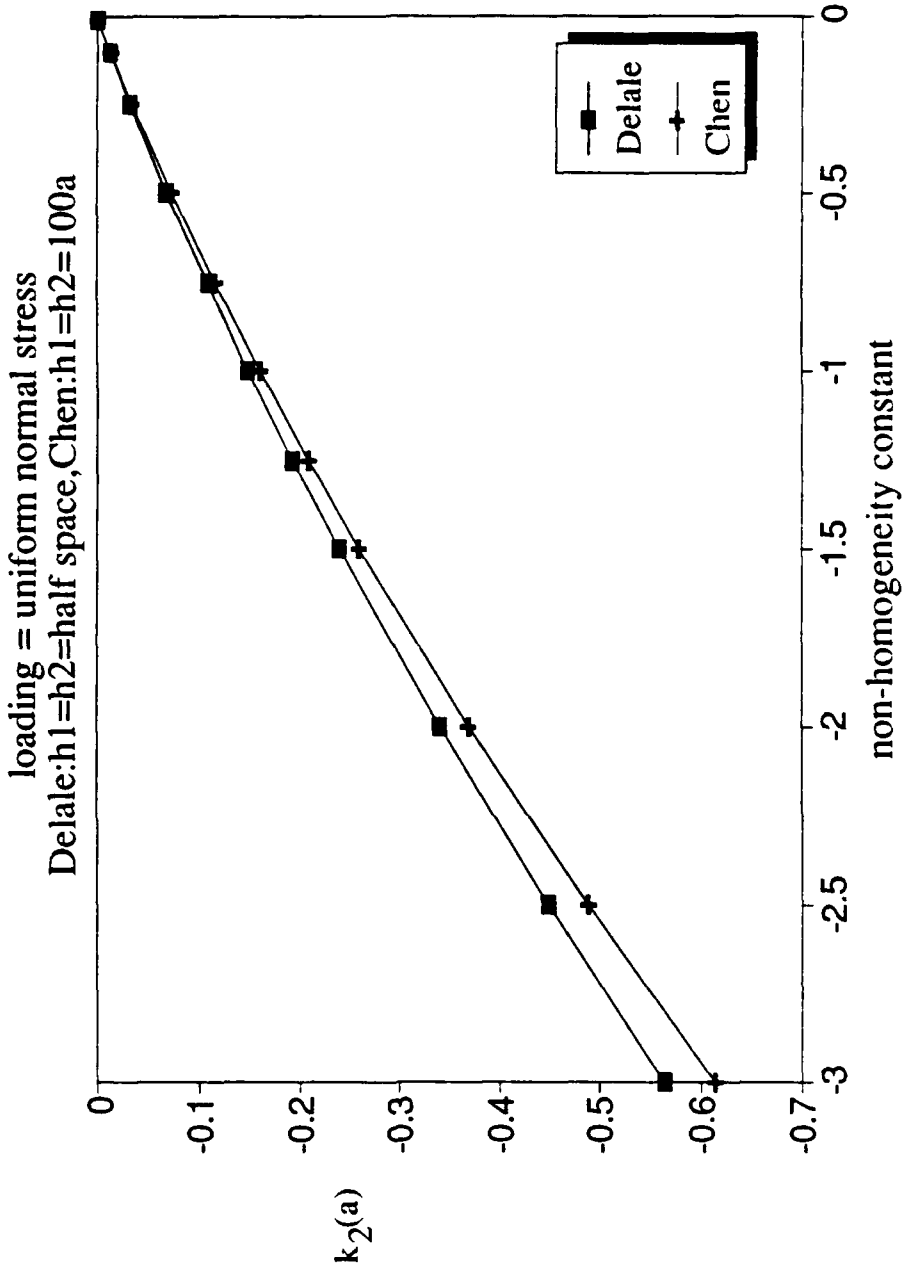

Figure 11. Comparison of Mode II SIF for interface crack between (1). two infinite half planes, and (2). $h_1=h_2=100a$ under loading of uniform normal stress.

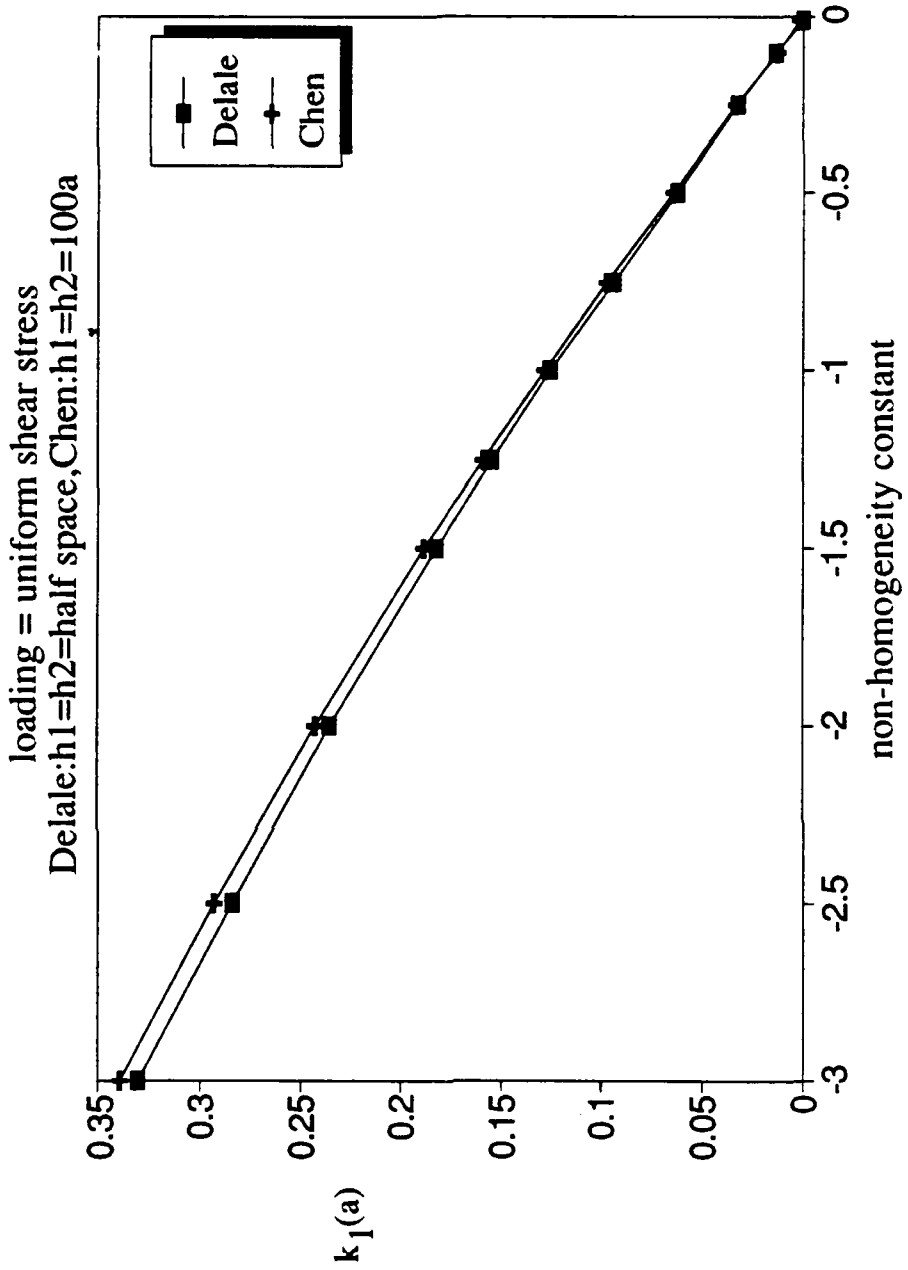

Figure 12. Comparison of Mode I SIF for interface crack between (1). two infinite half planes, and (2). $h_1=h_2=100a$ under loading of uniform shear.

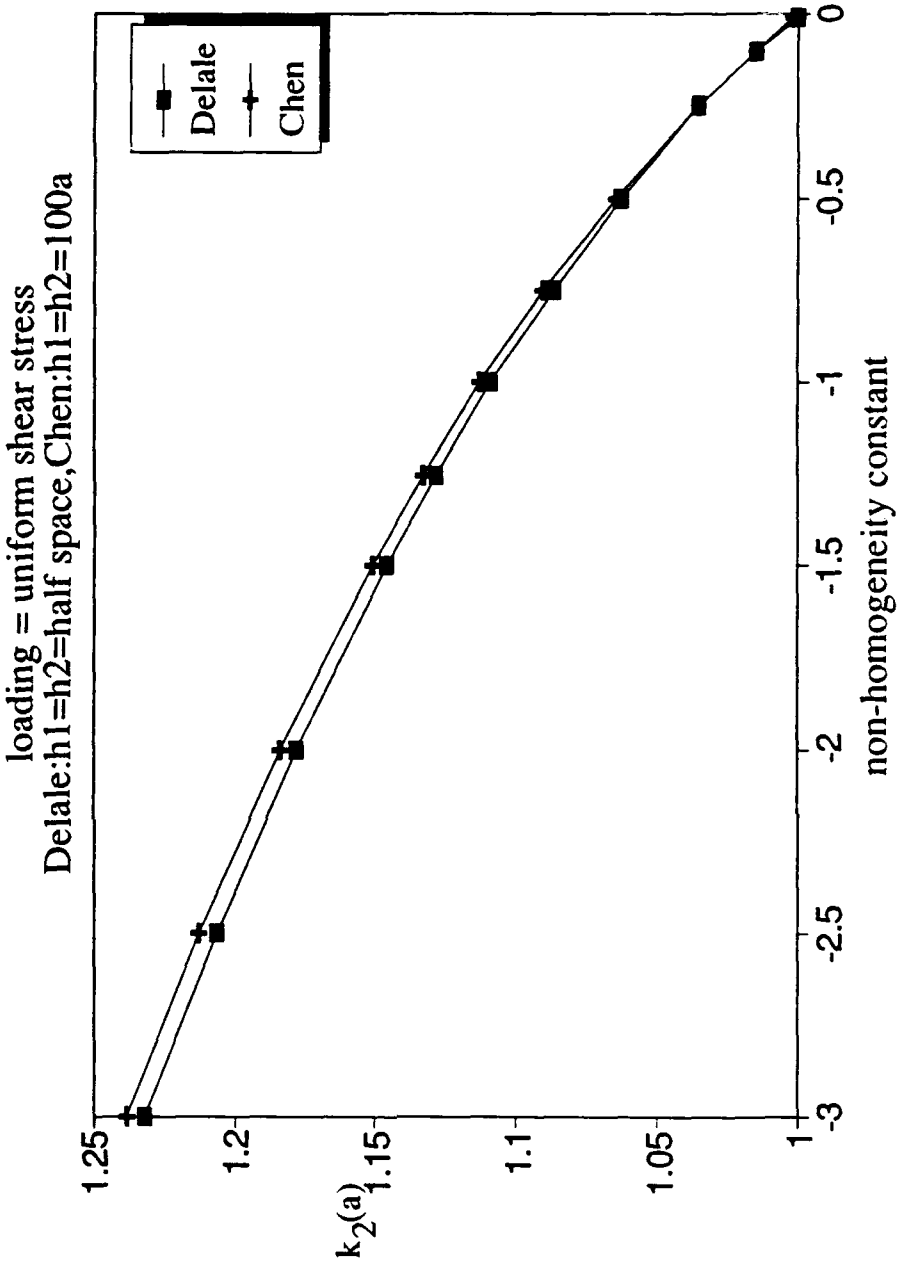

Figure 13. Comparison of Mode II SIF for interface crack between (1). two infinite half planes, and (2). $h_1=h_2=100a$ under loading of uniform shear.

correlated with differences perhaps attributed to the difference in Poisson's ratio.

We next examine the various cases computed in this work. Figure 14 through Figure 25 show the normalized strain energy release rate and Mode I and Mode II stress intensity factors for the cases where $h_1 = 100a$ remains unchanged, only h_2 varies, under the two loadings described in Figure 9.

First of all, all the parameters computed for cases (1), $h_1 = 100a$, $h_2 = 100a$, and (2). $h_1 = 100a$, $h_2 = 10a$, are identical to the third digit on the right hand side of the decimal point. This is why results of case (1) are not shown in Figure 14 through Figure 19. And it tells something about the nature of the cases when both materials are thick; as the nonhomogeneous material gets thicker, beyond $h_2 > 10$ (may be even less than 10), any further increase in h_2 has no effect on the outcome of the solution. When $\gamma < 0$, it is as if any material beyond $h_2 > 10$ does not exit, because large h_2 and the negative sign in the exponential have made μ_2 close to zero. On the other hand, the positive γ, together with large h_2 has made materials beyond $h_2 > 10$ to be like a rigid body. It explains why we see in Figure 14 through Figure 19 that the all parameters tend to converge at the two extremes of the nonhomogeneity constant where they are essentially the same as the half planes case. Only when γ is small do we see the deviation from the half planes case.

The Mode I stress intensity factor under both loadings exhibits a downward trend as the nonhomogeneity constant γ increases from negative to positive. This can be explained partly with the help of the discussions on the relative stiffness of the nonhomogeneous material as its thickness increases. The changes in the nonhomogeneity constant is showing a similar effect. Large γ on the negative side means the crack is closer to the free surface; smaller ligament thickness indicates

easier tear along the interface, therefore a larger mode I stress intensity factor as shown in Figure 15 and Figure 18. This argument explains clearly the upward trend of k_1 in the same figures as the nonhomogeneous layer gets thinner. Since case (2) $h_1 = 100a$, $h_2 = 10a$, is identical to the half planes case as far as the number of digits in the parameters we obtain, it is only appropriate that the stress intensity factors exhibit the same traits as the half planes case. That is why for $\gamma = 0$ we see for case (2). the Mode I SIF, $k_1(a) = 1.0$ and Mode II SIF, $k_2(a) = 0$ under uniform normal stress, as shown in Figure 15 and Figure 16. Similarly for the same case (2)., Mode I SIF, $k_1(a) = 0$ and Mode II SIF, $k_2(a) = 1.0$ when the loading is uniform shear, as shown in Figure 18 and Figure 19.

Due to the nonhomogeneity of the medium, the stress intensity factors exhibit mixed mode condition even though the loadings are of one mode. But in general, Mode II SIF is of secondary importance as compared to Mode I under uniform normal stress, just as Mode I SIF is secondary as compared to Mode II when the loading is uniform shear. These facts can be verified by the relative magnitude of k_1 and k_2 under respective loading as shown in Figure 15 through Figure 19. Furthermore, because the geometry of the problem is symmetric with respect to the y-axis, the shear stresses are anti-symmetric under uniform normal stress loading. Therefore the Mode II SIF under uniform normal stress has different signs at each end of the crack tip. This can also help to explain why $k_2(a)$ goes through a sign change as γ changes from negative to positive in Figure 16. We know that when $\gamma < 0$, the homogeneous material is stiffer than the nonhomogeneous material. Whereas the reverse is true when $\gamma > 0$. We can envision the change of sign in shear stress as γ goes from negative to positive as if the geometry of the problem has been rotated 180 degrees.

Because what used to be stiffer (material 1) when $\gamma < 0$ is "softer" when $\gamma > 0$, the sign of the shear stresses at $x = -a$ when $\gamma < 0$, which is positive, is exactly what it should be at $x = a$ when $\gamma > 0$. But as h_2 gets thinner and thinner, the tendency of this Mode II SIF under normal stress to change sign as γ goes from negative to positive because of the relative material stiffness explained earlier as shown in Figure 16 is being offset by the less and less ligament between the crack and the free surface. As a result the tendency to change sign is less as h_2 becomes thinner. This is reflected clearly in Figure 22 where we see for $h_2 = a$, k_2 changes its sign at $\gamma = 2$, whereas for $h_2 = 0.5a$ and $h_2 = 0.25a$, k_2 remains negative.

It should be pointed out that for uniform shear loading, σ_{xy} is symmetric with respect to the y-axis and σ_{yy} becomes anti-symmetric. As a result k_2 is positive at either tip of the crack whereas k_1 undergoes a sign change from one crack tip to another. But examination of the vertical crack opening displacement under this loading (see Figure 41) reveals that $(v^+ - v^-)$ is negative on the left half of the crack. This means the upper crack surface has penetrated into the lower crack surface, which is not permissible. What actually would have happened is that the crack would have opened for only a portion of the crack length, and would remain closed for the remainder. The problem needs to be reformulated if we want to solve it under this loading.

The normalized strain energy release rate would reflect the combined effect of both k_1 and k_2 in each loading for it is a function of $(k_1^2 + k_2^2)$ as discussed in Chapter 3.

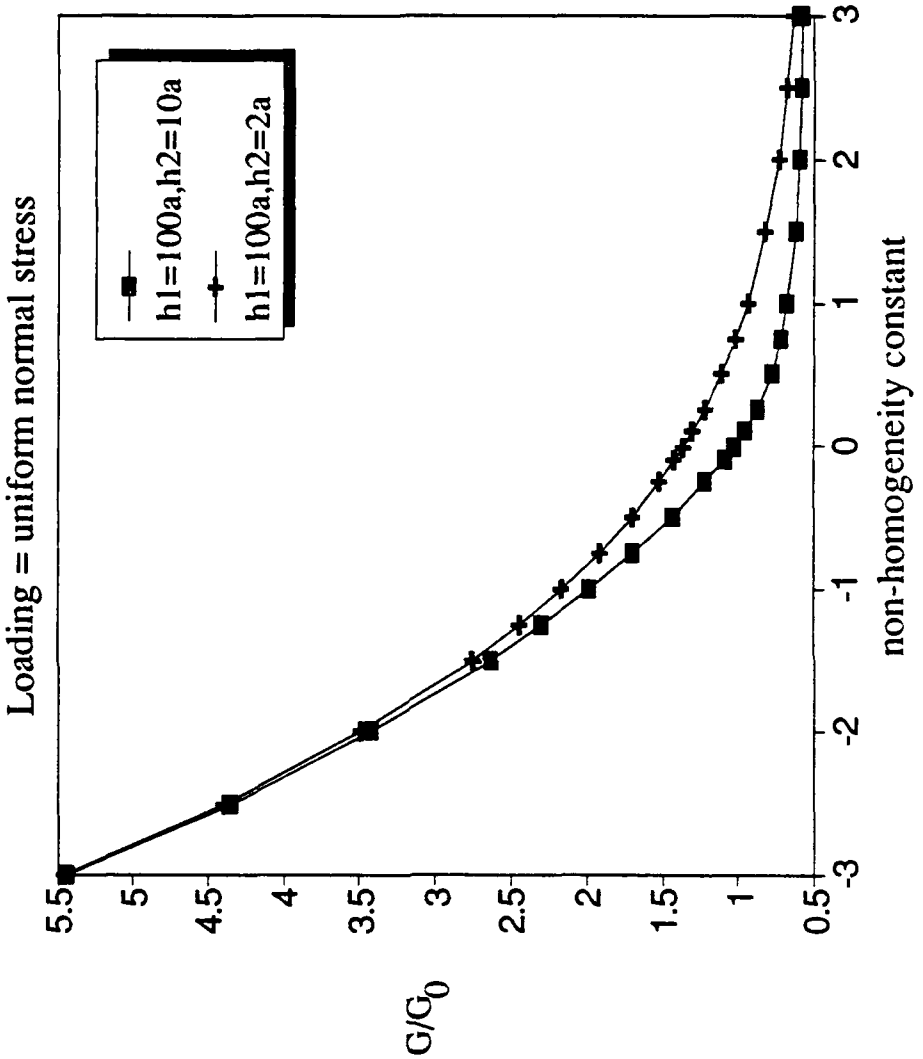

Figure 14. Normalized strain energy release rate of interface crack for (1). h_1=100a, h_2=10a, (2). h_1=100a, h_2=2a, under loading of uniform normal stress.

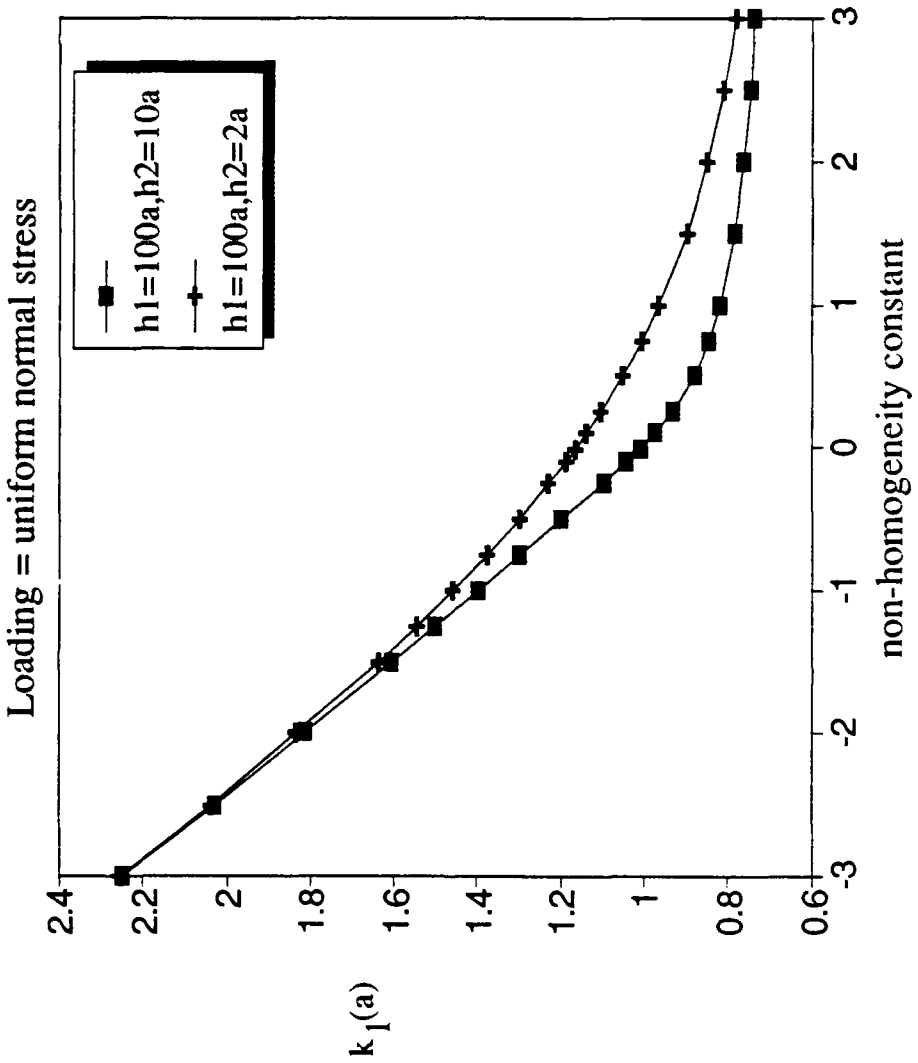

Figure 15. Normalized Mode I SIF of interface crack for (1). h_1=100a, h_2=10a, (2). h_1=100a, h_2=2a, under loading of uniform normal stress.

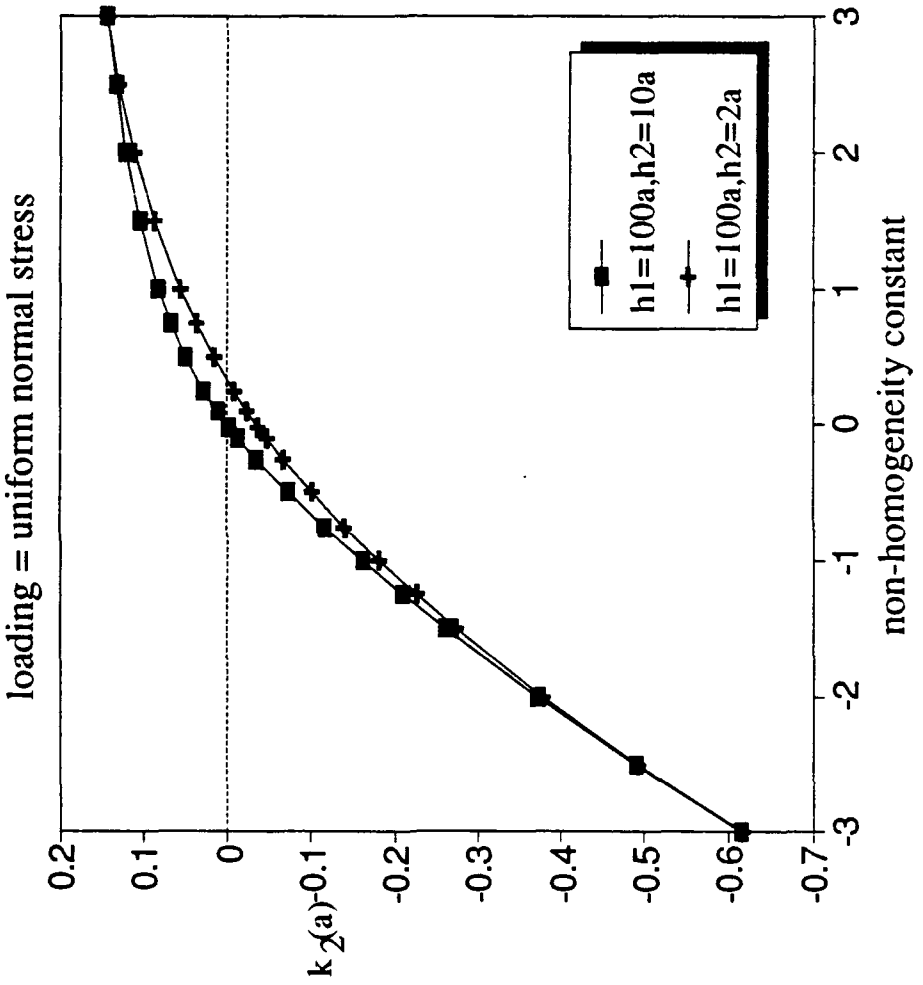

Figure 16. Normalized Mode II SIF of interface crack for (1). h_1=100a, h_2=10a, (2). h_1=100a, h_2=2a, under loading of uniform normal stress.

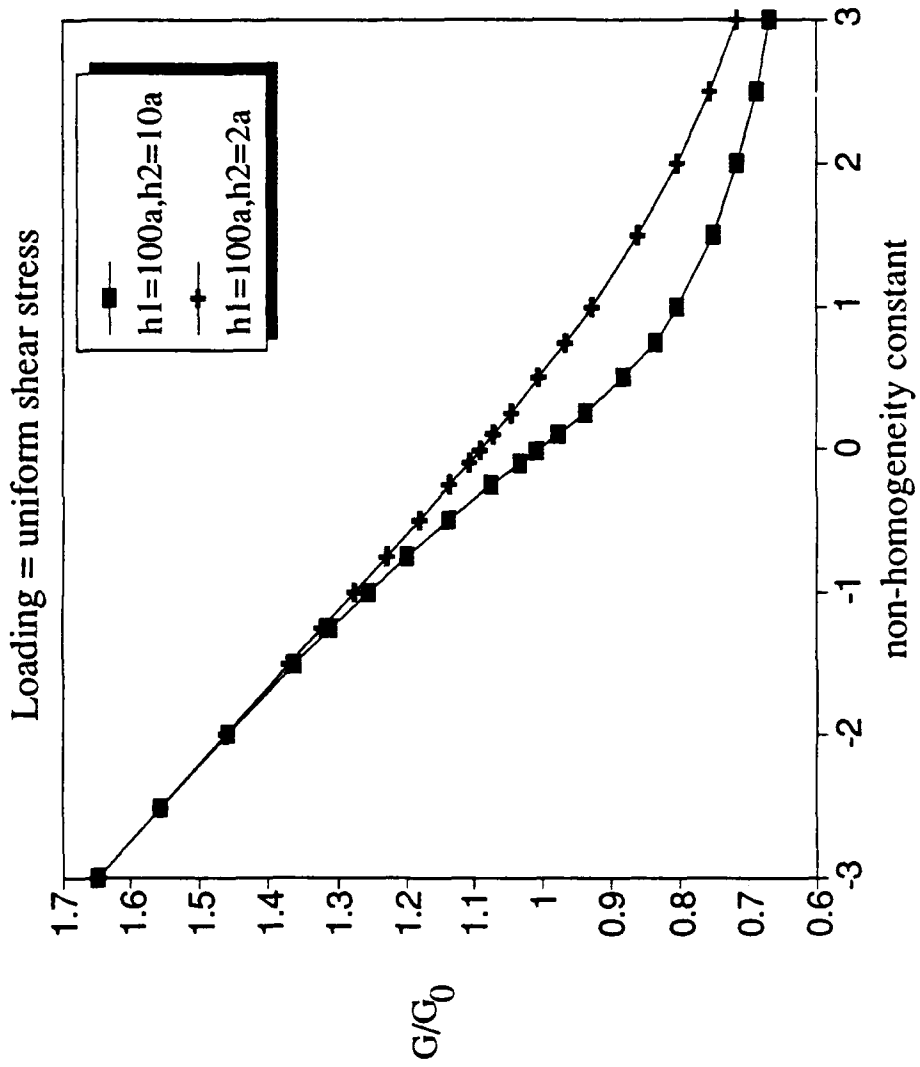

Figure 17. Normalized strain energy release rate of interface crack for (1). h_1=100a, h_2=10a, and (2). h_1=100a, h_2=2a, under loading of uniform shear.

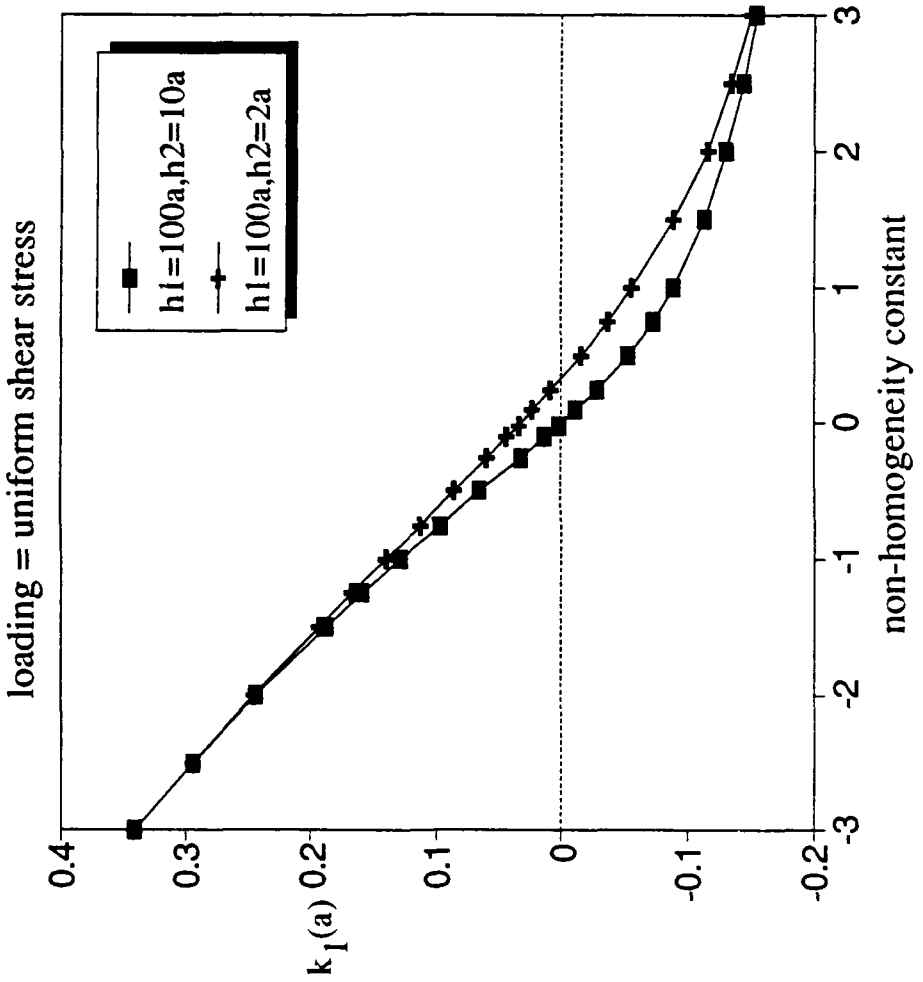

Figure 18. Normalized Mode I SIF of interface crack for (1). h_1=100a, h_2=10a, (2). h_1=100a, h_2=2a, under loading of uniform shear.

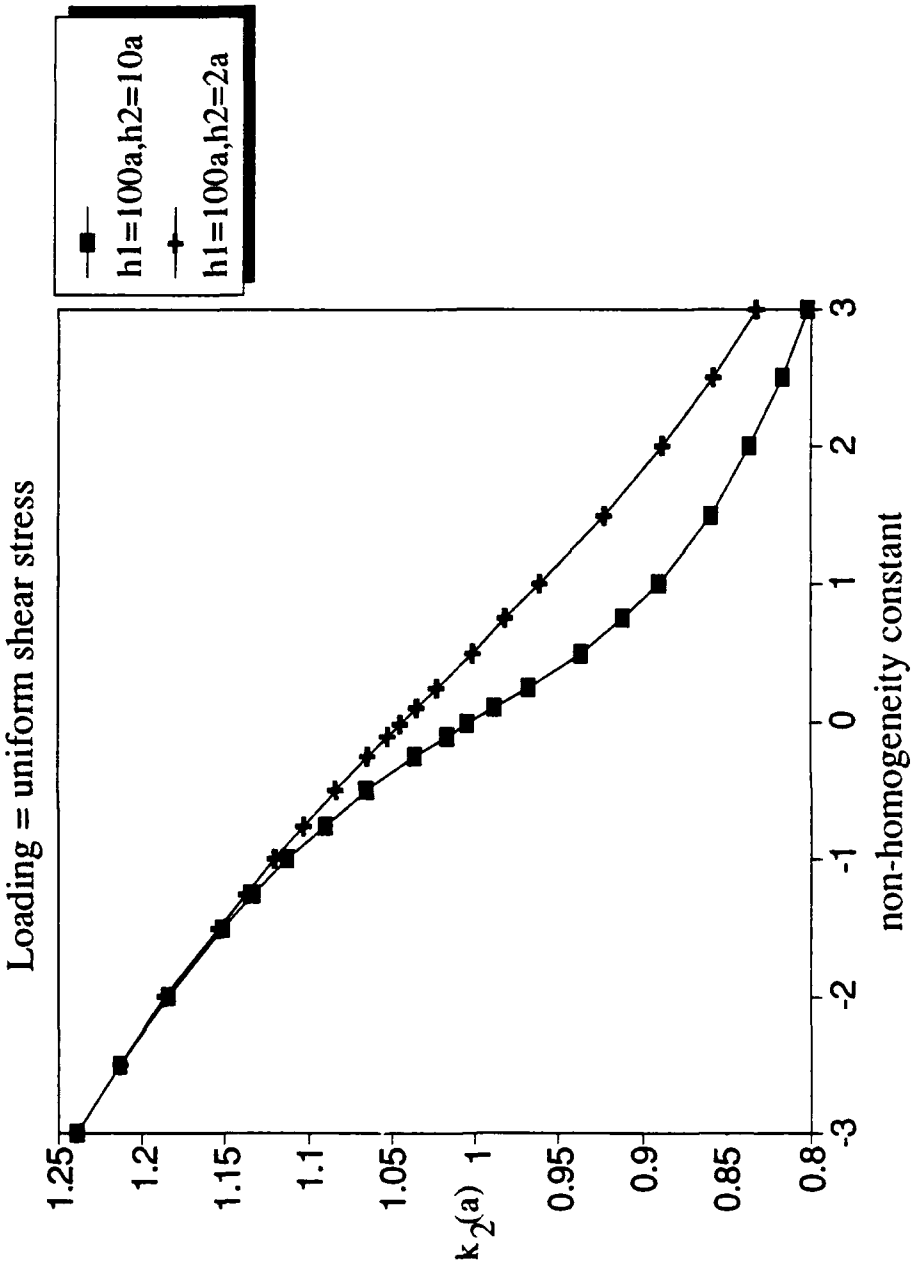

Figure 19. Normalized Mode II SIF of interface crack for (1). h_1=100a, h_2=10a, (2). h_1=100a, h_2=2a, under loading of uniform shear.

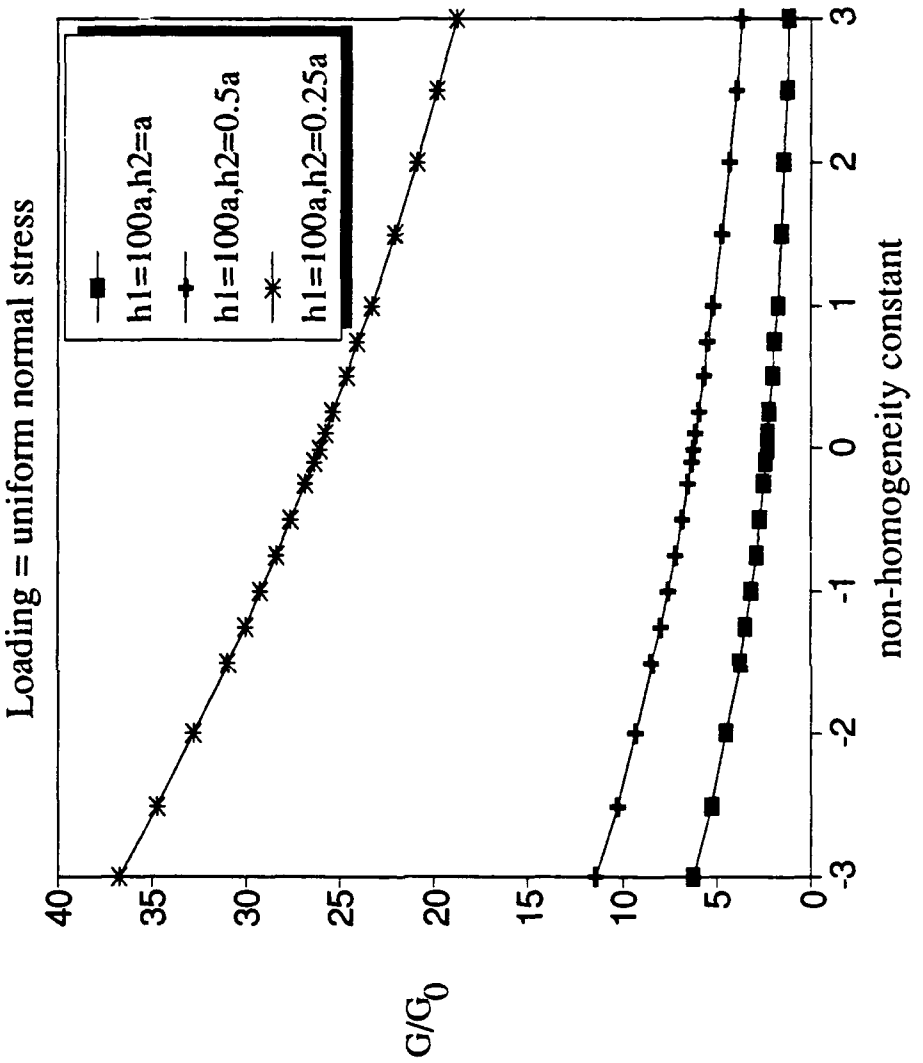

Figure 20. Normalized strain energy release rate of interface crack for (1). h_1=100a, h_2=a, (2). h_1=100a, h_2=0.5a, (3). h_1=100a, h_2=0.25a, under loading of uniform normal stress.

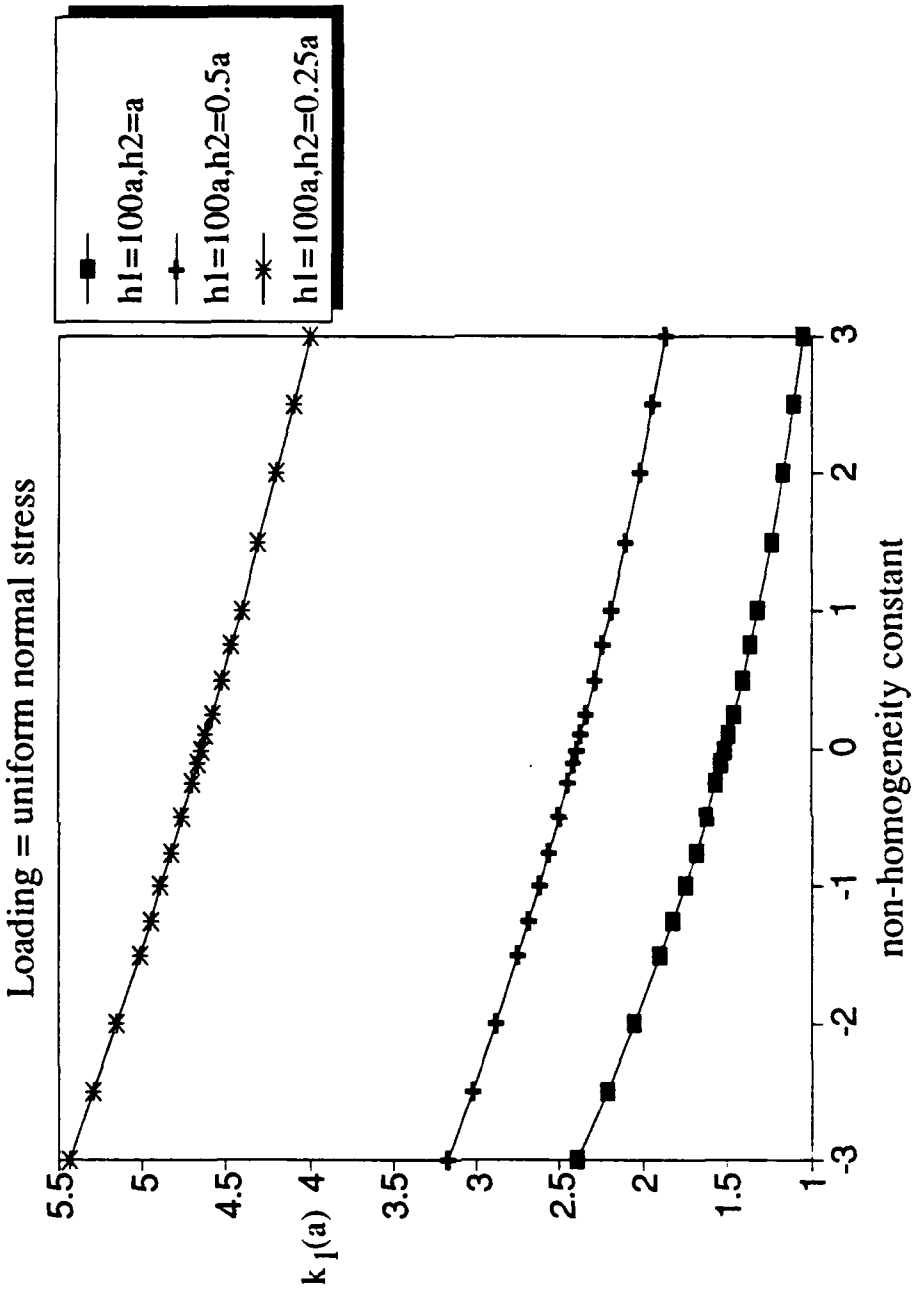

Figure 21. Normalized Mode I SIF of interface crack for (1). h_1=100a, h_2=a, (2). h_1=100a, h_2=0.5a, (3). h_1=100a, h_2=0.25a, under loading of uniform normal stress.

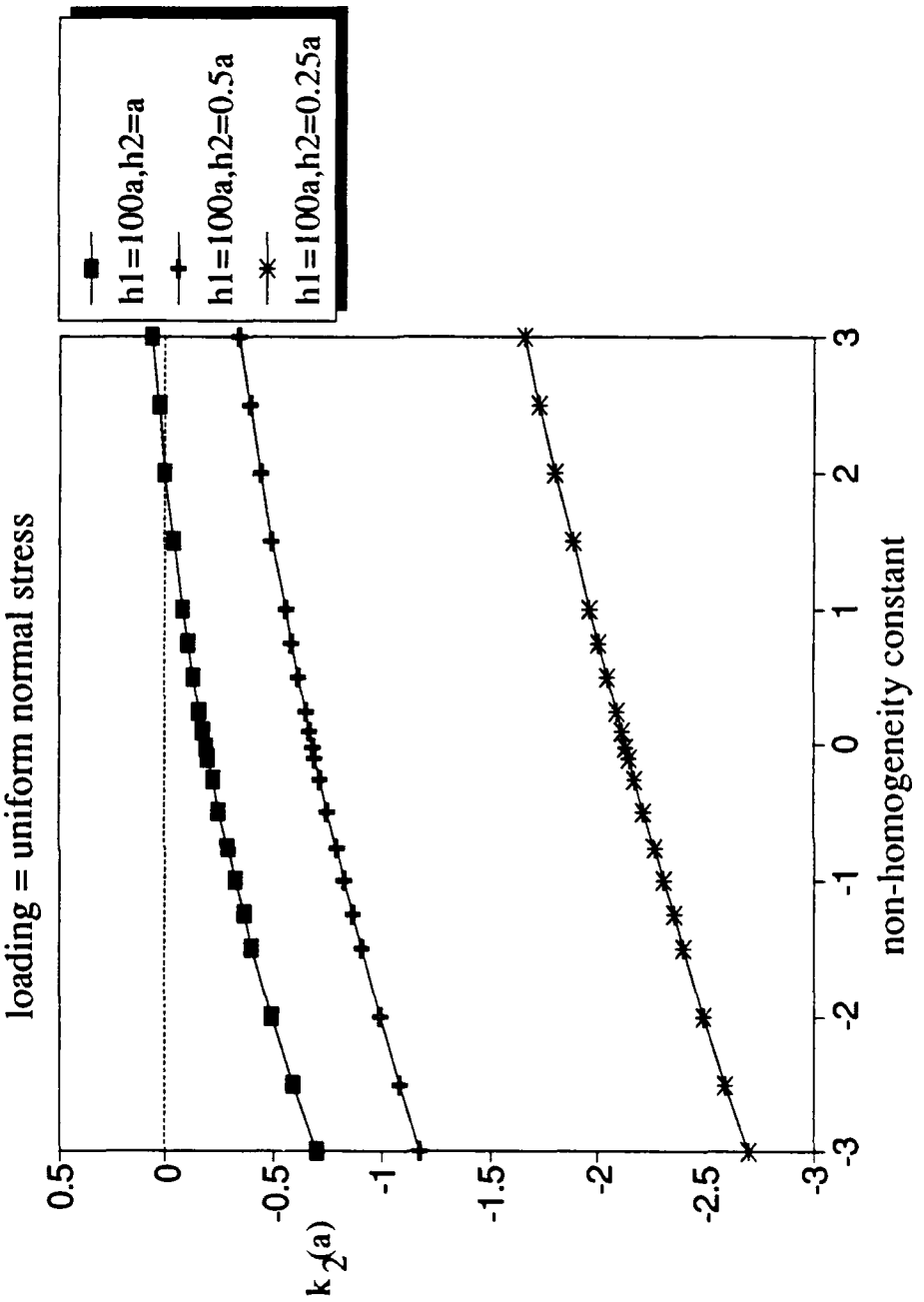

Figure 22. Normalized Mode II SIF of interface crack for (1). h_1=100a, h_2=a, (2). h_1=100a, h_2=0.5a, (3). h_1=100a, h_2=0.25a, under loading of uniform normal stress.

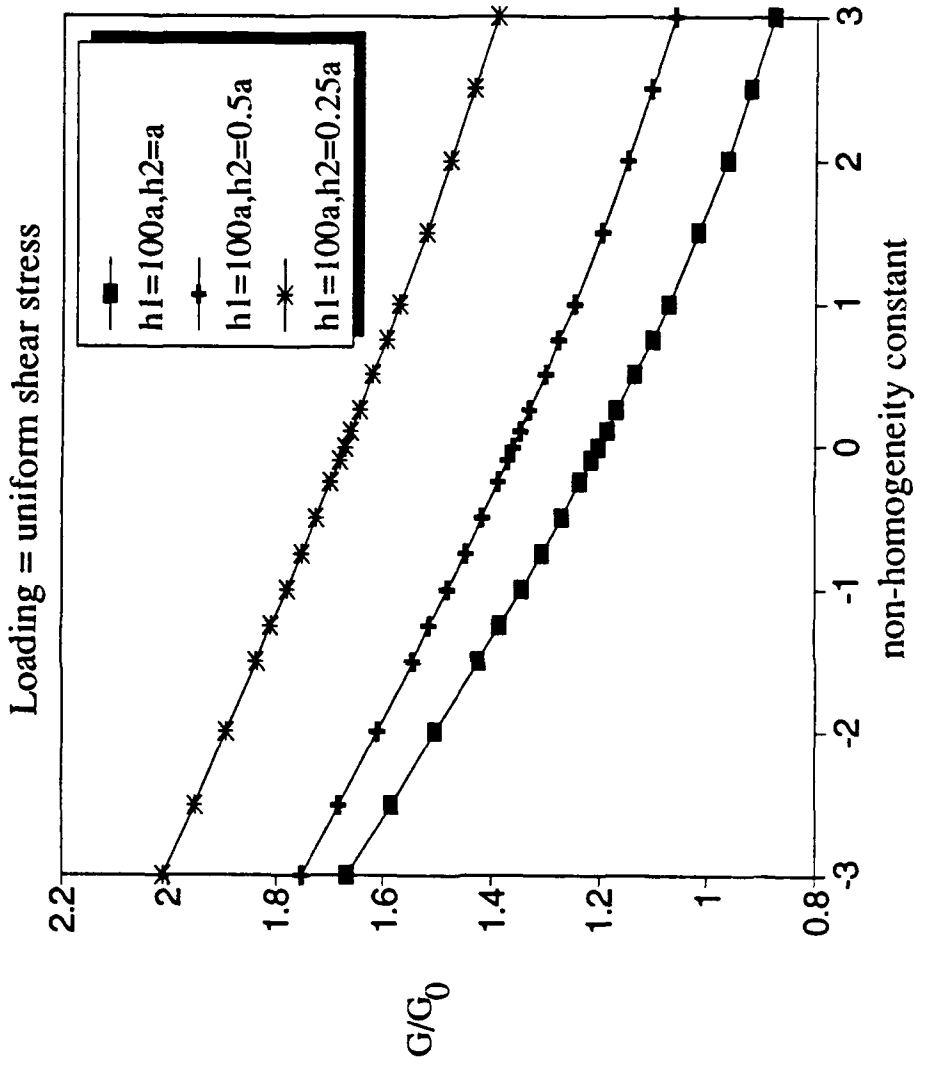

Figure 23. Normalized strain energy release rate of interface crack for (1). h_1=100a, h_2=a, (2). h_1=100a, h_2=0.5a, (3). h_1=100a, h_2=0.25a, under loading of uniform shear.

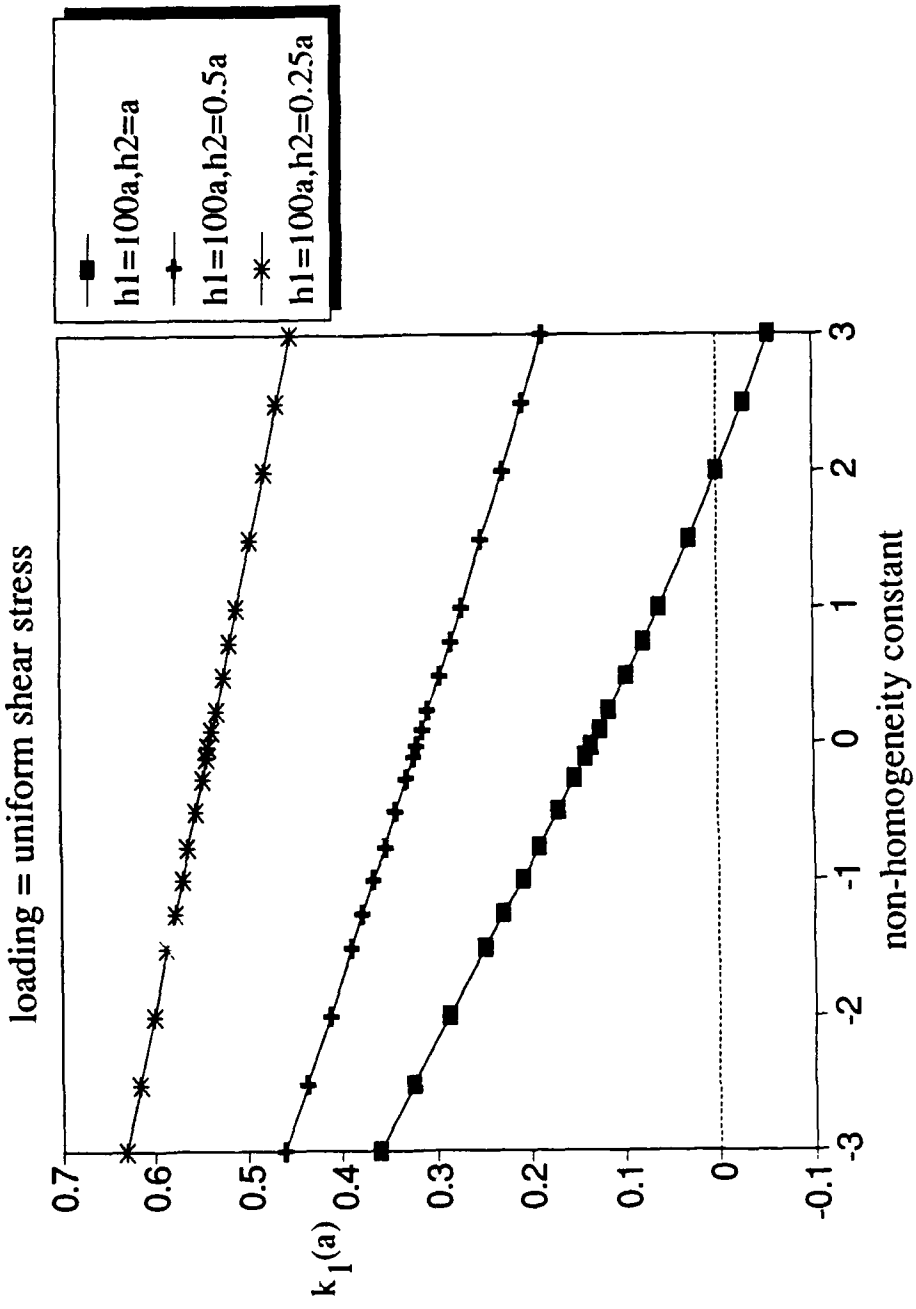

Figure 24. Normalized Mode I SIF of interface crack for (1). h_1=100a, h_2=a, (2). h_1=100a, h_2=0.5a, (3). h_1=100a, h_2=0.25a, under loading of uniform shear.

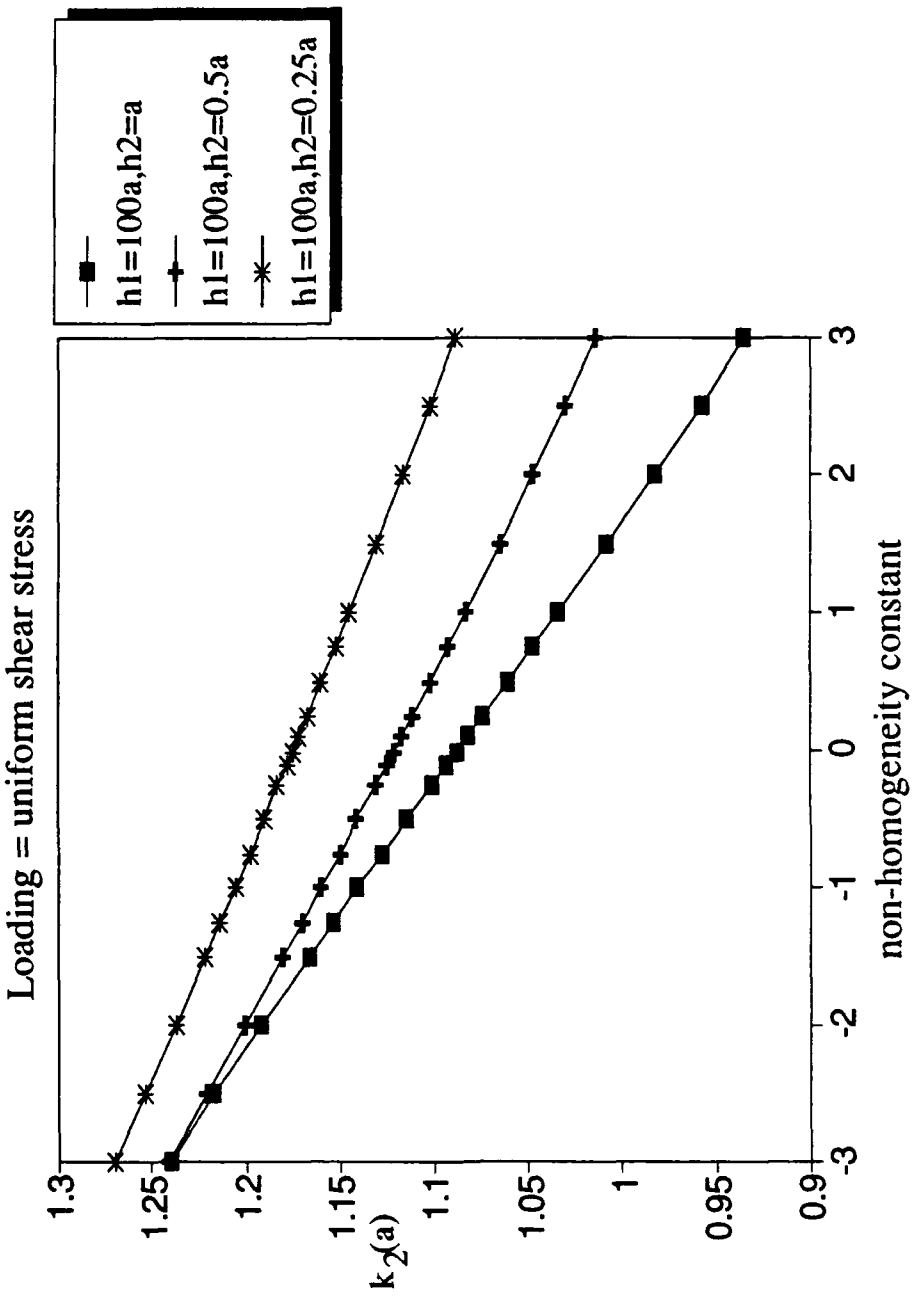

Figure 25. Normalized Mode II SIF of interface crack for (1). h_1=100a, h_2=a, (2). h_1=100a, h_2=0.5a, (3). h_1=100a, h_2=0.25a, under loading of uniform shear.

Figure 26 through Figure 31 show the normalized strain energy release rate and Mode I and Mode II stress intensity factors when $h_2 = a$ and h_1 varies under the two loading conditions. Again, the Mode I stress intensity factor under uniform normal stress decreases as γ goes from negative to positive. It also increases with decreasing ligament size in material 1, as can be seen in Figure 27. The Mode II SIF under uniform normal stress shows the same tendency to change sign as γ goes from negative to positive. For the same reason in the cases where $h_1 = 100a$ and h_2 varies, Figure 28 shows that the tendency for the sign change is discouraged as h_1 becomes thinner. It is worth noting that only when $h_1 = h_2 = a$ and $\gamma = 0$ do we see one mode as signified by $k_2 = 0$ under uniform normal stress in Figure 28 and $k_1 = 0$ under uniform shear as seen in Figure 30. The rest of the cases, either because nonsymmetric geometry or nonsymmetric material constant (nonhomogeneity), are of mixed mode.

The effect of the changes in Poisson's ratio on the strain energy release rate and stress intensity factors for the case $h_1 = 100a$, $h_2 = a$ under the two loadings are shown in Figure 32 through Figure 37. We note that for plane strain $\kappa = 3 - 4\nu$, therefore κ is equal to 1 and 3 respectively for Poisson's ratio of 0.5 and 0. Either of these two values of κ causes some term in the denominator to become zero during the course of numerical computation (see Eqn. (1) in Chapter 2). To avoid dividing by zero, Poisson's ratios of 0.01 and 0.499 are used instead. From Figure 32 through Figure 37, we see that changes in Poisson's ratio does not have a pronounced effect on the parameters calculated, except for very large values of γ, as evidenced by the closeness of the curves. These comparisons also show that when the materials are homogeneous, the stress intensity factors are independent of the Poisson's ratio. It

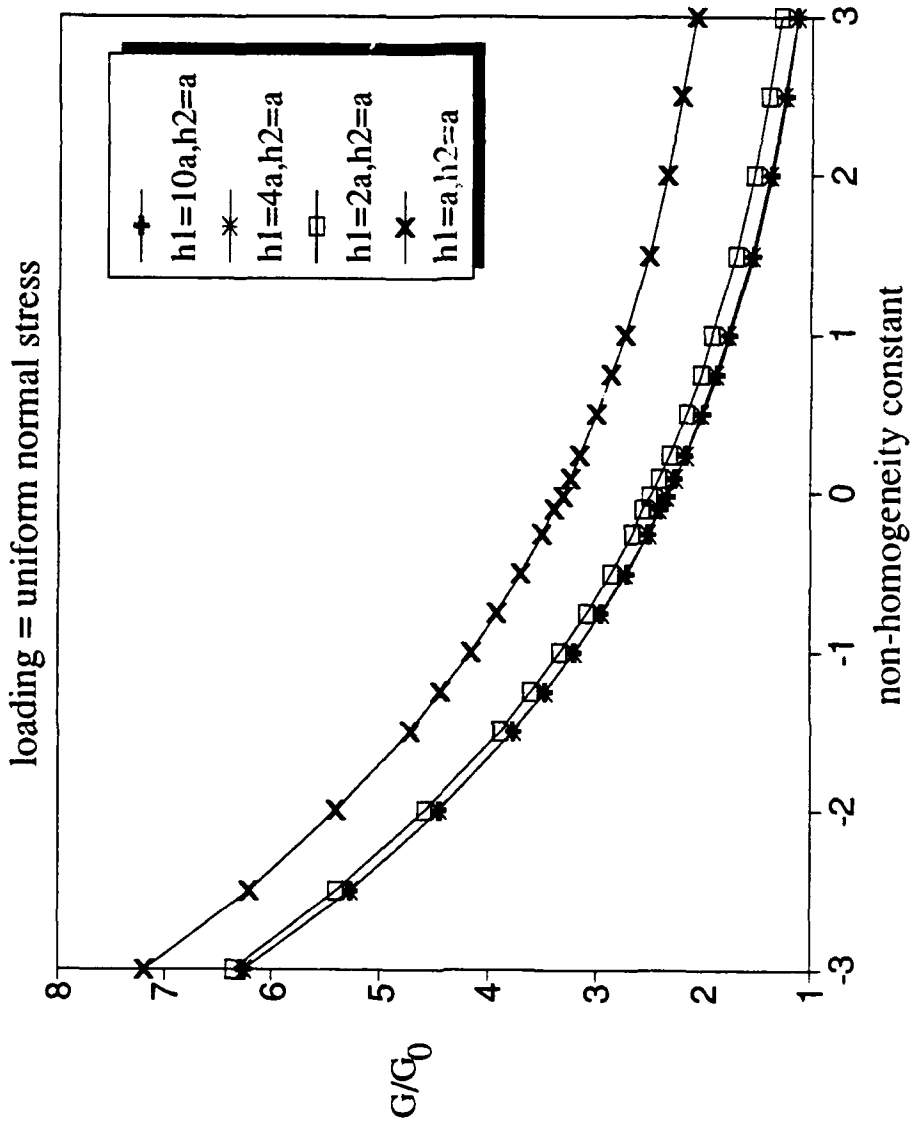

Figure 26. Normalized strain energy release rate of interface crack for (1). h_1=10a, h_2=a, (2). h_1=4a, h_2=a, (3). h_1=2a, h_2=a, (4). h_1=h_2=a, under loading of uniform normal stress.

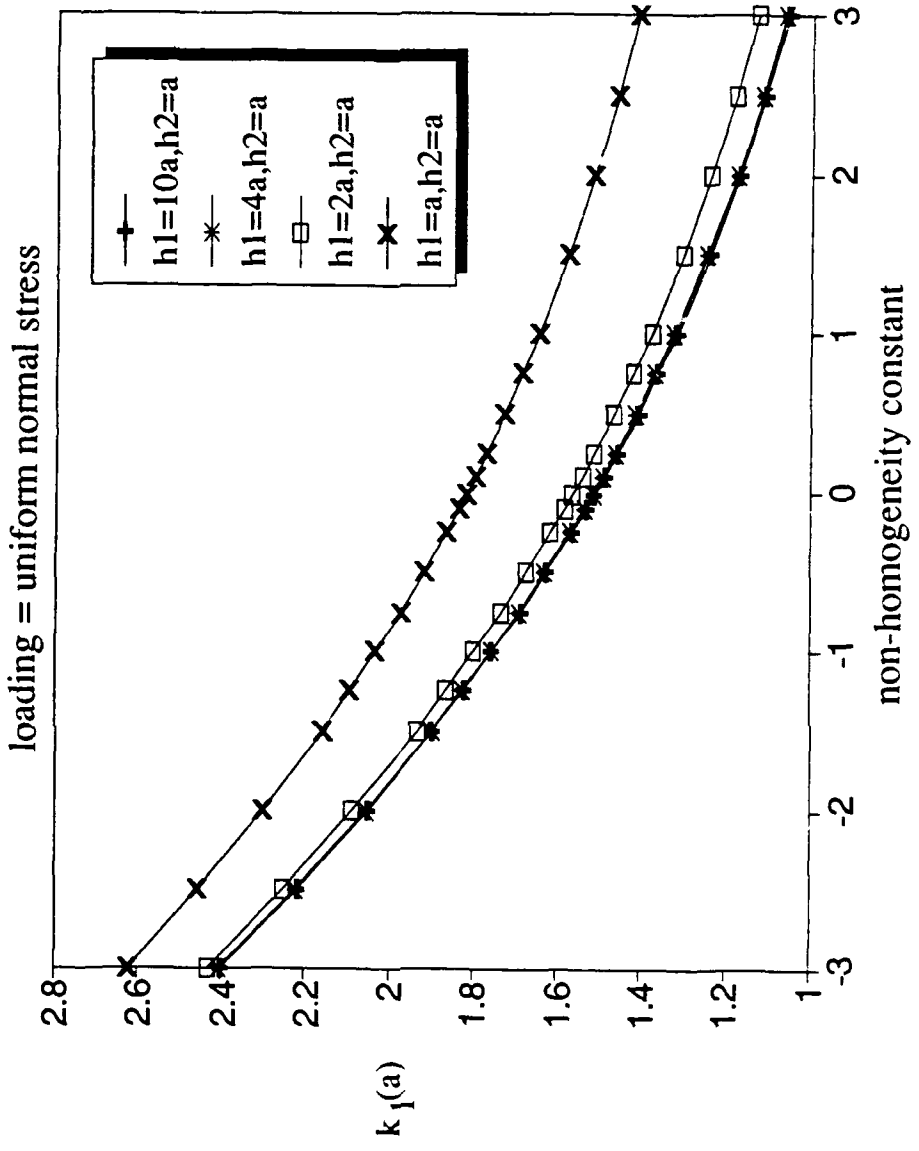

Figure 27. Normalized Mode I SIF of interface crack for (1). h_1=10a, h_2=a, (2). h_1=4a, h_2=a, (3). h_1=2a, h_2=a, (4). h_1=h_2=a, under loading of uniform normal stress.

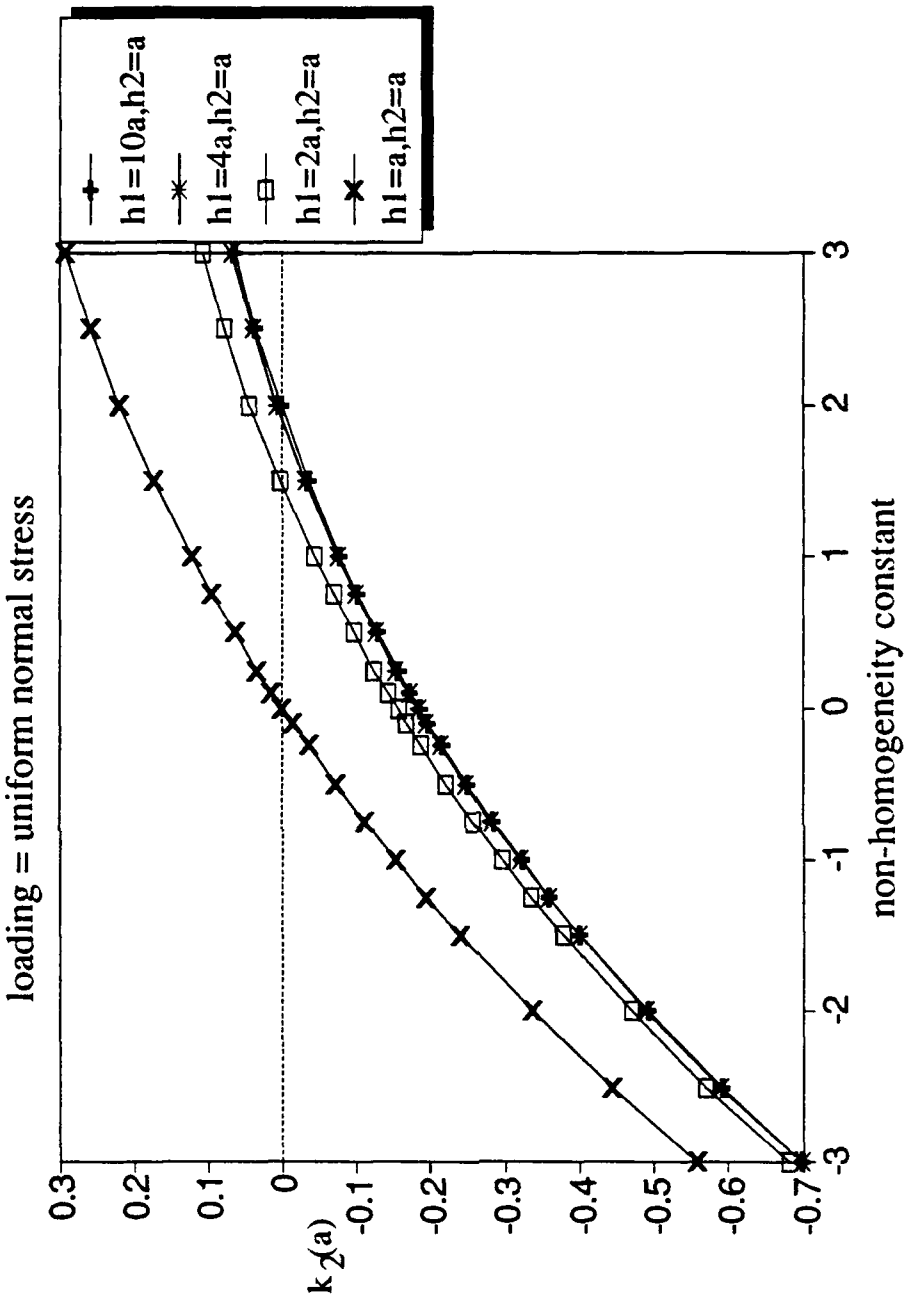

Figure 28. Normalized Mode II SIF of interface crack for (1). h_1=10a, h_2=a, (2). h_1=4a, h_2=a, (3). h_1=2a, h_2=a, (4). h_1=h_2=a, under loading of uniform normal stress.

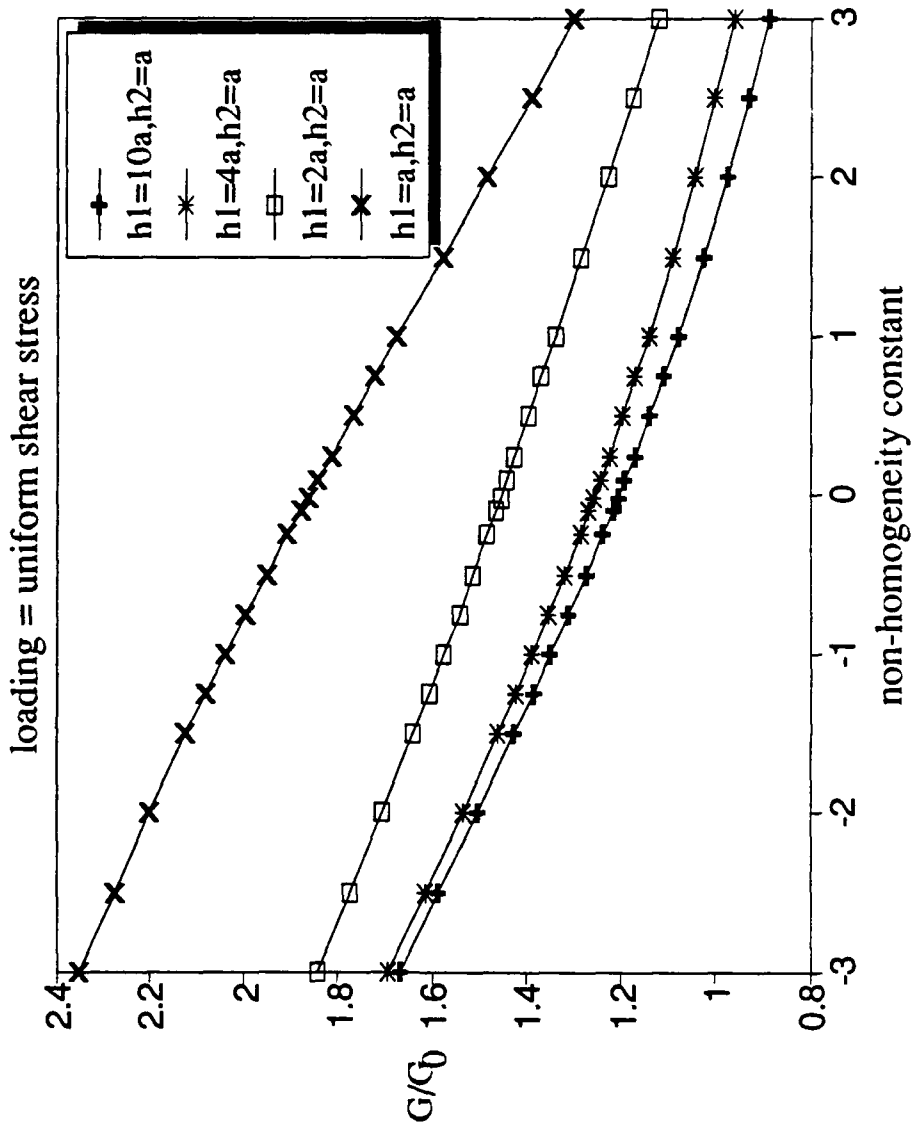

Figure 29. Normalized strain energy release rate of interface crack for (1). h_1=10a, h_2=a, (2). h_1=4a, h_2=a, (3). h_1=2a, h_2=a, (4). h_1=h_2=a, under loading of uniform shear.

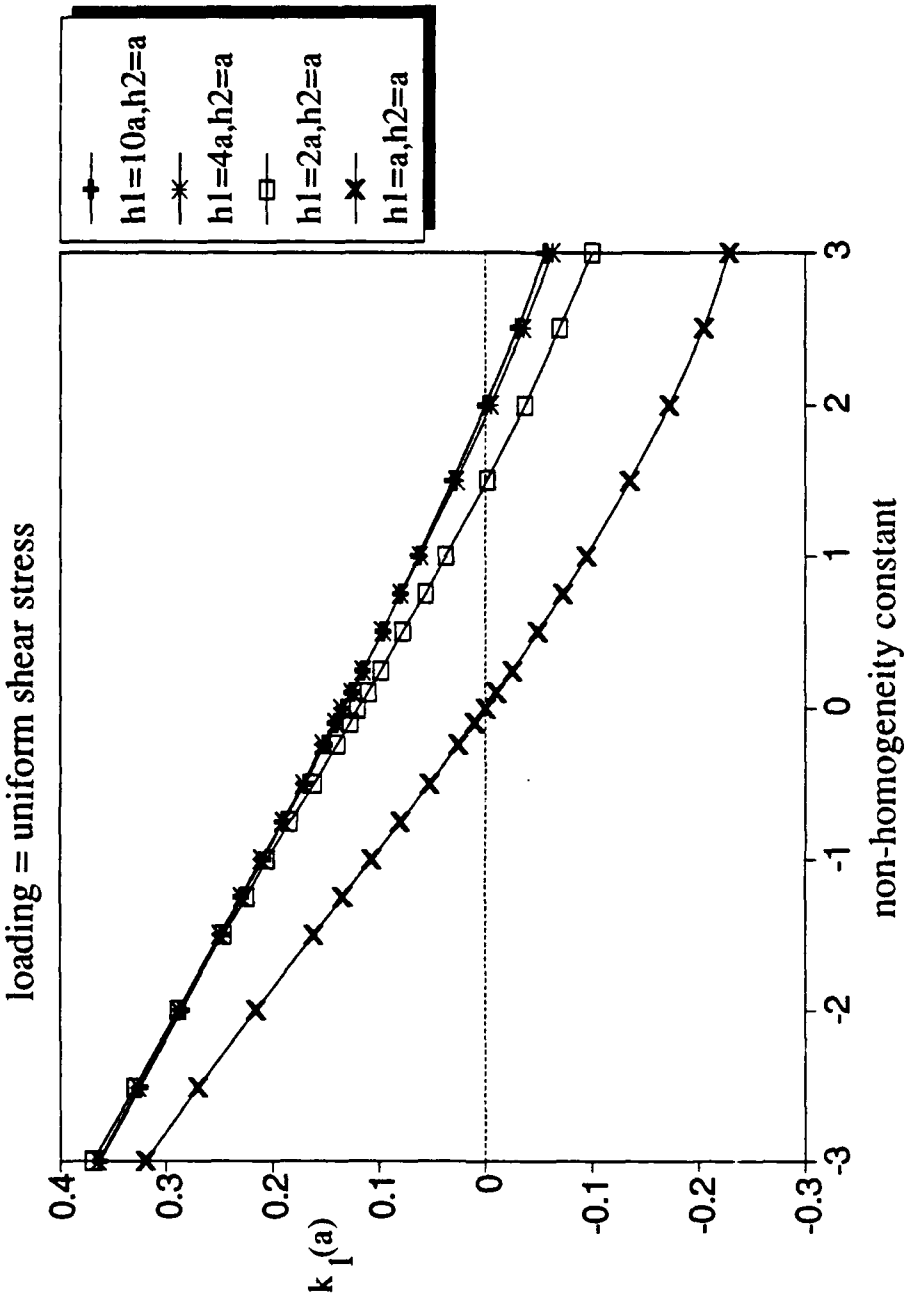

Figure 30. Normalized Mode I SIF of interface crack for (1). h_1=10a, h_2=a, (2). h_1=4a, h_2=a, (3). h_1=2a, h_2=a, (4). h_1=h_2=a, under loading of uniform shear.

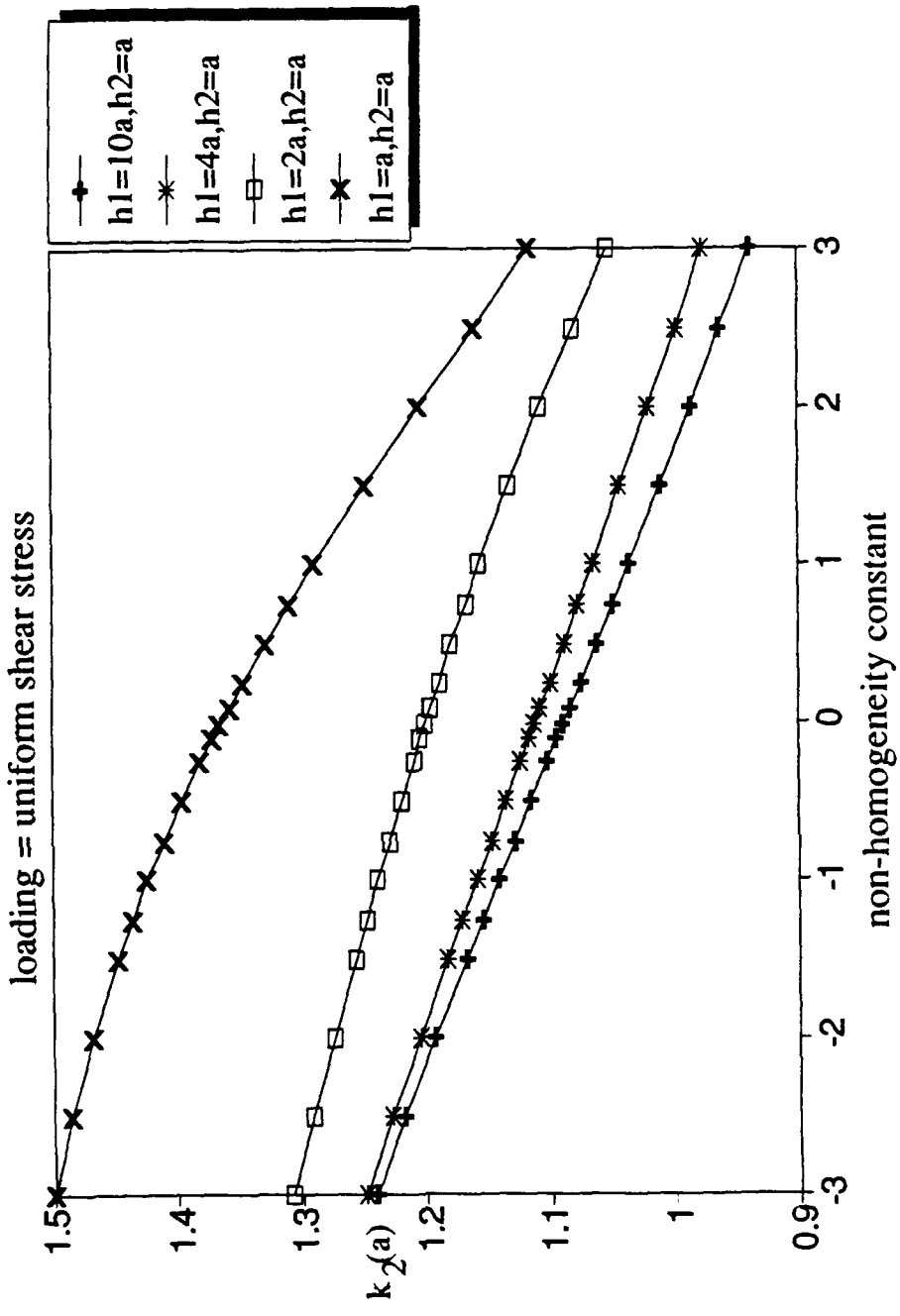

Figure 31. Normalized Mode II SIF of interface crack for (1). h_1=10a, h_2=a, (2). h_1=4a, h_2=a, (3). h_1=2a, h_2=a, (4). h_1=h_2=a, under loading of uniform shear.

is evidenced by the SIF's for all values of Poisson's ratio converging at $\gamma = 0$. Before we attempt to justify the behavior of the parameters shown in Figure 32 through Figure 37, we recognize that $\nu = 0$ signifies no lateral strain and $\nu = 0.5$ represents no volume change, which is also the maximum lateral strain allowed. Poisson's ratio of value larger than 0.5 is unlikely because in the case of tensile loading it means there is a volume decrease. Based on the above discussions, when $\gamma < 0$, we can interpret $\nu = 0$ to be stiffer than $\nu = 0.5$, therefore a smaller SIF as seen in Figure 33 and Figure 37. But the same can not be said for cases when $\gamma > 0$. Actually we see just the reverse. The above argument can also be applied to explain the small difference between the parameters computed in [16] and case (1). in this work. As mentioned earlier, the Poisson's ratio is treated as a constant in this work and varies the same way as does the shear modulus for material 2 in reference [16]. As a result, everything else being equal, for $\gamma < 0$ the nonhomogeneous material in [16] is actually stiffer than when ν remains constant as y increases. Therefore Figure 10 and Figure 13 show the result in this work to have a larger stress intensity factor.

Figure 38 through Figure 41 show crack opening displacements for the case $h_1 = 100a$, $h_2 = a$ and $\gamma = -3.0$ whereas Figure 42 through Figure 45 show COD's for the same geometry except $\gamma = 3.0$. Figure 38 and Figure 39 are typical of the crack opening displacements one would expect under uniform normal stress. The horizontal component displays a movement toward the center of the crack at which point the horizontal displacement is zero. The vertical component of the COD, on the other hand, has an elliptical shape. The crack opening displacements under uniform shear, however, is a reverse of what have just been described. The horizontal component has an elliptical distribution whereas the vertical component shows a change in direction

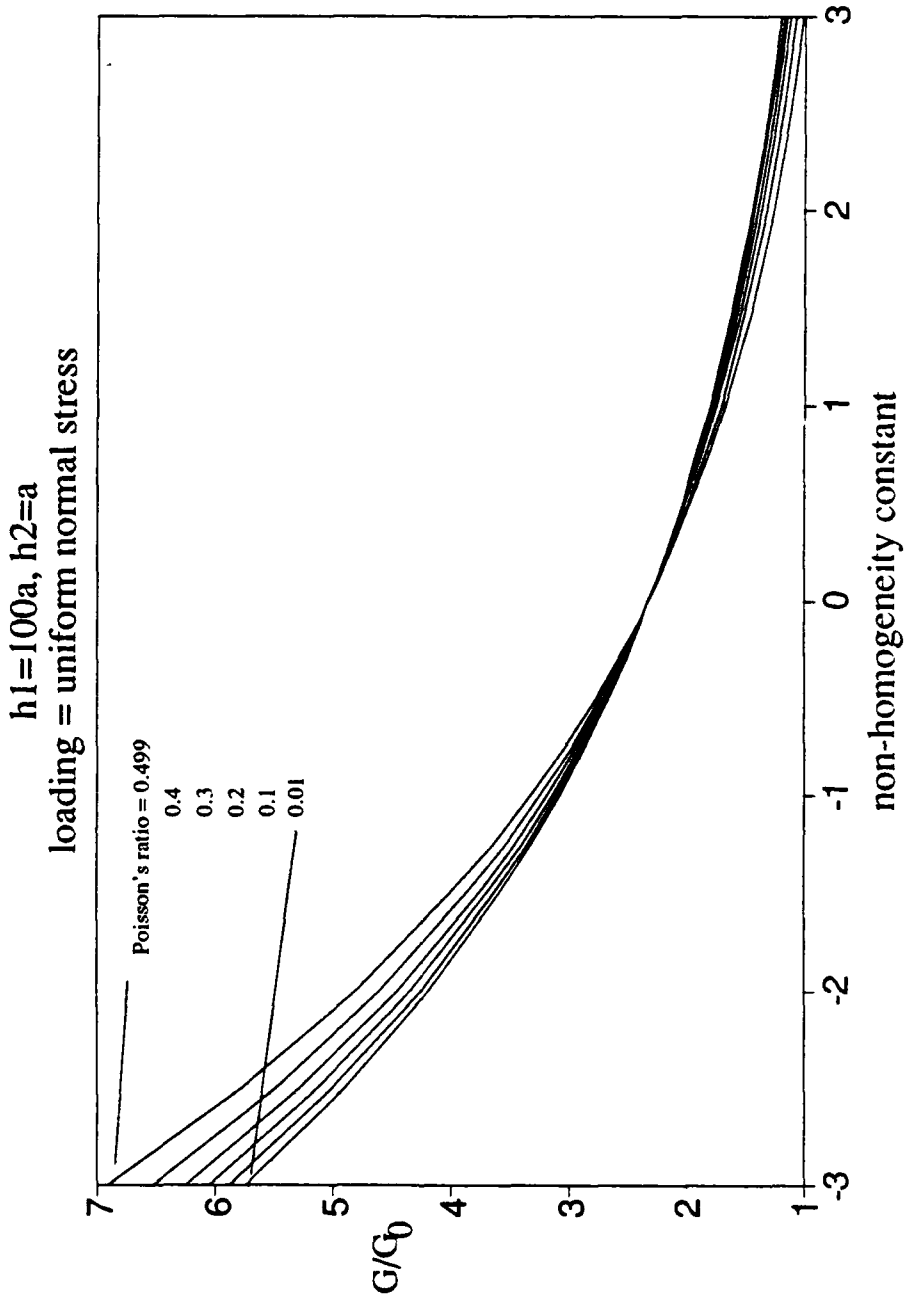

Figure 32. Normalized strain energy release rate of interface crack for h_1=100a, h_2=a at ν=0.01, 0.1, 0.2, 0.3, 0.4, 0.499 under loading of uniform normal stress.

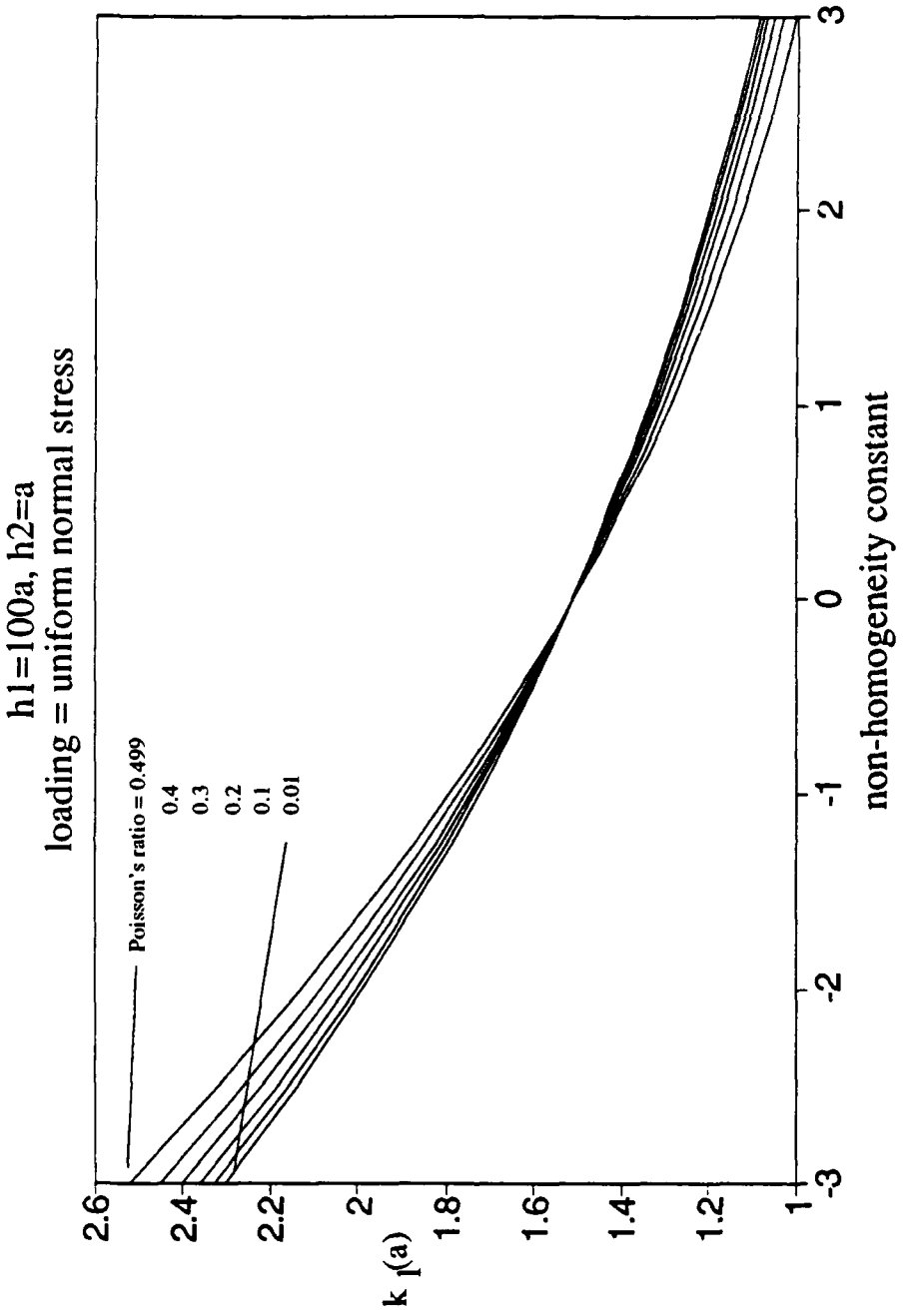

Figure 33. Normalized Mode I SIF of interface crack for h_1=100a, h_2=a at ν=0.01, 0.1, 0.2, 0.3, 0.4, 0.499 under loading of uniform normal stress.

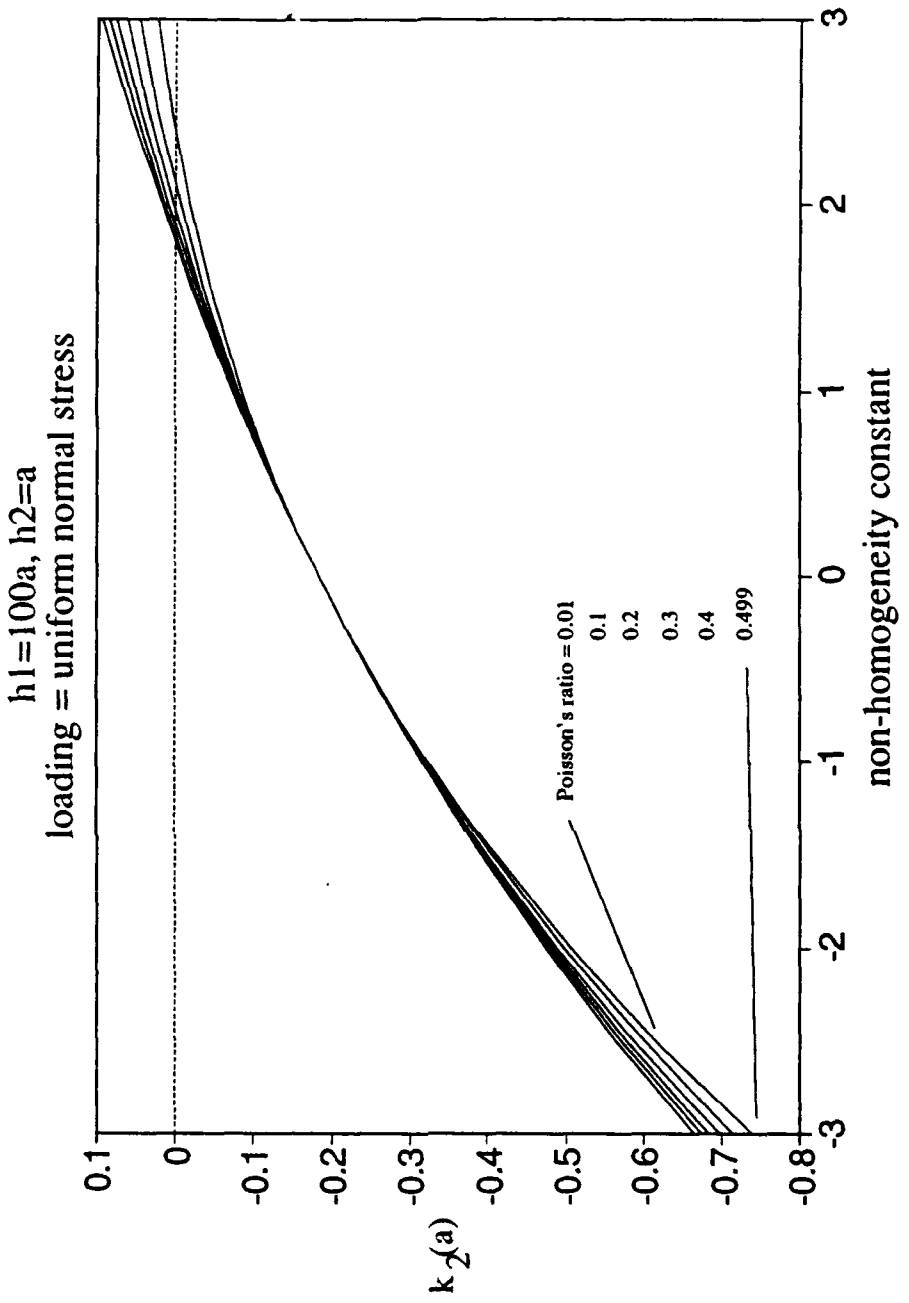

Figure 34. Normalized Mode II SIF of interface crack for h_1=100a, h_2=a at ν=0.01, 0.1, 0.2, 0.3, 0.4, 0.499 under loading of uniform normal stress.

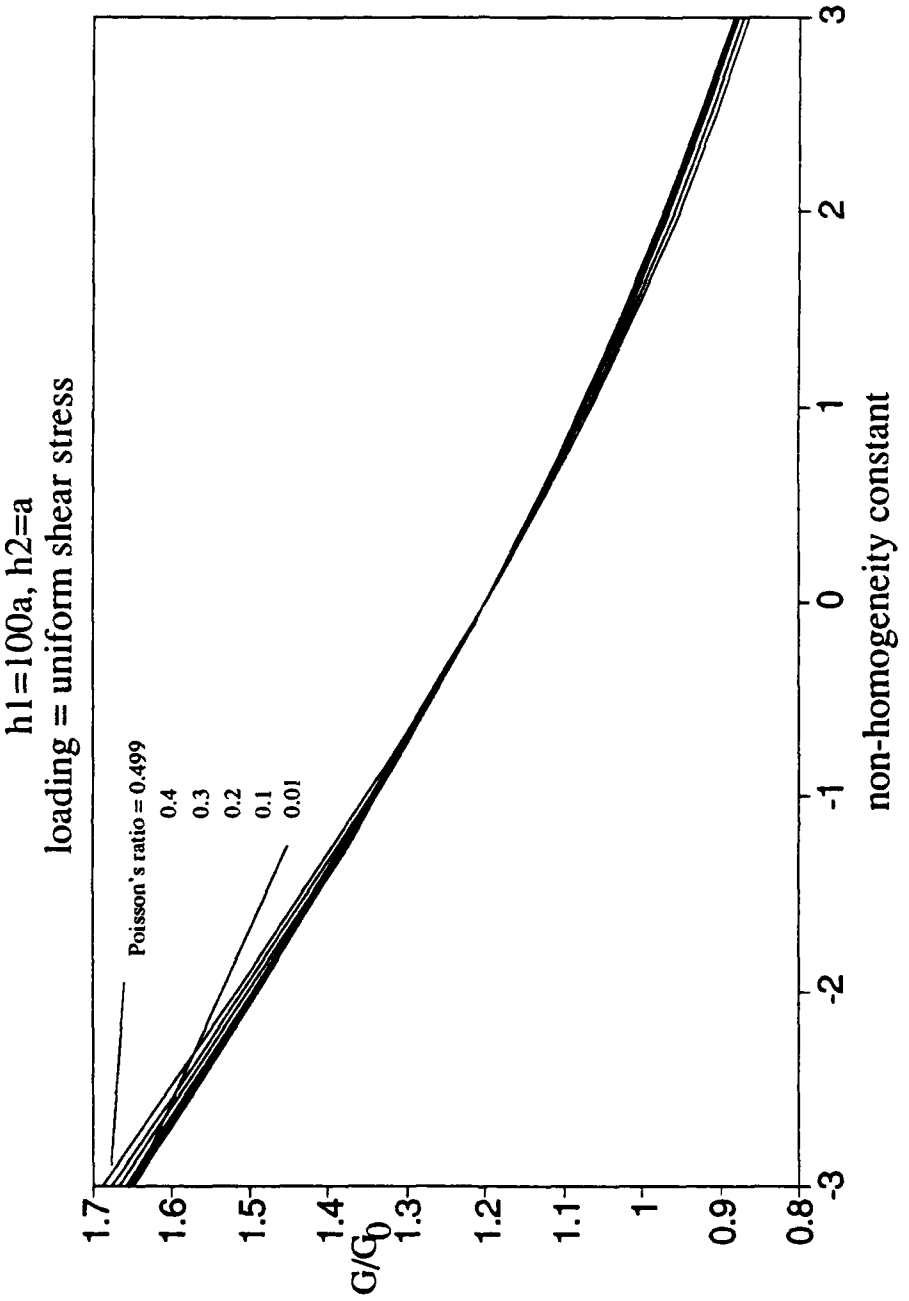

Figure 35. Normalized strain energy release rate of interface crack for h_1=100a, h_2=a at ν=0.01, 0.1, 0.2, 0.3, 0.4, 0.499 under loading of uniform shear.

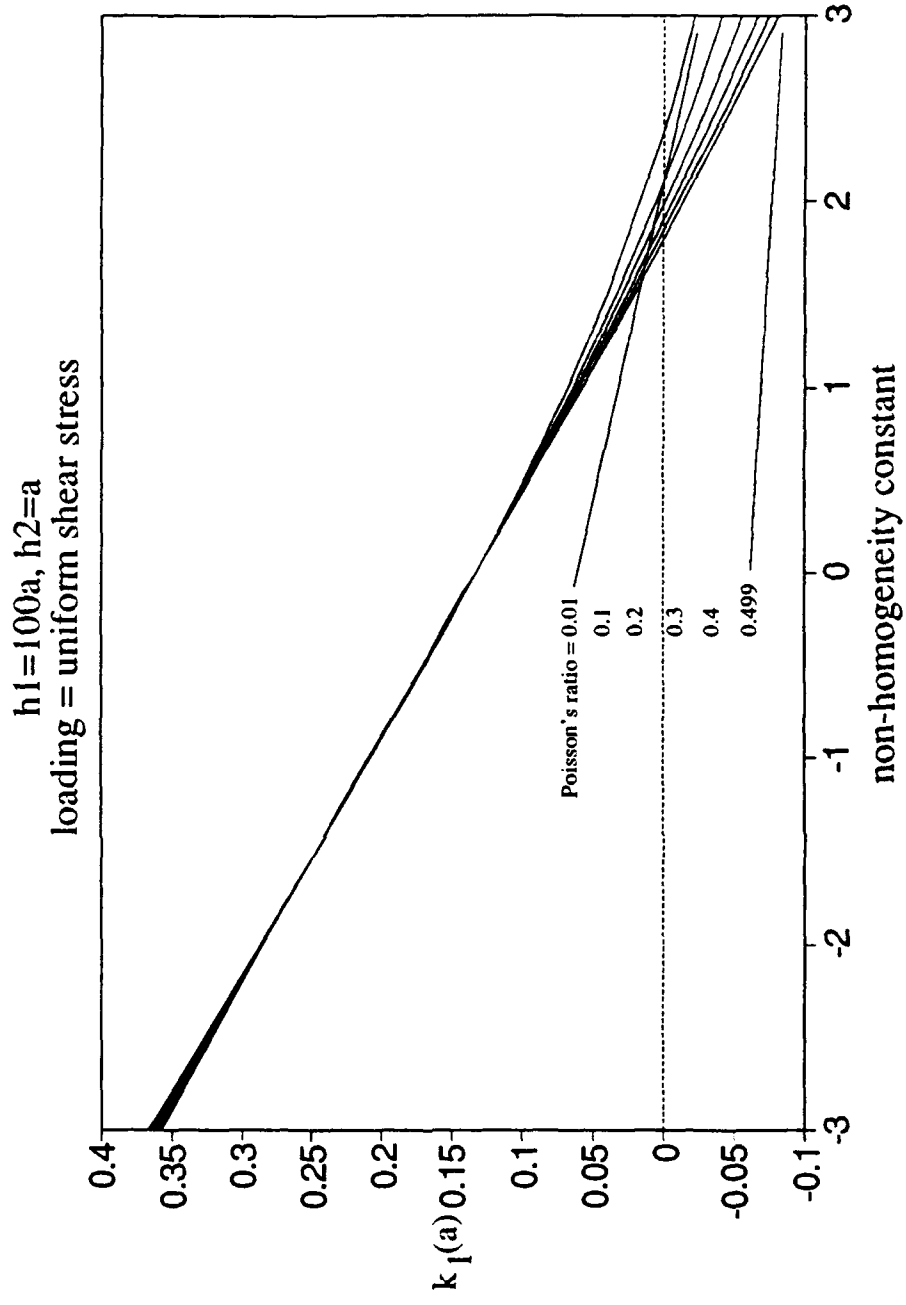

Figure 36. Normalized Mode I SIF of interface crack for h_1=100a, h_2=a at ν=0.01, 0.1, 0.2, 0.3, 0.4, 0.499 under loading of uniform shear.

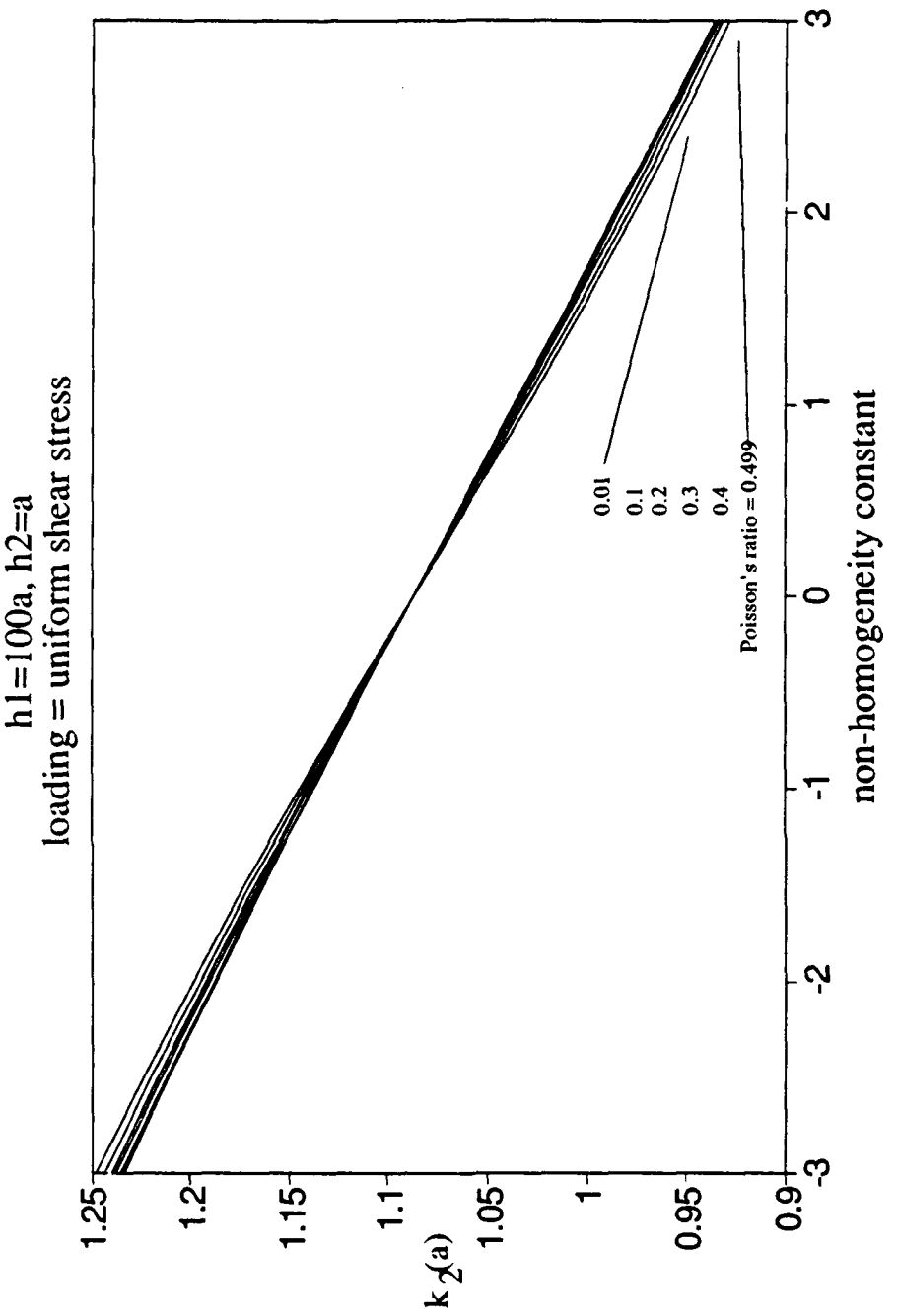

Figure 37. Normalized Mode II SIF of interface crack for h_1=100a, h_2=a at ν=0.01, 0.1, 0.2, 0.3, 0.4, 0.499 under loading of uniform shear.

of the relative crack surface movements on either half of the crack, as seen in Figure 40 and Figure 41. The implication of this behavior is quite different from the horizontal COD under uniform normal stress. Negative vertical COD is not permissible for an originally closed crack because it means the crack surfaces have penetrated each other. And as have been indicated earlier, in this case the crack would remain closed for some portion and the problem would have to be reformulated.

Figure 42 through Figure 45 show crack opening displacements for the case otherwise the same as those shown in Figure 38 through Figure 41 except $\gamma = 3.0$. One easily sees the difference in scale between corresponding displacement component in these two groups. The former represents when material 2 is very soft ($\gamma = -3.0$) therefore crack opening displacements are much larger than when it is very stiff ($\gamma = 3.0$). There is a peculiar behavior in the horizontal component of COD under normal stress as well as the vertical component od COD under uniform shear; that is in addition to the zero movement at the center of the crack, there are two additional zeroes.

The angle of probable crack extension at crack tip $x = a$ as measured from the x axis as a function of the nonhomogeneity constant is shown in Figure 46 and Figure 47. Because the uniform shear loading case shows negative Mode I SIF which requires problem reformulation due to portion of the crack not being open as discussed earlier, only the uniform normal stress loading is investigated. Generally, the two figures display the same trend; (1). For the same geometry, a shear modulus of the nonhomogeneous material going from weak to stiff will see the angle of crack extension change from large to small, and in the case where the two materials of the

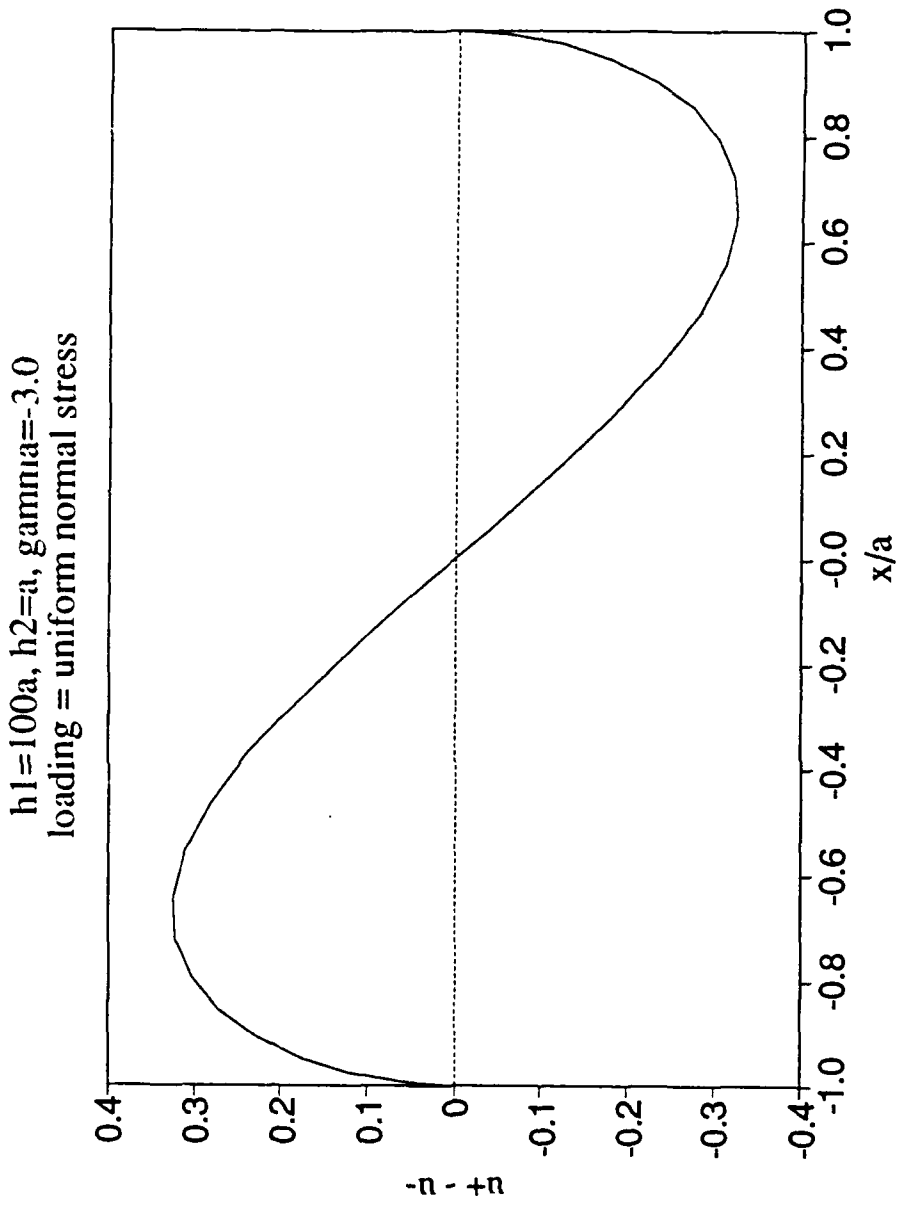

Figure 38. Crack opening displacements ($u^+ - u^-$) of interface crack for h_1=100a, h_2=a, γ= -3.0 under loading of uniform normal stress.

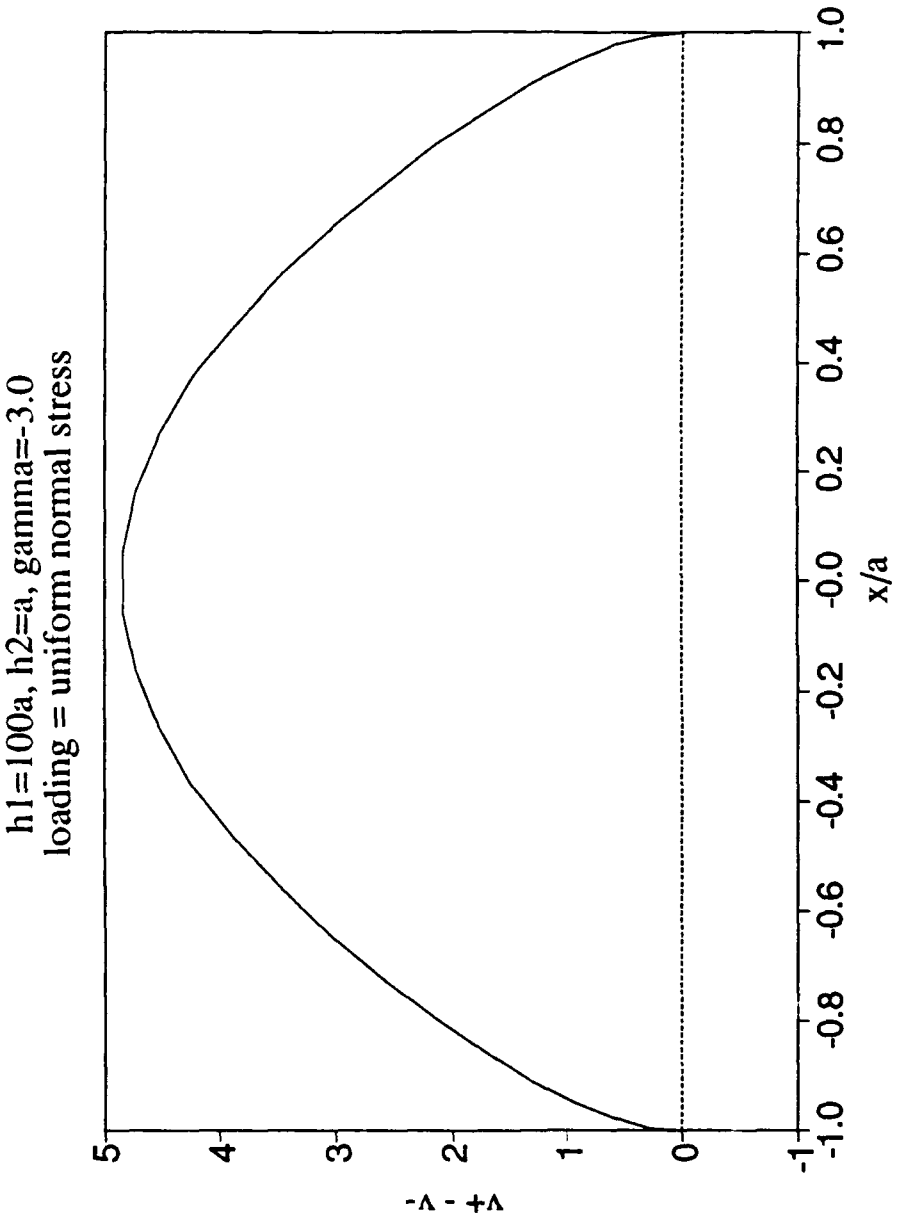

Figure 39. Crack opening displacements ($v^+ - v^-$) of interface crack for h_1=100a, h_2=a, γ= -3.0 under loading of uniform normal stress.

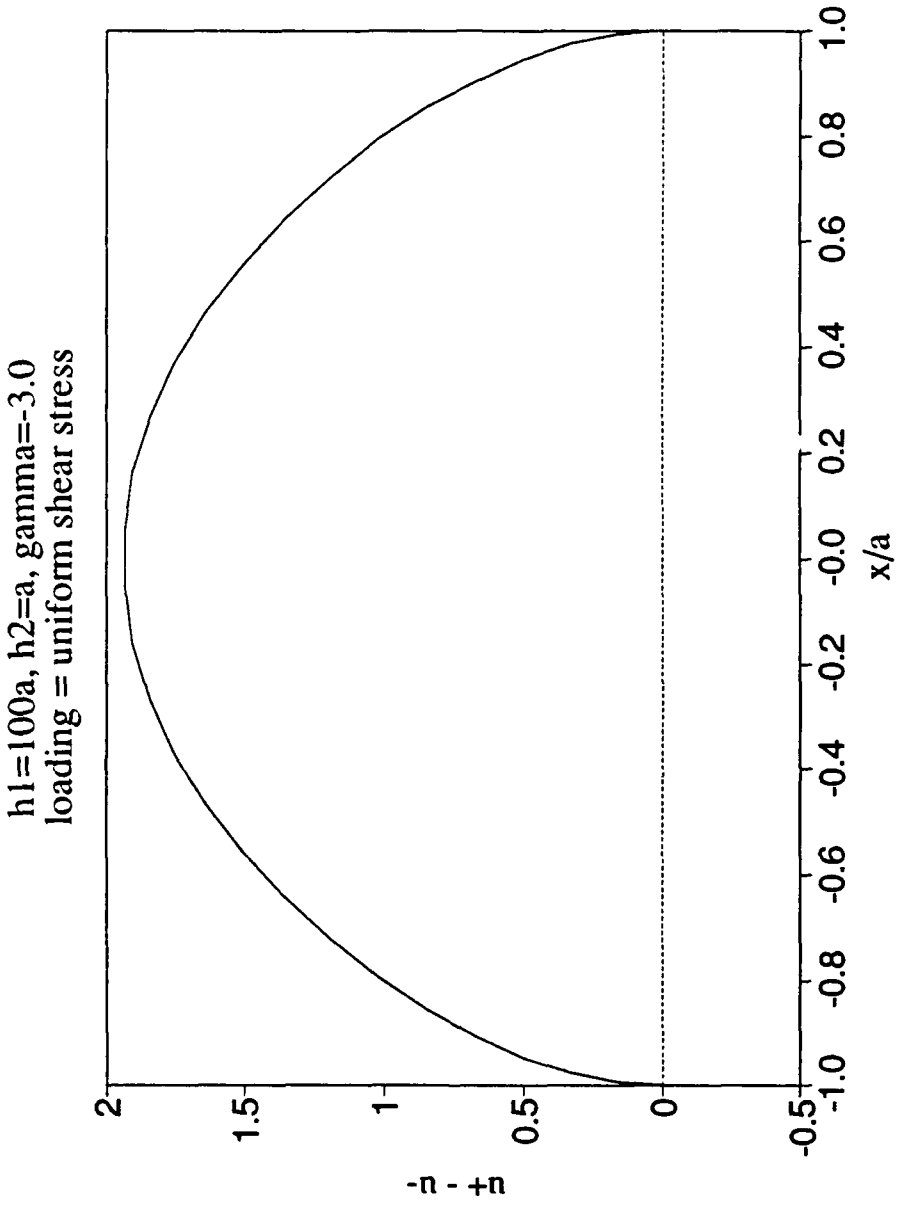

Figure 40. Crack opening displacements ($u^+ - u^-$) of interface crack for h_1=100a, h_2=a, γ= -3.0 under loading of uniform shear.

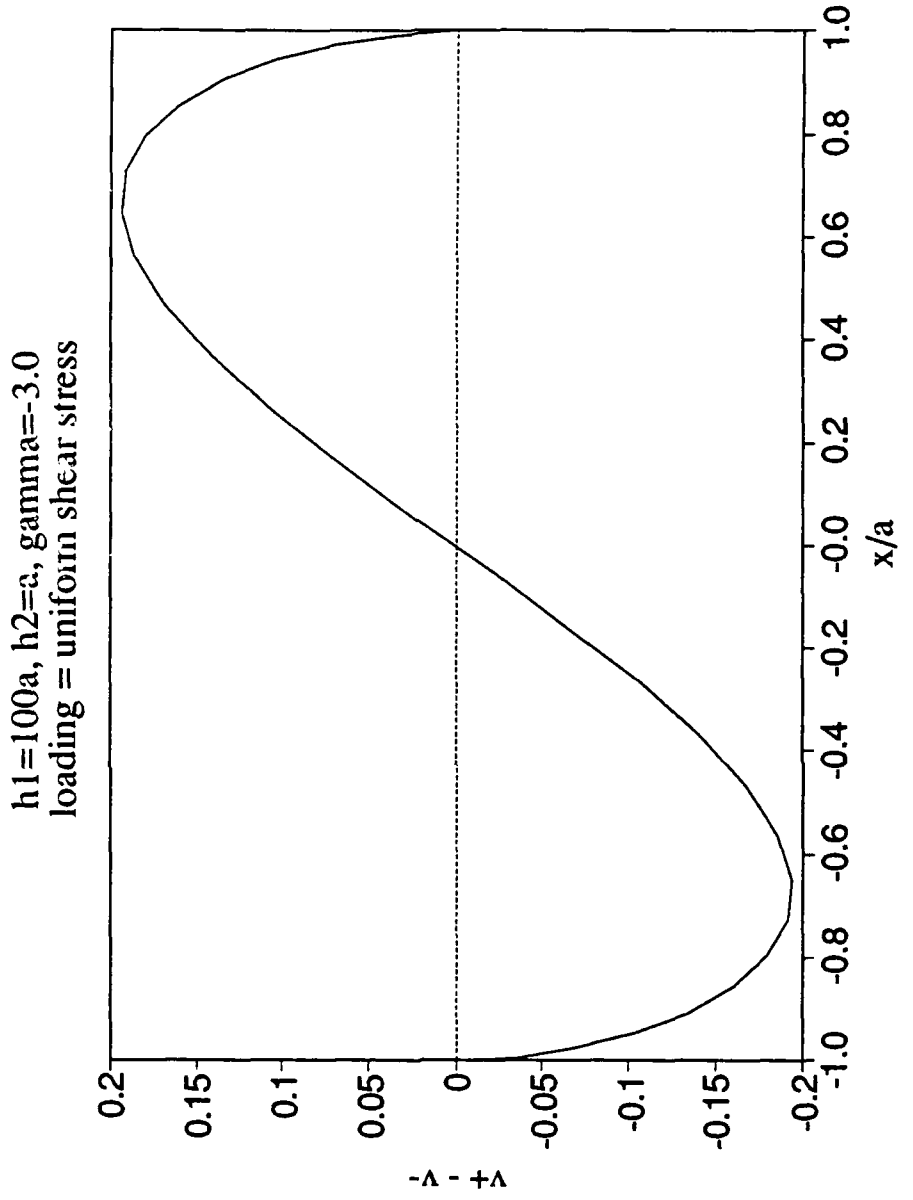

Figure 41. Crack opening displacements ($v^+ - v^-$) of interface crack for h_1=100a, h_2=a, γ= -3.0 under loading of uniform shear.

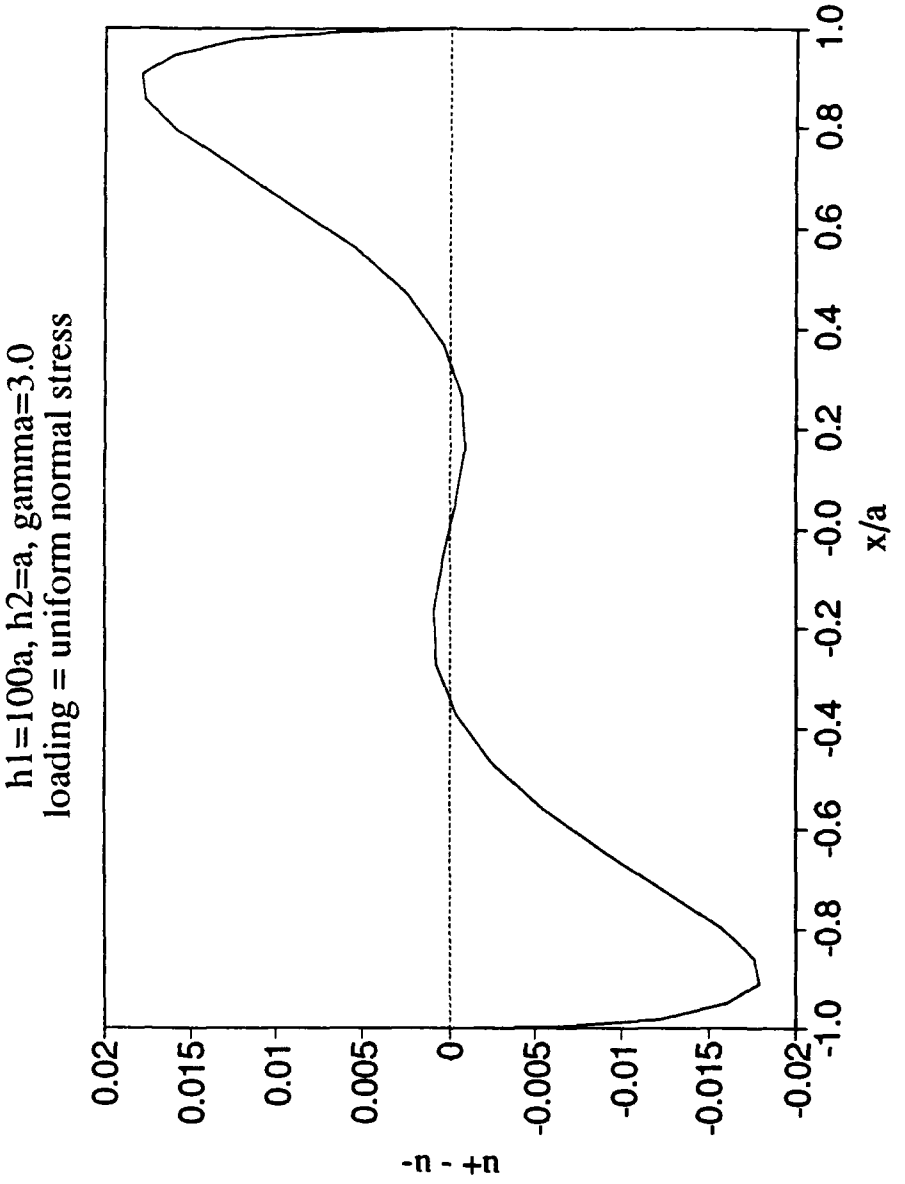

Figure 42. Crack opening displacements ($u^+ - u^-$) of interface crack for h_1=100a, h_2=a, γ=3.0 under loading of uniform normal stress.

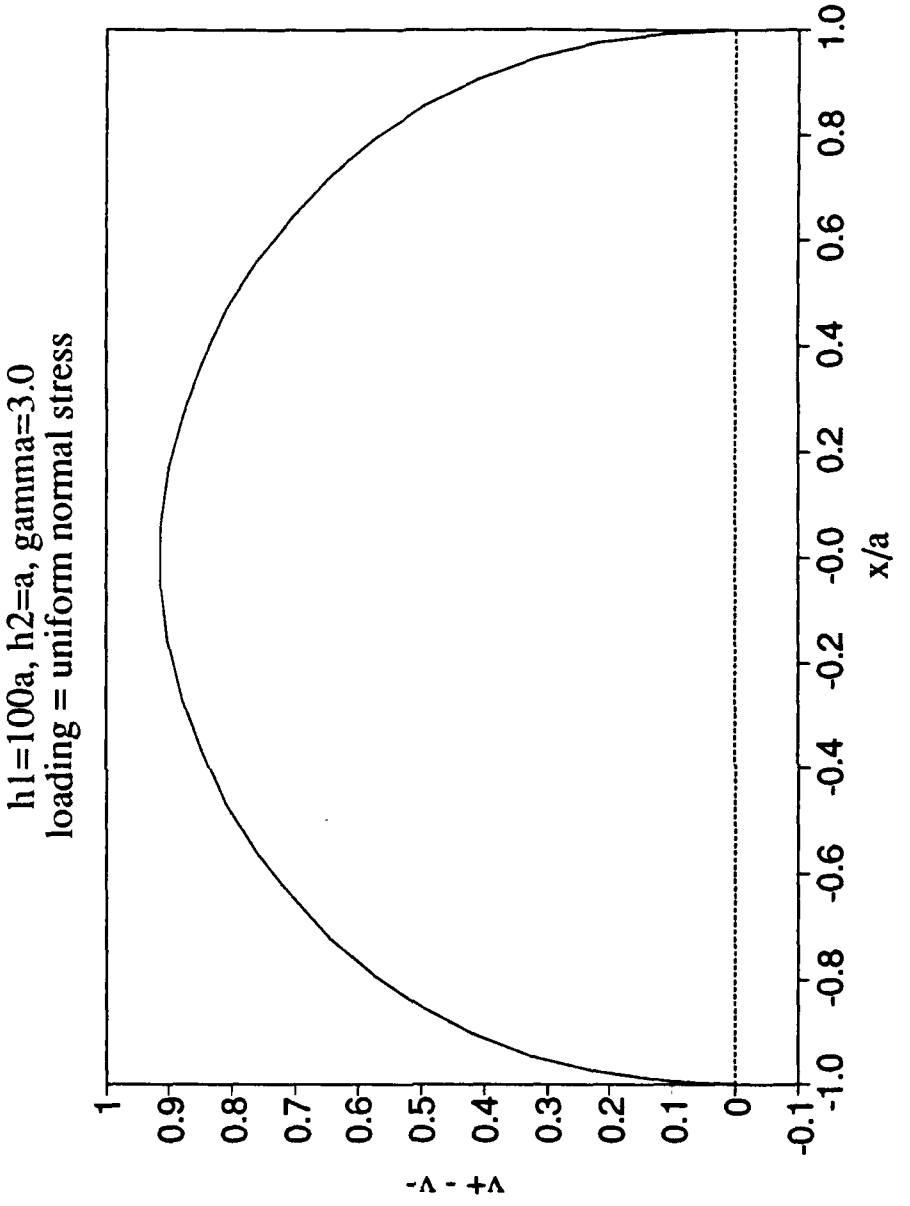

Figure 43. Crack opening displacements ($v^+ - v^-$) of interface crack for h_1=100a, h_2=a, γ=3.0 under loading of uniform normal stress.

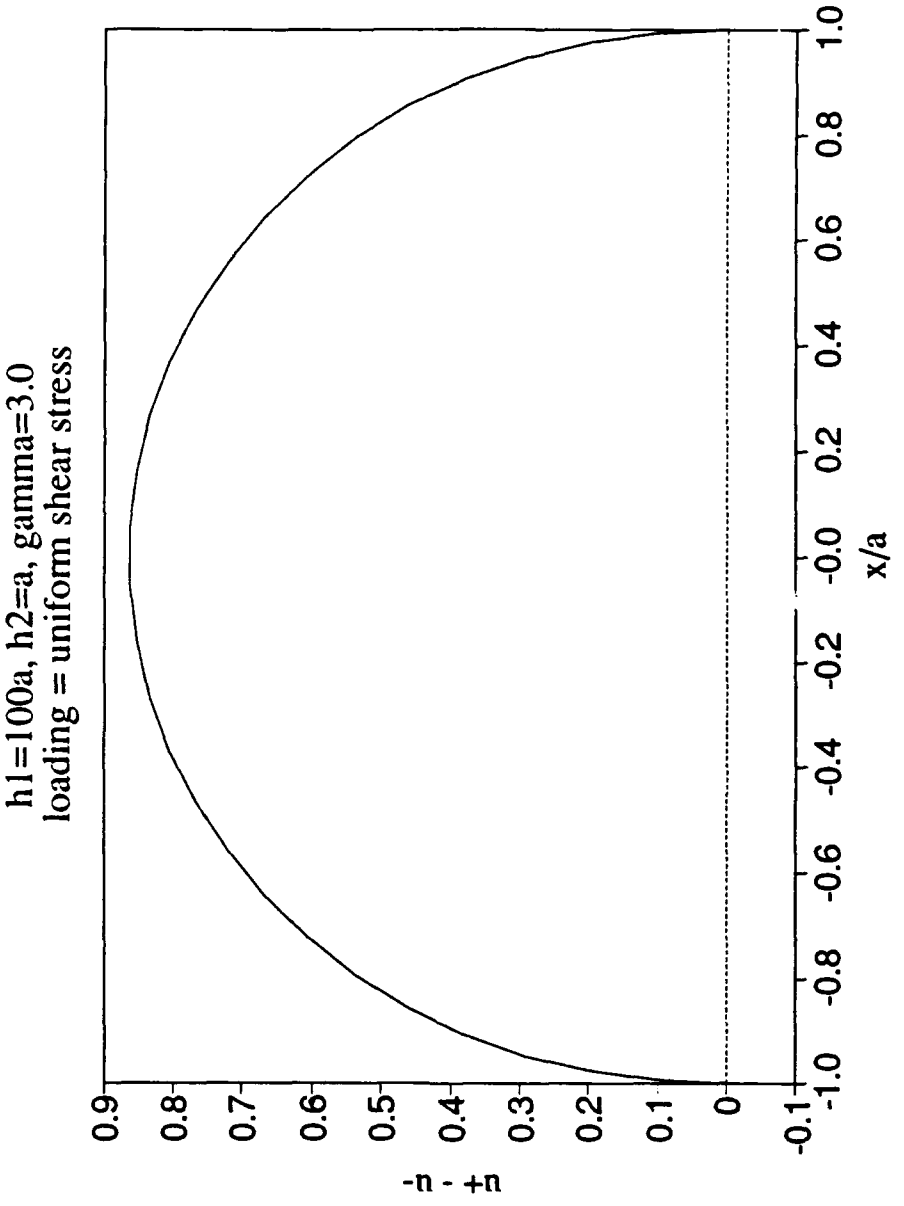

Figure 44. Crack opening displacements ($u^+ - u^-$) of interface crack for h_1=100a, h_2=a, γ=3.0 under loading of uniform shear.

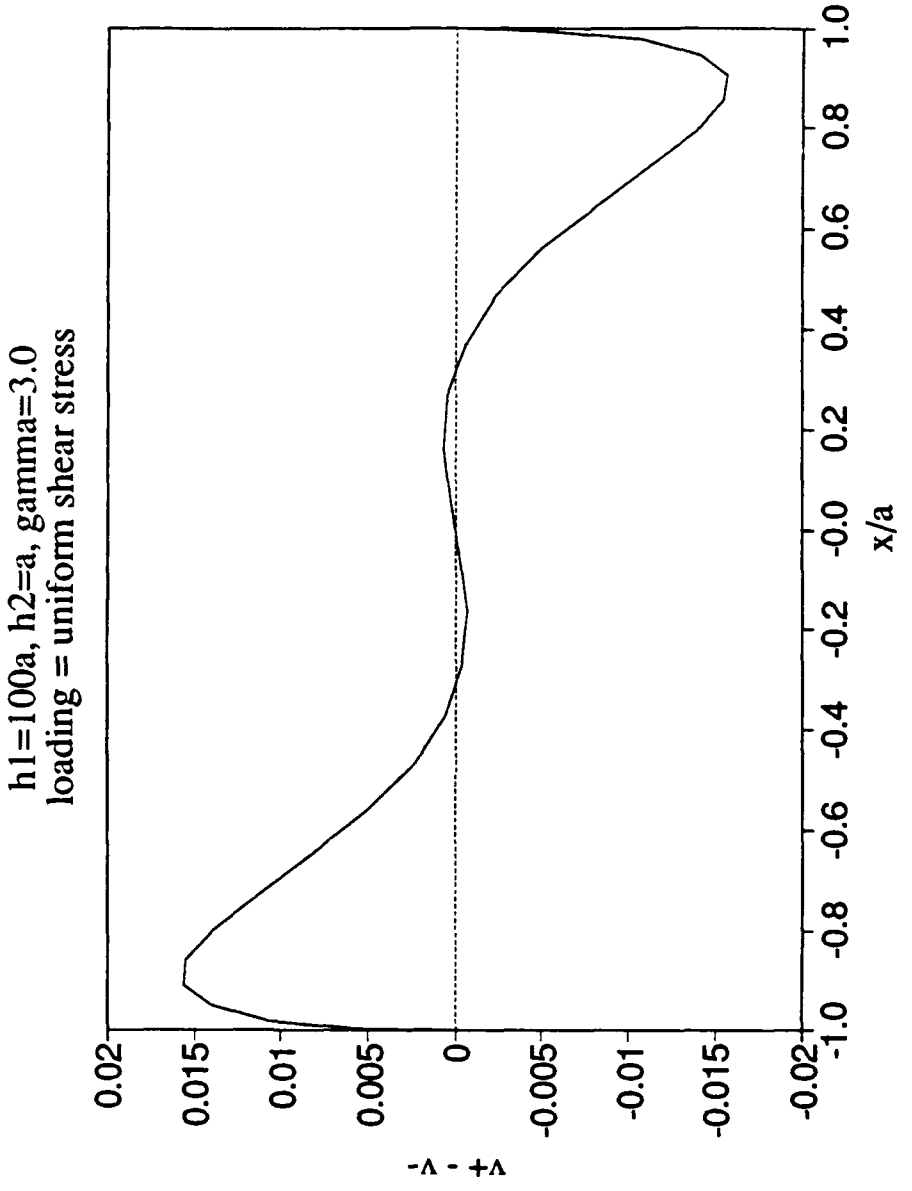

Figure 45. Crack opening displacements ($v^+ - v^-$) of interface crack for h_1=100a, h_2=a, γ=3.0 under loading of uniform shear.

same thicknesses from positive to negative. (2). A decrease in the relative ligament size will tend to discourage the trend describe in (1). Both explain the fact that crack tend to grow in the direction where the combination of material properties and geometry are favorable for such growth, namely a less stiff material property or a thinner ligament size. Again, the case $h_1 = 100a$, $h_2 = 100a$ and $h_1 = 100a$, $h_2 = 10a$ have the same angle of extension throughout the whole range of nonhomogeneity constant as can be seen in Figure 46. Similarly, the case $h_1 = 100a$, $h_2 = a$ and $h_1 = 10a$, $h_2 = a$ show exactly the same behavior as seen in Figure 47.

Table III through Table XX list the Mode I and Mode II stress intensity factors under the two loadings for relative dimensions No. 1 through No. 10 given in Table II.

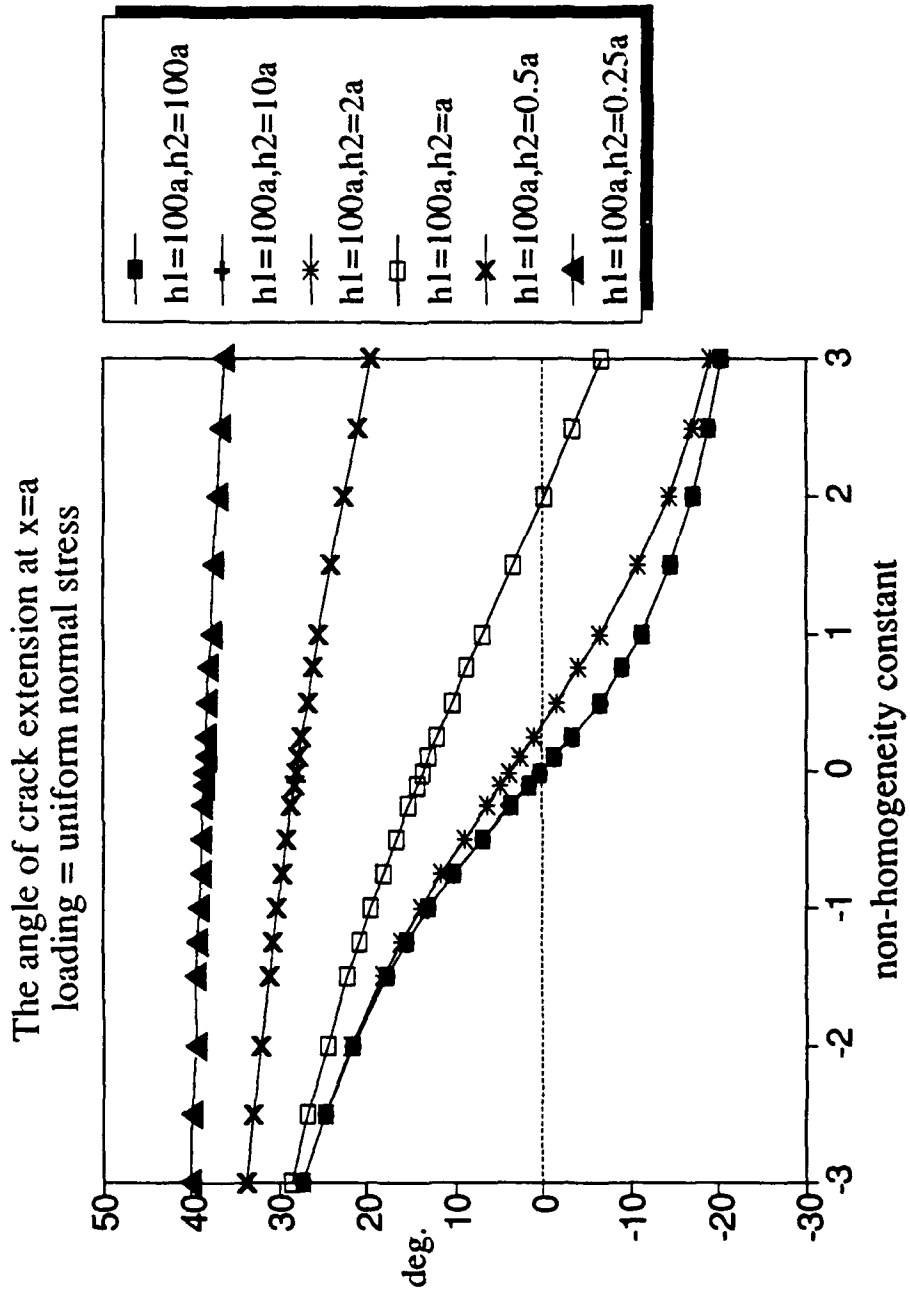

Figure 46. The angle of crack extension at x=a for h_1=100a, h_2=100a, 10a, 2a, a, 0.5a, 0.25a, respectively.

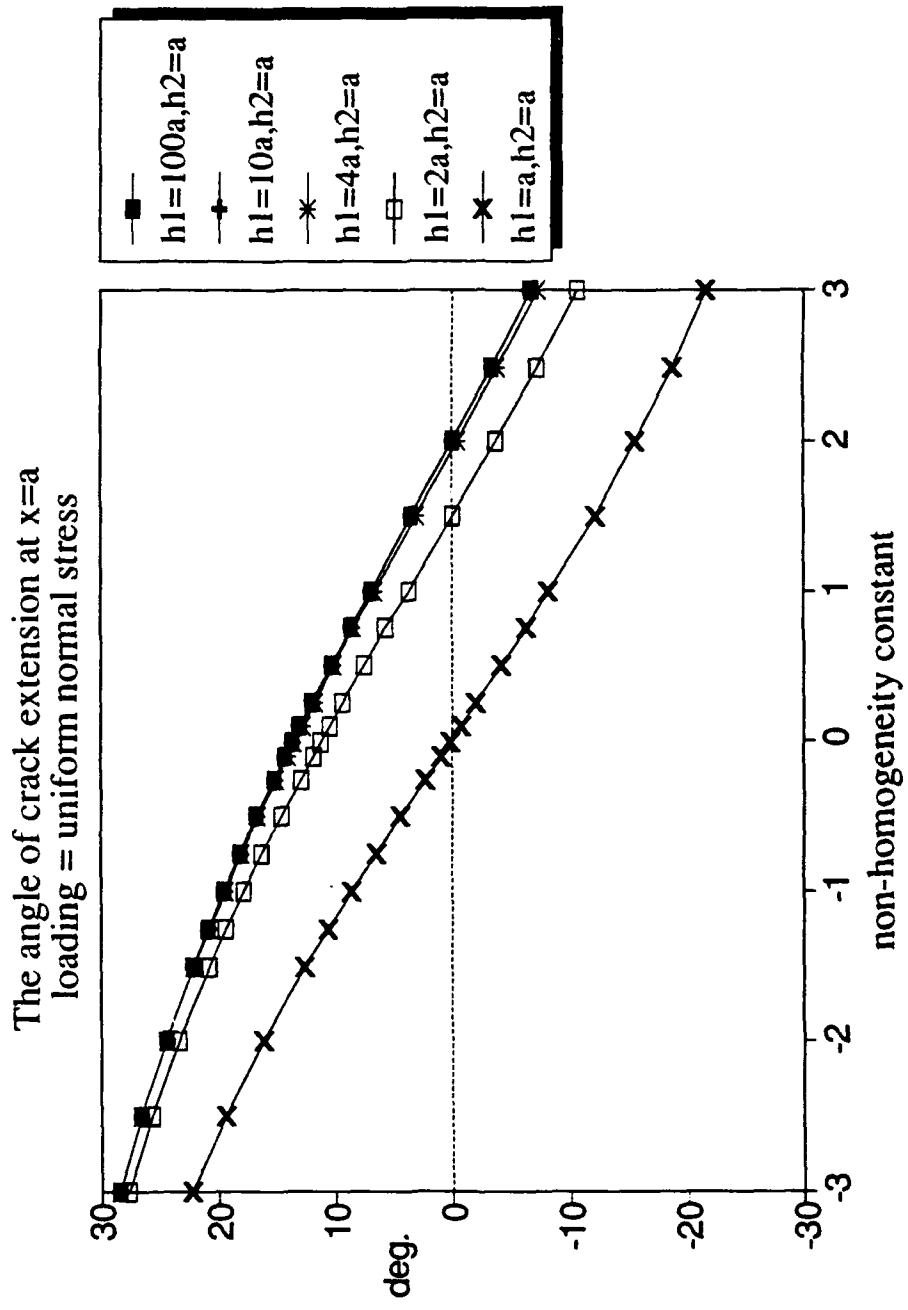

Figure 47. The angle of crack extension at x=a for h_2=a, h_1=10a, 4a, 2a, a, respectively.

Table III. Normalized stress intensity factors and strain energy release rates for h_1=100a, h_2=10a, ν = 0.3, when $\gamma < 0$.

	uniform normal stress			uniform shear		
γ	G/G_0	$k_1(a)/p_0a^{1/2}$	$k_2(a)/p_0a^{1/2}$	G/G_0	$k_1(a)/q_0a^{1/2}$	$k_2(a)/q_0a^{1/2}$
-0.01	1.008	1.011	-0.002	1.008	0.002	1.004
-0.1	1.087	1.043	-0.013	1.033	0.013	1.016
-0.25	1.209	1.099	-0.034	1.074	0.032	1.036
-0.5	1.437	1.197	-0.073	1.138	0.065	1.065
-0.75	1.694	1.296	-0.116	1.198	0.097	1.090
-1.0	1.978	1.397	-0.161	1.255	0.129	1.113
-1.25	2.291	1.499	-0.210	1.309	0.159	1.133
-1.5	2.635	1.602	-0.261	1.360	0.188	1.151
-2.0	3.422	1.812	-0.371	1.460	0.243	1.184
-2.5	4.350	2.027	-0.489	1.555	0.293	1.212
-3.0	5.432	2.248	-0.615	1.648	0.339	1.238

Table IV. Normalized stress intensity factors and strain energy release rates for h_1=100a, h_2=10a, ν = 0.3, when $\gamma > 0$.

	uniform normal stress			uniform shear		
γ	$G/G_0^{(1)}$	$k_1(a)/p_0a^{1/2}$	$k_2(a)/p_0a^{1/2}$	$G/G_0^{(2)}$	$k_1(a)/q_0a^{1/2}$	$k_2(a)/q_0a^{1/2}$
0.1	0.950	0.975	0.012	0.978	-0.012	0.989
0.25	0.870	0.932	0.028	0.938	-0.029	0.968
0.5	0.775	0.879	0.050	0.880	-0.053	0.937
0.75	0.715	0.843	0.067	0.835	-0.073	0.911
1.0	0.674	0.817	0.081	0.801	-0.089	0.891
1.5	0.624	0.784	0.103	0.751	-0.113	0.859
2.0	0.596	0.763	0.120	0.715	-0.131	0.836
2.5	0.577	0.748	0.132	0.688	-0.144	0.817
3.0	0.564	0.737	0.142	0.667	-0.155	0.802

Table V. Normalized stress intensity factors and strain energy release rates for h_1=100a, h_2=2a, ν = 0.3, when $\gamma < 0$.

	uniform normal stress			uniform shear		
γ	G/G_0	$k_1(a)/p_0a^{1/2}$	$k_2(a)/p_0a^{1/2}$	G/G_0	$k_1(a)/q_0a^{1/2}$	$k_2(a)/q_0a^{1/2}$
-0.01	1.361	1.166	-0.038	1.091	0.034	1.044
-0.1	1.415	1.189	-0.049	1.107	0.043	1.051
-0.25	1.513	1.228	-0.068	1.134	0.059	1.063
-0.5	1.699	1.299	-0.102	1.180	0.085	1.083
-0.75	1.913	1.376	-0.140	1.227	0.112	1.102
-1.0	2.159	1.458	-0.182	1.275	0.140	1.120
-1.25	2.439	1.545	-0.226	1.322	0.167	1.138
-1.5	2.754	1.637	-0.274	1.370	0.193	1.154
-2.0	3.495	1.831	-0.379	1.464	0.245	1.185
-2.5	4.393	2.037	-0.493	1.557	0.294	1.213
-3.0	5.457	2.253	-0.617	1.649	0.340	1.238

Table VI. Normalized stress intensity factors and strain energy release rates for h_1=100a, h_2=2a, ν = 0.3, when $\gamma > 0$.

	uniform normal stress			uniform shear		
γ	G/G_0	$k_1(a)/p_0a^{1/2}$	$k_2(a)/p_0a^{1/2}$	G/G_0	$k_1(a)/q_0a^{1/2}$	$k_2(a)/q_0a^{1/2}$
0.1	1.298	1.139	-0.025	1.072	0.023	1.035
0.25	1.220	1.105	-0.009	1.046	0.008	1.023
0.5	1.107	1.052	0.016	1.004	-0.015	1.002
0.75	1.013	1.006	0.037	0.965	-0.036	0.981
1.0	0.934	0.965	0.056	0.927	-0.056	0.961
1.5	0.815	0.898	0.087	0.860	-0.087	0.923
2.0	0.732	0.849	0.110	0.803	-0.115	0.888
2.5	0.674	0.811	0.128	0.754	-0.135	0.958
3.0	0.633	0.783	0.141	0.714	-0.150	0.832

Table VII. Normalized stress intensity factors and strain energy release rates for h_1=100a, h_2=a, ν = 0.3, when $\gamma < 0$.

	uniform normal stress			uniform shear		
γ	G/G_0	$k_1(a)/p_0a^{1/2}$	$k_2(a)/p_0a^{1/2}$	G/G_0	$k_1(a)/q_0a^{1/2}$	$k_2(a)/q_0a^{1/2}$
-0.01	2.324	1.513	-0.186	1.201	0.134	1.088
-0.1	2.389	1.533	-0.197	1.214	0.140	1.093
-0.25	2.502	1.567	-0.216	1.235	0.152	1.101
-0.5	2.706	1.626	-0.249	1.271	0.170	1.114
-0.75	2.932	1.689	-0.284	1.307	0.189	1.128
-1.0	3.180	1.754	-0.321	1.345	0.209	1.141
-1.25	3.454	1.823	-0.360	1.383	0.228	1.154
-1.5	3.755	1.896	-0.401	1.422	0.247	1.167
-2.0	4.448	2.051	-0.491	1.502	0.286	1.192
-2.5	5.273	2.219	-0.590	1.584	0.324	1.216
-3.0	6.250	2.400	-0.698	1.668	0.361	1.240

Table VIII. Normalized stress intensity factors and strain energy release rates for h_1=100a, h_2=a, ν = 0.3, when $\gamma > 0$.

	uniform normal stress			uniform shear		
γ	G/G_0	$k_1(a)/p_0a^{1/2}$	$k_2(a)/p_0a^{1/2}$	G/G_0	$k_1(a)/q_0a^{1/2}$	$k_2(a)/q_0a^{1/2}$
0.1	2.249	1.490	-0.173	1.186	0.126	1.082
0.25	2.151	1.458	-0.156	1.166	0.115	1.074
0.5	2.001	1.409	-0.129	1.134	0.097	1.060
0.75	1.865	1.362	-0.103	1.103	0.079	1.047
1.0	1.743	1.318	-0.079	1.073	0.062	1.034
1.5	1.534	1.238	-0.036	1.016	0.029	1.008
2.0	1.365	1.168	0.001	0.965	-0.001	0.982
2.5	1.226	1.107	0.034	0.918	-0.029	0.958
3.0	1.113	1.053	0.063	0.876	-0.055	0.934

Table IX. Normalized stress intensity factors and strain energy release rates for h_1=100a, h_2=0.5a, ν = 0.3, when $\gamma < 0$.

	uniform normal stress			uniform shear		
γ	G/G_0	$k_1(a)/p_0a^{1/2}$	$k_2(a)/p_0a^{1/2}$	G/G_0	$k_1(a)/q_0a^{1/2}$	$k_2(a)/q_0a^{1/2}$
-0.01	6.223	2.400	-0.682	1.359	0.319	1.121
-0.1	6.333	2.419	-0.694	1.369	0.323	1.125
-0.25	6.522	2.452	-0.715	1.387	0.330	1.131
-0.5	6.852	2.507	-0.751	1.417	0.342	1.140
-0.75	7.201	2.565	-0.788	1.448	0.354	1.150
-1.0	7.572	2.625	-0.826	1.480	0.365	1.160
-1.25	7.965	2.686	-0.866	1.512	0.377	1.170
-1.5	8.381	2.749	-0.906	1.545	0.389	1.180
-2.0	9.288	2.882	-0.991	1.612	0.413	1.201
-2.5	10.304	3.022	-1.082	1.682	0.437	1.221
-3.0	11.441	3.171	-1.178	1.753	0.462	1.241

Table X. Normalized stress intensity factors and strain energy release rates for h_1=100a, h_2=0.5a, ν = 0.3, when $\gamma > 0$.

	uniform normal stress			uniform shear		
γ	G/G_0	$k_1(a)/p_0a^{1/2}$	$k_2(a)/p_0a^{1/2}$	G/G_0	$k_1(a)/q_0a^{1/2}$	$k_2(a)/q_0a^{1/2}$
0.1	6.091	2.376	-0.667	1.346	0.314	1.117
0.25	5.917	2.345	-0.647	1.329	0.307	1.111
0.5	5.640	2.294	-0.614	1.301	0.295	1.102
0.75	5.380	2.245	-0.583	1.273	0.283	1.092
1.0	5.133	2.197	-0.552	1.247	0.272	1.083
1.5	4.682	2.107	-0.494	1.196	0.249	1.065
2.0	4.281	2.022	-0.439	1.148	0.227	1.047
2.5	3.924	1.943	-0.387	1.103	0.205	1.030
3.0	3.605	1.868	-0.339	1.062	0.184	1.014

Table XI. Normalized stress intensity factors and strain energy release rates for h_1=100a, h_2=0.25a, ν = 0.3, when $\gamma < 0$.

	uniform normal stress			uniform shear		
γ	G/G_0	$k_1(a)/p_0a^{1/2}$	$k_2(a)/p_0a^{1/2}$	G/G_0	$k_1(a)/q_0a^{1/2}$	$k_2(a)/q_0a^{1/2}$
-0.01	26.103	4.642	-2.134	1.673	0.540	1.175
-0.1	26.369	4.664	-2.149	1.683	0.543	1.178
-0.25	26.818	4.699	-2.176	1.699	0.548	1.183
-0.5	27.586	4.760	-2.220	1.725	0.555	1.190
-0.75	28.379	4.822	-2.264	1.752	0.563	1.198
-1.0	29.297	4.885	-2.310	1.779	0.570	1.206
-1.25	30.041	4.949	-2.356	1.807	0.578	1.214
-1.5	30.913	5.014	-2.403	1.835	0.586	1.222
-2.0	32.740	5.148	-2.498	1.893	0.601	1.238
-2.5	34.687	5.286	-2.597	1.951	0.616	1.254
-3.0	36.760	5.429	-2.700	2.012	0.632	1.270

Table XII. Normalized stress intensity factors and strain energy release rates for h_1=100a, h_2=0.25a, ν = 0.3, when $\gamma > 0$.

	uniform normal stress			uniform shear		
γ	G/G_0	$k_1(a)/p_0a^{1/2}$	$k_2(a)/p_0a^{1/2}$	G/G_0	$k_1(a)/q_0a^{1/2}$	$k_2(a)/q_0a^{1/2}$
0.1	25.783	4.616	-2.115	1.662	0.537	1.172
0.25	25.353	4.581	-2.090	1.647	0.532	1.167
0.5	24.654	4.523	-2.048	1.621	0.525	1.160
0.75	23.977	4.467	-2.006	1.596	0.518	1.152
1.0	23.321	4.411	-1.966	1.571	0.510	1.145
1.5	22.070	4.303	-1.886	1.523	0.495	1.130
2.0	20.894	4.198	-1.809	1.477	0.481	1.116
2.5	19.790	4.097	-1.734	1.432	0.466	1.102
3.0	18.753	3.999	-1.662	1.389	0.452	1.088

Table XIII. Normalized stress intensity factors and strain energy release rates for h_1=10a, h_2=a, ν = 0.3, when $\gamma < 0$.

	uniform normal stress			uniform shear		
γ	G/G_0	$k_1(a)/p_0a^{1/2}$	$k_2(a)/p_0a^{1/2}$	G/G_0	$k_1(a)/q_0a^{1/2}$	$k_2(a)/q_0a^{1/2}$
-0.01	2.325	1.513	-0.186	1.205	0.134	1.090
-0.1	2.389	1.533	-0.197	1.217	0.141	1.094
-0.25	2.502	1.567	-0.216	1.238	0.152	1.102
-0.5	2.706	1.626	-0.249	1.273	0.171	1.115
-0.75	2.932	1.689	-0.284	1.310	0.190	1.129
-1.0	3.180	1.754	-0.321	1.347	0.209	1.142
-1.25	3.454	1.823	-0.360	1.385	0.228	1.155
-1.5	3.756	1.896	-0.401	1.424	0.247	1.168
-2.0	4.448	2.051	-0.491	1.504	0.286	1.193
-2.5	5.273	2.219	-0.590	1.586	0.324	1.217
-3.0	6.250	2.401	-0.698	1.669	0.361	1.240

Table XIV. Normalized stress intensity factors and strain energy release rates for h_1=10a, h_2=a, ν = 0.3, when $\gamma > 0$.

	uniform normal stress			uniform shear		
γ	G/G_0	$k_1(a)/p_0a^{1/2}$	$k_2(a)/p_0a^{1/2}$	G/G_0	$k_1(a)/q_0a^{1/2}$	$k_2(a)/q_0a^{1/2}$
0.1	2.249	1.490	-0.173	1.190	0.126	1.084
0.25	2.151	1.458	-0.156	1.170	0.115	1.076
0.5	2.001	1.409	-0.129	1.138	0.097	1.063
0.75	1.865	1.362	-0.103	1.108	0.079	1.049
1.0	1.742	1.318	-0.079	1.078	0.062	1.036
1.5	1.535	1.238	-0.036	1.023	0.030	1.011
2.0	1.365	1.168	-0.001	0.973	-0.001	0.987
2.5	1.227	1.107	0.034	0.928	-0.030	0.963
3.0	1.114	1.053	0.063	0.886	-0.056	0.940

Table XV. Normalized stress intensity factors and strain energy release rates for $h_1=4a$, $h_2=a$, $\nu = 0.3$, when $\gamma < 0$.

	uniform normal stress			uniform shear		
γ	G/G_0	$k_1(a)/p_0a^{1/2}$	$k_2(a)/p_0a^{1/2}$	G/G_0	$k_1(a)/q_0a^{1/2}$	$k_2(a)/q_0a^{1/2}$
-0.01	2.337	1.518	-0.184	1.256	0.135	1.113
-0.1	2.401	1.537	-0.195	1.267	0.141	1.117
-0.25	2.514	1.571	-0.214	1.286	0.153	1.124
-0.5	2.717	1.630	-0.247	1.319	0.172	1.136
-0.75	2.942	1.692	-0.282	1.353	0.191	1.147
-1.0	3.191	1.758	-0.319	1.388	0.210	1.159
-1.25	3.464	1.826	-0.358	1.423	0.230	1.171
-1.5	3.765	1.899	-0.400	1.460	0.249	1.182
-2.0	4.456	2.053	-0.490	1.536	0.288	1.205
-2.5	5.281	2.221	-0.589	1.614	0.326	1.228
-3.0	6.257	2.402	-0.697	1.694	0.363	1.250

Table XVI. Normalized stress intensity factors and strain energy release rates for $h_1=4a$, $h_2=a$, $\nu = 0.3$, when $\gamma > 0$.

	uniform normal stress			uniform shear		
γ	G/G_0	$k_1(a)/p_0a^{1/2}$	$k_2(a)/p_0a^{1/2}$	G/G_0	$k_1(a)/q_0a^{1/2}$	$k_2(a)/q_0a^{1/2}$
0.1	2.262	1.494	-0.171	1.242	0.126	1.107
0.25	2.164	1.463	-0.153	1.224	0.115	1.100
0.5	2.014	1.414	-0.126	1.195	0.097	1.089
0.75	1.880	1.367	-0.100	1.167	0.079	1.077
1.0	1.758	1.342	-0.076	1.140	0.061	1.066
1.5	1.550	1.245	-0.032	1.089	0.027	1.043
2.0	1.382	1.175	0.006	1.042	-0.005	1.021
2.5	1.244	1.115	0.039	0.999	-0.035	0.999
3.0	1.132	1.062	0.068	0.957	-0.062	0.977

Table XVII. Normalized stress intensity factors and strain energy release rates for $h_1=2a$, $h_2=a$, $\nu = 0.3$, when $\gamma < 0$.

	uniform normal stress			uniform shear		
γ	G/G_0	$k_1(a)/p_0a^{1/2}$	$k_2(a)/p_0a^{1/2}$	G/G_0	$k_1(a)/q_0a^{1/2}$	$k_2(a)/q_0a^{1/2}$
-0.01	2.478	1.566	-0.156	1.455	0.120	1.200
-0.1	2.542	1.585	-0.168	1.466	0.127	1.204
-0.25	2.653	1.618	-0.187	1.483	0.140	1.210
-0.5	2.854	1.675	-0.221	1.513	0.161	1.220
-0.75	3.077	1.735	-0.258	1.544	0.183	1.229
-1.0	3.323	1.799	-0.296	1.575	0.204	1.238
-1.25	3.594	1.866	-0.336	1.607	0.225	1.247
-1.5	3.892	1.936	-0.379	1.639	0.246	1.256
-2.0	4.577	2.087	-0.471	1.706	0.287	1.274
-2.5	5.397	2.252	-0.571	1.775	0.328	1.291
-3.0	6.367	2.430	-0.681	1.846	0.367	1.308

Table XVIII. Normalized stress intensity factors and strain energy release rates for $h_1=2a$, $h_2=a$, $\nu = 0.3$, when $\gamma > 0$.

	uniform normal stress			uniform shear		
γ	G/G_0	$k_1(a)/p_0a^{1/2}$	$k_2(a)/p_0a^{1/2}$	G/G_0	$k_1(a)/q_0a^{1/2}$	$k_2(a)/q_0a^{1/2}$
0.1	2.403	1.544	-0.143	1.442	0.111	1.196
0.25	2.307	1.514	-0.125	1.425	0.098	1.190
0.5	2.159	1.466	-0.096	1.396	0.077	1.179
0.75	2.026	1.422	-0.069	1.368	0.057	1.168
1.0	1.905	1.380	-0.044	1.340	0.037	1.157
1.5	1.700	1.304	0.002	1.284	-0.002	1.133
2.0	1.532	1.237	0.042	1.229	-0.038	1.108
2.5	1.396	1.179	0.077	1.174	-0.071	1.081
3.0	1.284	1.128	0.108	1.120	-0.101	1.053

Table XIX. Normalized stress intensity factors and strain energy release rates for $h_1=a$, $h_2=a$, $\nu = 0.3$, when $\gamma < 0$.

	uniform normal stress			uniform shear		
γ	G/G_0	$k_1(a)/p_0a^{1/2}$	$k_2(a)/p_0a^{1/2}$	G/G_0	$k_1(a)/q_0a^{1/2}$	$k_2(a)/q_0a^{1/2}$
-0.01	3.303	1.817	-0.001	1.864	0.001	1.365
-0.1	3.367	1.835	-0.014	1.881	0.010	1.371
-0.25	3.480	1.865	-0.035	1.908	0.026	1.381
-0.5	3.682	1.918	-0.072	1.953	0.052	1.397
-0.75	3.906	1.973	-0.111	1.997	0.079	1.411
-1.0	4.152	2.032	-0.152	2.040	0.107	1.424
-1.25	4.422	2.094	-0.195	2.082	0.134	1.437
-1.5	4.719	2.159	-0.241	2.123	0.161	1.448
-2.0	5.401	2.299	-0.338	2.202	0.216	1.468
-2.5	6.215	2.453	-0.444	2.277	0.269	1.485
-3.0	7.178	2.620	-0.559	2.349	0.320	1.499

Table XX. Normalized stress intensity factors and strain energy release rates for $h_1=a$, $h_2=a$, $\nu = 0.3$, when $\gamma > 0$.

	uniform normal stress			uniform shear		
γ	G/G_0	$k_1(a)/p_0a^{1/2}$	$k_2(a)/p_0a^{1/2}$	G/G_0	$k_1(a)/q_0a^{1/2}$	$k_2(a)/q_0a^{1/2}$
0.1	3.228	1.797	0.013	1.844	-0.010	1.358
0.25	3.130	1.769	0.033	1.816	-0.025	1.347
0.5	2.979	1.725	0.064	1.769	-0.050	1.329
0.75	2.843	1.684	0.094	1.721	-0.073	1.310
1.0	2.720	1.645	0.122	1.673	-0.095	1.290
1.5	2.508	1.574	0.172	1.577	-0.137	1.248
2.0	2.334	1.512	0.217	1.482	-0.173	1.205
2.5	2.191	1.458	0.256	1.389	-0.204	1.161
3.0	2.073	1.410	0.291	1.300	-0.230	1.117

Chapter 5

Conclusions And Future Work

5.1 Conclusions

For general fracture mechanics problems, a half crack-length to thickness ratio of approximately unity may be the practical limit for applications. If we consider an interface crack problem that involves thin films coatings, a defect in a solid lubricant coating as described in [3] for example, where the material thickness is in the μm (1.0×10^{-6} meter) range, an aspect ratio of one is still only a small defect. The importance of interface cracks in thin films, therefore, can not be overstated.

From the cases of different geometry and material constant combinations computed in this work, we may summarize the following conclusions,

(1). Under uniform normal stress, the dominant Mode I stress intensity factor decreases as property of the nonhomogeneous material changes from "soft" to "stiff"; the nonhomogeneity constant changes from negative to positive. Similarly, the Mode II stress intensity factor under uniform shear shows the same trend.

(2). Again speaking of only the dominant Mode stress intensity factors under respective loading, considering everything else to be equal, a decrease in material thickness, whether it is the homogeneous material or nonhomogeneous material, causes a corresponding increase in stress intensity factor. we see from (1) and (2) two competing factors that would affect stress intensity factors, namely the degree of nonhomogeneity and the material thickness.

(3). Even though the crack tip characteristics are of mixed mode because either material constants and geometry is not symmetric, the nature of the loadings is such

that the primary mode is dominant under respective loading, Mode I is dominant under uniform normal stress and Mode II is dominant under uniform shear. The strain energy release rate under respective loadings therefore follows the trend of only the dominant mode stress intensity factor.

(4). Similar to their effect on the stress intensity factors, the material thickness and the nonhomogeneity constant are the two competing parameters influencing the probable angle of extension of the interface crack. The crack extension angle tends to turn toward the material is "soft" or where the ligament is slim.

(5). Effect of the changes in Poisson's ratio on the stress intensity factors is small, except for very large nonhomogeneity constant ($\gamma < -2.0$). A Poisson's ratio of 0.3 is good for practical purposes.

(6). The most important information that can be obtained from the crack opening displacements, if nothing else, is to see whether any compatibility condition is violated. Because the crack surfaces are surfaces where traction boundary conditions are applied, their displacements must be kept in check to make sure no inter-penetration occurs. When it does, the problem requires reformulation as a crack-contact problem.

5.2 Remarks on future research

Computer software in algebraic manipulation such as REDUCE, MACSYMA, MAPLE and the recently introduced Mathematica which, in contrast to other software and programming languages that deal with numerical operations, excels in doing symbolic computations and has broken new grounds for research in a number of problems previously considered being not feasible because of their inherent analytical

complexities. Coupled with advances in computer hardware in terms of computing speed and available memory as well as software development in user interface, more problems are being attempted with much efficiency. Specific tasks facilitated by these symbolic manipulators in helping to solve research problems similar to this study is the derivation, simplification, and bookkeeping of very large number of terms and expressions in the Fredholm kernels. Without such computer algebra software, it is not possible to solve the 8 by 8 system of linear algebraic equations and to undertake the extensive asymptotic analysis described in this study. Yet what was utilized in this undertaking barely scratch the surface of the many faceted features these symbolic manipulators have to offer. The vast potential of these software is yet to be tapped with the ever expanding progress in computing power that is reaching new horizons everyday.

On the other hand, it is also dangerous to assume these software to be all powerful to solve any kind of problem that is fed into it without the user's careful planning and thinking ahead. Brute force is sure to fail miserably as problems attempted get larger and more complicated, for sometimes the complexity of the task grows exponentially as the problem size increases. It is especially true when one deals with matrix inversion which requires expanding determinants that contain symbolic elements. Case in point is the asymptotic expansion of the 8 by 8 and 7 by 7 determinants described in this work. Without proper analytical ground work, or without correct understanding of the nature of the problem, one has no choice but to rely on raw computing power which resulted in the analysis quickly grinds to a halt. Only after careful planning and comprehension of the available computing resources, as well as devising ways to work around the limitations could one secure a

satisfactory completion of the task. It proves once again that there is still no substitute for sound analytical reasoning. Unlike numerical software, which always returns numbers good or otherwise, symbolic software usually refuses to work when told to accomplish something that is beyond its limitations.

In light of the capabilities symbolic manipulation software afforded us, a number of problems similar in nature to what has been done in this dissertation could, without much difficulty, be solved. Considering the fact that the nature of materials described in this work does not possess a distinct interface, but rather the material composition and properties go though a transition from one to the other. Also consider that as long as the properties of the two materials and in the interfacial zone are continuous, the formulation does not change much. An immediate extension of the present problem would be that a crack parallel to the free surface could exist any where in the interfacial zone.

Cracks of orientations parallel to the y-axis, with the crack spanning the interface, or the crack tip terminating at the interface or approaching the free surface, or an edge crack are also prospective problems of interest. These problems have the same Navier's equations with constant coefficients as in this study. The boundary conditions will be somewhat different and there will only be one unknown density function to be solved. Furthermore, cracks terminating at the interface and crack tip approaching the free surface will have different characteristics from that in this study. But the solution of these problems are all attainable because of the available computer algebra software described earlier.

As has been pointed out in the beginning of this dissertation, one of the common causes that composite materials fail is the existence of residual stresses.

These stresses come about because the temperature which the composite is processed differs considerably from that under which it usually operates. This is also one of the incentives to have a graded interfacial zone. It is therefore very desirable to study the fracture mechanics behavior of this and similar problems under residual stresses caused by thermal mismatch. But until appropriate material property characterizations such as the coefficients of thermal expansion of the graded material are known, proper assumptions will have to be made in order to try problems of this nature.

Acknowledgements

This study was supported by the Office of Naval Research under the contract N00014-89-J3188. Partial support was also provided by The National Science Foundation, the Semiconductor Research Corporation and General Electric Corporation.

List of References

[1]. R. F. Bunshah, "Deposition Technologies: An Overview", Deposition Technologies for Films and Coatings - Developments and Applications, Noyes Publications, 1982.

[2]. N. A. G. Ahmed, "Ion Plating Technology, Developments and Applications". John Wiley & Sons, 1987.

[3]. Talivaldis Spalvins, "The Structure of Ion Plated Films in Relation to Coating Properties". Ion Plating and Implantation Applications to Materials, Proceedings of a conference on the applications of ion plating and implantation to materials, 3-5 June, 1985, American Society of Metals.

[4]. ONRFE Science Information Bulletin, Vol. 15, No.3, 1990.

[5]. M. Sasaki, Y. Wang, T. Hirano, T. Hirai, "Design of SiC/C Functionally Gradient Material and its Preparation by Chemical Vapor Deposition". Journal of the Ceramic Society of Japan, Vol. 97, No. 5, pp. 539-543, 1989.

[6]. Y. Fukui, "Fundamental Investigation of Functionally Gradient Material Manufacturing System Using Centrifugal Force". Trans. JSME, Part C. Vol. 56, No. 521, pp. 67-70, 1990.

[7]. O. Yamada, "Fabrication of TiC-Ni Functionally Gradient Materials by the Gas-pressure Combustion Sintering". Journal of the Japan Society of Powder and Powder Metallurgy, Vol. 36, No. 6, pp. 712-715, 1988.

[8]. M. Koizumi, and K. Urabe, "Functionally Gradient Composites". Tetsu Hagan, Vol. 75, No. 6, pp. 887-893, 1989.

[9]. F. Erdogan and G. D. Gupta, "Layered Composites with an Interface Flaw", International Journal of Solids and Structures, Vol. 7, pp. 1089-1107, 1971.

[10]. J. R. Rice and G. C. Sih, "Plane Problems of Cracks in Dissimilar Media", ASME Journal of Applied Mechanics, Vol. 30, pp. 232-236, 1963.

[11]. F. Erdogan, "Stress Distribution in Bonded Dissimilar Materials with Cracks", ASME Journal of Applied Mechanics, Vol. 32, pp. 403-410, 1965.

[12]. A. H. England, "A Crack Between Dissimilar Media", ASME Journal of Applied Mechanics, Vol. 32, pp. 418-423, 1965.

[13]. M. Comninou, "The Interface Crack", ASME Journal of Applied Mechanics, Vol. 44, pp. 631-636, 1977.

[14]. C. Atkinson, "On Stress Singularities and Interfaces in Linear Elastic Fracture Mechanics", International Journal of Fracture, Vol. 13, pp. 807-820, 1977.

[15]. F. Delale and F. Erdogan, "Interfacial Crack in a Nonhomogeneous Elastic Medium", Lehigh University, Bethlehem, PA, Sept. 1987.

[16]. F. Delale and F. Erdogan, "On the Mechanical Modeling of the Interfacial Region in Bonded Half-Planes", ASME Journal of Applied Mechanics, Vol. 55, pp. 317-324, 1988.

[17]. R. H. Rand, "Computer Algebra in Applied Mathematics: An Introduction to MACSYMA". Pitman Publishing Inc., 1984.

[18]. Bruce W. Char, "MAPLE (Computer System)". Version 4.1, WATCOM Publications Limited, Ontario, Canada. 1988.

[19]. F. Erdogan, "Simultaneous Dual Integral Equations with Trigonometric and Bessel Kernels". Zeitchrift für Angewandte Mathematik und Mechanik, Band 48, Heft 4, pp. 217-225, June 1968.

[20]. N. I. Muskhelishvili, "Singular Integral Equations". Nooedhoff, Groningen, The Netherlands, 1953.

[21]. F. Erdogan, and G. D. Gupta, "On The Numerical Solution of Singular Integral Equations". Quarterly of Applied Mathematics, vol. 29, pp. 525-534, January 1972.

[22]. A. C. Kaya, and F. Erdogan, "On The Solution of Integral Equation with a Generalized Cauchy Kernel". Quarterly of Applied Mathematics, vol. xlv, pp 455-469, 1987.

[23]. M. Abramowitz, and I. E. Stegun, "Handbook of Mathematical Functions". National Bureau of Standards, June 1964.

[24]. F. Erdogan. "Approximate Solutions of Systems of Singular Integral Equations". SIAM Applied Mathematics, Vol. 17, No. 6, November 1969.

[25]. P. F. Joseph, "Plates and Shells Containing a Surface Crack under General Loading Conditions". Ph. D. dissertation, Lehigh University, 1987.

[26]. G. C. Sih, and H. Liebowitz, "Mathematical Theories of Brittle Fracture". in "Fracture, An Advanced Treatise", Vol. 2, Mathematical Fundamentals, ed. H. Liebowitz, Academic Press, 1968.

[27]. G. C. Sih, "Handbook of Stress Intensity Factors". Institute of Fracture and Solid Mechanics, Lehigh University, Bethlehem, PA, 1973.

[28]. M. L. Williams, "On the Stress Distribution at the Base of a Stationary Crack". Journal of Applied Mechanics, Vol. 24, Trans. ASME, Vol. 79, pp. 109-114, 1957.

[29]. F. Erdogan, G. C. Sih, "On the Crack Extension in Plates Under Plane Loading and Transverse Shear". Journal of Basic Engineering, Trans. ASME, Vol. 85, Series D, pp. 519-525, 1963.

[30]. F. Erdogan, "Fracture Problems in Composite Materials". Engineering Fracture Mechanics, Vol. 4, pp. 811-840, 1972.

[31]. F. B. Hildebrand, "Introduction to Numerical Analysis". 2nd ed., McGraw-Hill, New York, 1974.

[32]. Control Data Corporation, "FORTRAN Version 1 for NOS/VE Language Definition". 1988.

Appendix A

Boundary Conditions

In deriving the system of singular integral equations in Chapter 2, we applied Fourier transforms to Navier's equations to convert the coupled PDE's to ODE's (Eqn. (10)). The solution to the ODE's contain eight undetermined coefficients, where four are dependent. These procedures are applied to both the homogeneous and the nonhomogeneous materials of the problem at hand, which resulted in a total of eight unknown coefficients in place of the two displacement components that we defined as the original unknowns (Eqns. (11) and (18)). A set of new unknowns called density functions are then defined as the x derivative of the crack opening displacements (Eqn. (20)). Let the Fourier transforms of the density functions be the new unknown variables (Eqn. (21)). By taking the Fourier transforms of the six homogeneous boundary conditions and the two displacement boundary conditions of the mixed condition, we can create a new set of eight boundary conditions. This new set of boundary conditions, including six homogeneous condition and two where the right-hand-side are the new unknown variable (see Eqns. (22) through (28)), is what ties the eight unknown coefficient functions and the two new unknown variables together. Writing each of the new set of boundary conditions out explicitly, we obtain an 8 by 8 linear system to solve for the eight unknown coefficient functions in terms of the two new unknown variables. The linear system is written as follows:

$$a_{15}C_1 + a_{16}C_2 + a_{17}C_3 + a_{18}C_4 = 0, \tag{A.1}$$

$$a_{25}C_1 + a_{26}C_2 + a_{27}C_3 + a_{28}C_4 = 0, \tag{A.2}$$

$$a_{31}A_1 + a_{32}A_2 + a_{33}A_3 + a_{34}A_4 = 0, \tag{A.3}$$

$$a_{41}A_1 + a_{42}A_2 + a_{43}A_3 + a_{44}A_4 = 0, \tag{A.4}$$

$$a_{51}A_1 + a_{52}A_2 + a_{53}A_3 + a_{54}A_4 + a_{55}C_1 + a_{56}C_2 + a_{57}C_3 + a_{58}C_4 = 0, \tag{A.5}$$

$$a_{61}A_1 + a_{62}A_2 + a_{63}A_3 + a_{64}A_4 + a_{65}C_1 + a_{66}C_2 + a_{67}C_3 + a_{68}C_4 = 0, \tag{A.6}$$

$$a_{71}A_1 + a_{72}A_2 + a_{73}A_3 + a_{74}A_4 + a_{75}C_1 + a_{76}C_2 + a_{77}C_3 + a_{78}C_4 = F_1, \tag{A.7}$$

$$a_{81}A_1 + a_{83}A_3 + a_{85}C_1 + a_{86}C_2 + a_{87}C_3 + a_{88}C_4 = F_2, \tag{A.8}$$

where F_1 and F_2 are the Fourier transforms of the density functions that have been defined in Chapter 2. The coefficients a_{ij}, $i, j = 1 \cdots 8$, are all expressed in terms of α, κ, γ, h_1 and h_2, which are material and geometry constants also defined in Chapter 2. The actual combining of terms and simplifying of expressions with respect to their fundamental variable and material as well as geometry constants were carried out on a VAX-8300 using the symbolic software MACSYMA. We list the expressions for each element as follows

$$a_{31} = 2|\alpha| e^{-h_1|\alpha|}, \tag{A.9}$$

$$a_{32} = -[2h_1|\alpha| + \kappa - 1] e^{-h_1|\alpha|}, \tag{A.10}$$

$$a_{33} = -2|\alpha| e^{h_1|\alpha|}, \tag{A.11}$$

$$a_{34} = [2h_1|\alpha| - \kappa + 1]e^{h_1|\alpha|}, \tag{A.12}$$

$$a_{41} = -2i\alpha(\kappa - 1)e^{-h_1|\alpha|}, \tag{A.13}$$

$$a_{42} = i\alpha(\kappa - 1)[\frac{\kappa + 1}{|\alpha|} + 2h_1]e^{-h_1\alpha}, \tag{A.14}$$

$$a_{43} = -2i\alpha(\kappa - 1)e^{h_1|\alpha|}, \tag{A.15}$$

$$a_{44} = -i\alpha(\kappa - 1)[\frac{\kappa + 1}{|\alpha|} - 2h_1]e^{h_1\alpha}, \tag{A.16}$$

$$a_{51} = a_{53} = -2i\alpha(\kappa - 1), \tag{A.17}$$

$$a_{52} = i(\kappa^2 - 1)\frac{\alpha}{|\alpha|}, \tag{A.18}$$

$$a_{54} = -a_{52}, \tag{A.19}$$

$$a_{55} = -\{(\kappa + 1)R^3e^{3i\theta} - i\gamma(\kappa - 1)R^2e^{2i\theta} - [4(\kappa + 5)\alpha^2 + i\gamma^2(\kappa + 1)]$$
$$Re^{i\theta} - 4\gamma\alpha^2(\kappa - 11) + \gamma^3(\kappa + 1)\}\frac{i(\kappa - 1)}{8\alpha[Re^{i\theta} - \gamma(2 - \kappa)]}, \tag{A.20}$$

$$a_{56} = -\{(\kappa + 1)R^3e^{-3i\theta} - i\gamma(\kappa - 1)R^2e^{-2i\theta} - [4(\kappa + 5)\alpha^2 + i\gamma^2(\kappa + 1)]$$
$$Re^{-i\theta} - 4\gamma\alpha^2(\kappa - 11) + \gamma^3(\kappa + 1)\}\frac{i(\kappa - 1)}{8\alpha[Re^{-i\theta} - \gamma(2 - \kappa)]}, \tag{A.21}$$

$$a_{57} = -\{(\kappa+1)R^3e^{-3i\theta} + i\gamma(\kappa-1)R^2e^{-2i\theta} - [4(\kappa+5)\alpha^2 + i\gamma^2(\kappa+1)]$$

$$Re^{-i\theta} + 4\gamma\alpha^2(\kappa-11) - \gamma^3(\kappa+1)\}\frac{i(\kappa-1)}{8\alpha[Re^{-i\theta}+\gamma(2-\kappa)]}, \tag{A.22}$$

$$a_{58} = -\{(\kappa+1)R^3e^{3i\theta} + i\gamma(\kappa-1)R^2e^{2i\theta} - [4(\kappa+5)\alpha^2 + i\gamma^2(\kappa+1)]$$

$$Re^{i\theta} + 4\gamma\alpha^2(\kappa-11) - \gamma^3(\kappa+1)\}\frac{i(\kappa-1)}{8\alpha[Re^{i\theta}+\gamma(2-\kappa)]}, \tag{A.23}$$

$$a_{61} = 2|\alpha|, \tag{A.24}$$

$$a_{62} = 1-\kappa, \tag{A.25}$$

$$a_{63} = -a_{61}, \tag{A.26}$$

$$a_{64} = a_{62}, \tag{A.27}$$

$$a_{65} = \frac{-(3-\kappa)R^2e^{2i\theta} + 2\gamma(3-\kappa)Re^{i\theta} - 4(\kappa+1)\alpha^2 - \gamma^2(3-\kappa)}{4[Re^{i\theta}-\gamma(2-\kappa)]}, \tag{A.28}$$

$$a_{66} = \frac{-(3-\kappa)R^2e^{-2i\theta} + 2\gamma(3-\kappa)Re^{-i\theta} - 4(\kappa+1)\alpha^2 - \gamma^2(3-\kappa)}{4[Re^{-i\theta}-\gamma(2-\kappa)]}, \tag{A.29}$$

$$a_{67} = \frac{(3-\kappa)R^2e^{-2i\theta} + 2\gamma(3-\kappa)Re^{-i\theta} + 4(\kappa+1)\alpha^2 + \gamma^2(3-\kappa)}{4[Re^{-i\theta}+\gamma(2-\kappa)]}, \tag{A.30}$$

$$a_{68} = \frac{(3-\kappa)R^2e^{2i\theta} + 2\gamma(3-\kappa)Re^{i\theta} + 4(\kappa+1)\alpha^2 + \gamma^2(3-\kappa)}{4[Re^{-i\theta}+\gamma(2-\kappa)]}, \tag{A.31}$$

$$a_{15} = -a_{65} e^{\frac{h_2}{2}(Re^{i\theta} - \gamma)}, \tag{A.32}$$

$$a_{16} = -a_{66} e^{\frac{h_2}{2}(Re^{-i\theta} - \gamma)}, \tag{A.33}$$

$$a_{17} = -a_{67} e^{\frac{h_2}{2}(-Re^{-i\theta} - \gamma)}, \tag{A.34}$$

$$a_{18} = -a_{68} e^{\frac{h_2}{2}(-Re^{i\theta} - \gamma)}, \tag{A.35}$$

$$a_{25} = -a_{55} e^{\frac{h_2}{2}(Re^{-i\theta} - \gamma)}, \tag{A.36}$$

$$a_{26} = -a_{56} e^{\frac{h_2}{2}(Re^{-i\theta} - \gamma)}, \tag{A.37}$$

$$a_{27} = -a_{57} e^{\frac{h_2}{2}(-Re^{-i\theta} - \gamma)}, \tag{A.38}$$

$$a_{28} = -a_{58} e^{\frac{h_2}{2}(-Re^{i\theta} - \gamma)}, \tag{A.39}$$

$$a_{71} = -|\alpha|, \tag{A.40}$$

$$a_{72} = a_{74} = \kappa, \tag{A.41}$$

$$a_{73} = -a_{71}, \tag{A.42}$$

$$a_{75} = \frac{-(\kappa-1)R^2e^{2i\theta}+4(\kappa+1)\alpha^2+\gamma^2(\kappa-1)}{4[Re^{i\theta}-\gamma(2-\kappa)]}, \tag{A.43}$$

$$a_{76} = \frac{-(\kappa-1)R^2e^{-2i\theta}+4(\kappa+1)\alpha^2+\gamma^2(\kappa-1)}{4[Re^{-i\theta}-\gamma(2-\kappa)]}, \tag{A.44}$$

$$a_{77} = \frac{(\kappa-1)R^2e^{-2i\theta}-4(\kappa+1)\alpha^2-\gamma^2(\kappa-1)}{4[Re^{-i\theta}+\gamma(2-\kappa)]}, \tag{A.45}$$

$$a_{78} = \frac{(\kappa-1)R^2e^{2i\theta}-4(\kappa+1)\alpha^2-\gamma^2(\kappa-1)}{4[Re^{i\theta}+\gamma(2-\kappa)]}, \tag{A.46}$$

$$a_{81} = a_{83} = -i\alpha, \tag{A.47}$$

$$a_{85} = a_{86} = a_{87} = a_{88} = i\alpha, \tag{A.48}$$

where R and θ, both defined in Chapter 2, are shown again as follows,

$$R = \sqrt[4]{(\gamma^2+4\alpha^2)^2+16\alpha^2\gamma^2\frac{3-\kappa}{1+\kappa}}, \tag{A.49}$$

$$\theta = \frac{1}{2}\tan^{-1}\left(\frac{4\alpha\gamma}{\gamma^2+4\alpha^2}\sqrt{\frac{3-\kappa}{1+\kappa}}\right).$$

Appendix B

Asymptotic Expansions

B.1 Introduction

In the derivation of the system of singular integral equations, an important step is finding the asymptotic values of the integrands of some infinite integrals (Eqns. (47) to (50)). The asymptotic analysis is necessary for the following two reasons,

1. The leading term of the integrands in asymptotic expansion gives the Cauchy kernel in the singular integral equations.
2. Subsequent terms in the expansion facilitate computational efficiency when we numerically solve the SIE's. The more terms that can be asymptotically extracted, the less effort is required for the numerical computation.

The major task of the analysis is the asymptotic expansion of the 8 by 8 determinant and eight 7 by 7 cofactors which form the integrands in the infinite integrals. These cofactors and the determinant constitute the solution of the 8 by 8 linear system as depicted by Eqn. (29). The leading terms of $\frac{D_{ij}}{D}, \quad i = 1 \cdots 4, j = 1, 2$ in Eqn. (30) are desired.

B.2 Algebraic vs. numeric operations

One may wonder why in solving the linear system (29), the inefficient Cramer's rule was used in lieu of more efficient methods (see Eqn. (30) and (31)). The answer to this has to do with the inherently different nature of algebraic manipulations and

numeric operations. Consider the problem of inverting an n by n matrix. What we learned from numerical analysis tells us that the problem requires operations on the order of n^3 [31]. But this kind of analysis does not apply when we are dealing with algebraic entities. Consider now the number of terms in the determinant of a fully occupied n by n matrix whose elements are the symbols a_{ij}. The determinant, when fully expanded, which is necessary in computing the inverse, has $n!$ terms. For an 8 by 8 matrix with each element being a single symbol, the fully expanded determinant has 40,320 terms, and this is vastly different from the number of operations ($8^3 = 512$) needed to invert the matrix numerically. For the problem at hand where each element in the 8 by 8 matrix is a complex expression rather than a single symbol, the number of terms in the expanded determinant is even more. The complexity of determinant expansion will quickly make the asymptotic analysis come to a halt if brute force determinant expansion was used.

A straight forward approach would be to asymptotically expand each element in the matrix to compute the determinant and cofactors by direct expansion. One soon finds that such a procedure breaks down quickly as matrix size and number of terms expanded in each element increases. The reason for the break-down is obvious. As the matrix size increases, even if there is only one term in each element, the number of terms in the expanded determinant increases exponentially as explained earlier. When there are more terms in each element, and each term is in turn complex expressions, it soon becomes more than even a mainframe computer can handle. On a VAX-8530 in which 20,000 pages of dynamic memory was allocated, the computation breaks down with a two term expansion in each element of an 8 by 8 matrix to analytically expand its determinant.

The successful asymptotic expansion of the 8 by 8 determinant and its cofactors to as many terms as the aforementioned restraint would allow, lies in recognizing that out of the nominally required astronomical number of multiplications, only a relevant few need to be carried out to produce the leading terms in the determinant. Those expansions not carried out contribute only to low order terms which can be ignored. In what follows each relevant element of the 8 by 8 matrix undergoes a 12-term asymptotic expansion. These expansions in turn produce a 12-term asymptotic polynomial out of $\frac{D_{ij}}{D}$, (see Eqns. (51) through (54)) which gives a 11-term asymptotic analysis in the integrands of infinite integrals (Eqns. (47) through (50)). The memory constraint is the only factor that controls the number of terms that can be asymptotically expanded in each element, therefore it also determines the number of terms that can be expanded in the integrands of Fredholm kernels.

B.3 Asymptotic expansion

To asymptotically expand the 8 by 8 determinant and eight 7 by 7 cofactors, we first examine the asymptotic behavior of the elements that make up these determinants. Referring to expressions of each element in Appendix A, we note that,

$$R = \sqrt[4]{(\gamma^2+4\alpha^2)^2+16\alpha^2\gamma^2\frac{3-\kappa}{1+\kappa}} = 2\alpha + O(0),$$

$$\theta = \frac{1}{2}\tan^{-1}\left(\frac{4\alpha\gamma}{\gamma^2+4\alpha^2}\sqrt{\frac{3-\kappa}{1+\kappa}}\right) = \frac{1}{2}\gamma\sqrt{\frac{3-\kappa}{1+\kappa}}\ \frac{1}{\alpha} + O\left(\frac{1}{\alpha^2}\right), \qquad \textbf{(B.1)}$$

$$\alpha \rightarrow \infty,$$

therefore,

$$Re^{i\theta} = 2\alpha + O(0),$$

$$Re^{-i\theta} = 2\alpha + O(0), \text{ as } \alpha \to \infty. \tag{B.2}$$

As have been defined in Chapter 2, $O(\frac{1}{\alpha^2})$ indicates polynomials with leading term of degree -2 in α, and so on. With these observations, we found that a_{15}, a_{16}, and a_{25}, a_{26} contain a term like $e^{\alpha h_2}$ in their asymptotic behavior. Similarly, elements a_{33}, a_{34}, and a_{43} , a_{44} have a term like $e^{\alpha h_1}$. We bear in mind that in expanding a determinant, no two elements that belong to the same column or row may appear in the form of product in any expansion. It is apparent that the dominant term in both the numerator and denominator must carry a term like $e^{2\alpha(h_1 + h_2)}$ so that the leading terms are derived from their quotient. Since the denominator, the determinant of the 8 by 8 matrix, will always carry the term $e^{2\alpha(h_1 + h_2)}$, any term in the numerator without $e^{2\alpha(h_1 + h_2)}$ will only contribute to lower order terms in the rational expression. Our objective then, becomes to identify all relevant elements that contribute to this dominant term in each 8 by 8 or 7 by 7 determinant expansions and ignore the rest as they are insignificant to the analysis.

The foregoing analysis is the key to the successful asymptotic analysis of the problem. It reduces what appeared to be an insurmountably complicated task to a manageable job that can be better explained by rewriting the 8 by 8 matrix in a different way as shown in Eqn. (B.3). Following the rule in expanding a determinant as stated earlier, we observe that the dominant term in the determinant must include two elements from columns 3, 4 and two from columns 5, 6 with the exponential term. Another way of getting the dominant terms is through row-wise expansion, in which case the leading terms of the determinant must include two elements from rows 1, 2

$$\begin{bmatrix} 0 & 0 & 0 & 0 & -a_{65}e^{\alpha h_2} & -a_{66}e^{\alpha h_2} & I & I \\ 0 & 0 & 0 & 0 & -a_{55}e^{\alpha h_2} & -a_{56}e^{\alpha h_2} & I & I \\ I & I & O(\alpha)e^{\alpha h_1} & O(\alpha)e^{\alpha h_1} & 0 & 0 & 0 & 0 \\ I & I & O(\alpha)e^{\alpha h_1} & O(\alpha)e^{\alpha h_1} & 0 & 0 & 0 & 0 \\ a_{51} & a_{52} & I & I & I & I & a_{57} & a_{58} \\ a_{61} & a_{62} & I & I & I & I & a_{67} & a_{68} \\ a_{71} & a_{72} & I & I & I & I & a_{77} & a_{78} \\ a_{81} & 0 & I & 0 & I & I & a_{87} & a_{88} \end{bmatrix} \quad \textbf{(B.3)}$$

and two from rows 3, 4 that have the exponential term. With these elements in the product, the rest will have to come from those elements explicitly written in Eqn. (B.3), observing the rule that only one element in a column or row may participate in forming the product. The remaining elements are either zero occupied or do not contribute to the leading terms of our analysis and are marked as "*I*".

Having established the ground rule of obtaining the leading terms of asymptotic analysis in the determinants, we can now explicitly write the exact expressions to get the leading terms of the 8 by 8 determinant and 7 by 7 cofactors. Note that they are written in terms of truncated asymptotically expanded expressions of only those elements associated with products that give the dominant terms. Let us denote the truncated asymptotic expressions of elements as $a'_{i\,j}$, and those of the determinant and cofactors as d and $d_{i\,j}$ respectively. We have

$$d_{11} = (a'_{55}\cdot a'_{66} - a'_{65}\cdot a'_{56})\cdot(a'_{34}\cdot a'_{43} - a'_{33}\cdot a'_{44})\cdot[a'_{52}\cdot (a'_{67}\cdot a'_{88} - a'_{87}\cdot a'_{68}) - a'_{62}\cdot(a'_{58}\cdot a'_{87} - a'_{57}\cdot a'_{88})], \tag{B.4}$$

$$d_{12} = -(a'_{55}\cdot a'_{66} - a'_{65}\cdot a'_{56})\cdot(a'_{34}\cdot a'_{43} - a'_{33}\cdot a'_{44})\cdot[a'_{52}\cdot(a'_{67}\cdot a'_{78} - a'_{77}\cdot a'_{68}) - a'_{57}\cdot(a'_{62}\cdot a'_{78} - a'_{72}\cdot a'_{68}) + a'_{58}\cdot(a'_{62}\cdot a'_{77} - a'_{72}\cdot a'_{67})], \tag{B.5}$$

$$d_{21} = -(a'_{55}\cdot a'_{66} - a'_{65}\cdot a'_{56})\cdot(a'_{34}\cdot a'_{43} - a'_{33}\cdot a'_{44})\cdot[a'_{51}\cdot(a'_{67}\cdot a'_{88} - a'_{87}\cdot a'_{68}) - a'_{57}\cdot(a'_{61}\cdot a'_{88} - a'_{81}\cdot a'_{68}) + a'_{58}\cdot(a'_{61}\cdot a'_{87} - a'_{81}\cdot a'_{67})], \tag{B.6}$$

$$d_{22} = (a'_{55}\cdot a'_{66} - a'_{65}\cdot a'_{56})\cdot(a'_{34}\cdot a'_{43} - a'_{33}\cdot a'_{44})\cdot[a'_{51}\cdot(a'_{67}\cdot a'_{78} - a'_{77}\cdot a'_{68}) - a'_{57}\cdot(a'_{61}\cdot a'_{78} - a'_{71}\cdot a'_{68}) + a'_{58}\cdot(a'_{61}\cdot a'_{77} - a'_{71}\cdot a'_{67})], \tag{B.7}$$

$$\begin{aligned} d = {} & -(a'_{55}\cdot a'_{66} - a'_{65}\cdot a'_{56})\cdot(a'_{34}\cdot a'_{43} - a'_{33}\cdot a'_{44})\cdot\{a'_{51}\cdot[a'_{62}\cdot(a'_{87}\cdot a'_{78} - a'_{77}\cdot a'_{88}) + a'_{72}\cdot(a'_{67}\cdot a'_{88} - a'_{87}\cdot a'_{68})] - a'_{52}\cdot[a'_{61}\cdot(a'_{87}\cdot a'_{78} - a'_{77}\cdot a'_{88}) + a'_{72}\cdot(a'_{81}\cdot a'_{78} - a'_{71}\cdot a'_{88}) + a'_{68}\cdot(a'_{81}\cdot a'_{77} - a'_{71}\cdot a'_{87})] + a'_{57}\cdot[-a'_{62}\cdot(a'_{81}\cdot a'_{78} - a'_{71}\cdot a'_{88}) - a'_{72}\cdot(a'_{61}\cdot a'_{88} - a'_{81}\cdot a'_{68})] - a'_{58}\cdot[-a'_{62}\cdot(a'_{81}\cdot a'_{77} - a'_{71}\cdot a'_{87}) - a'_{72}\cdot(a'_{61}\cdot a'_{87} - a'_{81}\cdot a'_{67})]\}, \end{aligned} \tag{B.8}$$

It is amazing that there are only 54 terms required to obtain the leading terms of the 8 by 8 determinant, out of the possible 40320 (8!), as shown in Eqn. (B.8). Of course the number of terms will be something less if full determinant expansion was carried out because there are 18 zero occupied elements in our 8 by 8 determinant (see Eqn. (B.3)). But the reduction in the number of terms needed to compute the leading terms

of the determinant paves the way for a promising prospect that perhaps more terms can be expanded from our asymptotic analysis. It is also worth noting that expressions for d_{31}, d_{32}, d_{41}, and d_{42} need not be written. The reason for this is apparent when we notice that the corresponding cofactors D_{31}, D_{32}, D_{41}, and D_{42} were obtained from the 8 by 8 matrix by deleting column 3 or 4. In any case one of the dominant terms $e^{\alpha h_1}$ was lost thus making these cofactors of much lower order than that of determinant D. Therefore the resulting rational polynomials are analytic at $\alpha = \infty$ when such lower order cofactors appear in the numerators. In other words, $\frac{D_{31}}{D}$, $\frac{D_{32}}{D}$, $\frac{D_{41}}{D}$, and $\frac{D_{42}}{D}$ do not contribute to Cauchy kernel or any of the leading terms in the asymptotic analysis that aids numerical efficiency, but become part of the massive Fredholm kernels.

Due to the constraint in memory allocated on the VAX-8530, there are only so many leading terms we can expand out of the asymptotic analysis. We shall now try to establish the relationship between the number of leading terms in the overall asymptotic analysis with that of each element in the matrix. Let $-n$ be the lowest power that can be asymptotically expanded in a particular element. We denote the range of terms that can be expanded within the constraint for an element as $O(\alpha,m,-n)$, where m is the power of the leading term and α is the variable of the asymptotic expansion. We can write number of terms expanded for each significant element and exact asymptotic expression for some elements in Eqn. (B.3) as follows,

$$a'_{33} = O(\alpha,1) = -2\alpha, \tag{B.9}$$

$$a'_{34} = O(\alpha,1,0) = 2h_1\alpha - \kappa + 1, \tag{B.10}$$

$$a'_{43} = O(\alpha,1) = -2i\alpha(\kappa-1), \tag{B.11}$$

$$a'_{44} = O(\alpha,1,0) = i(\kappa-1)(2h_1\alpha-\kappa+1), \tag{B.12}$$

$$a'_{51} = O(\alpha,1) = -2i\alpha(\kappa-1), \tag{B.13}$$

$$a'_{52} = O(\alpha,0) = i(\kappa^2-1), \tag{B.14}$$

$$a'_{61} = O(\alpha,1) = 2\alpha, \tag{B.15}$$

$$a'_{62} = O(\alpha,0) = 1-\kappa, \tag{B.16}$$

$$a'_{71} = O(\alpha,1) = -\alpha, \tag{B.17}$$

$$-a'_{81} = a'_{87} = a'_{88} = O(\alpha,1) = i\alpha, \tag{B.18}$$

$$a'_{55} = O(\alpha,1,-n) = c_{55,1}\alpha + c_{55,0} + \frac{c_{55,-1}}{\alpha} + \frac{c_{55,-2}}{\alpha^2} + \frac{c_{55,-3}}{\alpha^3} + \frac{c_{55,-4}}{\alpha^4} + \cdots + \frac{c_{55,-n}}{\alpha^n}, \tag{B.19}$$

$$a'_{56} = O(\alpha,1,-n) = c_{56,1}\alpha + c_{56,0} + \frac{c_{56,-1}}{\alpha} + \frac{c_{56,-2}}{\alpha^2} + \frac{c_{56,-3}}{\alpha^3} + \frac{c_{56,-4}}{\alpha^4} + \cdots + \frac{c_{56,-n}}{\alpha^n}, \tag{B.20}$$

$$a'_{57} = O(\alpha,1,-n) = c_{57,1}\alpha + c_{57,0} + \frac{c_{57,-1}}{\alpha} + \frac{c_{57,-2}}{\alpha^2} + \frac{c_{57,-3}}{\alpha^3} + \frac{c_{57,-4}}{\alpha^4} + \cdots + \frac{c_{57,-n}}{\alpha^n}, \tag{B.21}$$

$$a'_{58} = O(\alpha,1,-n) = c_{58,1}\alpha + c_{58,0} + \frac{c_{58,-1}}{\alpha} + \frac{c_{58,-2}}{\alpha^2} + \frac{c_{58,-3}}{\alpha^3} + \frac{c_{58,-4}}{\alpha^4} + \cdots + \frac{c_{58,-n}}{\alpha^n}, \tag{B.22}$$

$$a'_{65} = O(\alpha,1,-n) = c_{65,1}\alpha + c_{65,0} + \frac{c_{65,-1}}{\alpha} + \frac{c_{65,-2}}{\alpha^2} + \frac{c_{65,-3}}{\alpha^3} + \frac{c_{65,-4}}{\alpha^4} + \cdots + \frac{c_{65,-n}}{\alpha^n}, \tag{B.23}$$

$$a'_{72} = O(\alpha,0) = \kappa, \tag{B.24}$$

$$a'_{66} = O(\alpha,1,-n) = c_{66,1}\alpha + c_{66,0} + \frac{c_{66,-1}}{\alpha} + \frac{c_{66,-2}}{\alpha^2} + \frac{c_{66,-3}}{\alpha^3} + \frac{c_{66,-4}}{\alpha^4} + \cdots + \frac{c_{66,-n}}{\alpha^n}, \qquad \textbf{(B.25)}$$

$$a'_{67} = O(\alpha,1,-n) = c_{67,1}\alpha + c_{67,0} + \frac{c_{67,-1}}{\alpha} + \frac{c_{67,-2}}{\alpha^2} + \frac{c_{67,-3}}{\alpha^3} + \frac{c_{67,-4}}{\alpha^4} + \cdots + \frac{c_{67,-n}}{\alpha^n}, \qquad \textbf{(B.26)}$$

$$a'_{68} = O(\alpha,1,-n) = c_{68,1}\alpha + c_{68,0} + \frac{c_{68,-1}}{\alpha} + \frac{c_{68,-2}}{\alpha^2} + \frac{c_{68,-3}}{\alpha^3} + \frac{c_{68,-4}}{\alpha^4} + \cdots + \frac{c_{68,-n}}{\alpha^n}, \qquad \textbf{(B.27)}$$

$$a'_{77} = O(\alpha,1,-n) = c_{77,1}\alpha + c_{77,0} + \frac{c_{77,-1}}{\alpha} + \frac{c_{77,-2}}{\alpha^2} + \frac{c_{77,-3}}{\alpha^3} + \frac{c_{77,-4}}{\alpha^4} + \cdots + \frac{c_{77,-n}}{\alpha^n}, \qquad \textbf{(B.28)}$$

$$a'_{78} = O(\alpha,1,-n) = c_{78,1}\alpha + c_{78,0} + \frac{c_{78,-1}}{\alpha} + \frac{c_{78,-2}}{\alpha^2} + \frac{c_{78,-3}}{\alpha^3} + \frac{c_{78,-4}}{\alpha^4} + \cdots + \frac{c_{78,-n}}{\alpha^n}, \qquad \textbf{(B.29)}$$

where $c_{i,j,k}$ represents the coefficient of the α^k term of the truncated polynomial a'_{ij}. Note that elements a'_{33}, a'_{34}, a'_{43}, and a'_{44} were written without the term $e^{\alpha h_1}$. Also a'_{15} and a'_{16} differ from a'_{65}, and a'_{66} by the factor $-e^{\alpha h_2}$, as can be seen from Eqns. (A.32), (A.33) and (B.2), the latter is written instead. For the same reason a'_{55}, and a'_{56} are written instead of a'_{25}, and a'_{26}. The reason that both $e^{\alpha h_1}$ and $e^{\alpha h_2}$ are excluded from the analysis is that they factor out since they appear in both the numerator and the denominator when $\frac{D_{ij}}{D}$ is divided. Eqns. (B.9) through (B.18) are those elements whose exact representations are simple polynomials. Therefore, no asymptotic expansions are needed. They are directly constructed from Appendix A. Eqns. (B.19) through (B.29), however, are those elements that have complex rational polynomial expressions. We shall apply asymptotic expansion to these elements, and their exact expressions up to the lowest power expandable will be shown later in the appendix.

If one tries to substitute Eqns. (B.9) through (B.29) into Eqns (B.4) through (B.8) now, considering that the necessary asymptotic analysis has been done on the elements shown in Eqns. (B.19) through (B.29) and all the coefficients $c_{i,j,k}$ are known, one still can not expect to extract the most leading terms out of the determinant and cofactors. The reason is as follows. Remember that a'_{ij} are truncated polynomials, therefore any operation on them, especially multiplications and divisions, will produce nonsignificant terms. If steps are not taken to keep only the significant terms and to throw away the excess baggage, before very long these nonsignificant terms will accumulate to a monstrous proportion and defeat the economizing that we have accomplished earlier. Therefore, we now establish the following rules as regard to operations on these truncated polynomials

$$
\begin{aligned}
O(\alpha, n_1, -n_2) + O(\alpha, n_3, -n_4) &= O(\alpha, \max[n_1, n_3], \max[-n_2, -n_4]), \\
O(\alpha, n_1, -n_2) - O(\alpha, n_3, -n_4) &= O(\alpha, \max[n_1, n_3], \max[-n_2, -n_4]), \\
O(\alpha, n_1, -n_2) \cdot O(\alpha, n_3, -n_4) &= O(\alpha, n_1 + n_3, \max[n_3 - n_2, n_1 - n_4]), \\
\frac{O(\alpha, n_1, -n_2)}{O(\alpha, n_3, -n_4)} &= O(\alpha, n_1 - n_3, -n_2 - n_3).
\end{aligned}
\qquad \textbf{(B.30)}
$$

We can now substitute all the expressions in Eqns. (B.18) through (B.29) into Eqns. (B.4) through (B.8) to obtain the significant expanded terms in the cofactors and determinant. The resulting range of significant terms are

$$d_{11} = O(\alpha, 6, 4-n),$$

$$d_{12} = O(\alpha, 6, 4-n),$$

$$d_{21} = O(\alpha, 7, 5-n), \qquad \textbf{(B.31)}$$

$$d_{22} = O(\alpha, 7, 5-n),$$

$$d = O(\alpha, 7, 5-n),$$

The actual asymptotic expansion was done on VAX-8530 using the symbolic software MAPLE. It gives $n = 12$, which is the limit to which the asymptotic expansion of those elements in Eqns. (B.19) through (B.29) can be carried out. During the asymptotic expansion process for those elements in Eqns. (B.19) through (B.29), it was found that

$$a'_{57} = c_{55,1}\alpha - c_{55,0} + \frac{c_{55,-1}}{\alpha} - \frac{c_{55,-2}}{\alpha^2} + \frac{c_{55,-3}}{\alpha^3} - \frac{c_{55,-4}}{\alpha^4} + \cdots + (-1)^{(n+1)}\frac{c_{55,-n}}{\alpha^n}, \qquad \textbf{(B.32)}$$

$$a'_{58} = c_{56,1}\alpha - c_{56,0} + \frac{c_{56,-1}}{\alpha} - \frac{c_{56,-2}}{\alpha^2} + \frac{c_{56,-3}}{\alpha^3} - \frac{c_{56,-4}}{\alpha^4} + \cdots + (-1)^{(n+1)}\frac{c_{56,-n}}{\alpha^n}, \qquad \textbf{(B.33)}$$

$$a'_{67} = -c_{65,1}\alpha + c_{65,0} - \frac{c_{65,-1}}{\alpha} + \frac{c_{65,-2}}{\alpha^2} - \frac{c_{65,-3}}{\alpha^3} + \frac{c_{65,-4}}{\alpha^4} - \cdots + (-1)^{n}\frac{c_{65,-n}}{\alpha^n}, \qquad \textbf{(B.34)}$$

$$a'_{68} = -c_{66,1}\alpha + c_{66,0} - \frac{c_{66,-1}}{\alpha} + \frac{c_{66,-2}}{\alpha^2} - \frac{c_{66,-3}}{\alpha^3} + \frac{c_{66,-4}}{\alpha^4} - \cdots + (-1)^{n}\frac{c_{66,-n}}{\alpha^n}. \qquad \textbf{(B.35)}$$

As a result, we need to show only the expanded terms of elements a_{55}, a_{56}, a_{65}, a_{66}, a_{77}, a_{78}. They are as follows,

$$Re[a'_{55}] = \{\frac{\gamma}{2}(\kappa+1) - \frac{\gamma^2}{4\alpha}\kappa(\kappa+1) + \frac{\gamma^3}{8\alpha^2}(\kappa^3-3\kappa-2) - \frac{\gamma^4}{16\alpha^3}(\kappa^4-\kappa^3-$$

$$5\kappa^2-\kappa+4) + \frac{\gamma^5}{32\alpha^4}(\kappa^5-2\kappa^4-6\kappa^3+4\kappa^2+13\kappa+6) - \frac{\gamma^6}{64\alpha^5(\kappa+1)}$$

$$(\kappa^7-2\kappa^6-9\kappa^5+6\kappa^4+33\kappa^3+18\kappa^2-21\kappa-32) + \frac{\gamma^7}{128\alpha^6}(\kappa^7-4\kappa^6-$$

$$5\kappa^5+22\kappa^4+23\kappa^3-32\kappa^2-51\kappa-18) - \frac{\gamma^8}{256\alpha^7(\kappa+1)^2}(\kappa^{10}-3\kappa^9-$$

$$12\kappa^8+22\kappa^7+78\kappa^6-18\kappa^5-222\kappa^4-198\kappa^3+63\kappa^2+225\kappa+252) +$$

$$\frac{\gamma^9}{512\alpha^8}(\kappa^9-6\kappa^8+44\kappa^6-6\kappa^5-144\kappa^4-56\kappa^3+180\kappa^2+189\kappa+54) -$$

$$\frac{\gamma^{10}}{1024\alpha^9(\kappa+1)^3}(\kappa^{13}-4\kappa^{12}-14\kappa^{11}+46\kappa^{10}+125\kappa^9-170\kappa^8-660\kappa^7- \qquad \textbf{(B.36)}$$

$$120\kappa^6+1425\kappa^5+1820\kappa^4+262\kappa^3-1380\kappa^2-1709\kappa-2192) +$$

$$\frac{\gamma^{11}}{2048\alpha^{10}}(\kappa^{11}-8\kappa^{10}+9\kappa^9+62\kappa^8-94\kappa^7-264\kappa^6+250\kappa^5+724\kappa^4-3\kappa^3-$$

$$864\kappa^2-675\kappa-162) - \frac{\gamma^{12}}{4096\alpha^{11}(\kappa+1)^4}(\kappa^{16}-5\kappa^{15}-15\kappa^{14}+77\kappa^{13}+$$

$$161\kappa^{12}-483\kappa^{11}-1253\kappa^{10}+1015\kappa^9+5355\kappa^8+2975\kappa^7-8323\kappa^6-$$

$$15015\kappa^5-7175\kappa^4+6347\kappa^3+13341\kappa^2+11437\kappa+21052) +$$

$$\frac{\gamma^{13}}{8192\alpha^{12}}(\kappa^{13}-10\kappa^{12}+22\kappa^{11}+68\kappa^{10}-245\kappa^9-262\kappa^8+1060\kappa^7+$$

$$1016\kappa^6-2201\kappa^5-3030\kappa^4+1062\kappa^3+3780\kappa^2+2349\kappa+486)\}\sqrt{\frac{3-\kappa}{1+\kappa}},$$

$$Im[a'_{55}] = 2\alpha - \frac{\gamma}{2}(\kappa+1) + \frac{\gamma^2}{4\alpha}(\kappa^2-\kappa-2) - \frac{\gamma^3}{8\alpha^2}(\kappa^3-2\kappa^2-3\kappa+2) +$$

$$\frac{\gamma^4}{16\alpha^3}(\kappa^4-3\kappa^3-3\kappa^2+7\kappa+6) + \frac{\gamma^5}{32\alpha^4(\kappa+1)}(\kappa^6-3\kappa^5-6\kappa^4+$$

$$12\kappa^3+21\kappa^2-3\kappa-20) + \frac{\gamma^6}{64\alpha^5}(\kappa^6-5\kappa^5+22\kappa^3+\kappa^2-33\kappa-$$

$$18) - \frac{\gamma^7}{128\alpha^6(\kappa+1)^2}(\kappa^9-4\kappa^8-8\kappa^7+30\kappa^6+48\kappa^5-66\kappa^4-$$

$$156\kappa^3-42\kappa^2+103\kappa+154) + \frac{\gamma^8}{256\alpha^7}(\kappa^8-7\kappa^7+7\kappa^6+37\kappa^5-$$

$$43\kappa^4-101\kappa^3+45\kappa^2+135\kappa+54) - \frac{\gamma^9}{512\alpha^8(\kappa+1)^3}(\kappa^{12}-5\kappa^{11}-$$

$$9\kappa^{10}+55\kappa^9+70\kappa^8-240\kappa^7-420\kappa^6+300\kappa^5+1125\kappa^4+695\kappa^3-$$

$$435\kappa^2-885\kappa-1270) + \frac{\gamma^{10}}{1024\alpha^9}(\kappa^{10}-9\kappa^9+18\kappa^8+44\kappa^7- \qquad \textbf{(B.37)}$$

$$138\kappa^6-126\kappa^5+376\kappa^4+348\kappa^3-351\kappa^2-513\kappa-162) -$$

$$\frac{\gamma^{11}}{2048\alpha^{10}(\kappa+1)^4}(\kappa^{15}-6\kappa^{14}-9\kappa^{13}+86\kappa^{12}+75\kappa^{11}-558\kappa^{10}-$$

$$695\kappa^9+1710\kappa^8+3645\kappa^7-670\kappa^6-7653\kappa^5-7362\kappa^4+$$

$$185\kappa^3+6258\kappa^2+5823\kappa+11638) + \frac{\gamma^{12}}{4096\alpha^{11}}(\kappa^{12}-11\kappa^{11}+$$

$$33\kappa^{10}+35\kappa^9-280\kappa^8+18\kappa^7+1042\kappa^6-26\kappa^5-2175\kappa^4-$$

$$855\kappa^3+1917\kappa^2+1863\kappa+486) - \frac{\gamma^{13}}{8192\alpha^{12}(\kappa+1)^5}(\kappa^{18}-$$

$$7\kappa^{17}-8\kappa^{16}+122\kappa^{15}+52\kappa^{14}-1036\kappa^{13}-770\kappa^{12}+4970\kappa^{11}+$$

$$7084\kappa^{10}-10780\kappa^9-30338\kappa^8-7294\kappa^7+47824\kappa^6+65744\kappa^5+$$

$$22052\kappa^4-32186\kappa^3-56905\kappa^2-29345\kappa-116376),$$

$$Re[a'_{56}] = -Re[a'_{55}],$$

$$Im[a'_{56}] = Im[a'_{55}], \tag{B.38}$$

$$\begin{aligned}
Re[a'_{65}] = {} & -2\alpha + \frac{\gamma}{2}(\kappa-1) - \frac{\gamma^2}{4\alpha(\kappa+1)}(\kappa^3-2\kappa^2-3\kappa+4) + \frac{\gamma^3}{8\alpha^2}(\kappa^3-4\kappa^2+ \\
& \kappa+6) - \frac{\gamma^4}{16\alpha^3(\kappa+1)^2}(\kappa^6-3\kappa^5-6\kappa^4+12\kappa^3+21\kappa^2-\kappa-28) + \frac{\gamma^5}{32\alpha^4} \\
& (\kappa^5-6\kappa^4+6\kappa^3+16\kappa^2-15\kappa-18) - \frac{\gamma^6}{64\alpha^5(\kappa+1)^3}(\kappa^9-4\kappa^8-8\kappa^7+ \\
& 30\kappa^6+48\kappa^5-66\kappa^4-156\kappa^3-40\kappa^2+79\kappa+212) + \frac{\gamma^7}{128\alpha^6}(\kappa^7-8\kappa^6+ \\
& 15\kappa^5+22\kappa^4-55\kappa^3-36\kappa^2+81\kappa+54) - \frac{\gamma^8}{256\alpha^7(\kappa+1)^4}(\kappa^{12}-5\kappa^{11}- \\
& 9\kappa^{10}+55\kappa^9+70\kappa^8-240\kappa^7-420\kappa^6+300\kappa^5+1125\kappa^4+697\kappa^3-483\kappa^2- \\
& 591\kappa-1784) + \frac{\gamma^9}{512\alpha^8}(\kappa^9-10\kappa^8+28\kappa^7+16\kappa^6-154\kappa^5+28\kappa^4+ \\
& 348\kappa^3-351\kappa-162) - \frac{\gamma^{10}}{1024\alpha^9(\kappa+1)^5}(\kappa^{15}-6\kappa^{14}-9\kappa^{13}+86\kappa^{12}+ \\
& 75\kappa^{11}-558\kappa^{10}-695\kappa^9+1710\kappa^8+3645\kappa^7-670\kappa^6-7653\kappa^5-7360\kappa^4+ \\
& 105\kappa^3+7150\kappa^2+2135\kappa) + \frac{\gamma^{11}}{2048\alpha^{10}}(\kappa^{11}-12\kappa^{10}+45\kappa^9-10\kappa^8- \\
& 270\kappa^7+288\kappa^6+754\kappa^5-780\kappa^4-1395\kappa^3+540\kappa^2+1377\kappa+486) - \\
& \frac{\gamma^{12}}{4096\alpha^{11}(\kappa+1)^6}(\kappa^{18}-7\kappa^{17}-8\kappa^{16}+122\kappa^{15}+52\kappa^{14}-1036\kappa^{13}- \\
& 770\kappa^{12}+4970\kappa^{11}+7084\kappa^{10}-10780\kappa^9-30338\kappa^8-7294\kappa^7+ \\
& 47824\kappa^6+65746\kappa^5+21932\kappa^4-30086\kappa^3-71965\kappa^2+17725\kappa- \\
& 169596) + \frac{\gamma^{13}}{8192\alpha^{12}}(\kappa^{13}-14\kappa^{12}+66\kappa^{11}-64\kappa^{10}-385\kappa^9+858\kappa^8+ \\
& 988\kappa^7-3156\kappa^6-2097\kappa^5+5670\kappa^4+4482\kappa^3-3888\kappa^2-5103\kappa- \\
& 1458),
\end{aligned} \tag{B.39}$$

$$Im[a'_{65}] = \{\frac{\gamma}{2}(\kappa-1) - \frac{\gamma^2}{4\alpha}(\kappa^2-\kappa-2) + \frac{\gamma^3}{8\alpha^2(\kappa+1)}(\kappa^4-\kappa^3-5\kappa^2-\kappa+6) -$$

$$\frac{\gamma^4}{16\alpha^3}(\kappa^4-3\kappa^3-3\kappa^2+7\kappa+6) + \frac{\gamma^5}{32\alpha^4(\kappa+1)^2}(\kappa^7-2\kappa^6-9\kappa^5+$$

$$6\kappa^4+33\kappa^3+18\kappa^2-19\kappa-44) - \frac{\gamma^6}{64\alpha^5}(\kappa^6-5\kappa^5+22\kappa^3+\kappa^2-$$

$$33\kappa-18) + \frac{\gamma^7}{128\alpha^6(\kappa+1)^3}(\kappa^{10}-3\kappa^9-12\kappa^8+22\kappa^7+78\kappa^6-$$

$$18\kappa^5-222\kappa^4-198\kappa^3+65\kappa^2+193\kappa+350) - \frac{\gamma^8}{256\alpha}(\kappa^8-7\kappa^7+$$

$$7\kappa^6+37\kappa^5-43\kappa^4-101\kappa^3+45\kappa^2+135\kappa+54) - \frac{\gamma^9}{512\alpha^8(\kappa+1)^4}$$

$$(\kappa^{13}-4\kappa^{12}-14\kappa^{11}+46\kappa^{10}+125\kappa^9-170\kappa^8-660\kappa^7-120\kappa^6+$$

$$1425\kappa^5+1820\kappa^4+264\kappa^3-1440\kappa^2-1263\kappa-3114) - \frac{\gamma^{10}}{1024\alpha^9}$$

$$(\kappa^{10}-9\kappa^9+18\kappa^8+44\kappa^7-138\kappa^6-126\kappa^5+376\kappa^4+348\kappa^3-351\kappa^2-$$

$$513\kappa-162) + \frac{\gamma^{11}}{2048\alpha^{10}(\kappa+1)^5}(\kappa^{16}-5\kappa^{15}-15\kappa^{14}+77\kappa^{13}+ \quad \textbf{(B.40)}$$

$$161\kappa^{12}-483\kappa^{11}-1253\kappa^{10}+1015\kappa^9+5355\kappa^8+2975\kappa^7-$$

$$8323\kappa^6-15015\kappa^5-7173\kappa^4+6251\kappa^3+14601\kappa^2+5413\kappa+$$

$$30466) - \frac{\gamma^{12}}{4096\alpha^{11}}(\kappa^{12}-11\kappa^{11}+33\kappa^{10}+35\kappa^9-280\kappa^8+18\kappa^7+$$

$$1042\kappa^6-26\kappa^5-2175\kappa^4-855\kappa^3+1917\kappa^2+1863\kappa+486) +$$

$$\frac{\gamma^{13}}{8192\alpha^{12}(\kappa+1)^6}(\kappa^{19}-6\kappa^{18}-15\kappa^{17}+114\kappa^{16}+174\kappa^{15}-984\kappa^{14}-$$

$$1806\kappa^{13}+4200\kappa^{12}+12054\kappa^{11}-3696\kappa^{10}-41118\kappa^9-37632\kappa^8+$$

$$40530\kappa^7+113568\kappa^6+87800\kappa^5-10414\kappa^4-83451\kappa^3-$$

$$132210\kappa^2-15619\kappa-319176)\}\sqrt{\frac{3-\kappa}{1+\kappa}},$$

$$Re[a'_{66}] = Re[a'_{65}],$$
$$Im[a'_{66}] = -Im[a'_{65}], \tag{B.41}$$

$$\begin{aligned}
Re[a'_{77}] = {} & -\alpha - \frac{\gamma}{2}(\kappa-2) - \frac{\gamma^2}{4\alpha(\kappa+1)}(\kappa^3-2\kappa^2-3\kappa+2) - \frac{\gamma^3}{8\alpha^2}(\kappa^3-4\kappa^2+ \\
& \kappa+6) - \frac{\gamma^4}{16\alpha^3(\kappa+1)^2}(\kappa^6-3\kappa^5-6\kappa^4+12\kappa^3+21\kappa^2-3\kappa-20) - \frac{\gamma^5}{32\alpha^4} \\
& (\kappa^5-6\kappa^4+6\kappa^3+16\kappa^2-15\kappa-18) - \frac{\gamma^6}{64\alpha^5(\kappa+1)^3}(\kappa^9-4\kappa^8-8\kappa^7+ \\
& 30\kappa^6+48\kappa^5-66\kappa^4-156\kappa^3-42\kappa^2+103\kappa+154) - \frac{\gamma^7}{128\alpha^6}(\kappa^7-8\kappa^6+ \\
& 15\kappa^5+22\kappa^4-65\kappa^3-36\kappa^2+81\kappa+54) - \frac{\gamma^8}{256\alpha^7(\kappa+1)^4}(\kappa^{12}-5\kappa^{11}- \\
& 9\kappa^{10}+55\kappa^9+70\kappa^8-240\kappa^7-420\kappa^6+300\kappa^5+1125\kappa^4+695\kappa^3-435\kappa^2- \\
& 885\kappa-1270) + \frac{\gamma^9}{512\alpha^8}(\kappa^9-10\kappa^8+28\kappa^7+16\kappa^6-154\kappa^5+28\kappa^4+ \\
& 348\kappa^3-351\kappa-162) - \frac{\gamma^{10}}{1024\alpha^9(\kappa+1)^5}(\kappa^{15}-6\kappa^{14}-9\kappa^{13}+86\kappa^{12}+ \\
& 75\kappa^{11}-558\kappa^{10}-695\kappa^9+1710\kappa^8+3645\kappa^7-670\kappa^6-7653\kappa^5- \\
& 7362\kappa^4+185\kappa^3+6258\kappa^2+5823\kappa) - \frac{\gamma^{11}}{2048\alpha^{10}}(\kappa^{11}-12\kappa^{10}+45\kappa^9- \\
& 10\kappa^8-270\kappa^7+288\kappa^6+754\kappa^5-780\kappa^4-1395\kappa^3+540\kappa^2+1377\kappa+ \\
& 486) - \frac{\gamma^{12}}{4096\alpha^{11}(\kappa+1)^6}(\kappa^{18}-7\kappa^{17}-8\kappa^{16}+122\kappa^{15}+52\kappa^{14}- \\
& 1036\kappa^{13}-770\kappa^{12}+4970\kappa^{11}+7084\kappa^{10}-10780\kappa^9-30338\kappa^8- \\
& 7294\kappa^7+47824\kappa^6+65744\kappa^5+22052\kappa^4-32186\kappa^3-56905\kappa^2- \\
& 29345\kappa) - \frac{\gamma^{13}}{8192\alpha^{12}}(\kappa^{13}-14\kappa^{12}+66\kappa^{11}-64\kappa^{10}-385\kappa^9+858\kappa^8+ \\
& 988\kappa^7-3156\kappa^6-2097\kappa^5+5670\kappa^4+4482\kappa^3-3888\kappa^2-5103\kappa- \\
& 1458),
\end{aligned} \tag{B.42}$$

$$
\begin{aligned}
Im[a'_{78}] = \{ & -\frac{\gamma}{2}\kappa - \frac{\gamma 2}{4\alpha}(\kappa^2-\kappa-2) - \frac{\gamma^3}{8\alpha^2(\kappa+1)}(\kappa^4-\kappa^3-5\kappa^2-\kappa+4) - \\
& \frac{\gamma^4}{16\alpha^3}(\kappa^4-3\kappa^3-3\kappa^2+7\kappa+6) - \frac{\gamma^5}{32\alpha^4(\kappa+1)^2}(\kappa^7-2\kappa^6-9\kappa^5+ \\
& 6\kappa^4+33\kappa^3+18\kappa^2-21\kappa-32) - \frac{\gamma^6}{64\alpha^5}(\kappa^6-5\kappa^5+22\kappa^3+\kappa^2- \\
& 33\kappa-18) - \frac{\gamma^7}{128\alpha^6(\kappa+1)^3}(\kappa^{10}-3\kappa^9-12\kappa^8+22\kappa^7+78\kappa^6- \\
& 18\kappa^5-222\kappa^4-198\kappa^3+63\kappa^2+225\kappa+252) - \frac{\gamma^8}{256\alpha^7}(\kappa^8-7\kappa^7+ \\
& 7\kappa^6+37\kappa^5-43\kappa^4-101\kappa^3+45\kappa^2+135\kappa+54) - \frac{\gamma^9}{512\alpha^8(\kappa+1)^4} \\
& (\kappa^{13}-4\kappa^{12}-14\kappa^{11}+46\kappa^{10}+125\kappa^9-170\kappa^8-660\kappa^7-120\kappa^6+ \\
& 1425\kappa^5+1820\kappa^4+262\kappa^3-1380\kappa^2-1709\kappa-2192) - \frac{\gamma^{10}}{1024\alpha^9} \\
& (\kappa^{10}-9\kappa^9+18\kappa^8+44\kappa^7-138\kappa^6-126\kappa^5+376\kappa^4+348\kappa^3-351\kappa^2- \\
& 513\kappa-162) - \frac{\gamma^{11}}{2048\alpha^{10}(\kappa+1)^5}(\kappa^{16}-5\kappa^{15}-15\kappa^{14}+77\kappa^{13}+ \\
& 161\kappa^{12}-483\kappa^{11}-1253\kappa^{10}+1015\kappa^9+5355\kappa^8+2975\kappa^7- \\
& 8323\kappa^6-15015\kappa^5-7175\kappa^4+6347\kappa^3+13341\kappa^2+11437\kappa+ \\
& 21052) - \frac{\gamma^{12}}{4096\alpha^{11}}(\kappa^{12}-11\kappa^{11}+33\kappa^{10}+35\kappa^9-280\kappa^8+18\kappa^7+ \\
& 1042\kappa^6-26\kappa^5-2175\kappa^4-855\kappa^3+1917\kappa^2+1863\kappa+486) - \\
& \frac{\gamma^{13}}{8192\alpha^{12}(\kappa+1)^6}(\kappa^{19}-6\kappa^{18}-15\kappa^{17}+114\kappa^{16}+174\kappa^{15}-984\kappa^{14}- \\
& 1806\kappa^{13}+4200\kappa^{12}+12054\kappa^{11}-3696\kappa^{10}-41118\kappa^9-37632\kappa^8+ \\
& 40530\kappa^7+113568\kappa^6+87798\kappa^5-10274\kappa^4-86271\kappa^3- \\
& 109230\kappa^2-65051\kappa-217776)\Big| \sqrt{\frac{3-\kappa}{1+\kappa}}\,,
\end{aligned}
\tag{B.43}
$$

$$Re[a'_{87}] = Re[a'_{77}],$$

$$Im[a'_{87}] = -Im[a'_{77}], \tag{B.44}$$

While substituting Eqns. (B.9) through (B.29) into Eqns. (B.4) through (B.8), some of the coefficients in the leading terms of expansion become zero when the actual computation was done. As a result, instead of seeing the power of leading terms as shown in the second parameters in Eqn. (B.31), we obtain the following

$$d_{11} = O(\alpha,3,-8),$$

$$d_{12} = O(\alpha,3,-8),$$

$$d_{21} = O(\alpha,4,-7), \tag{B.45}$$

$$d_{22} = O(\alpha,4,-7),$$

$$d = O(\alpha,4,-7).$$

Using the rules set forth in Eqn. (B.30), the final asymptotic expansions are as follows,

$$\frac{d_{11}}{d} = O(\alpha,-1,-12),$$

$$\frac{d_{12}}{d} = O(\alpha,-1,-12),$$

$$\frac{d_{21}}{d} = O(\alpha,0,-11), \tag{B.46}$$

$$\frac{d_{22}}{d} = O(\alpha,0,-11).$$

Written explicitly, they are

$$\frac{d_{11}}{d} = \frac{1}{\alpha(\kappa+1)}(\kappa-1)+\frac{\gamma}{4\alpha^2(\kappa+1)^2}(\kappa-3)-\frac{\gamma^2}{8\alpha^3(\kappa+1)^3}(3\kappa^2-\kappa-6)+$$

$$\frac{\gamma^3}{16\alpha^4(\kappa+1)^4}(\kappa^3-8\kappa^2+17\kappa+10)-\frac{\gamma^4}{32\alpha^5(\kappa+1)^5}(3\kappa^4-21\kappa^3+17\kappa^2+5\kappa-$$

$$4)+\frac{\gamma^5}{64\alpha^6(\kappa+1)^6}(\kappa^5-17\kappa^4+76\kappa^3-72\kappa^2-173\kappa-71)-\frac{\gamma^6}{128\alpha^7(\kappa+1)^7}\cdot$$

$$(3\kappa^6-50\kappa^5+159\kappa^4-4\kappa^3-127\kappa^2-10\kappa+29)+\frac{\gamma^7}{256\alpha^8(\kappa+1)^8}(\kappa^7-$$

$$30\kappa^6+241\kappa^5-629\kappa^4-225\kappa^3+1836\kappa^2+2039\kappa+623)-\frac{\gamma^8}{512\alpha^9(\kappa+1)^9}\cdot$$

$$(3\kappa^8-91\kappa^7+635\kappa^6-946\kappa^5-1308\kappa^4+921\kappa^3+1183\kappa^2-140\kappa-257)+ \qquad \textbf{(B.47)}$$

$$\frac{\gamma^9}{1024\alpha^{10}(\kappa+1)^{10}}(\kappa^9-47\kappa^8+608\kappa^7-2900\kappa^6+3328\kappa^5+10552\kappa^4-$$

$$10316\kappa^3-34016\kappa^2-25109\kappa-6101)-\frac{\gamma^{10}}{2048\alpha^{11}(\kappa+1)^{11}}(3\kappa^{10}-144\kappa^9+$$

$$1749\kappa^8-6484\kappa^7+744\kappa^6+20824\kappa^5+6536\kappa^4-18804\kappa^3-10539\kappa^2+$$

$$3584\kappa+2531)+\frac{\gamma^{11}}{4096\alpha^{12}(\kappa+1)^{12}}(\kappa^{11}-68\kappa^{10}+1305\kappa^9-9860\kappa^8+$$

$$27560\kappa^7+13328\kappa^6-149276\kappa^5-73340\kappa^4+370775\kappa^3+569292\kappa^2+$$

$$316995\kappa+63912),$$

$$\frac{d_{12}}{d} = i[\frac{1}{\alpha} + \frac{\gamma}{4\alpha^2(\kappa+1)} + \frac{\gamma^2}{8\alpha^3(\kappa+1)^2}(\kappa-1) + \frac{\gamma^3}{16\alpha^4(\kappa+1)^3}(\kappa^2-\kappa-6) +$$

$$\frac{\gamma^4}{32\alpha^5(\kappa+1)^4}(\kappa^3-8\kappa^2+3\kappa+4) + \frac{\gamma^5}{64\alpha^6(\kappa+1)^5}(\kappa^4+6\kappa^3-14\kappa^2+54\kappa+45) +$$

$$\frac{\gamma^6}{128\alpha^7(\kappa+1)^6}(\kappa^5-19\kappa^4+60\kappa^3+32\kappa^2-45\kappa-29) + \frac{\gamma^7}{256\alpha^8(\kappa+1)^7}\cdot(\kappa^6-$$

$$15\kappa^5+8\kappa^4+271\kappa^3-256\kappa^2-844\kappa-405) + \frac{\gamma^8}{512\alpha^9(\kappa+)^8}\cdot(\kappa^7-34\kappa^6+251\kappa^5-$$

$$309\kappa^4-803\kappa^3+22\kappa^2+615\kappa+257) + \frac{\gamma^9}{1024\alpha^{10}(\kappa+1)^9}\cdot(\kappa^8-28\kappa^7+124\kappa^6+ \qquad \textbf{(B.48)}$$

$$576\kappa^5-3008\kappa^4-1816\kappa^3+9196\kappa^2+11860\kappa+4023) + \frac{\gamma^{10}}{2048\alpha^{11}(\kappa+1)^{10}}\cdot$$

$$(\kappa^9-53\kappa^8+688\kappa^7-2540\kappa^6-836\kappa^5+9844\kappa^4+8596\kappa^3-4976\kappa^2-8193\kappa-$$

$$2531) + \frac{\gamma^{11}}{4096\alpha^{12}(\kappa+1)^{11}}(\kappa^{10}-45\kappa^9+430\kappa^8+150\kappa^7-12270\kappa^6+19534\kappa^5+$$

$$65073\kappa^4-44178\kappa^3-198071\kappa^2-161797\kappa-42528)],$$

$$\frac{d_{21}}{d} = \frac{1}{\kappa+1} + \frac{\gamma}{\alpha(\kappa+1)^2} - \frac{\gamma^2}{2\alpha^2(\kappa+1)^3}(\kappa-1) + \frac{\gamma^3}{4\alpha^3(\kappa+1)^4}(\kappa^2-4\kappa-1) -$$

$$\frac{\gamma^4}{8\alpha^4(\kappa+1)^5}(\kappa^3-7\kappa^2+3\kappa+3) + \frac{\gamma^5}{16\alpha^5(\kappa+1)^6}(\kappa^4-12\kappa^3+20\kappa^2+24\kappa+7) -$$

$$\frac{\gamma^6}{32\alpha^6(\kappa+1)^7}\cdot(\kappa^5 17\kappa^4+50\kappa^3+22\kappa^2-35\kappa-21) + \frac{\gamma^7}{64\alpha^7(\kappa+1)^8}\cdot(\kappa^6-24\kappa^5+$$

$$119\kappa^4-36\kappa^3-301\kappa^2-244\kappa-59) - \frac{\gamma^8}{128\alpha^8(\kappa+1)^9}\cdot(\kappa^7-31\kappa^6+213\kappa^5-$$

$$251\kappa^4+605\kappa^3+35\kappa^2+455\kappa+183) + \frac{\gamma^9}{256\alpha^9(\kappa+1)^{10}}\cdot(\kappa^8-40\kappa^7+384\kappa^6- \qquad \textbf{(B.49)}$$

$$904\kappa^5-1184\kappa^4+2320\kappa^3+4636\kappa^2+2768\kappa+563) - \frac{\gamma^{10}}{512\alpha^{10}(\kappa+1)^{11}}\cdot(\kappa^9-$$

$$49\kappa^8+596\kappa^7-2084\kappa^6-658\kappa^5+7458\kappa^4+6244\kappa^3-3796\kappa^2-5927\kappa-1785)$$

$$+\frac{\gamma^{11}}{1024\alpha^{11}(\kappa+1)^{12}}(\kappa^{10}-60\kappa^9+935\kappa^8-4720\kappa^7+2840\kappa^6+23272\kappa^5-316\kappa^4$$

$$-58720\kappa^3-70049\kappa^2-33180\kappa-5795),$$

$$\frac{d_{22}}{d} = i[\frac{1}{\kappa+1} + \frac{\gamma^3}{4\alpha^3(\kappa+1)^3} - \frac{\gamma^4}{8\alpha^4(\kappa+1)^4}(\kappa-1) + \frac{\gamma^5}{8\alpha^5(\kappa+1)^5}(\kappa^2-4\kappa-3) -$$

$$\frac{\gamma^6}{16\alpha^6(\kappa+1)^6}(\kappa^3-6\kappa^2+\kappa+4) + \frac{\gamma^7}{64\alpha^7(\kappa+1)^7}(3\kappa^4-32\kappa^3+41\kappa^2+110\kappa+50) -$$

$$\frac{\gamma^8}{128\alpha^8(\kappa+1)^8}\cdot(3\kappa^5-41\kappa^4+99\kappa^3+99\kappa^2-86\kappa-74) + \frac{\gamma^9}{64\alpha^9(\kappa+1)^9}(\kappa^6-20\kappa^5$$

$$+86\kappa^4+30\kappa^3-306\kappa^2-364\kappa-119) - \frac{\gamma^{10}}{256\alpha^{10}(\kappa+1)^{10}}\cdot(2\kappa^7-48\kappa^6+276\kappa^5- \quad \textbf{(B.50)}$$

$$187\kappa^4-1006\kappa^3-170\kappa^2+760\kappa+373) + \frac{\gamma^{11}}{1024\alpha^{11}(\kappa+1)^{11}}\cdot(5\kappa^8-160\kappa^7+$$

$$1330\kappa^6-2340\kappa^5-6786\kappa^4+7168\kappa^3+24634\kappa^2+19156\kappa+4897)].$$

B.4 Leading terms of the integrands in Fredholm kernels

It is shown in Chapter 2 that the Fredholm kernels in the singular integral equations are in the form of infinite integrals with their integrands composed of two multiplicative parts (Eqns.' (51) through (54)). The first is made up of sums of analytical rational functions whose numerators and denominators are determinants as described in Chapter 2. These expressions are multiplied by either a sine or cosine function that makes the integrands oscillating.

In Chapter 3, we choose to evaluate each infinite integral by two parts. The first part is an integral with limits of integration from 0 to a finite value "*A*" (see Chapter 3), and the integral is evaluated numerically by straightforward Gauss' formula. The second is an integral with limits of integration from "*A*" to infinity. We have chosen to evaluate only the leading terms of the integrand from the asymptotic

expansion, together with the oscillating part, in closed form. The remaining part is ignored, provided a sufficiently large "A" is chosen so that contributions to the integral from terms of order higher than what could be extracted asymptotically were insignificant. Convergence of the evaluation of each infinite integral is achieved by varying the value "A" and by noting the numerical results are identical to a certain digit.

In what follows, we shall give the leading terms of asymptotic expansion of the integrands in the Fredholm kernels as described above. They are derived simply from combining terms and expressions already established in Eqns. (B.47) through (B.50).

Let us rewrite Eqns. (47) through (54) as follows,

$$k_{11}(x,t) = \int_0^{\infty} D_{11}^{*}(\alpha)\sin\alpha(t-x)\,d\alpha, \tag{B.51}$$

$$k_{12}(x,t) = \int_0^{\infty} D_{12}^{*}(\alpha)\cos\alpha(t-x)\,d\alpha, \tag{B.52}$$

$$k_{21}(x,t) = \int_0^{\infty} D_{21}^{*}(\alpha)\cos\alpha(t-x)\,d\alpha, \tag{B.53}$$

$$k_{22}(x,t) = \int_0^{\infty} D_{22}^{*}(\alpha)\sin\alpha(t-x)\,d\alpha, \tag{B.54}$$

$$D_{11}^{*}(\alpha) = -\frac{\kappa+1}{2}\left[2\alpha\left(\frac{D_{11}}{D}+\frac{D_{31}}{D}-\frac{\kappa-1}{2\alpha(\kappa+1)}\right)+(\kappa+1)\left(\frac{D_{21}}{D}-\frac{D_{41}}{D}-\frac{1}{\kappa+1}\right)\right], \tag{B.55}$$

$$D_{12}^{*}(\alpha) = -\frac{\kappa+1}{2}\,i\left[2\alpha\left(\frac{D_{12}}{D}+\frac{D_{32}}{D}\right)-(\kappa+1)\left(\frac{D_{22}}{D}-\frac{D_{42}}{D}\right)\right], \tag{B.56}$$

$$D_{21}^{*}(\alpha) = \frac{\kappa+1}{2}[2\alpha(\frac{D_{11}}{D} - \frac{D_{31}}{D}) - (\kappa-1)(\frac{D_{21}}{D} + \frac{D_{41}}{D})], \tag{B.57}$$

$$D_{22}^{*}(\alpha) = -\frac{\kappa+1}{2} i[2\alpha(\frac{D_{12}}{D} - \frac{D_{32}}{D} - \frac{i}{2\alpha}) - (\kappa-1)(\frac{D_{22}}{D} + \frac{D_{42}}{D} - \frac{i}{\kappa+1})]. \tag{B.58}$$

Let d_{11}^{*}, d_{12}^{*}, d_{21}^{*} and d_{22}^{*} represent the leading asymptotic terms of D_{11}^{*}, D_{12}^{*}, D_{21}^{*} and D_{22}^{*} respectively. Substituting $\frac{d_{11}}{d}$, $\frac{d_{12}}{d}$, $\frac{d_{21}}{d}$ and $\frac{d_{22}}{d}$ from Eqns. (B.47) through (B.50), which are the first eleven leading asymptotic terms of the respective rational expression resulting from the 7 by 7 determinant in the numerator and the 8 by 8 determinant in the denominator, for $\frac{D_{11}}{D}$, $\frac{D_{12}}{D}$, $\frac{D_{21}}{D}$ and $\frac{D_{22}}{D}$ in Eqns. (B.55) through (B.58), we obtain a set of truncated polynomials in α^{-1}. Again, any term that involves $\frac{D_{13}}{D}$, $\frac{D_{14}}{D}$, $\frac{D_{23}}{D}$ or $\frac{D_{24}}{D}$ is ignored for the same reason given earlier, that they are of much lower order terms and do not participate in the asymptotic analysis or contribute to the leading terms. The expressions for $d^{*}_{11}(\alpha)$, $d^{*}_{12}(\alpha)$, $d^{*}_{21}(\alpha)$ and $d^{*}_{22}(\alpha)$ are shown in the following few pages.

$$d_{11}^{*}(\alpha) = \frac{\gamma}{4\alpha} + \frac{\gamma^2}{8\alpha^2(\kappa+1)^2}(\kappa-1)(\kappa-3) + \frac{\gamma^3}{16\alpha^3(\kappa+1)^3}\cdot$$

$$(\kappa^3+2\kappa^2-27\kappa-12) + \frac{\gamma^4}{32\alpha^4(\kappa+1)^4}(\kappa-1)(\kappa^3-8\kappa^2+17\kappa+10) +$$

$$\frac{\gamma^5}{64\alpha^5(\kappa+1)^5}(\kappa^5-5\kappa^4-60\kappa^3+160\kappa^2+235\kappa+85) + \frac{\gamma^6}{128\alpha^6(\kappa+1)^6}\cdot$$

$$(\kappa^5-17\kappa^4+76\kappa^3-72\kappa^2-173\kappa-71) + \frac{\gamma^7}{256\alpha^7(\kappa+1)^7}\cdot(\kappa^7-16\kappa^6-$$

$$51\kappa^5+795\kappa^4-449\kappa^3-2926\kappa^2-2645\kappa-741) + \frac{\gamma^8}{512\alpha^8(\kappa+1)^8}\cdot$$

$$(\kappa-1)(\kappa^7-30\kappa^6+241\kappa^5-629\kappa^4-225\kappa^3+1836\kappa^2+2039\kappa+623) +$$

$$\frac{\gamma^9}{1024\alpha^9(\kappa+1)^9}\cdot(\kappa^9-31\kappa^8+80\kappa^7+1860\kappa^6-7504\kappa^5-8280\kappa^4+ \qquad \textbf{(B.59)}$$

$$24228\kappa^3+48824\kappa^2+31771\kappa+7227) + \frac{\gamma^{10}}{2048\alpha^{10}(\kappa+1)^{10}}\cdot(\kappa-1)$$

$$(\kappa^9-47\kappa^8+608\kappa^7-2900\kappa^6+3328\kappa^5+10552\kappa^4-10316\kappa^3-$$

$$34016\kappa^2-25109\kappa-6101) + \frac{\gamma^{11}}{4096\alpha^{11}(\kappa+1)^{11}}(\kappa^{11}-50\kappa^{10}+$$

$$445\kappa^9+2290\kappa^8-31320\kappa^7+38896\kappa^6+195188\kappa^5-44732\kappa^4-$$

$$628313\kappa^3-775750\kappa^2-394945\kappa-75502)$$

$$= \sum_{j=1}^{11} \frac{c_{11,j}^{*}}{\alpha^j},$$

$$d_{12}^{*}(\alpha) = \frac{\gamma}{4\alpha} + \frac{\gamma^2}{8\alpha^2(\kappa+1)}(\kappa-1) + \frac{\gamma^3}{16\alpha^3(\kappa+1)^2}\cdot(\kappa^2-3\kappa-8) +$$

$$\frac{\gamma^4}{32\alpha^4(\kappa+1)^3}(\kappa-1)(\kappa^2-5\kappa-2) + \frac{\gamma^5}{64\alpha^5(\kappa+1)^4}\cdot(\kappa^4-10\kappa^3-2\kappa^2+$$

$$82\kappa+57) + \frac{\gamma^6}{128\alpha^6(\kappa+1)^5}\cdot(\kappa^4-14\kappa^3+26\kappa^2+38\kappa+13) +$$

$$\frac{\gamma^7}{256\alpha^7(\kappa+1)^6}\cdot(\kappa^6-21\kappa^5+66\kappa^4+253\kappa^3-558\kappa^2-1164\kappa-505) +$$

$$\frac{\gamma^8}{512\alpha^8(\kappa+1)^7}\cdot(\kappa-1)(\kappa^6-27\kappa^5+148\kappa^4-45\kappa^3-452\kappa^2-404\kappa-$$

$$109) + \frac{\gamma^9}{1024\alpha^9(\kappa+1)^8}\cdot(\kappa^8-36\kappa^7+276\kappa^6+48\kappa^5-3936\kappa^4+ \qquad \textbf{(B.60)}$$

$$392\kappa^3+14556\kappa^2+15724\kappa+4975) + \frac{\gamma^{10}}{2048\alpha^{10}(\kappa+1)^9}\cdot(\kappa-1)$$

$$(\kappa^8-44\kappa^7+460\kappa^6-1168\kappa^5-1648\kappa^4+3424\kappa^3+7316\kappa^2+4700\kappa+$$

$$1039) + \frac{\gamma^{11}}{4096\alpha^{11}(\kappa+1)^{10}}\cdot(\kappa^{10}-55\kappa^9+740\kappa^8-2190\kappa^7-10250\kappa^6+$$

$$37786\kappa^5+64314\kappa^4-107782\kappa^3-285651\kappa^2-209903\kappa-52322)$$

$$= \sum_{j=1}^{11} \frac{c_{12j}^{*}}{\alpha^j},$$

$$d_{21}^{*}(\alpha) = -d_{12}^{*}(\alpha), \qquad \textbf{(B.61)}$$

$$d_{22}^{*}(\alpha) = \frac{\gamma}{4\alpha} + \frac{\gamma^2}{8\alpha^2(\kappa+1)}(\kappa-1) + \frac{\gamma^3}{16\alpha^3(\kappa+1)}\cdot(\kappa-4) +$$

$$\frac{\gamma^4}{32\alpha^4(\kappa+1)^2}(\kappa-1)(\kappa-6) + \frac{\gamma^5}{64\alpha^5(\kappa+1)^3}\cdot(\kappa^3-11\kappa^2+$$

$$17\kappa+33) + \frac{\gamma^6}{128\alpha^6(\kappa+1)^4}\cdot(\kappa-1)(\kappa^3-15\kappa^2+33\kappa+45) +$$

$$\frac{\gamma^7}{256\alpha^7(\kappa+1)^5}\cdot(\kappa^5-22\kappa^4+100\kappa^3+25\kappa^2-419\kappa-305) +$$

$$\frac{\gamma^8}{512\alpha^8(\kappa+1)^6}\cdot(\kappa-1)(\kappa^5-28\kappa^4+164\kappa^3-57\kappa^2-639\kappa-$$

$$405) + \frac{\gamma^9}{1024\alpha^9(\kappa+1)^7}\cdot(\kappa^7-37\kappa^6+329\kappa^5-601\kappa^4+ \qquad \textbf{(B.62)}$$

$$1959\kappa^3+2831\kappa^2+6829\kappa+3071) + \frac{\gamma^{10}}{2048\alpha^{10}(\kappa+1)^8}\cdot(\kappa-1)$$

$$(\kappa^7+45\kappa^6-489\kappa^5-1289\kappa^4-2199\kappa^3+5279\kappa^2+9741\kappa+$$

$$4023) + \frac{\gamma^{11}}{4096\alpha^{11}(\kappa+1)^9}(\kappa^9-56\kappa^8+816\kappa^7-3646\kappa^6-$$

$$1284\kappa^5+29710\kappa^4+7460\kappa^3-86570\kappa^2-100545\kappa-32734)$$

$$= \sum_{j=1}^{11} \frac{c_{22j}^{*}}{\alpha^j},$$

Appendix C

Formula Derived From Sine And Cosine Integrals

We start with the definitions of sine and cosine integrals [23],

$$Si(x) = \int_0^x \frac{\sin t}{t}\, dt, \tag{C.1}$$

$$Ci(x) = -\int_x^\infty \frac{\cos t}{t}\, dt = \gamma_o + \log|x| + \int_0^{|x|} \frac{\cos t - 1}{t}\, dt, \tag{C.2}$$

$$si(x) = -\int_x^\infty \frac{\sin t}{t}\, dt, \tag{C.3}$$

where γ_0=0.57721566490, is the Euler's constant. To change Eqns. (C.1) (C.2), and (C.3) to a form that is suitable to be used in our problem, we can show that it can be expressed, by a simple change of variable, as follows

$$\int_0^A \frac{\sin\alpha(t-x)}{\alpha}\, d\alpha = Si(A(t-x)), \tag{C.4}$$

$$\begin{aligned}\int_A^\infty \frac{\cos\alpha(t-x)}{\alpha}\, d\alpha &= -Ci(A(t-x)) \\ &= -\gamma_o - \log|A(t-x)| - \int_0^{|A(t-x)|} \frac{\cos\alpha - 1}{\alpha}\, d\alpha,\end{aligned} \tag{C.5}$$

$$\int_A^\infty \frac{\sin\alpha(t-x)}{\alpha}\, d\alpha = si(A(t-x)). \tag{C.6}$$

We also note that

$$\int_0^{\infty} \frac{\sin\alpha(t-x)}{\alpha}\, d\alpha = sign(t-x)\, \frac{\pi}{2}. \tag{C.7}$$

Therefore

$$si(A(t-x)) = Si(A(t-x)) - sign(t-x)\frac{\pi}{2}. \tag{C.8}$$

Now we are ready to derive the necessary closed form expressions for integrals to be used in Chapter 3. Integrating Eqn. (C.6) by parts as

$$\int_A^{\infty} \frac{\sin\alpha(t-x)}{\alpha}\, d\alpha + \int_A^{\infty} \frac{\cos\alpha(t-x)}{\alpha^2(t-x)}\, d\alpha = -\frac{\cos\alpha(t-x)}{\alpha(t-x)}\Big|_A^{\infty} = \frac{\cos A(t-x)}{A(t-x)}, \tag{C.9}$$

and after simplifying, we obtain

$$\int_A^{\infty} \frac{\cos\alpha(t-x)}{\alpha^2} d\alpha = \frac{\cos A(t-x)}{A} + (t-x)si(A(t-x)). \tag{C.10}$$

Again integrating Eqn. (C.10) by parts and simplifying, we obtain

$$\int_A^{\infty} \frac{\sin\alpha(t-x)}{\alpha^3} d\alpha = \frac{t-x}{2A}\cos A(t-x) + \frac{1}{2A^2}\sin A(t-x) + \frac{(t-x)^2}{2} si(A(t-x)). \tag{C.11}$$

By repeating the above process several times, we can deduce the following identities,

$$\int_A^{\infty} \frac{\cos\alpha(t-x)}{\alpha^{2n}} d\alpha = \cos A(t-x)\sum_{j=1}^{n} \frac{(-1)^{j+1}(t-x)^{2(j-1)}(2n-2j)!}{(2n-1)!A^{2n-2j+1}} + \tag{C.12}$$

$$\sin A(t-x)\sum_{j=1}^{n-1} \frac{(-1)^j(t-x)^{2j-1}(2n-2j-1)!}{(2n-1)!A^{2n-2j}} + (-1)^{n+1}\frac{(t-x)^{2n-1}}{(2n-1)!} si(A(t-x)).$$

$$\int_A^{\infty} \frac{\sin\alpha(t-x)}{\alpha^{2n-1}}\,d\alpha = \cos A(t-x)\sum_{j=1}^{n-1}\frac{(-1)^{j+1}(t-x)^{2(j-1)}(2n-2j-2)!}{(2n-2)!A^{2n-2j-1}} +$$

(C.13)

$$\sin A(t-x)\sum_{j=1}^{n-1}\frac{(-1)^{j+1}(t-x)^{2(j-1)}(2n-2j-1)!}{(2n-2)!A^{2n-2j}} + (-1)^{n+1}\frac{(t-x)^{2n-2}}{(2n-2)!}si(A(t-x)).$$

where n is any positive integer. Here we have derived expressions for infinite integrals with a definite lower limit of integration whose integrand involves cosine functions with even algebraic decaying power functions as well as for similar integrals with integrands that have sine functions and odd algebraic decaying power functions.

Applying the above procedure to the cosine integral as we do to the sine integral, integrating Eqn. (C.5) by parts and simplifying, we obtain

$$\int_A^{\infty} \frac{\sin\alpha(t-x)}{\alpha^2}d\alpha = \frac{1}{A}\sin\alpha(t-x) - (t-x)Ci(A(t-x)). \qquad \textbf{(C.14)}$$

Once again repeating the integration by parts several times, we deduce the following identities,

$$\int_A^{\infty} \frac{\cos\alpha(t-x)}{\alpha^{2n-1}}\,d\alpha = \cos A(t-x)\sum_{j=1}^{n-1}\frac{(-1)^{j+1}(t-x)^{2(j-1)}(2n-2j-1)!}{(2n-2)!A^{2n-2j}} +$$

(C.15)

$$\sin A(t-x)\sum_{j=1}^{n-1}\frac{(-1)^{j}(t-x)^{2j-1}(2n-2j-2)!}{(2n-2)!A^{2n-2j-1}} + (-1)^{n}\frac{(t-x)^{2n-2}}{(2n-2)!}Ci(A(t-x)).$$

$$\int_A^{\infty} \frac{\sin\alpha(t-x)}{\alpha^{2n}}d\alpha = \cos A(t-x)\sum_{j=1}^{n-1}\frac{(-1)^{j+1}(t-x)^{2j-1}(2n-2j-1)!}{(2n-1)!A^{2n-2j}} +$$

(C.16)

$$\sin A(t-x)\sum_{j=1}^{n}\frac{(-1)^{j+1}(t-x)^{2(j-1)}(2n-2j)!}{(2n-1)!A^{2n-2j+1}} + (-1)^{n}\frac{(t-x)^{2n-1}}{(2n-1)!}Ci(A(t-x)).$$

again, n is any positive integer. Eqn. (C.15) and (C.16) show expressions for infinite integrals with their integrands having cosine or sine functions and corresponding odd and even algebraic decaying power functions.

Appendix D

Approximation Of Step Function and Logarithm Function

D.1 Gauss' formula and its approximation of a step function

The famous Gauss' formula for the evaluation of integrals of bounded functions is as follows [23]

$$\int_{-1}^{1} f(t)\,dt = \sum_{i=1}^{n} w_i\, f(t_i) + R_n, \tag{D.1}$$

where t_i is the *i-th* zero of the Legendre polynomial $P_n(t)$. The weight function $w_i(t)$ and remainder R_n are as follows,

$$w_i = \frac{2}{(1-t_i^2)}\,[P'_n(t_i)]^2,$$

$$R_n = \frac{2^{2n+1}(n!)^4}{(2n+1)[(2n)!]^3}\, f^{(2n)}(\xi),\ -1<\xi<1. \tag{D.2}$$

For smooth bounded functions, the Gauss' formula provides an accurate evaluation of definite integrals. To evaluate certain functions that have discontinuities, however, Gauss' formula, or any numerical scheme for that matter, will fail if proper care is not taken to address the discontinuities. In the case of a step function, we will find that straight away Gauss' formula fails miserably. The reason is that general numerical schemes which use polynomials, and in the case of Gauss' formula which uses orthogonal Legendre polynomials, are simply unable to properly approximate a step function. Compared to evaluating integrals with a step function, those with a logarithm function fare much better when using the Gauss' formula. But the error

is still significant. We shall illustrate this by using the Gauss' formula to evaluate integrals with a simple step function and functions involving step function and simple power functions to compare them with the values computed from exact analytical expression. Integrals involving a logarithm function and a power function will be demonstrated likewise.

In Chapter 3, we evaluated infinite integrals with a definite lower limit having integrands with power functions in the denominator and oscillatory sine or cosine terms of the form

$$\int_A^\infty \frac{\sin\alpha(t-x)}{\alpha^n}\,d\alpha, \quad \int_A^\infty \frac{\cos\alpha(t-x)}{\alpha^n}\,d\alpha, \quad n = 1 \cdots 11. \tag{D.3}$$

From the closed form expressions of Eqn. (D.3) (see Eqns. (C.12) ,(C.13), (C.15) and (C.16) in Appendix C), we know that these integrals contain terms like $(t-x)^n\, si(A(t-x))$, and $(t-x)^n\, Ci(A(t-x))$. From Eqn. (C.5) in Appendix C, we see that $Ci(A(t-x))$ contains a logarithm term like $\log|t-x|$. Furthermore, from Eqn. (D.4), we know that $si(A(t-x))$ contains a step function $sign(t-x)$. This implies that the Fredholm kernels may be expressed as follows

$$k_{ij}(x,t) = \sum_{n=0}^{\infty} (t-x)^n \left[c_{ij,n}\, sign(t-x) + d_{ij,n} \log|t-x|\right] + F_{ij}(t,x),\ i, j = 1, 2. \tag{D.4}$$

where $c_{i\,j,\,l}$ and $d_{i\,j,\,l}$ are constants and $F_{i\,j}(t,x)$ are smooth bounded functions. The terms involving the sign function in the summation is a step function as shown in Figure 48. The $n=1$ term, which gives $(t-x)\, sign(t-x)$, is continuous, but its derivative is not. This can be seen from the presence of a kink in Figure 49. When n is 2 or larger, each term becomes increasingly smoother, even though there is a step function, and it becomes easier to approximate it with a polynomial. Figure 50 portrays this

fact by the plot of the function $(t-x)^2\ sign(t-x)$ and shows that even with the presence of a step function, the function is sufficiently smooth so that the function itself and its first derivative is continuous, only its second derivative is discontinuous.

Table XXI further illustrates the fact stated above by the tabulated result of numerical integration from -1 to 1 of functions plotted in Figure 48 to Figure 50 by three different schemes.

(a). Use a 20-point Gauss' formulas over the limits of integration from -1 to 1 disregarding the presence of step function.

(b). The same 20-point Gauss rule, but splitting it into two integrals at the point of sign change.

(c). Exact analytical evaluation.

We make several observations based on the results of the three cases computed, see Table XXI.

(1). Completely disregarding the presence of step function while integrating numerically could make the integral very inaccurate, with error reaching as much as 25% in the cases illustrated.

(2). The increasing exponent of the power functions serves to dampen the effect of the step function in making the integrand discontinuous. This can be seen in the increasing digits of accuracy for the integral as the power goes up.

(3). Splitting the integral in two when there is a step function in the integrand at the point of sign change is perhaps the best way to evaluate these integrals. This can be seen in Table XXI that the results are virtually the same for splitting the integral and the exact

analytical evaluation. This also shows the superb accuracy Gauss' formula possesses when dealing with bounded smooth functions in definite integrals.

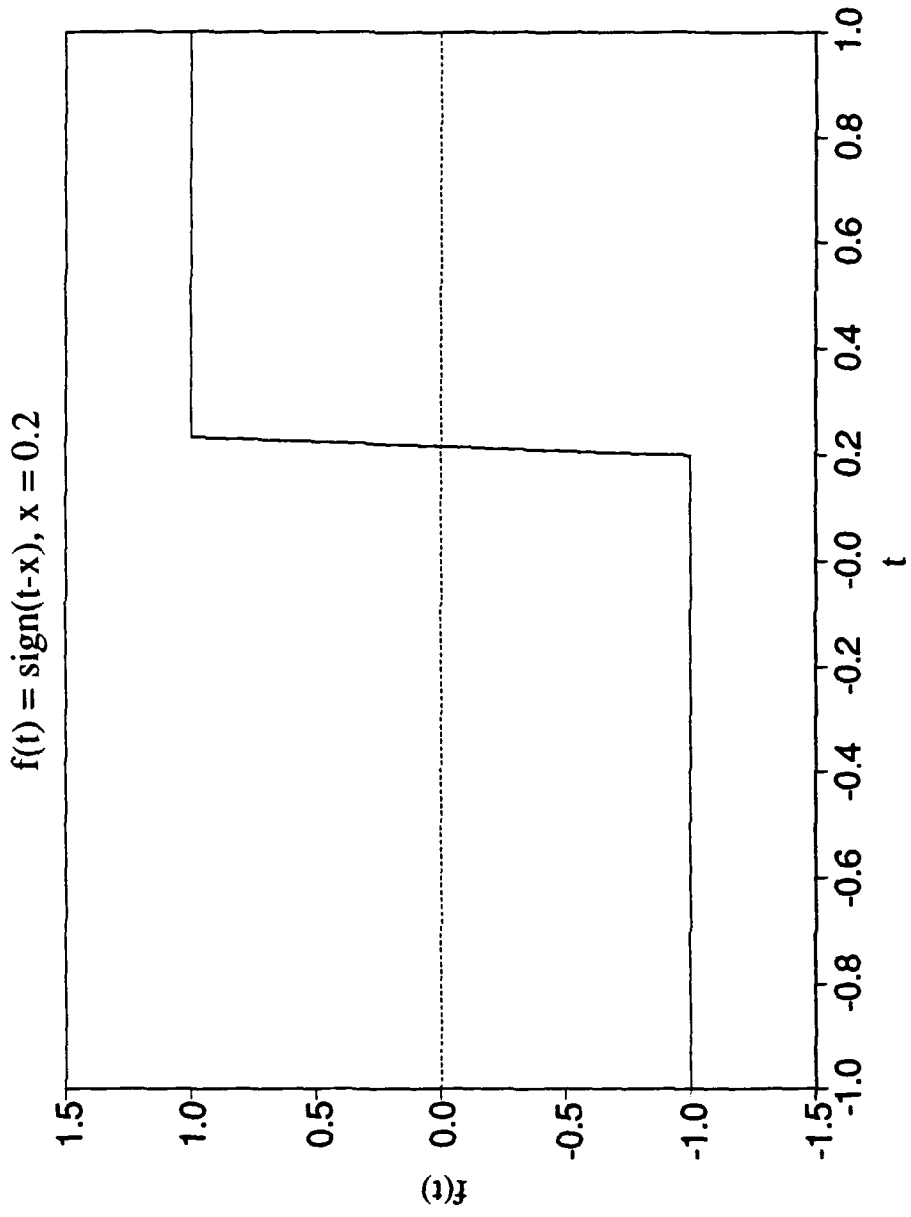

Figure 48 *sign(t-x), x=0.2*, a step function.

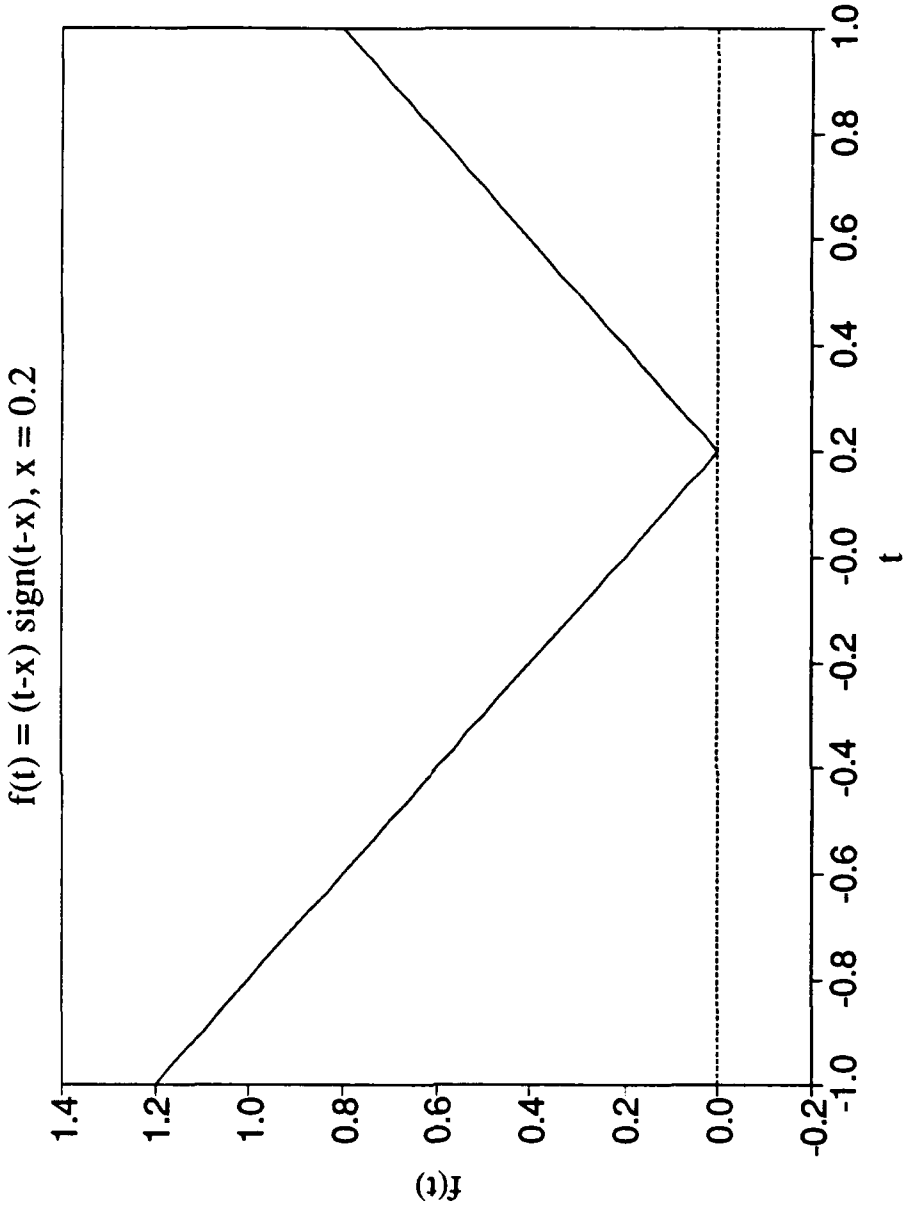

Figure 49 *f(t)=(t-x) sign(t-x), x=0.2, f'(t)* is discontinuous.

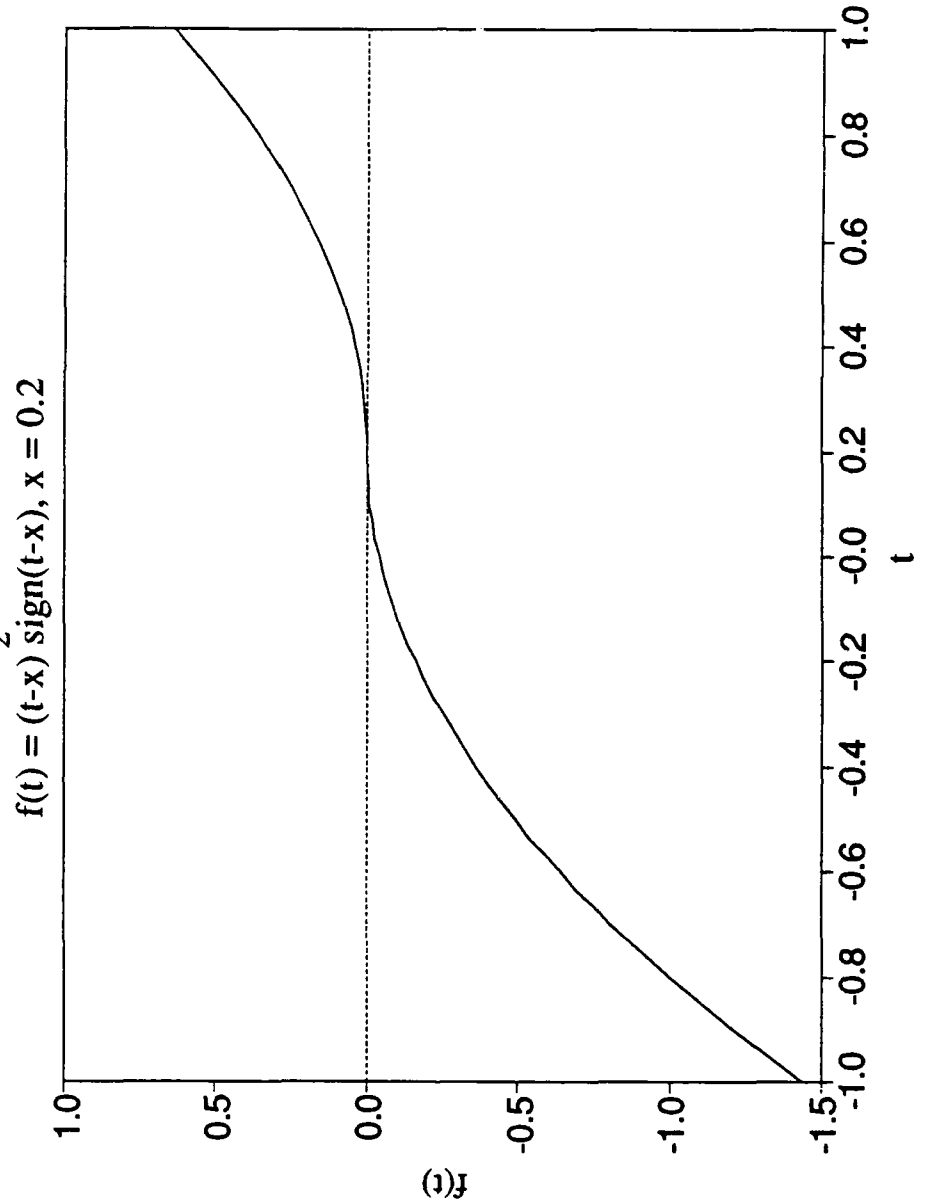

Figure 50 *f(t)=(t-x)² sign(t-x), x=0.2,* **both** *f(t)* **and** *f'(t)* **are continuous.**

Table XXI Evaluation of $\int_{-1}^{1} f(t,x)\,dt$, with different schemes for selected x values. f(t,x) contains a step function.

	f(t,x)	Gauss (a)	Gauss/split int. (b)	Exact (c)
x=0.2	sign(t-x)	-0.305506	-0.400000	-0.400000
	(t-x) sign(t-x)	1.039683	1.040000	1.040000
	$(t-x)^2$ sign(t-x)	-0.405442	-0.405333	-0.405333
x=0.4	sign(t-x)	-0.888045	-0.800000	-0.800000
	(t-x) sign(t-x)	1.159637	1.160000	1.160000
	$(t-x)^2$ sign(t-x)	-0.842581	-0.842667	-0.842667
x=0.6	sign(t-x)	-1.151422	-1.200000	-1.200000
	(t-x) sign(t-x)	1.360721	1.360000	1.360000
	$(t-x)^2$ sign(t-x)	-1.344049	-1.344000	-1.344000

Note:

(a). Gauss' formula with 20 Gauss points.

(b). Split the integral in two at the point of sign change in the step function, then use Gauss' formula for each integral.

(c). Exact.

D.2 Approximation of a logarithm function

The terms in Eqn. (D.4) that contain a logarithm function do not behave as badly as those that contain a step function, as far as numerical integration is concerned. As a matter of fact, for terms like $(t-x)^n \log|t-x|$, $n \geq 1$, the function is continuous and so are its derivatives. It is due to the stronger term $(t-x)^n$ suppressing a weak singularity at $(t-x) = 0$ of a logarithm function. This can be seen by the behavior of the functions in Figure 52 and Figure 53. Only when there is a logarithm function without the presence of power function do we see a singularity, as shown in Figure 51.

From the behavior of those functions that contain a logarithm term as shown in Figure 51 through Figure 53, and the discussions in the previous section regarding numerical approximation of integrals, we could very well anticipate that only the logarithm function alone would need particular attention in numerical computation. Those integrals that have terms like $(t-x)^n \log|t-x|$, $n \geq 1$ pose no special problem. Similar to what has been done in the previously section, a table is compiled to list the result of numerical integration from -1 to 1 of functions plotted in Figure 51 to Figure 53, again using three different schemes for comparison. Indeed we find such is the case that only integration of the log term itself by direct application of Gauss' formula present a significant error.

Once again, we make the following observations based on the three schemes used for these functions with a logarithm term, see Table XXII.

(1). The inability, or difficulty of Gauss' formula to appropriately approximate functions with discontinuities is revealed once again by the discrepancy in the result of direct applying the formula to integrate a logarithm function

and the exact value. Although the relative error in evaluating a log function, 6%, is much smaller than in evaluating a step function.

(2). As expected, only the log function alone causes significant error in the numerical integration. So long as there is a power function like $(t-x)^n$, $n \geq 1$ to suppress the logarithm term, Gauss' formula can be applied directly without significant error.

(3). Once again, splitting the integral in two at the point of discontinuity proves to be a superior way of handling these integrals.

Unlike the case of a step function, splitting the integral when integrating a logarithm function from -1 to 1 does not produce as good an accuracy. This is because the logarithm function is unbounded at where the integral is being separated. Artificially separating the integral at point of singularity forces Gauss' formula to take the value 0 for the logarithm instead of infinity. But the error introduced is still small compared to if Gauss' formula is applied over the whole range without separation.

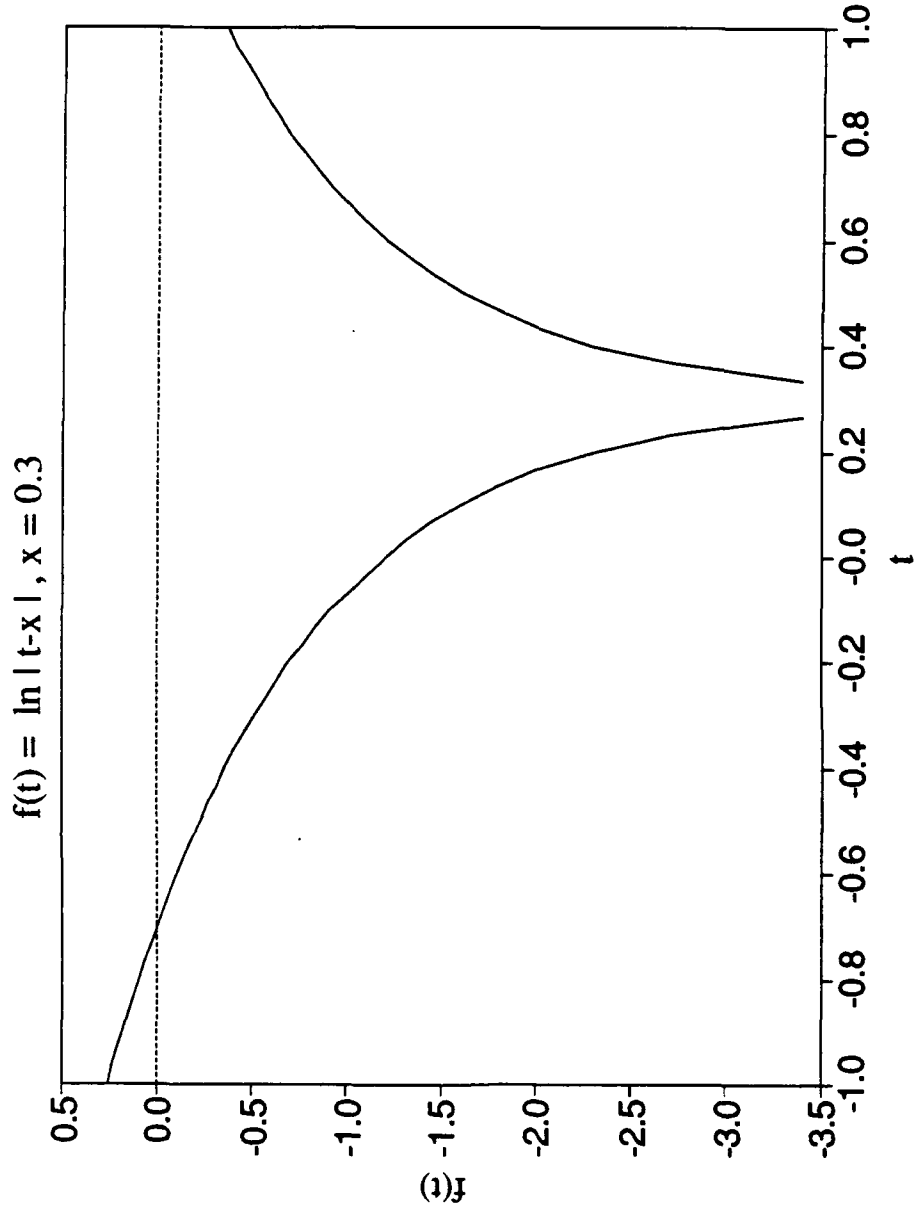

Figure 51 $\log|t\text{-}x|$, *x=0.3*.

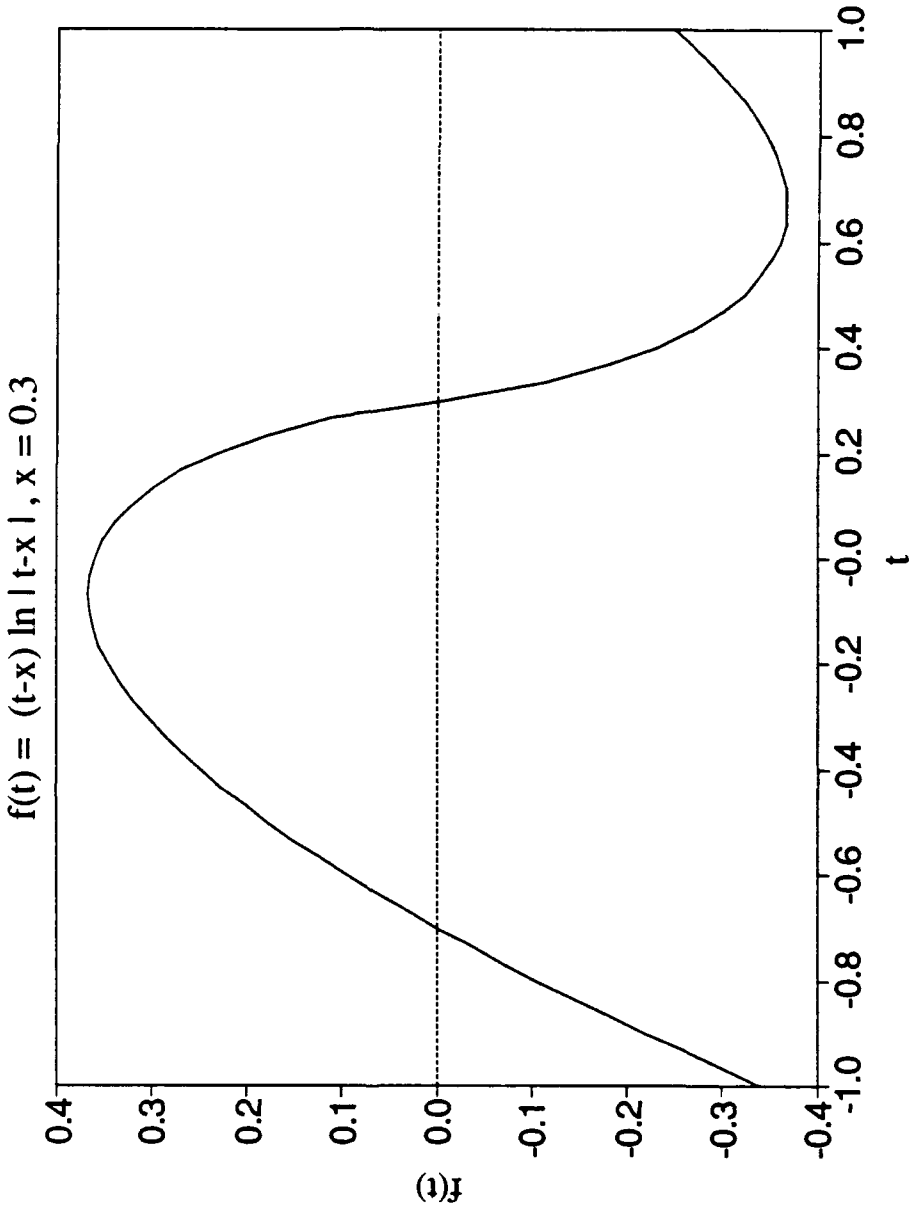

Figure 52 *f(t)=(t-x) log|t-x|, x=0.3.*

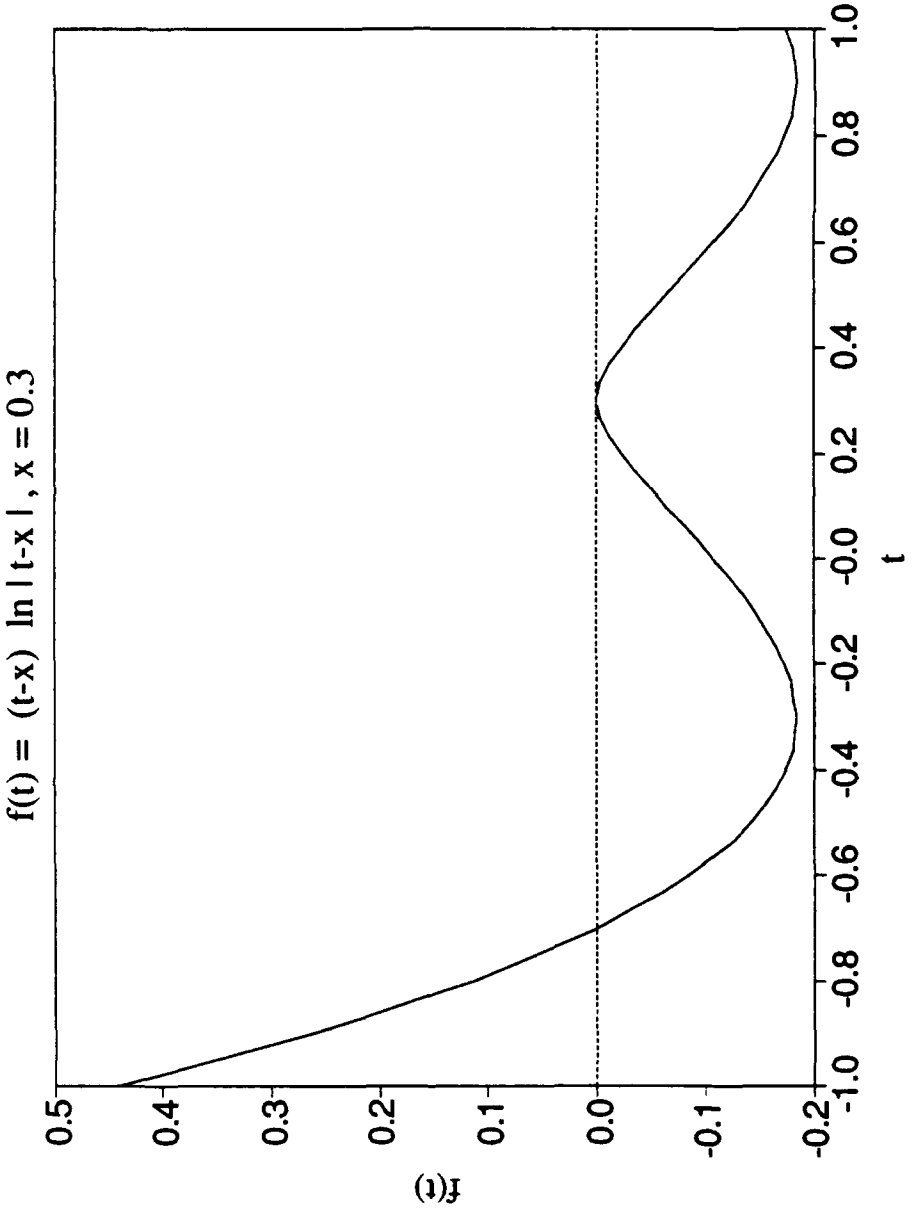

Figure 53 *f(t)=(t-x)² log|t-x|, x=0.3.*

Table XXII Evaluation of $\int_{-1}^{1} f(t,x)\,dt$, with different schemes for selected x values. f(t,x) contains a logarithm function.

	f(t,x)	Gauss (a)	Gauss/split int. (b)	Exact (c)
x=0.3	log(t-x)	-1.807367	-1.905593	-1.908599
	(t-x) log(t-x)	-0.008847	-0.009081	-0.009083
	$(t-x)^2$ log(t-x)	-0.131007	-0.130864	-0.130864
x=0.5	log(t-x)	-1.825950	-1.735370	-1.738376
	(t-x) log(t-x)	-0.045311	-0.042789	-0.042792
	$(t-x)^2$ log(t-x)	0.038481	0.038378	0.038378
x=0.7	log(t-x)	-1.384621	-1.456118	-1.459124
	(t-x) log(t-x)	-1.121327	-1.120933	-1.120937
	$(t-x)^2$ log(t-x)	0.309208	0.309268	0.309268

Note:

(a). Gauss' formula with 20 Gauss points.

(b). Split the integral in two at the point $(t-x) = 0$, then use Gauss' formula for each integral.

(c). Exact.

Appendix E

Numerical Evaluation Of Determinant

E.1 Introduction

In Chapter 3, we solved the SIE numerically by discretizing it at the collocation points. At each collocation point we evaluated the Fredholm kernels which are in the form of infinite integrals. Those integrals are each separated into two parts. The first part is obtained by using closed form expressions. The second part is a definite integral with limits of integration being 0 and a finite number "*A*", which we evaluated by using Gauss' formula.

We recall in Chapter 2 that the integrand of each Fredholm kernel is the algebraic sum of four terms each being the quotient of a 7 by 7 and an 8 by 8 determinant (see Eqns. (51) through (54)). From the discussions in Chapter 3 and Appendix B, we realized that in the actual numerical computation these determinants are to be evaluated by a full expansion. Since full determinant expansion requires a very large number of operations, we can expect this is where the major computing effort will be in the numerical analysis.

E.2 Floating point overflow

In order to learn how to be more efficient in computing the 8 by 8 and 7 by 7 determinants, let us write again the 8 by 8 determinant shown in Eqn. (B.3), but in a slightly different format as shown in Eqn. (E.1). Following discussions in Appendix B, we know that the leading terms of the 8 by 8 determinant and the eight 7 by 7 cofactors appear in the integrands of Fredholm kernels must carry a term like

$$\begin{bmatrix} 0 & 0 & 0 & 0 & -a_{65}e^{\alpha h_2} & -a_{66}e^{\alpha h_2} & -a_{67}e^{-\alpha h_2} & -a_{68}e^{-\alpha h_2} \\ 0 & 0 & 0 & 0 & -a_{55}e^{\alpha h_2} & -a_{56}e^{\alpha h_2} & -a_{57}e^{-\alpha h_2} & -a_{58}e^{-\alpha h_2} \\ O(\alpha)e^{-\alpha h_1} & O(\alpha)e^{-\alpha h_1} & O(\alpha)e^{\alpha h_1} & O(\alpha)e^{\alpha h_1} & 0 & 0 & 0 & 0 \\ O(\alpha)e^{-\alpha h_1} & O(\alpha)e^{-\alpha h_1} & O(\alpha)e^{\alpha h_1} & O(\alpha)e^{\alpha h_1} & 0 & 0 & 0 & 0 \\ a_{51} & a_{52} & a_{53} & a_{54} & a_{55} & a_{56} & a_{57} & a_{58} \\ a_{61} & a_{62} & a_{63} & a_{64} & a_{65} & a_{66} & a_{67} & a_{68} \\ a_{71} & a_{72} & a_{73} & a_{74} & a_{75} & a_{76} & a_{77} & a_{78} \\ a_{81} & 0 & a_{83} & 0 & a_{85} & a_{86} & a_{87} & a_{88} \end{bmatrix}. \quad \textbf{(E.1)}$$

$e^{2\alpha(h_1+h_2)}$. Depending on the relative value of α, h_1 and h_2, this $e^{2\alpha(h_1+h_2)}$ term can get very large very easily. Floating point overflow in numerical computations is consequently something we should watch out for in this determinant expansion.

Let's take the maximum floating point number prescribed in a particular computer to be R, a machine constant. This number is hardware dependent as well as programming language dependent. Let's further restrict the programming language used to be FORTRAN, which is the programming language numerical procedures in this study is written. R is therefore the maximum real number, single or double precision, that can appear anywhere in a FORTRAN program before overflow occurs. In the 8 by 8 determinant that we are dealing with, however, all numerical operations are in complex arithmetic. The maximum floating point number that can appear in our numerical procedure in either the real part or the imaginary part, therefore, becomes $R^{\frac{1}{2}}$. The numerical computation for this work is carried

out on a Cyber 180 Model 850 where the R value allowed in FORTRAN is defined to be $5.2\text{x}10^{1232}$ [32]. From this we can deduce that the following condition must exist or a floating point overflow would occur.

$$e^{2\alpha(h_1+h_2)} \le R^{\frac{1}{2}}, \Rightarrow \alpha(h_1+h_2) \le \frac{1}{4}\log R = 709.61 \qquad \textbf{(E.2)}$$

Based on the analysis above, we now know that in evaluating the Fredholm kernels, as the integration variable gets larger, there is increasing danger of floating point overflow. One way to avoid the floating point overflow is to have checkpoints in the numerical procedure so that whenever a particular element with the exponential term gets too large, the entire row is divided by a constant to keep it in check. This division on rows has to be done on both the numerator and the denominator so that the quotient is unchanged. But as this division is carried out, there are elements on the same rows that will run the risk of floating point underflow. These elements are those that carry the negative exponential as shown in Eqn. (E.1). To remedy the situation another checkpoint will have to be installed to set those elements under risk of floating point underflow to zero.

While this method works, there is another way of computing these determinants more efficiently. We shall describe it as follows. The value $\frac{1}{4}\log R$ in Eqn. (E.2) serve as a guide below which full expansion should be used to

numerically compute the determinants. When $\alpha\,(h_1 + h_2) > \frac{1}{4}\log R$, the term $e^{2\alpha(h_1+h_2)}$ is so overwhelmingly large that, as a result, the product of the rest of the terms of the fully expanded determinant are lost in the trailing digits of this huge number so that we are in effect computing the leading terms of the determinants. If we recognize this fact, the complicated procedure of computing all the terms of the determinant shrunk to just computing the leading term only, that is the term with the common factor $e^{2\alpha(h_1+h_2)}$. When this happens, we don't compute the term $e^{2\alpha(h_1+h_2)}$ in the numerator nor in the denominator because they factor out. What follows is a much simplified computation of the determinants exactly as described in Appendix B. This reflects a much reduced effort in our numerical computation. $\frac{1}{4}\log R$ in Eqn. (E.2) therefore becomes a parameter to flag between full expansion and leading terms expansion.

To avoid any possibility of floating point overflow in numerical computation, we purposely keep the value of $\alpha(h_1 + h_2)$ smaller than $\frac{1}{4}\log R$ by some margin. Since in full determinant expansion, we have eight elements to contend with in each product, and $e^{2\alpha(h_1+h_2)}$ constitutes only the exponential term of two elements. A limit of *500.0* was used for the computation in this work instead of *709.61* as given by Eqn. (E.2).

There is yet another interesting point one may make as a result of this floating point overflow discussion made above. Take the integral in Fredholm kernels that we have chosen to ignore in Chapter 3, namely

$$\int_A^{\infty}[D_{11}^{*}(\alpha)-d_{11}^{*}(\alpha)]\sin\alpha(t-x)\ d\alpha,$$

$$\int_A^{\infty}[D_{22}^{*}(\alpha)-d_{22}^{*}(\alpha)]\sin\alpha(t-x)\ d\alpha,$$

$$\int_A^{\infty}[D_{12}^{*}(\alpha)-d_{12}^{*}(\alpha)]\cos\alpha(t-x)\ d\alpha, \qquad \textbf{(E.3)}$$

$$\int_A^{\infty}[D_{21}^{*}(\alpha)-d_{21}^{*}(\alpha)]\cos\alpha(t-x)\ d\alpha.$$

From Chapter 2 we know that D_{ij}^{*}'s are the algebraic sum of $\frac{D_{ij}}{D}$, which are quotients of full expanded determinants. Likewise d_{ij}^{*} are the algebraic sum of $\frac{d_{ij}}{d}$, which are quotients of the leading terms of determinants. From the discussions stated earlier, we conclude that if the integration variable α gets too large, floating point overflow can occur. Here we must point out that the term "large" depends also on the sum $(h_1 + h_2)$. For large $(h_1 + h_2)$, α can be quite small when floating point overflow happens. When it happens, D_{ij}^{*}'s are evaluated the same way as d_{ij}^{*} as pointed out earlier, that is by leading terms expansion. As a result we have no way to reliably evaluate the integrals in Eqn. (E.3) since at large α, we can not evaluate D_{ij}^{*} exactly due to limitation of the machine constant. Putting it in another way, for sufficiently large "A", D_{ij}^{*} is equal to d_{ij}^{*} as far as numerical computation is concerned, therefore the integral is zero. This proves once more that these integrals can be ignored as we have done in Chapter 3.

E.3 Case of thin film on thick substrate

The discussions above applies to all cases of material thicknesses except that which we are going to address in this section. While it is generally true that when

the order of magnitude of the determinant reaches the limit of machine constant (the value R in the previous section, $R^{\frac{1}{2}}$ for complex arithmetic), it is as though we are computing the leading terms of the determinant and it is more efficient that way. But as the ratio of the thickness of the two materials $\frac{h_2}{h_1}$ gets smaller, it reaches a point where the numerical scheme of computing the determinants based on the leading terms expansion no longer suffice. Therefore for the case of very thin film on thick substrate, we need to re-examine the numerical procedure because the usual leading term expansion applicable to the general case would lead to difficulties in the convergence of solution and an unsatisfactory result. We shall now investigate this situation as follows. Consider the case of a very thin nonhomogeneous film as material 2

$$h_2 = \delta h_1. \tag{E.4}$$

Eqn. (E.2) becomes

$$\begin{aligned} \alpha h_1(1+\delta) &\le \frac{1}{4}\log R, \\ \approx \alpha h_1 &\le \frac{1}{4}\log R, \end{aligned} \tag{E.5}$$

since δ is very small. We now consider the next higher order term in the determinant that is ignored by the leading term expansion but a term that becomes increasingly important as $\frac{h_2}{h_1}$ becomes smaller, they are terms with a factor like $e^{2\alpha h_1}$ (see Eqn. (E.1)). We actually do not know under what circumstance the dropping of the term $e^{2\alpha h_1}$ will affect the result. Let us illustrate by assuming conservatively that when the second highest order term is larger than 1% of the highest order term, computing the determinant based on only the leading terms will give a distorted result. In other

words, when

$$e^{2\alpha h_1} > 1\%\ e^{2\alpha(h_1+h_2)}, \tag{E.6}$$

the solution will be disturbed if terms including $e^{2\alpha h_1}$ and lower are dropped. Taking logarithm on both sides of the inequality and simplifying, we obtain

$$\delta < \frac{\log 100}{2\alpha h_1}. \tag{E.7}$$

As mentioned earlier, as $e^{2\alpha(h_1+h_2)}$ reaches the machine constant, we resort to leading term expansion in computing the determinants. When that happens, αh_1 is at least equal to $\frac{1}{4}\log R$, see Eqn. (E.5). Substituting this into (E.7), we obtain the limiting value of δ under which, based on the assumption we have made in keeping only the highest order term when the second highest order term is larger than 1% of the highest order term, using the leading terms expansion to compute the determinants is no longer valid. For Cyber 850, we get $\delta < 0.00324$, which means that at approximately $\frac{h_1}{h_2} > 300$, dropping lower order terms as have been done in leading terms expansion will affect the accuracy of our solution.

The fix for these borderline cases when $\frac{h_1}{h_2}$ gets large is to simply go back to the less efficient full determinant expansion and employ row-wise division to avoid floating point overflow as well as setting small numbers to zero to avoid floating point underflow. To be on the safe side, in the cases that we have computed in Chapter 4, two worst cases where $\frac{h_1}{h_2}$ equals *200* and *400* respectively ($h_1 = 100\ a$, $h_2 = 0.5\ a$, and $h_1 = 100\ a$, $h_2 = 0.25\ a$) are computed using full determinant expansion. The rest of the cases were computed by employing the leading terms expansion. We found the results to be quite satisfactory as have been shown in Chapter 4.

Appendix F

Behavior of Cauchy Integral

Let there be a function of position $\phi(t)$ defined on an arc $[a_1, a_2]$. $\phi(t)$ is said to satisfy the Hölder condition on $[a_1, a_2]$, if for any two points t_1, t_2 on the arc

$$|\phi(t_2)-\phi(t_1)| \le A\,|t_2-t_1|^{\mu},\ 0<\mu\le 1, \tag{F.1}$$

where A is a positive constant. A is called the Hölder constant and μ the Hölder index. The implication that the function $\phi(t)$ satisfies the Hölder condition is that $\phi(t)$ is bounded and $d\phi(t)/dt$ is integrable within the closed interval $[a_1, a_2]$.

Consider the Cauchy integral

$$\Phi(z) = \frac{1}{2\pi i}\int_{a_1}^{a_2}\frac{\phi(t)}{t-z}\,dt, \tag{F.2}$$

where $\phi(t)$ has at most an integrable singularity and may be expressed as

$$\phi(t) = \frac{\phi_1^*(t)}{(t-a_1)^{\gamma_1}} + \frac{\phi_2^*(t)}{(t-a_2)^{\gamma_2}} + \phi_3^*(t),\ 0<Re[\gamma_1],\ Re[\gamma_2]<1. \tag{F.3}$$

$\phi_k^*(t)$, $k = 1, 2$ satisfy the Hölder condition on the closed interval of $[a_1, a_2]$ and $\phi_1^*(a_1) \neq 0$, $\phi_2^*(a_2) \neq 0$. Substituting Eqn. (F.3) into Eqn. (F.2), $\Phi(z)$ may be expressed as

$$\Phi(z) = \frac{1}{2\pi i}\,[\phi_1^*(a_1)\int_{a_1}^{a_2}\frac{dt}{(t-a_1)^{\gamma_1}(t-z)} + \phi_2^*(a_2)\int_{a_1}^{a_2}\frac{dt}{(t-a_2)^{\gamma_2}(t-z)} +$$

$$(I_1) \qquad\qquad (I_2)$$

$$\int_{a_1}^{a_2}\frac{\phi_1^*(t)-\phi_1^*(a_1)}{(t-a_1)^{\gamma_1}(t-z)}\,dt + \int_{a_1}^{a_2}\frac{\phi_2^*(t)-\phi_2^*(a_2)}{(t-a_2)^{\gamma_2}(t-z)}\,dt + \int_{a_1}^{a_2}\frac{\phi_3^*(t)}{t-z}\,dt\ ]. \tag{F.4}$$

$$(I_3) \qquad\qquad (I_4) \qquad\qquad (I_5)$$

Since, $\phi_1^*(t)$ satisfies the Hölder condition, we have

$$|\phi_1^*(t)-\phi^*(a)| < A\,|t-a|^{\mu},\ A>0,\ 0<\mu<1. \tag{F.5}$$

It follows that

$$I_3 < A\,|\frac{1}{2\pi i}\int_{a_1}^{a_2}\frac{dt}{(t-a_1)^{\gamma_1-\mu}(t-z)}\ | < K|\frac{1}{(z-a_1)^{\gamma_1-\mu}}|, \tag{F.6}$$

where A and K are both positive constants. From this we conclude that I_3 is of higher order than $(z - a_1)^{-\gamma_1}$. By a similar argument, I_4 is of higher order than $(z - a_2)^{-\gamma_2}$. $\phi_3^*(t)$ also satisfies the Hölder condition, therefore I_5 has at most a log singularity. As for I_1 and I_2, we shall show that they both have singularities at the end points that is stronger than any of I_3, I_4, or I_5. Let t_o be a point on (a_1, a_2). From the Plemelj formula (see [20]) we obtain the boundary value of I_1 as follows

$$I_1(t_0)^+ - I_1(t_0)^- = \phi_1^*(a_1)(t_0-a_1)^{\gamma_1},$$

$$I_1(t_0)^+ + I_1(t_0)^- = \frac{\phi_1^*(a_1)}{\pi i}\int_{a_1}^{a_2}\frac{dt}{(t-a_1)^{\gamma_1}(t-t_0)}. \tag{F.7}$$

Define the function

$$\Omega(z) = \frac{\phi_1^*(a_1)}{(1-e^{-2\pi i\gamma_1})(z-a_1)^{\gamma_1}}, \tag{F.8}$$

on any definite branch that is single valued and varies continuously on the interval (a_1, a_2). We obtain its boundary values as

$$\begin{aligned}
\Omega(t_0)^+ &= \frac{\phi_1^*(a_1)}{1-e^{-2\pi i\gamma_1}}\,(t_0-a_1)^{-\gamma_1}, \\
\Omega(t_o)^- &= \frac{\phi_1^*(a_1)e^{-2\pi i\gamma_1}}{1-e^{-2\pi i\gamma_1}}\,(t_0-a_1)^{-\gamma_1}, \\
\Omega(t_0)^+ - \Omega(t_0)^- &= \phi_1^*(a_1)(t_0-a_1)^{-\gamma_1}.
\end{aligned} \tag{F.9}$$

From Eqn. (F.7) and Eqn. (F.9), we obtain

$$[I_1(t_0)-\Omega(t_0)]^+ - [I_1(t_0)-\Omega(t_0)]^- = 0. \tag{F.10}$$

which means that $[I_1(z) - \Omega(z)]$ is holomorphic on the entire plane. We can write

$$\begin{aligned}
I_1(z) - \Omega(z) &= P_1(z), \\
I_1(z) &= \frac{\phi_1^*(a_1)}{1-e^{-2\pi i\gamma_1}}(z-a_1)^{-\gamma_1} + P_1(z), \\
&= \frac{\phi_1^*(a_1)e^{\pi i\gamma_1}}{2i\sin\pi\gamma_1}(z-a_1)^{-\gamma_1} + P_1(z).
\end{aligned} \tag{F.11}$$

where $P_1(z)$ is holomorphic. To obtain the boundary value of $I_1(z)$ on $[a_1, a_2]$, use Eqn. (F.9) and the Plemelj formula

$$I_1(t_0) = \frac{1}{2}\,[I_1(t_0)^+ + I_1(t_0)^-]$$

$$= \frac{1}{2}\phi_1^*(a_1)\,(t_0-a_1)^{-\gamma_1}\frac{1+e^{-2\pi i\gamma_1}}{1-e^{-2\pi i\gamma_1}} \qquad \textbf{(F.12)}$$

$$= \frac{1}{2i}\phi_1^*(a_1)\,(t_0-a_1)^{-\gamma_1}\cot\pi\gamma_1.$$

I_2 can be obtained in a similar manner in terms of its leading term and a holomorphic function. By Plemelj formula I_2 has boundary values as follows

$$I_2(t_0)^+ - I_2(t_0)^- = \phi_2^*(a_2)(t_0-a_2)^{\gamma_2},$$

$$I_2(t_0)^+ + I_2(t_0)^- = \frac{\phi_2^*(a_2)}{\pi i}\int_{a_1}^{a_2}\frac{dt}{(t-a_2)^{\gamma_2}(t-t_0)}. \qquad \textbf{(F.13)}$$

Again, define a function $\Psi(z)$ that is single valued and varies continuously on any definite branch

$$\Psi(z) = \frac{\phi_2^*(a_2)}{(1-e^{2\pi i\gamma_2})(z-a_2)^{\gamma_2}}. \qquad \textbf{(F.14)}$$

The boundary values of $\Psi(z)$ become

$$\Psi(t_0)^+ = \frac{\phi_2^*(a_2)}{1-e^{2\pi i\gamma_2}}\,(t_0-a_2)^{-\gamma_2},$$

$$\Psi(t_o)^- = \frac{\phi_2^*(a_2)e^{-2\pi i\gamma_2}}{1-e^{2\pi i\gamma_2}}\,(t_0-a_2)^{-\gamma_2}, \qquad \textbf{(F.15)}$$

$$\Psi(t_0)^+ - \Psi(t_0)^- = \phi_2^*(a_2)(t_0-a_2)^{-\gamma_2}.$$

From Eqn. (F.13) and (F.15), we conclude that $I_2(z) - \Psi(z)$ is holomorphic and write

$$I_2(z) - \Psi(z) = P_2(z),$$

$$I_2(z) = \frac{\phi_2^*(a_2)}{1-e^{2\pi i\gamma_2}}(z-a_2)^{-\gamma_2} + P_2(z), \tag{F.16}$$

$$= -\frac{\phi_2^*(a_2)e^{-\pi i\gamma_2}}{2i\sin\pi\gamma_2}(z-a_2)^{-\gamma_2} + P_2(z).$$

Similar to Eqn. (F.11), $P_2(z)$ is a holomorphic function. The boundary values of $I_2(z)$ on $[a_1, a_2]$ can be obtained from Eqn. (F.15) by using Plemelj formula again as follows

$$I_2(t_0) = \frac{1}{2}\left[I_2(t_0)^+ + I_2(t_0)^-\right]$$

$$= \frac{1}{2}\phi_2^*(a_2)\,(t_0-a_2)^{-\gamma_2}\frac{1+e^{2\pi i\gamma_2}}{1-e^{2\pi i\gamma_2}} \tag{F.17}$$

$$= \frac{1}{2i}\phi_2^*(a_2)\,(t_0-a_2)^{-\gamma_2}\cot\pi\gamma_2.$$

We have now shown that $I_1(z)$ and $I_2(z)$ have higher order leading terms than either $I_3(z)$ or $I_4(z)$. As for $I_5(z)$ which has a log singularity, we shall assume temporarily that it has a weaker singularity than either $I_1(z)$ or $I_2(z)$. We can now write the Cauchy integral and the boundary values in terms of its leading terms as follows

$$\Phi(z) = \frac{1}{2\pi i}\int_{a_1}^{a_2}\frac{\phi(t)}{t-z}\,dt,$$

$$= \frac{\phi_1^*(a_1)e^{\pi i\gamma_1}}{2i\sin\pi\gamma_1}(z-a_1)^{-\gamma_1} - \frac{\phi_2^*(a_2)e^{-\pi i\gamma_2}}{2i\sin\pi\gamma_2}(z-a_2)^{-\gamma_2} + P(z). \tag{F.18}$$

$$\Phi(t_0) = \frac{1}{2i}\phi_1^*(a_1)\cot\pi\gamma_1(t_0-a_1)^{-\gamma_1} - \frac{1}{2i}\phi_2^*(a_2)\cot\pi\gamma_2(t_0-a_2)^{-\gamma_2} + P(t_0). \tag{F.19}$$

$P(z)$ is bounded everywhere except possibly at the end points a, b, where it has

singularities no higher than those of the leading terms in Eqn. (F.18).

Multiplying Eqn. (F.19) by $(z - a_1)^{-\gamma_1}$ and let $t_o \to a_1$, we obtain the following characteristic equation

$$\frac{\phi_1^*(a_1)\cot\pi\gamma_1}{2i} = 0. \tag{F.20}$$

Since $\phi_1^*(a_1) \neq 0$, we have

$$\cot\pi\gamma_1 = 0,\ \gamma_1 = \pm\frac{1}{2}, \pm\frac{3}{2}, \pm\frac{5}{2}, \pm\frac{7}{2}, \cdots, \tag{F.21}$$

where γ_1 represent the stress singularity at end a_1. We obtain $\gamma_1 = \frac{1}{2}$ as the only acceptable solution since $0 < \text{Re}\ [\gamma] < 1$. At the end a_2 we can follow a similar procedure giving $\gamma_1 = \frac{1}{2}$. This is the well-known square root singularity for most crack problems. It also justifies the assumption we made earlier that I_5 has a weaker singularity than that of I_1 and I_2, since log singularity is weaker than square root singularity. From the discussions we had so far, we conclude that for singular integral equations with a simple Cauchy kernel. The density function $\phi(t)$ may be written as

$$\phi(t) = \frac{\phi^*(t)}{(t-a_1)^{1/2}(a_2-t)^{1/2}}, \tag{F.22}$$

$$\phi^*(t) = \phi_1^*(t)(a_2-t)^{1/2} + i\phi_2^*(t)(t-a_1)^{1/2} + \phi_3^*(t)(t-a_1)^{1/2}(a_2-t)^{1/2}.$$

where $\phi^*(t)$ is bounded everywhere on $[a_1, a_2]$.